Université de Montréal

Self-Assembly of PS-PVP Block Copolymers and Their Complexes at the Air/Water Interface

par

Iryna I. Perepichka

Département de chimie
Faculté des arts et des sciences

Thèse présentée à la Faculté des arts et des sciences
en vue de l'obtention du grade de
Ph.D. en chimie

Janvier 2011

Université de Montréal
Faculté des études supérieures et postdoctorales

Cette thèse intitulée:

Self-Assembly of PS-PVP Block Copolymers and Their Complexes at the Air/Water Interface

Présentée par:

Iryna I. Perepichka

a été évaluée par un jury composé des personnes suivantes:

Prof. Robert E. Prud'homme, président-rapporteur

Prof. C. Géraldine Bazuin, directrice de recherche

Prof. Antonella Badia, co-directrice

Prof. Christian Pellerin, membre du jury

Prof. Matthew G. Moffitt, examinateur externe

Prof. Pierrette Thibault, représentante du doyen de la FES

Résumé

Une compréhension approfondie et un meilleur contrôle de l'auto-assemblage des copolymères diblocs (séquencés) et de leurs complexes à l'interface air/eau permettent la formation contrôlée de nanostructures dont les propriétés sont connues comme alternative à la nanolithographie. Dans cette thèse, des monocouches obtenues par les techniques de Langmuir et de Langmuir-Blodgett (LB) avec le copolymère dibloc polystyrène-poly(4-vinyl pyridine) (PS-PVP), seul ou complexé avec de petites molécules par liaison hydrogène [en particulier, le 3-n-pentadécylphénol (PDP)], ont été étudiées.

Une partie importante de notre recherche a été consacrée à l'étude d'une monocouche assemblée atypique baptisée réseau de nanostries. Des monocouches LB composées de nanostries ont déjà été rapportées dans la littérature mais elles coexistent souvent avec d'autres morphologies, ce qui les rend inutilisables pour des applications potentielles. Nous avons déterminé les paramètres moléculaires et les conditions expérimentales qui contrôlent cette morphologie, la rendant très reproductible. Nous avons aussi proposé un mécanisme original pour la formation de cette morphologie. De plus, nous avons montré que l'utilisation de solvants à haut point d'ébullition, non couramment utilisés pour la préparation des films Langmuir, peut améliorer l'ordre des nanostries.

En étudiant une large gamme de PS-PVP avec des rapports PS/PVP et des masses molaires différents, avec ou sans la présence de PDP, nous avons établi la dépendance des types principaux de morphologie (planaire, stries, nodules) en fonction de la composition et de la concentration des solutions. Ces observations ont mené à une discussion sur les mécanismes de formation des morphologies, incluant la cinétique, l'assemblage moléculaire et l'effet du démouillage. Nous avons aussi démontré pour la première fois que le plateau dans l'isotherme des PS-PVP/PDP avec morphologie de type nodules est relié à une transition ordre-ordre des nodules (héxagonal-tétragonal) qui se produit simultanément avec la réorientation du PDP, les deux aspects étant clairement observés par AFM.

Ces études ouvrent aussi la voie à l'utilisation de films PS-PVP/PDP ultraminces comme masque. La capacité de produire des films nanostructurés bien contrôlés sur différents substrats a été démontrée et la stabilité des films a été vérifiée. Le retrait de la petite molécule des nanostructures a fait apparaître une structure interne à explorer lors d'études futures.

Mots-clés: auto-assemblage, films ultraminces nanostructurés, copolymères bloc, réseau de nanostries, monocouches Langmuir et Langmuir-Blodgett, interface air/eau, approche supramoléculaire, polystyrène-poly(4-vinyl pyridine).

Abstract

Deeper understanding and control of the self-assembly of diblock copolymers and their complexes at the air/water interface allow the formation of nanopatterns with known properties to provide a competitive substitute to nanolithography. In this dissertation, Langmuir and Langmuir-Blodgett (LB) monolayers obtained from polystyrene-poly(4-vinyl pyridine) diblock copolymers (PS-PVP), alone and hydrogen-bonded by various small molecules [particularly, 3-n-pentadecylphenol (PDP)], have been extensively investigated.

A major part of the research was devoted to the study of an uncommon monolayer pattern that we term the nanostrand network. LB monolayers consisting of nanostrands have sometimes been reported in the literature, but are often coexistent with other morphologies, which is not useful for potential applications. We have determined the molecular parameters and experimental conditions that control this morphology, making it highly reproducible, and have proposed a novel mechanism for the formation of this morphology. In addition, we have shown that the use of high-boiling spreading solvents, not usually used for Langmuir film preparation, can improve the nanostrand order.

By investigation of a wide range of PS-PVP's with various block ratios and molecular weights, with and without PDP present, we have established the composition dependence of the main LB morphology types (planar, nanostrand, nanodot) and the influence of each type on spreading solution concentration. This led to an extensive discussion concerning the mechanisms of morphology formation, including kinetic, molecular association, and dewetting contributions. We have also shown that the isotherm plateau transition for nanodot-forming PS-PVP/PDP is related to an order–order transition that occurs simultaneously with PDP reorientation, both aspects being clearly observed by AFM.

These studies also form the basis for the use of ultrathin PS-PVP/PDP films as templates. The ability to produce well-controlled nanopatterned films on various substrates has been demonstrated, and film stability has been verified. Removal of small molecules from the nanostructures has revealed the appearance of new substructure of interest for further study.

Keywords: self-assembly, nanostructured ultrathin films, block copolymers, nanostrand network, Langmuir and Langmuir-Blodgett monolayers, air/water interface, supramolecular approach, polystyrene-poly(4-vinyl pyridine).

Dedicated to my father, who first showed me the spectacular world of Chemistry,
to my husband, who always and everywhere was nearby supporting me, and
to my daughter, whose childhood is indissolubly connected with UdeM

Disclosure

This dissertation is written in the form of one published paper and two thesis chapters. The latter will be submitted shortly to peer-reviewed journals.

The first paper is co-authored by the research director, Prof. C. Geraldine Bazuin, and co-director, Prof. Antonella Badia. Here, based on proposals of my supervisors and my own ideas, I did all experimental studies (including film preparation, variation of experimental parameters, imaging of film morphology, etc.), prepared the article for publication (wrote the manuscript, modified it in accordance to feedback from my supervisors, and made final corrections after peer-review). Permission to reproduce this paper in my dissertation has been granted by the American Chemical Society (ACS), and copyright clearance was given by the co-authors.

The Chapter 3 is an "almost ready for submission" paper that will be co-authored with Dr. Qing Lu, Prof. C. G. Bazuin, and Prof. A. Badia. My contribution to this research is at least 80% of the experimental part (obtaining of Langmuir isotherms, preparation of LB films, surface characterization), and participation in the manuscript preparation. The contribution of co-authors other than my research supervisors is as follows: Qing Lu (a former postdoc in Prof. Bazuin's group) obtained results for a limited series of block copolymers using dilute solutions and using the "solvent-assisted" technique (specifically, Figure 3-6), which are complementary to my conditions. Dr. Qing Lu gave me permission to use the above data in the present thesis.

Acknowledgements

This dissertation work would not be possible without my supervisors, Prof. Géraldine Bazuin and Prof. Antonella Badia. Many thanks for their valuable advice, critical discussions, and sincere joy for my success, as well as for financial support, including coverage of my trips to many scientific conferences. To Prof. Géraldine Bazuin, I also want to say special thanks for her careful reviewing all my paperwork (including this dissertation) and great editorial efforts, and also for just being a very kind person; I will never forget the care and support that she provided.

I thank all the funding sources that generously supported my studies. I thank the Faculté des études supérieures et postdoctorales (FESP, Université de Montréal) for a Bourse d'exemption des droits de scolarité supplémentaires (2005–2007), a Bourse pour le passage accéléré de la maîtrise au doctorat (2006–2007), and a Bourse de fin d'études doctorales (2010). I thank Le fonds québécois de la recherche sur la nature et les technologies (FQRNT, Quebec, Canada) for granting me the Merit Scholarship for Foreign Students (2007–2010) and a Postdoctoral Fellowship (2011–2013; though I have not benefited from the latter one yet, this award gave me an additional force during the last year of my PhD). I appreciated my membership in the interuniversity Centre for Self-Assembled Chemical Structures (CSACS/CRMAA) and Le regroupement québécois sur les matériaux de pointe (RQMP) that allowed me to broaden my experience due to communication with other scientists in the area of nanomaterials and chemical self-assembly, and participation in various multidisciplinary trainings.

I am deeply grateful to Prof. Christian Pellerin (Université de Montréal) and Damien Mauran for their welcome help with infrared spectroscopy and for always being available to discuss results. I also thank Prof. Michel Pézolet (Université Laval, Canada) for allowing me to do *in-situ* infrared spectroscopy in his lab, and Jean-François Rioux-Dubé for assistance in the experiments.

I also thank Andrey Krayev (Aist-NT, USA) for collaboration in AFM imaging.

I am grateful to many former and present members of the Bazuin and Badia groups, especially to Dr. Alexis Laforgue (for introducing me to AFM), Jacqueline Sanchez (for training me in LB film preparation and assistance in BAM experiments), Dr. Lana Norman and Eric Dionne [for preparation of gold substrates, which I used in my research; and also to Lana, for the friendship, and to Eric, for involving me in his research that resulted in my discovery of how acetone affects the nanostrands (Chapter 4)], Ximin Chen and Sébastien Roland (for sharing their experience in thin films, and for making the routine days filled with jokes); and Gwénaëlle Bazin (Prof. Zhu group) for help in organization of student meetings. I also thank Kateryna Borozenko (a summer student from Donetsk National University, Ukraine) for her diligent work during her training in summer 2010. I sincerely hope that, from our collaborative work, she gained as much positive experience in the lab as I gained in teaching.

I acknowledge Lyne Laurin and Prof. André Beauchamp for guiding me through the bureaucratic labyrinths of graduate school.

Sanna Rantanen and Denis Le Bras (Attension & KSV Nima, Finland) are acknowledged for providing high-resolution images illustrating LB and LS methods (Figure 1-7) used in the Chapter 1.

I thank Prof. Federico Rosei (INRS, Canada) for inspiring me to never give up.

I am very thankful to Dr. Oleksandr Ivasenko for his help, countless research ideas, and open-hearted friendship.

A very special acknowledgements goes to my mentors (both in Chemistry and in life): to my father, Prof. Igor Perepichka (Bangor University, United Kingdom) and to my uncle, Prof. Dmitrii Perepichka (McGill University, Canada), for their inestimable advice and fruitful discussions. They showed me in detail what it means to be a professor, and made me appreciate (and understand) that this profession is not easy (and sometimes thankless) but (always) fascinating and fun.

I thank Dr. Inna Perepichka, one of the perfect women-in-science, to my mind, for her kindness and the ability to infuse self-confidence. I thank my grandmother, Prof. Svitlana Bila ("Beekah"), for the cognitive lessons of Physics and the wisdom lessons of life philosophy. And I thank my mother Lyudmyla Perepichka and sister Olga, for supporting me when I decided to continue my graduate studies abroad and for never complaining, though I know how it was (and is) difficult for them that I am so far away.

I am infinitely grateful to my loved and loving husband, Maksym Kryuchkov, who always supported me both in daily life at home and with help in the lab, constantly giving me force to go ahead. I want to use this opportunity to tell him how I appreciate his care and patience. Besides, we both know that he was to defend his PhD thesis first, but as a real gentleman, he let me go ahead of him. Finally, I am obliged to my dear daughter, little Diana, who let me feel the happiness of motherhood and enjoy a scientific career simultaneously. I love you. A woman can reach a goal and have success, but all those are especially valued only if her family is proud of her. Thanks for making me happy in Science!

TABLE OF CONTENTS

CHAPTER 1

CHAPTER 2

Nanostrand Formation of Block Copolymers At the Air/Water Interface …………………………………………………… 51

CHAPTER 5

List of Figures

List of Tables

List of Abbreviations and Symbols Used

π	surface pressure
μm	micrometer(s)
^{1}H NMR	proton nuclear magnetic resonance spectroscopy
2D	two-dimensional
3D	three-dimensional
Å	Angstrom(s)
AFM	atomic force microscopy
A_{on}	onset area
A_{lim}	limiting area
ATR	attenuated total reflection
b.p.	boiling point
BAM	Brewster angle microscopy
C (or C*)	cylindrical morphology
C_{16}diol	1,16-hexadecanediol
$C_2H_2Cl_4$	1,1,2,2-tetrachloroethane
$C_2H_4Cl_2$	1,2-dichloroethane
C_3Cl_6	hexachloropropene
CNSL	cashew nut shell liquid
CwL	cylinders within lamellar matrix
DBSA	4-dodecylbenzenesulfonic acid
DDP	4-dodecylphenol
EO-SA	oligo(ethylene oxide) sulfonic acids
FOH	1H,1H,2H,2H-perfluoro-1-octanol
FTIR	Fourier transform infrared spectroscopy
GwL	gyroid within lamellar matrix
H-bond	hydrogen-bond
HOPG	highly ordered pyrolytic graphite
ITO	indium tin oxide

L	lamellar morphology
LB	Langmuir-Blodgett
LS	Langmuir-Schaefer
LwC	lamellae within cylindrical matrix
LwL	lamellae within lamellar matrix
LwS	lamellae within spherical matrix
M_n	number average molecular weight
M_w	weight average molecular weight
M_w/M_n	polydispersity index
mN/m	millinewton per meter
mol%	molar fraction (in percents)
MSA	methane sulfonic acid
n_{PS}	number of repeat units in the polymer chain of PS
NDP	4-*n*-nonadecylphenol
nm	nanometer(s)
NOH	1-naphthol
OBA	4-*n*-octylbenzoic acid
OctOH	1-octanol
OctPh	4-*n*-octylphenol
OS	oligostyrene
PVP	poly(4-vinyl pyridine)
P2VP	poly(2-vinyl pyridine)
PBA	poly(*tert*-butyl acrylate)
PBMA	poly(*n*- or *tert*-butyl methacrylate)
PCDA	10,12-pentacosadiynoic acid
PDMS	poly(dimethylsiloxane)
PDP	3-*n*-pentadecylphenol
PEO	poly(ethylene oxide)
PFS	poly(ferrocenyl silane)
$PhNO_2$	nitrobenzene
PM-IRRAS	polarization modulation infrared reflection–absorption spectroscopy

PMMA	poly(methyl methacrylate)
PPE	poly(2,6-dimethyl-1,4-diphenyl oxide)
PS	polystyrene
PS-PVP	polystyrene-*b*-poly(4-vinyl pyridine) [in the form PS_x-PVP_y, *x* and *y* are numbers of repeat units; in the form PS(x)-PVP(y), *x* and *y* are molecular weights of blocks]
PS-PVP/PDP	polystyrene-*b*-poly(4-vinyl pyridine) hydrogen-complexed with 3-*n*-pentadecylphenol [in the form PS-PVP/PDP_x, *x* denotes the PDP:VP molar ratio]
rms	root mean square
S (or S*)	spherical morphology
SAXS	small-angle X-ray scattering
Si/SiO_2	silicon oxide wafer
SwL	spheres within lamellar matrix
T	temperature
T_g	glass transition temperature
TEM	transmission electron microscopy
TSA	4-toluenesulfonic acid
v.p.	vapour pressure
v/v	volume to volume ratio
VP	vinylpyridine
wt%	weight fraction (in percent)
$Zn[DBSA]_2$	zinc dodecylbenzenesulfonate

Prologue

“We live in a world of three dimensions. We measure objects by their length, breadth and thickness. … I propose to tell you of a real two-dimensional world” *

Irving Langmuir

“I will describe a simple method, which I have employed for several years” **

Agnes Pockels

---

* Langmuir, I. *Science* **1936**, *84*, 379.

** From a letter to Lord Rayleigh (Pockels, A. *Nature* **1891**, *43*, 437).

Chapter 1

General Introduction and Scope of the Thesis

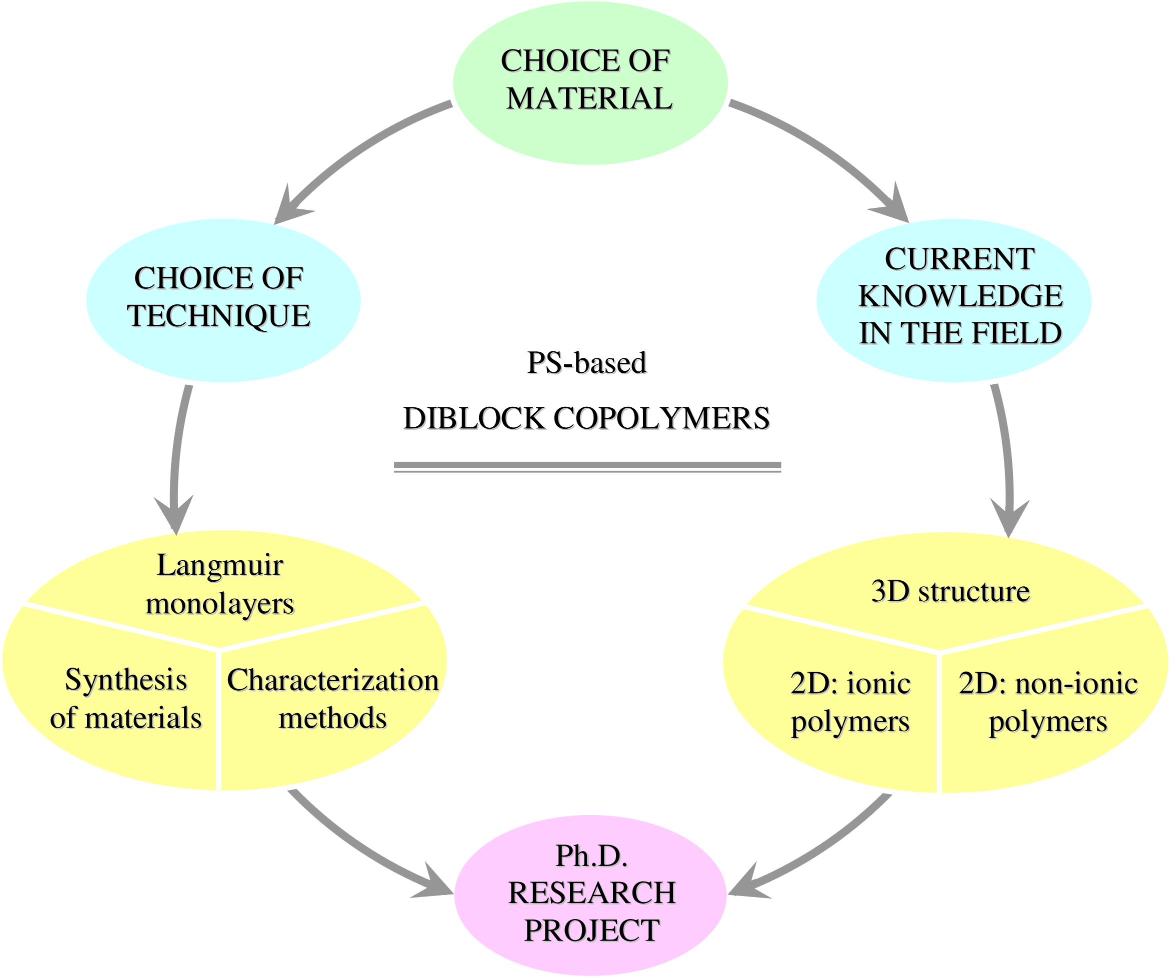

1.1. WHY BLOCK COPOLYMERS?

Block copolymers are currently receiving much attention due to their ability to self-assemble into well-defined and easily tunable nanostructures. They have many applications that range from biomedical to (opto-)electronic technologies.[1]

Block copolymers consist of two or more distinct homopolymers linked together via covalent bonds. Usually, two chemically different polymers macrophase separate when mixed together due to asymmetry in enthalpic and entropic contributions. Even weak repulsive interactions between repeat units in different polymers are magnified due to the large number of repeat units in each polymer. These interactions usually dominate the thermal motion of polymer chains causing macrophase separation. But when two incompatible polymers are linked together through a covalent bond they can separate only on a local molecular scale, leading to the formation of periodic structures of nanoscale order.[2,3]

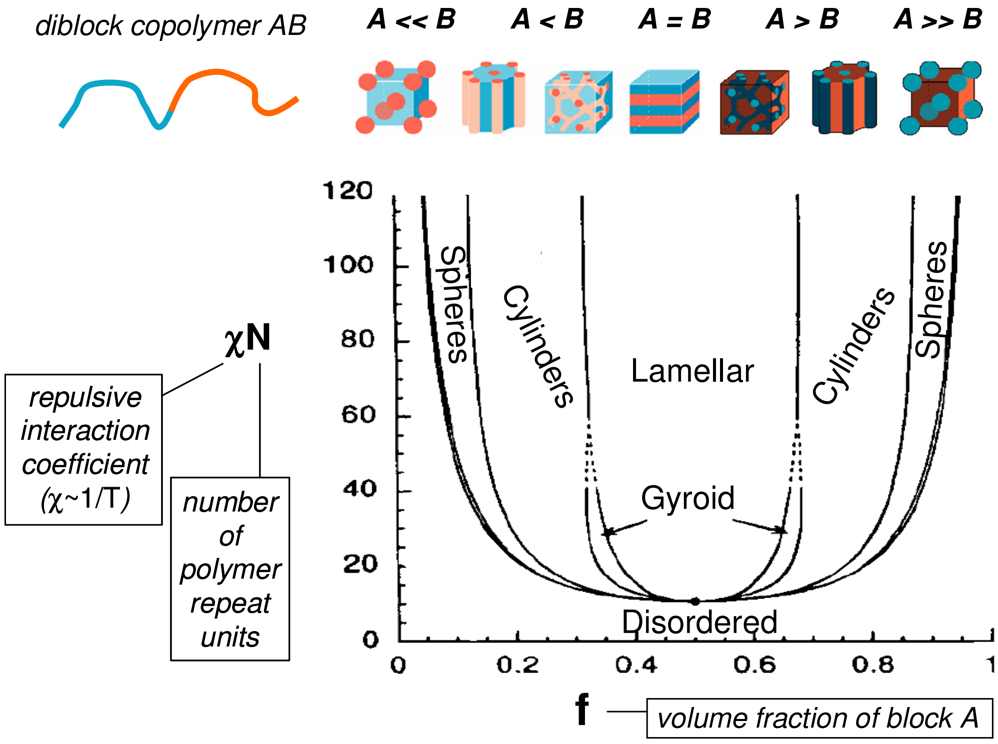

Figure 1-1. Theoretical phase diagram of diblock copolymers.

(Adapted with permission from ref. 4. Copyright 1996 American Chemical Society).

A theoretical phase diagram for diblock copolymers is shown in Figure 1-1. It illustrates how the different phase structures typically observed (spherical, cylindrical, gyroid, and lamellar) depend on block volume fraction, total degree of polymerization, and the Flory–Huggins interaction parameter χ. The latter indicates the strength of the interactions between the polymer blocks and depends inversely on temperature.

The relatively simple phase diagram for diblock copolymers can be made more complex in different ways, such as by adding a block selective homopolymer, or by turning to tri- and multi-block copolymers. Of most relevance to this thesis is the introduction of supramolecular chemistry to modify or control copolymer self-assembly. This approach is based on the use of non-covalent interactions, using, for example, block copolymers where one of the blocks has side groups capable of forming hydrogen or ionic bonds with other molecules having a complementary interacting group (*e.g.*, acid–base pairs or oppositely charged ionic groups). On the one hand, introducing surfactants or functionalized mesogens can lead to additional self-assembly within one of the blocks, so that new substructures appear (detailed structure-within-structure formation will be discussed later). On the other hand, an advantage of block copolymer supramolecular systems is that, after the desired film morphology is obtained, the small molecules can be rinsed out easily to give nanoporous materials (in bulk) or membranes (in thin films). Figure 1-2 illustrates one such example for a thin film of polystyrene-poly(4-vinyl pyridine) (PS-PVP) containing 1,5-dihydroxy-naphthalene (DHN) that hydrogen bonds to PVP.[5]

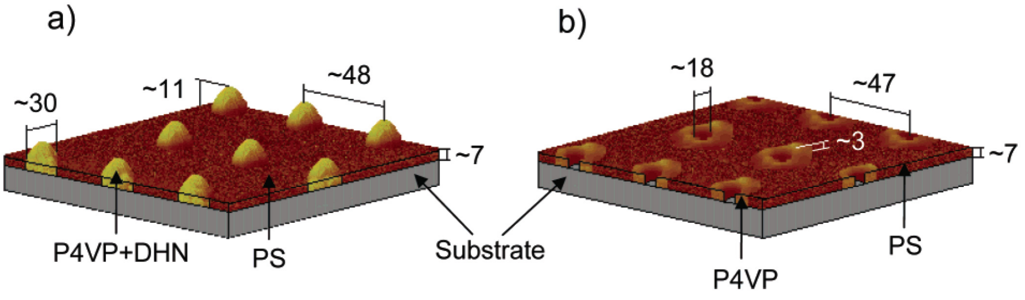

Figure 1-2. Morphology of thin (dip-coated) films of PS-PVP/DHN: a) as deposited; b) after immersion in methanol to eliminate DHN. Dimensions are in nm. (Reproduced with permission from ref. 5. Copyright 2006 American Chemical Society).

1.1.1. Bulk *vs*. Thin Films of Block Copolymers

It should be noted that thick and thin films of structured block copolymers are distinguished not by their exact thickness, but rather by a basic difference in the layer formation.[6] Though, in general, thin films are less than 500 nm and thick films may be several tens of micrometers in thickness, the most important point is that the microstructure in thin films has an orientation with respect to the underlying substrate, whereas thick films do not show such an orientation, but instead behave as in the bulk.[6]

In other words, thin films can have a different morphology than the equilibrium bulk morphology and show structural orientation due to the influence of interfacial energies, typically with a solid substrate and with air.[7] For example, cylinders lying parallel to the surface in very thin films may become perpendicular to it as the film thickness increases. Use of various solvents or different concentrations of solutions can also cause phase transitions in thin films.[8]

1.1.2. Potential Applications of Block Copolymer Thin Films

One of the examples of block copolymer thin film applications is their use in nanolithography. It was shown that ultrathin films can be used as a mask for the generation of nanoscale gold islands (Figure 1-3),[9] or as a template for titanium coatings due to the favourable PS/Ti interaction.[10]

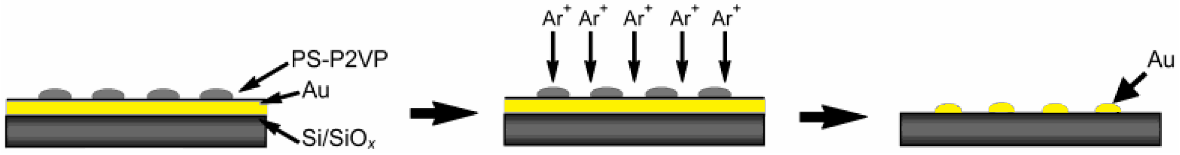

Figure 1-3. Schematic cross-sectional view of the formation of well-defined gold clusters *via* reactive ion etching of a silicon wafer covered with gold and an ultrathin mask of PS-P2VP. (Adapted with permission from ref. 9. Copyright 2003 American Chemical Society).

Another advanced application of block copolymer films is their use in medical diagnostics and water treatment engineering. Separation membranes prepared using block copolymers are characterized by nanoscale pores, high porosity, uniform pore size, and the possibility of selective functionalization.[11] As such, they can be used, for example, for virus filtration (Figure 1-4)[11] or for water purification.[12]

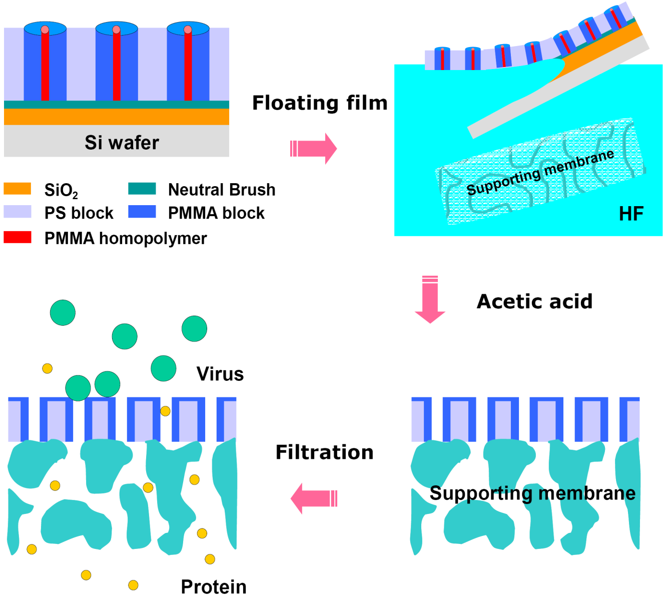

Figure 1-4. Schematic representation of nanoporous membrane preparation, and its use for filtration of viruses from proteins.

The nanopatterned ultrathin films can be used as nanotemplates for deposition of conjugated monomers for further polymerization, or metals to fabricate nanowires. Films with strand morphology obtained by multilayer transfers can be used as a nanoseparation membrane, or as a separation layer in sandwich materials where a porous wall is required.

1.2. ULTRATHIN FILMS

Our research is focussed on studies of monolayers of block copolymers obtained at the air/water interface, using the techniques described below.

1.2.1. Langmuir and Langmuir-Blodgett Films

1.2.1.1. First Investigations of Thin Insoluble Monolayers

Prior to 1910, many different theories of adsorption had been proposed, including those concerning the increased concentration of the adsorbed substance near the surface as analogous to the retention of the earth's atmosphere by the gravitational attraction of the earth.[13] Langmuir[*] first proposed a general theory of adsorption for solid and liquid surfaces based on the idea of satisfying unsaturated surface valence forces.[14] Based on early experiments of Pockels to measure the surface tension properties of water using a kitchen sink, string, and buttons,[15] Langmuir advanced the technique by designing a trough with an adjustable balance and a floating barrier, which allowed compressing and/or expanding the water surface area. Using this "Langmuir trough", he recorded the force, expressed as the surface pressure[†], and correlated it with the area occupied per molecule, which was determined by dividing the area between the fixed and floating barriers by the number of molecules placed on the surface.[16] These experiments enabled Langmuir to find the shape of molecules, and demonstrate that, when organic molecules containing -COOH, -CO-, or -OH polar head groups and a hydrocarbon tail $-(CH_2)_nCH_3$ are spread over the water surface, they become oriented with the hydrophilic polar group soluble in the water layer and the hydrophobic hydrocarbon portion of the molecule extended in the air.[16,17]

---

[*] *Irving Langmuir*, an American chemist and physicist, is known for his investigation of thin insoluble monolayers at the air-water interface, surface adsorption, and improvement of the technique used by Agnes Pockels. In 1932, he was awarded a Nobel Prize in Chemistry for "his discoveries and investigations in surface chemistry."

[†] "The net of forces exerted on the plate partially immersed into liquid subphase is constituted by the sum of the gravitational force and the surface tension pulling the plate downward, minus the buoyancy force pushing it upwards."(From description of Wilhelmy plate method).

1.2.1.2. Langmuir Compression Isotherm

A single layer of molecules on the water surface can refer to two-dimensional gases, two-dimensional liquids, or two-dimensional solids.[16]

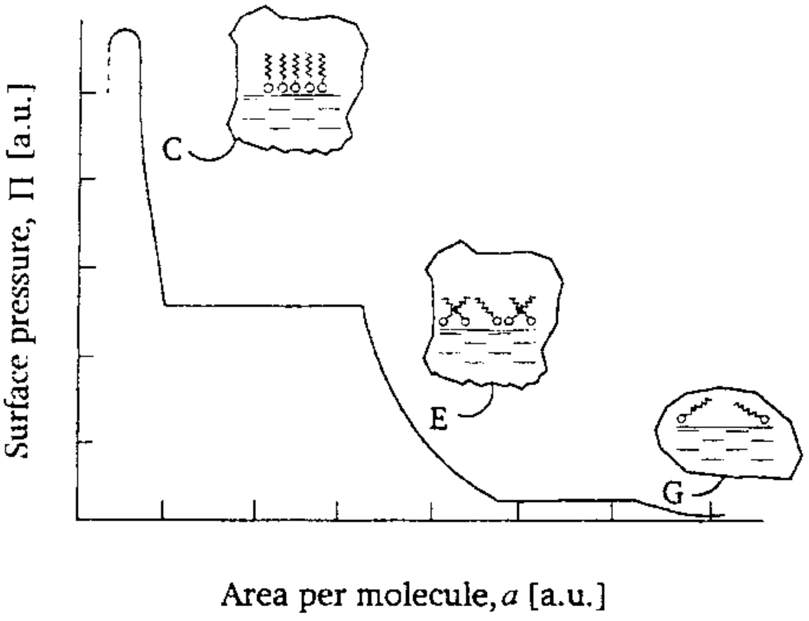

Figure 1-5. A typical surface pressure – mean molecular area isotherm for a long-chain organic compound showing the different phases: G – gaseous, E – liquid expanded, C – liquid condensed. (Reproduced from ref. 18 with the permission of Cambridge University Press).

The principal idea of Langmuir's experiments was based on measurement of surface tension: the stronger the intermolecular forces between molecules residing at the surface of a liquid, the stronger the surface tension. The high surface tension of pure water, for example, is caused by strong hydrogen bonding between H_2O molecules. The introduction of impurities to the water surface dramatically decreases its surface tension due to interaction between them leading to a change in the free energy of the water surface.[19] Thus, surface pressure (π) is a measure of the change in the free energy of the water surface before and after adsorption of organic solutes,[19] and can be defined as the difference between the surface tension of pure water (γ_0) and the surface tension in the presence of adsorbed solutes (γ):

$$\pi = \gamma_0 - \gamma$$

The Langmuir compression isotherm, which is expressed as the dependence of surface pressure *versus* area per molecule, indicates the molecular orientation of amphiphilic molecules at the air–water interface (Figure 1-5). The transition between phases can be detected by a plateau region that is characterized by an equilibrium state in which the surface pressure remains constant while the area is decreased.

1.2.1.3. Langmuir-Blodgett and Langmuir-Schaefer Films

The first experiments involving the deposition of mono- and multilayers onto solid substrates were performed by Blodgett[‡] using long-chain fatty acids.[20] Films were deposited from a trough covered with surfactants by displacement of a vertical plate out of a liquid bath.[21] The basic principle of Langmuir-Blodgett (LB) film deposition has not changed over almost a century. The modern Langmuir trough is presented in Figure 1-6.

Another technique used to transfer Langmuir monolayers onto solid substrates is the horizontal lifting method, where the substrate touches the film horizontally, and lifts it up into the air,[22] or lowers it onto the surface of the water.[23] Films deposited by this method usually are called Langmuir-Schaefer[§] (LS) films, in contrast to LB films, produced by conventional vertical deposition (Figure 1-7a,b).

[‡] *Katherine Blodgett* was Irving Langmuir's assistant, and the first female research scientist hired by General Electric Laboratory. Working in the field of surface chemistry, she discovered that several monolayer films could be transferred one on top of the other to produce multilayer films, and she invented non-reflective glass, produced by LB technique. Blodgett was the first woman to be awarded a Ph.D. degree in Physics from Cambridge University (England) in 1926.

[§] *Vincent Schaefer* was a research assistant of Irving Langmuir who was also, like Katherine Blodgett, involved in studies of monolayers and surface chemistry techniques. However, his main area of interests was in meteorology, where he became famous for his experiments on the creation of artificial rain and snow, and the discovery of the principle of cloud seeding.

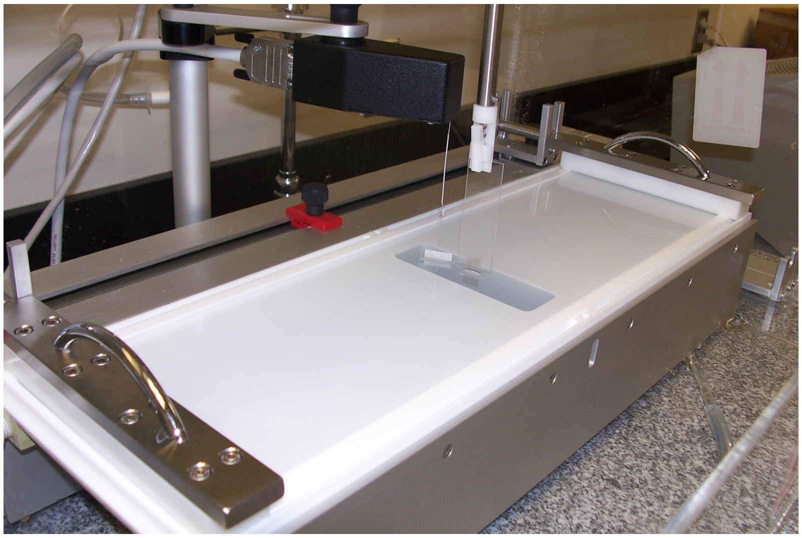

Figure 1-6. Langmuir trough (KSV 3000).
In the center is a Wilhelmy plate to measure surface tension, and a piece of mica (stuck to glass) immersed in the water subphase. After spreading a solution, barriers (on the left and right sides of the trough) are compressed to reach and hold a specified surface tension. Transfer of the monolayer onto mica is caused by the withdrawal of the substrate from the subphase at a constant speed.

The transfer ratio (TR) of monolayers, which is defined as the ratio of the area swept by the moving barriers during the transfer of a single monolayer to the area of film deposition on the substrate,[24] can be estimated in LB films; but quantification in LS films is difficult due to the difficulties of *in-situ* measuring of the horizontal transfer processes.[22]

Multilayer films can be transferred from water to a solid substrate by successive substrate immersion-withdrawal cycles. The three main types of multilayer films are: X-type, characterized by a hydrophilic surface because the monolayer at the air/water interface deposits onto the substrate during immersion only; Z-type, characterized by a hydrophobic surface because the monolayer deposits onto the substrate during withdrawal only; and Y-type, where the monolayer deposits onto the substrate both during immersion and withdrawal, and thus the hydrophilicity of the surface is determined by the last layer deposited (Figure 1-7c).[20]

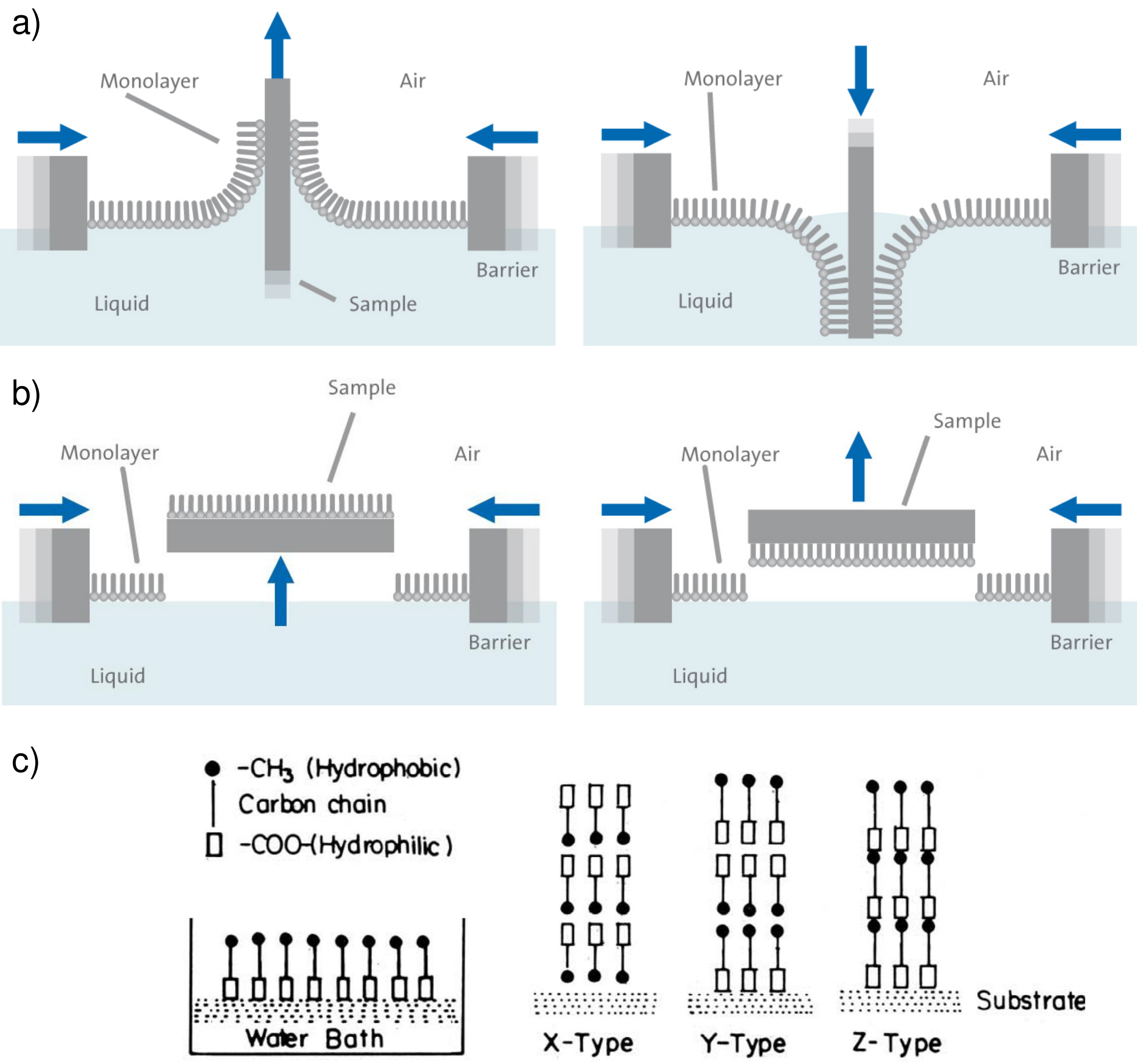

Figure 1-7. a) Langmuir-Blodgett method; b) Langmuir-Schaefer method; c) common types of multilayers deposited on a substrate. (Images *a* and *b* are reproduced from ref. 25 with permission of KSV-Nima. Image *c* is adapted from ref. 20 with permission of American Chemical Society).

During the last century, attention to Langmuir monolayers has alternately increased and declined. In spite of many pros and cons, nowadays the technique is used not only in research laboratories, but also has found applications in industry (*e.g.*, Nanometrix Inc. in Montreal).

1.2.2. Film Characterization

In our work, we used the following methods of characterization: 1) atomic force microscopy (AFM) and scanning tunnelling microscopy (STM) to image the film morphology, 2) Brewster angle microscopy (BAM) to image the monolayer at the water surface, 3) Fourier transform infrared (FTIR) spectroscopy in attenuated total reflection (ATR) and reflection–absorption (IRRAS) modes, to confirm complexation between the polymer and small molecules, and in polarization modulated infrared reflection–absorption (PM-IRRAS) mode to determine the orientation of alkyl chains of small molecules at the air/water interface, 4) proton nuclear magnetic resonance spectroscopy (^{1}H NMR) to study complexation and aging of solutions, and 5) time of flight static secondary ion mass spectrometry (TOF-SIMS) to analyze the composition of thin films after their treatment.

Of these techniques, AFM was the major one used, and thus will be the only one described here. The principles of the other methods, some of which were used just once or twice, can be found elsewhere.[26–31]

1.2.2.1. *Atomic Force Microscopy*

AFM is a type of scanning force microscopy that enables one to investigate nanoscale structures, dynamics, and forces at interfaces.[32] The first AFM was invented by Binning, Quate and Gerber in 1986. The principle of AFM operation is to scan a surface by means of a tip integrated at the end of a cantilever, making a constant force (or height) between tip and sample, which is controlled by a piezoelectric scanner. The interactions between the tip and the sample surface are detected by monitoring the reflection of a laser off the cantilever with a split-segment photodiode (Figure 1-8).[32] In contrast to STM, samples (and substrates) for imaging by AFM are not limited to conducting materials.

There are three types of AFM operation: non-contact, contact, and tapping modes. In non-contact mode, the cantilever tip, which is a few tens or hundreds of Angstroms (Å) above the sample surface, detects the *attractive* van der Waals forces acting between the tip and the sample. In contact mode, the tip is in much closer contact with the sample, so that the interaction forces between the tip and the sample are mainly *repulsive* in nature.[33] In our work, we used tapping mode AFM mode. In this mode, the cantilever is oscillated at or near its resonance frequency, and the vibrating tip thus scans the sample by lightly tapping the surface (Figure 1-9a).

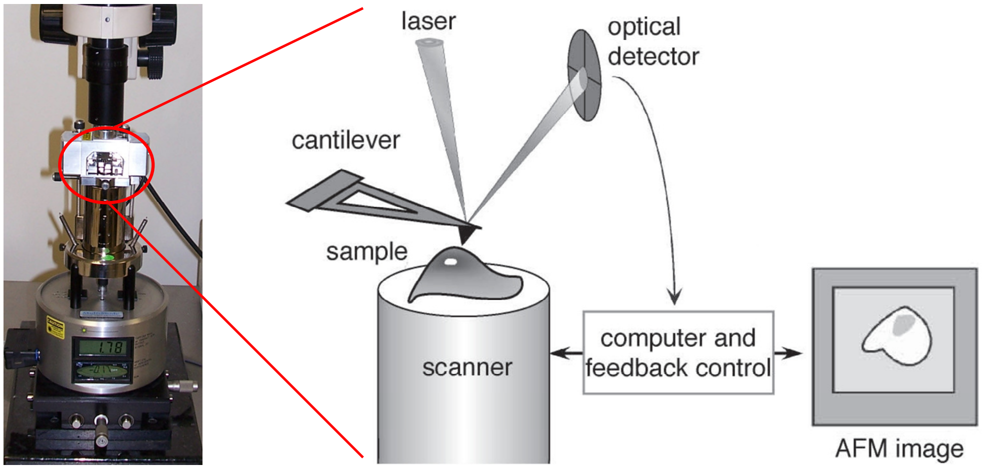

Figure 1-8. Schematic illustration of a common implementation of the AFM. (Right image is reproduced with permission from ref. 32. Copyright 2005 American Chemical Society).

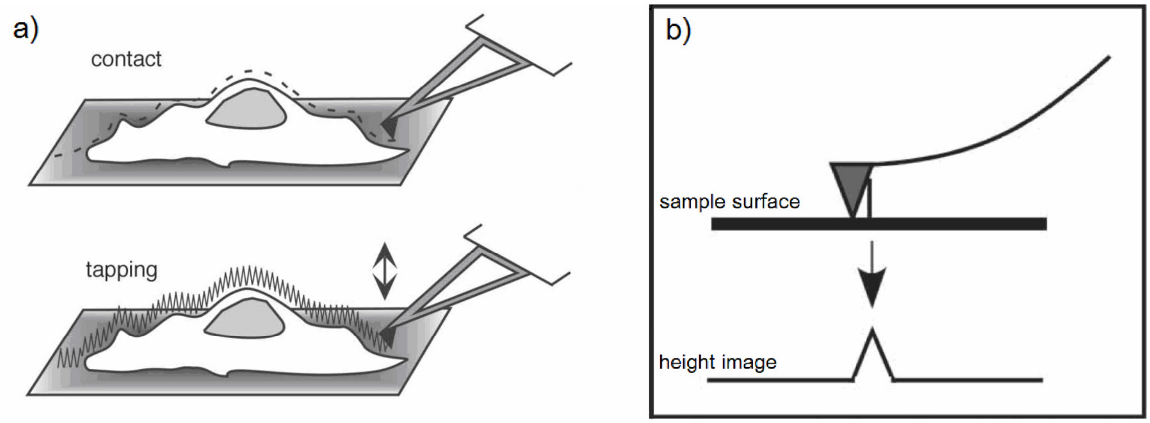

Figure 1-9. Illustration of: a) contact mode and tapping mode of AFM operation; b) the tip contribution to the features imaged.

(Adapted with permission from ref. 32. Copyright 2005 American Chemical Society).

The lateral resolution of an AFM image is determined by two factors: the step size of the image and the radius of the tip. For instance, a 1×1 μm image taken with a 512×512 line precision would have a step size (and lateral resolution) of about 2 nm (1μm ÷ 512 lines). Thus, the tip curvature (which is about 10 nm in our case) is a dominant factor here. The resolution of the z-scale (*i.e.*, normal to the surface) is more accurate (usually, 1 nm or less). One of the fundamental problems in AFM image interpretation is to distinguish features contributed by the tip from true molecular details. Such common effects as "shadowing" or "multiplication", which arise due to a double tip, are easy to recognize, while distinguishing the real lateral dimensions of structures from the height image, which also contains the information about the radius of tip curvature, is usually challenging. Because the sides of the tip can interact with the sample features before the apex of the tip does, resulting in broader images. Figure 1-9b illustrates how a vertical post is imaged as a much broader object due to this effect.[32]

1.3. MATERIALS

The diblock copolymers chosen for the investigations of this thesis are based on polystyrene-*b*-poly(4-vinyl pyridine) (PS-PVP) for two major reasons. One reason is practical, in that a wide variety of these copolymers are commercially available. The second, more fundamental, reason is that the PVP block is a functional block that can be modified by protonation, ionization, coordination chemistry and supramolecular chemistry. This allows additional control on the nanoscopic level, as will be shown below. In addition, when small molecules are incorporated by supramolecular means, they can be removed (*e.g.*, by dissolution) after structure formation, to give nanoporous materials, or they can be substituted with others substances such as metals.

Supramolecular PS-PVP diblock copolymer systems have been well studied in the bulk,[41–60] following extensive studies of supramolecular PVP comb polymer systems.[34,61–68] More recently, some of the same systems have been investigated in the form of thin films prepared by spin-coating. The small molecule most often used in these systems is 3-*n*-pentadecylphenol (PDP). These studies are a good background for further study in the form of ultrathin LB films, focussing mainly on PS-PVP/PDP. In addition, works devoted to LB monolayers of PS-based diblock copolymers and especially to block copolymers of fully quaternized (alkylated) PS-PVP,[77–79,81] which is architecturally similar to PS-PVP/PDP, are particularly relevant to the present research.

Although we used commercially available PS-PVP and PDP, it is worth describing briefly their syntheses.

1.3.1. Synthesis of PS-PVP

PS-PVP diblock copolymers are synthesized by sequential anionic polymerization of the styrene monomer followed by the 4-vinylpyridine monomer using *n*-butyllithium as initiator and tetrahydrofuran (THF) as a solvent (Figure 1-10).[35,36] The polymerization is performed at -78°C under nitrogen, and requires rigorously controlled synthetic conditions, in which air and water vapour must be excluded.[36]

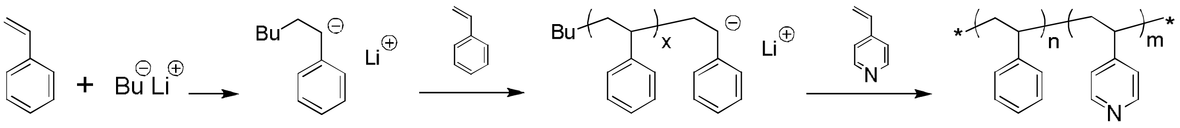

Figure 1-10. Anionic polymerization of PS-PVP.

The reaction is accomplished in an all-glass apparatus that allows the withdrawal of aliquots for characterization. The molecular weight of the PS block is easily determined by gel permeation chromatography (GPC) using monodisperse PS references. The PVP content is estimated by non-aqueous titration with dichloroethane.[36]

1.3.2. Synthesis of PDP

In contrast to long *para*- or 4-alkyl phenols, which are usually obtained by alkylation of phenols with alkenes,[37,38] *meta*- or 3-pentadecylphenol is derived from oil contained in cashew shell, known as cashew nut shell liquid (CNSL).[39]

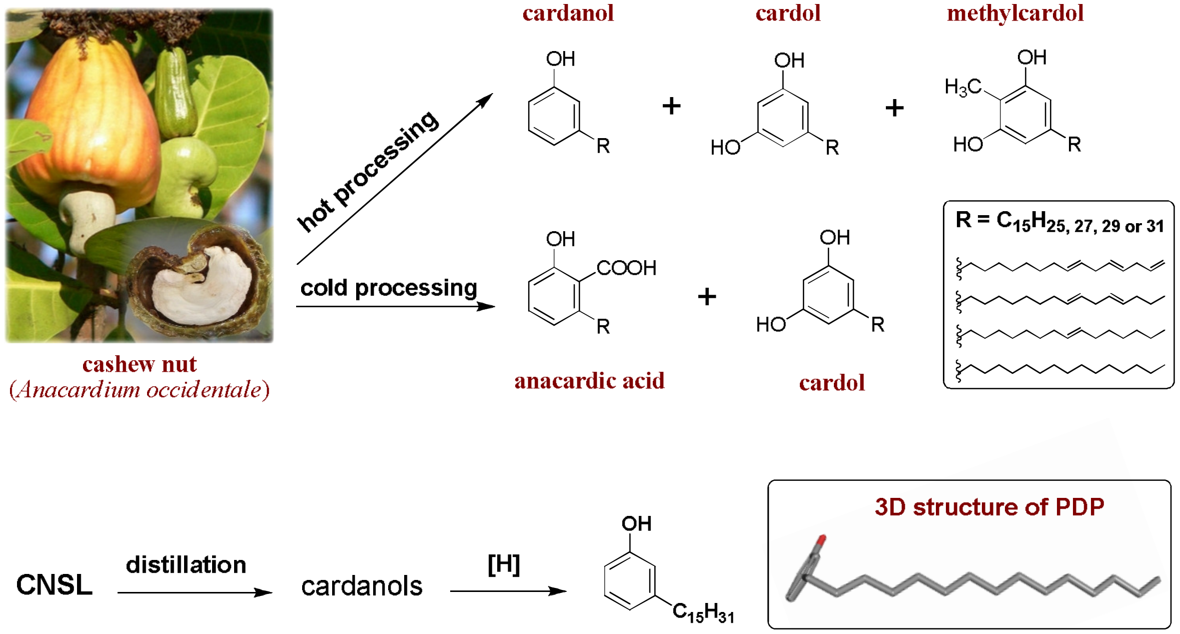

Figure 1-11. Production of CNSL and chemical structures of its major constituents (*top*); and commercial route to obtain PDP (*bottom*).

CNSL is a dark brown, viscous liquid, consisting of a mixture of long-chain alkylphenols and phenolic acids. Being a byproduct of the cashew nut processing industry developed in such countries as India, Tanzania, Brazil, Mozambique, and Kenya,[40] it is widely used in various industries around the world. Depending on the way of processing, two distinct commercial types of CNSL are available (Figure 1-11). Hot-processed CNSL is obtained by oozing out of a shell during roasting of the nuts for kernel separation. In this case, the major components of CNSL are cardanols (60–70%) and cardols (20–25%) with minor quantities of methylcardols. These constituents are separated by distillation.[39,40] Cold-processed CNSL is obtained by extraction of the cashew nut shells with solvents (alcohols). This type of CNSL mainly consists of anacardic acids (60–70%) and cardols (20–25%). These constituents are separated by chromatography, because anacardic acids are thermolabile and decompose to cardanols and CO_2 upon heating.[40]

PDP is obtained by distillation of CNSL under reduced pressure, followed by hydrogenation of unsaturated chains of 3-pentadecadienyl- and 3-pentadecatrienylphenols.

1.4. CURRENT KNOWLEDGE IN THE FIELD

The present work is devoted to the study of PS-PVP diblock copolymers and their supramolecular complexes at the air/water interface. Studies of PS-PVP complexes in the bulk are a good background for making comparisons and sometimes for predicting the type of morphology in thin films. Below, the literature review of PS-PVP in the bulk is summarized, followed by a review of Langmuir and LB monolayers of PS-based diblock copolymers.

1.4.1. Supramolecular PS-PVP Diblock Copolymers in Bulk

Ikkala and ten Brinke and co-workers studied bulk structures of PS-PVP complexed with: 3-*n*-pentadecyl phenol (PDP),[41–46] PDP with methane sulfonic acid (MSA),[43,45,47,48] 4-*n*-nonadecylphenol (NDP),[49] oligo(ethylene oxide) sulfonic acids (EO-SA),[50] 4-dodecylbenzenesulfonic acid (DBSA),[51] zinc dodecylbenzenesulfonate (Zn[DBSA]$_2$),[52] 4-toluenesulfonic acid (TSA),[53] phosphoric acid (H_3PO_4),[54] 4-dodecylphenol (DDP),[55] DDP with poly(2,6-dimethyl-1,4-diphenyl oxide) (PPE),[55] PDP with PPE,[56] fullerene (C_{60}),[57] phenolic resin,[58] and cholesteryl hemisuccinate (CholHS)[59] (Figure 1-12).

The sample preparation was as follows. Generally, the substances were dissolved in chloroform,[41–45,48,51–53,55,56,59] and sometimes in dimethylformamide (DMF),[46,49] tetrahydrofuran (THF),[50,58] dimethyl sulfoxide (DMSO),[54] or xylene[57] to obtain the low concentrated solution (to ensure homogeneous complex formation). Then, the solvent was evaporated very slowly, and the final drying was performed under vacuum for a few days. After that, some samples were annealed,[41,45,46,49,52,57] while others not.[42–44,48,50,51,53–56,59] Annealing step is usually applied to facilitate or accelerate microdomain formation by increasing the mobility of the copolymer molecules resulting in more rapid achievement of the final structure.[2] In thin films, in addition to thermal annealing, solvent vapour treatment is usually applied.[60]

Some experiments required removal of the small molecules after structure formation. To wash out PDP[44] and DDP[55], the material was placed in a dialysis tube and dialyzed against ethanol for 2 weeks. To remove Zn[DBSA]$_2$, the sample was immersed in methanol for 12 h.[52] Thin films of PS-PVP/PDP were prepared by spin-casting from chloroform solution.[60]

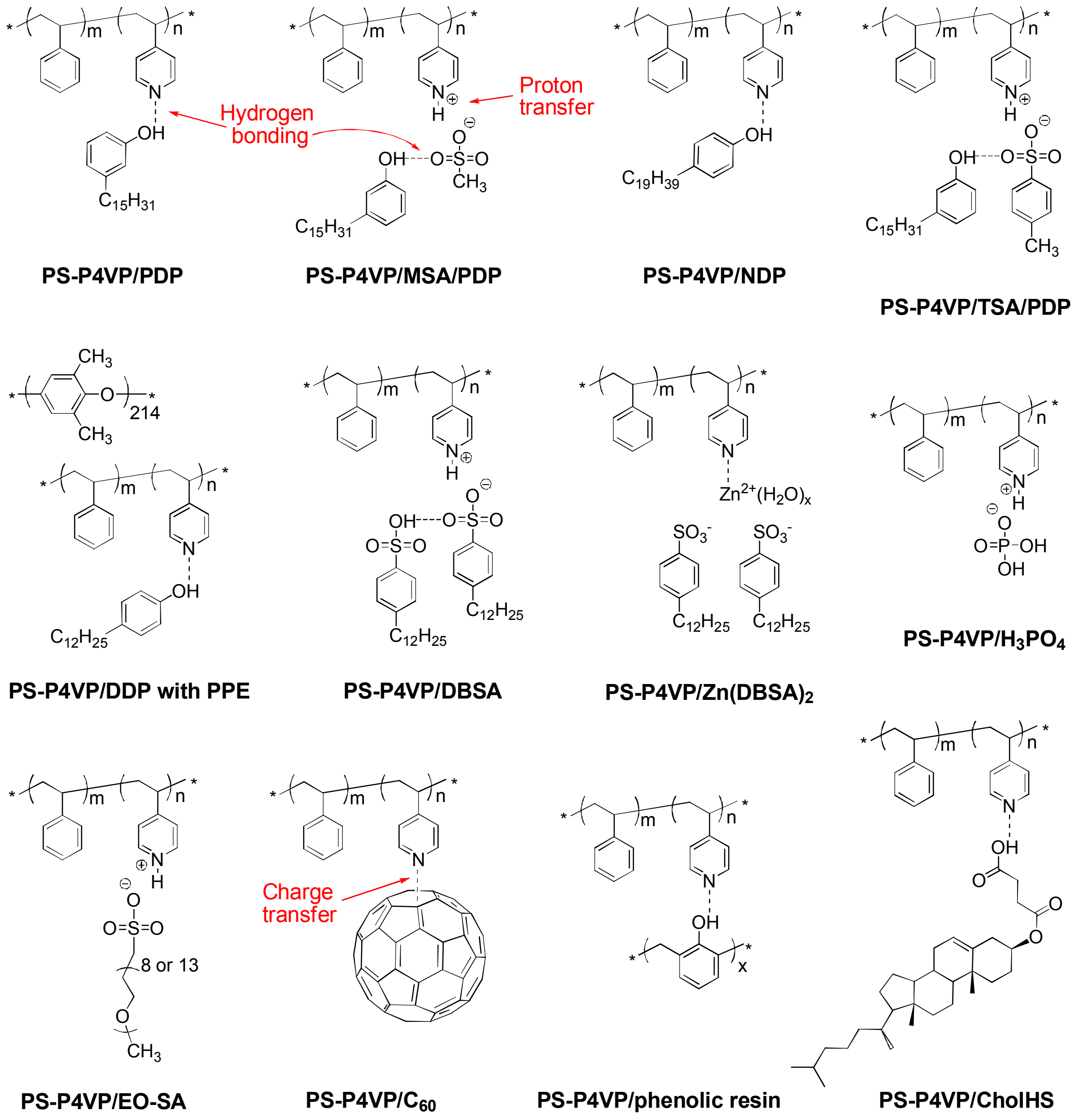

PS-P4VP/PDP

PS-P4VP/MSA/PDP

PS-P4VP/NDP

PS-P4VP/TSA/PDP

PS-P4VP/DDP with PPE

PS-P4VP/DBSA

PS-P4VP/Zn(DBSA)$_2$

PS-P4VP/H_3PO_4

PS-P4VP/EO-SA

PS-P4VP/C_{60}

PS-P4VP/phenolic resin

PS-P4VP/CholHS

Figure 1-12. PS-PVP supramolecular complexes in bulk studied in the literature.[41–68]

1.4.1.1. Confirmation of Supramolecule Formation

In the literature studies, the formation of supramolecular complexes in the above complexes is generally determined by FTIR.

Hydrogen Bonding. Early studies of infrared spectra of pyridine in hydrogen donor solvents (H_2O, D_2O, CH_3OH, C_2H_5OH)[61] demonstrated that changes in the electron distribution of the pyridine ring are observed for pyridine bands at 606, 992, 1438, and 1583 cm^{-1}. Upon formation of hydrogen bonding, these bands shift to higher frequencies 617–618, 1000–1002, 1443, 1593–1595 cm^{-1}, respectively. Later studies of PVP showed similar results: the characteristic absorption bands of free pyridine at 993, 1415, and 1597 cm^{-1} are shifted to 1008, 1421, and 1603 cm^{-1} when it is hydrogen-bonded to PDP,[62] and from 993 to 1003 cm^{-1} when it is hydrogen bonded to NDP. [63] They also showed that, at low temperatures, most of the alkylphenols are hydrogen-bonded to pyridine groups until the alkyl tail length exceeds *ca.* 23 methylene units where macrophase separation takes place (perhaps due to higher driving force for crystallisation).[50] At temperatures higher than *ca.* 120°C, considerable decoupling is observed.[63] It was also noted that the fraction of free pyridine groups in PVP/NDP is larger than in PVP/PDP, which is explained by higher repulsion between longer alkyl tails.[63] It is also worth noting that full complexation of dodecanoic acid with PVP is not achieved, as shown by FTIR, SAXS and WAXS data.[64]

Proton Transfer. When PVP is protonated using strong acids (EO-SA,[50] DBSA,[51] TSA,[53] H_3PO_4[54]), the stretching band of PVP at 1597 cm^{-1} shifts to 1637–1639 cm^{-1}. In the case of PVP and DBSA, both protonation and strong hydrogen bonding may take place. The presence of a shoulder at *ca.* 1620 cm^{-1} when the degree of complexation is equimolar is considered to be an indication of hydrogen bonding between DBSA and PVP.[51] In the presence of two DBSA molecules per VP unit, the shoulder is reduced suggesting that the equilibrium shifts towards protonation.[51] The complexation of PDP to the sulfonates of PS-PVP/TSA is not evident by FTIR due to the complicated spectra of sulfonate bands near 1200–1300 cm^{-1}.[53] In this case, hydrogen bonding between TSA and PDP is inferred indirectly from SAXS.

Metal Coordination and Charge-Transfer Complexation. Coordination of Zn^{2+} to PVP was shown by the shift of the pyridine band at 1597 cm^{-1} to 1619 cm^{-1} due to metal–ligand π-bonding.[52] Complexation between PS-PVP and C_{60} is shown by the decrease in intensity of the pyridine band at 993 cm^{-1} and the appearance of a new band at 1003 cm^{-1}.[57] In this case, however, only a fraction of the pyridine units interacts with C_{60}, and only upon aging in solution as C_{60} molecules slowly penetrate into the micellar cores of PS-PVP to form charge-transfer complexes.

1.4.1.2. Role of Small Molecules and Influence of Polymer Composition on Morphology

In contrast to classical diblock copolymers, where the ratio between blocks is fixed by synthesis, the relative weight fractions[**] in supramolecular complexes can be easily tuned by the addition of the block-selective small molecules. Using PS-PVP/PDP_x [M_n(PS)=40,000; M_n(PVP)=5,600; x denotes the molar ratio of phenol to pyridine units], Ruokolainen *et al.*[41] demonstrated that for a pure block copolymer that gives a spherical morphology, complexation with PDP can produce cylindrical or lamellar structures, depending on the amount of PDP added. This is consistent with a change in weight fraction of the comb block ($wt_{(PVP/PDP)}\%$) that varied from 12 % ($x = 0$) to 26 % ($x = 0.5$) to 35 % ($x = 1.0$). The phase diagram for PS-PVP/$PDP_{1.0}$ shows a transition from spherical to cylindrical morphology at 22 $wt_{(PVP/PDP)}\%$, from cylindrical to lamellar at 32 $wt_{(PVP/PDP)}\%$, then there is an extended range of PS cylindrical structure for 54–82 $wt_{(PVP/PDP)}\%$, followed by a PS spherical morphology.[41]

Furthermore, the effect of temperature on the phase diagram is more complex for PS-PVP/PDP than for PS-PVP. Because the extent of hydrogen-bonding between the PVP block and PDP depends on temperature (T),[65–67] heating results in several transitions:

[**] Weight fraction rather than volume fraction is used for simplicity. The densities of the two phases are only slightly different: 1.047 g/cm^3 for PS (literature value) and 0.98 g/cm^3 for PVP/$PDP_{1.0}$ (measured value).[41]

structures that were organized at 25°C exhibit an order–disorder transition within the comb block at *ca.* 60°C, followed by other ordered block copolymer structures at higher temperatures. In particular, cylindrical and lamellar structures, typically formed at room temperature, change to spheres and/or cylinders, respectively, at *ca.* 170°C, respectively, and both turn into spheres at *ca.* 210°C.[45] At room temperature, PVP is hydrogen bonded to PDP; but upon heating, the hydrogen bond gradually breaks. Thus, at T > 120°C, PDP becomes soluble in both PS and PVP (Figure 1-13) and, at T > 175°C, PDP dissolves selectively in PS only. Thus the effective volume of PS-containing domains increases.[45] The phase sequence is reversed on cooling. This thermoreversibility may lead to new types of responsive materials, since structural transitions are usually not accessible by temperature changes in the Flory-Huggins interaction parameter, χ.[45]

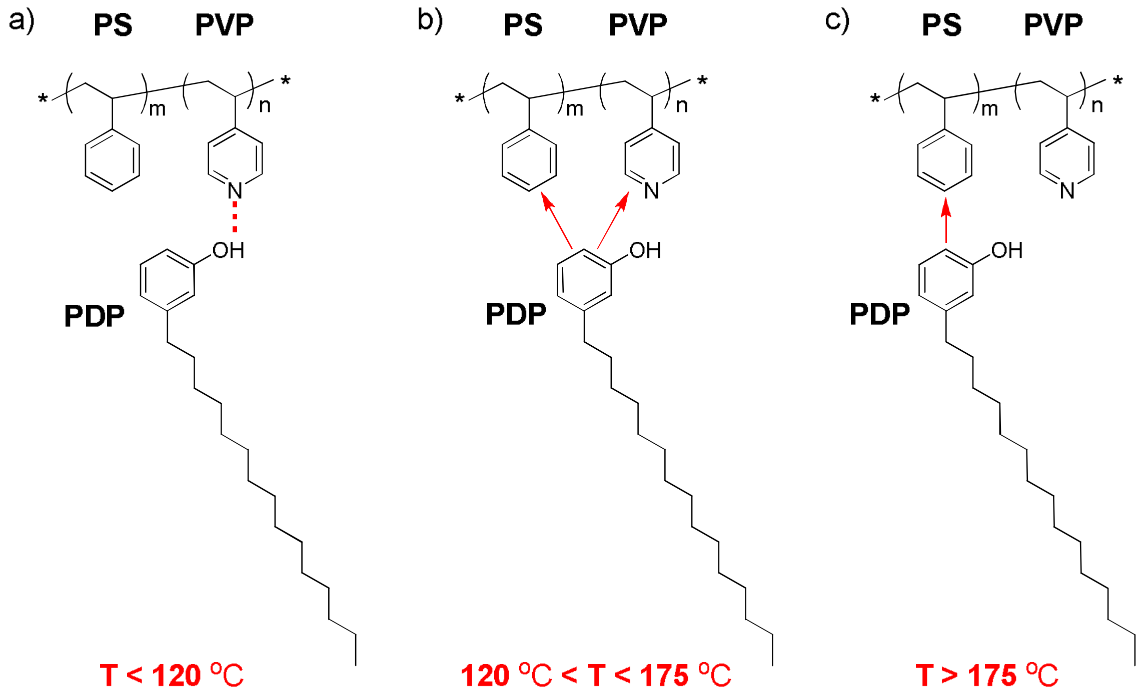

Figure 1-13. Interaction of PDP with PS-PVP at various temperatures: a) at room temperature, PDP is hydrogen-bonded to PVP; b) upon heating, the hydrogen bond is broken, and at temperatures between *ca.* 120 and 175 °C, PDP is soluble in both PVP and PS domains; c) at higher temperatures, PDP is expelled from PVP and is miscible in PS only.[45]

1.4.1.3. Structure-Within-Structure

Early work on homopolymer complexes of PVP/PDP[67] and PVP/NDP[68] showed that repulsion between the polar backbone and the nonpolar alkyl tails is sufficient for nanophase separation resulting in a liquid crystalline lamellar structure (Figure 1-14) with a periodicity of *ca.* 4 nm,[45,68] as determined by small-angle X-ray scattering (SAXS) and transmission electron microscopy (TEM). It was also noted that this structure was observed only when the linear alkyl chains were composed of 12–23 carbons. For shorter alkyl tails the system remains disordered (isotropic), whereas for longer tails there is macroscopic phase separation with crystallisation of the small molecules.[45]

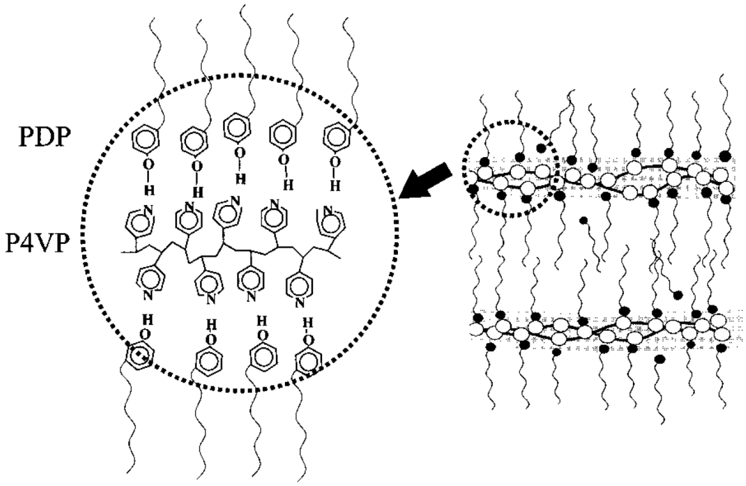

Figure 1-14. Schematic illustration of the PVP/PDP lamellar structure. (Reproduced with permission from ref. 67. Copyright 1997 American Chemical Society).

Similarly, modification of block copolymers by complexation with surfactants or mesogens leads to self-assembly within the complexed block. This results in the formation of a substructure within the block copolymer structure, or a morphology with two length scales.[45,65] For example, the main (longer length scale) morphology of PS-PVP/PDP$_{1.0}$ with M_n(PS) = 34,000 and M_n(PVP) = 2,900 ($f_{(PVP/PDP)}$ = 25 wt%) is hexagonally assembled PVP/PDP cylinders within a PS matrix, with a periodicity of 24 nm (determined by SAXS). Within the cylinders, there is a (shorter length scale) lamellar structure with a periodicity of *ca.* 3.7 nm.[65] This morphology is termed a lamellar-within-cylindrical structure. Similarly, a lamellar-within-spherical morphology is formed in PS-PVP/NDP$_{1.0}$ with $f_{(PVP/NDP)}$ = *ca.* 20 wt%.[49] If the weight fraction of the comb block is much higher and the coil block forms the minority phase, the morphology is reversed. Here, PS cylinders or PS spherical domains are embedded in a lamellar matrix, called cylindrical-within-lamellar or spherical-within-lamellar matrix morphology, respectively.[49] If the weight fractions of the coil and comb blocks are similar, the long lengthscale morphology is lamellar, with the PVP domains containing an internal lamellar structure of alternating small molecules and PVP layers, giving the lamellar-within-lamellar structure. In these morphologies, the long period is controlled by the molecular weight of the block copolymer, and the short period depends on the length of the small molecule. Examples of the periodicities associated with the latter morphology are summarized in Table 1-1.

Table 1-1. Periodicities in lamellar-within-lamellar structures of coil–comb complexes.

Sample	Molecular weight, g/mol		Fraction of comb block PVP/small molecule		Periodicity, nm	
	M$_n$(PS)	M$_n$(PVP)	mol %	wt %	long length scale	short length scale
PS-PVP/NDP$_{1.0}$ [42]	238,100	49,500	17	48	90	4.5
PS-PVP/DBSA$_{1.0}$ [51]	238,100	49,500	17	46	97	3
PS-PVP/DBSA$_{1.5}$ [51]	238,100	49,500	17	54	130	3
PS-PVP/DBSA$_{2.0}$ [51]	238,100	49,500	17	60	140	3
PS-PVP/[Zn/DBSA$_{2.0}$]$_{0.9}$ [52]	238,100	49,500	17	60	110	> 3
PS-PVP/[Zn/DBSA$_{2.0}$]$_{0.8}$ [52]	41,400	1,900	4	23	27	5
PS-PVP/[Zn/DBSA$_{2.0}$]$_{0.6}$ [52]	41,400	1,900	4	19	22	5
PS-PVP/MSA$_{1.0}$/PDP$_{1.0}$ [47]	40,000	5,600	12	40	35	4.8
PS-PVP/(H$_3$PO$_4$)$_{2.2}$ [54]	35,500	3,600	9	9	45	n/a

In Table 1-1, the sequence involving PS-PVP/DBSA$_x$ is noteworthy. It is observed that its short period is invariable (here, the lamellar structure was assumed but could not be confirmed[48]), whereas the long period ranges from 97 to 140 nm.[51] In comparison, pure PS-

PVP has a periodicity of *ca*. 70 nm (its structure could not be determined due to the lack of higher order peaks in X-ray scattering) and pure DBSA is an isotropic fluid, with a scattering vector corresponding to 2 nm. The change in long period and the constant short period suggest that the PVP chains have to stretch further for $x \geq 1.0$.[51]

The structures of the PS-PVP supramolecular complexes described in ref. 41–68 are summarized in the Appendix to Chapter 1 (Table 1-2). Their morphologies as a function of total molecular weight and weight percent of the comb block are combined in Figure 1-15. The overall trend in morphology evolution with weight fraction is as expected. However, there is morphological overlap for the different systems, suggesting that the type of small molecule used has some influence on the longer length-scale morphology.

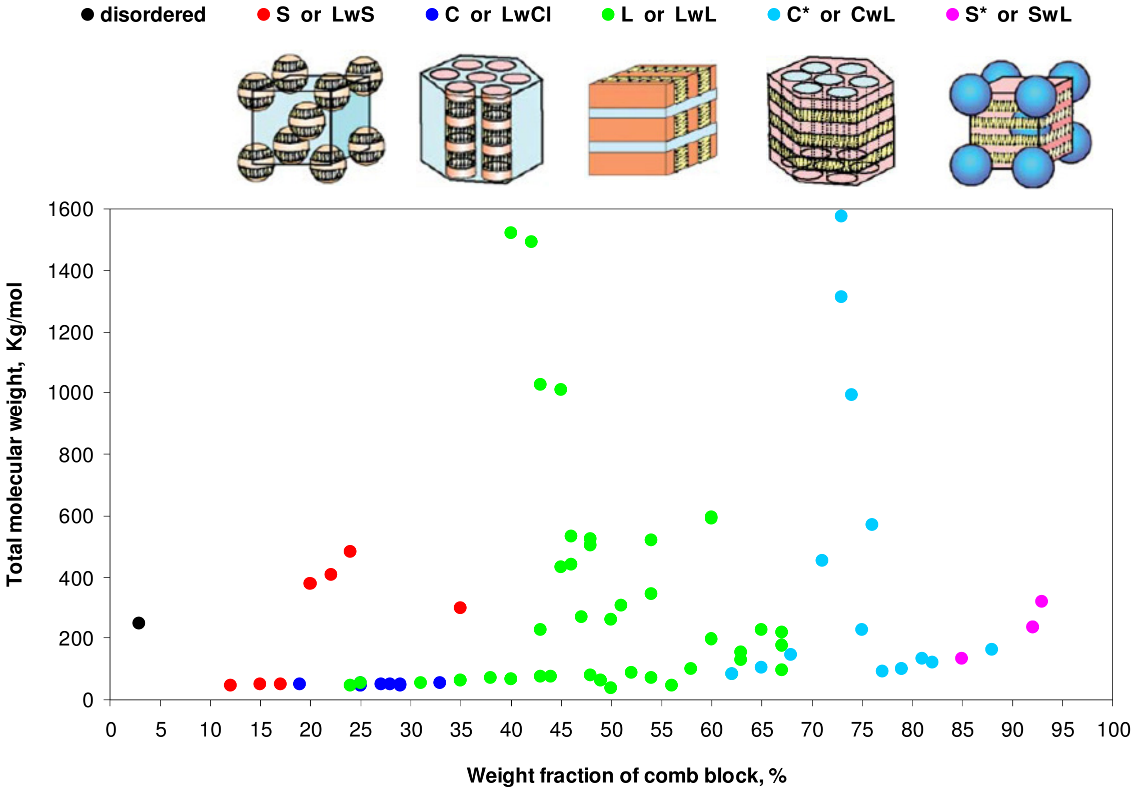

Figure 1-15. Morphology diagram of PS-PVP, complexed with the various molecules listed in the Appendix (Table 1-2), giving the total molecular weight of the complex *vs*. the weight fraction of the comb block, at room temperature. (The top image is adapted from ref. 65).

1.4.2. Diblock Copolymers in Thin Films

The morphology of thin block copolymer films is strongly affected by the vicinity of the interface.[69] Due to differences in interfacial energies, a particular block generally tends to preferentially wet each interface (typically substrate and air), resulting in parallel orientation of microdomains.[60,70] Only neutral surfaces (obtained, *e.g.*, by grafting a random copolymer onto a substrate) encourage the presence of both blocks at the surface allowing the assembly of perpendicular lamellae and cylinders.[2,70] To facilitate the molecular mobility and reach the equilibrium structure in thin films, thermal or (more often) solvent vapour annealing is usually applied.

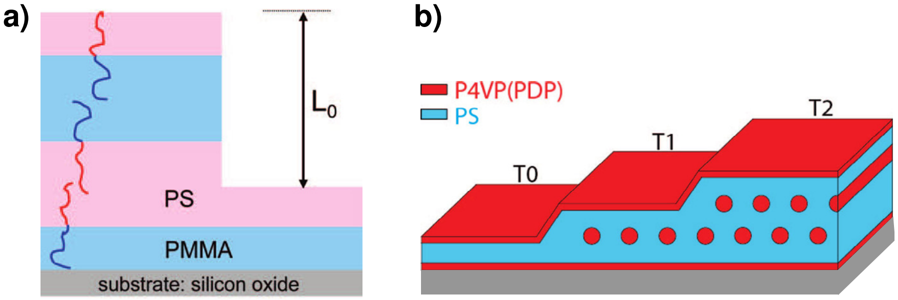

Figure 1-16. Schematic representation of ordered thin films:
a) PS-PMMA lamellae on a selective surface; b) terraces of PS-PVP/PDP cylindrical domains.
(Adapted with permission from refs. 2, 60. Copyright 2008, 2010 American Chemical Society).

Figure 1-16 schematically illustrates the molecular orientation of diblock copolymer thin films on a selective substrate. In particular, when a solution of symmetric PS-PMMA is spin-cast on silicon oxide (SiO_2), the polar PMMA block first covers the hydrophilic substrate and nonpolar PS is exposed to the air (Figure 1-16a).[69,71] Lamellae, formed in this case, orient parallel to the substrate and tend to form a film of thickness equal to an integral value of the lamellar periodicity, L_0.[69] If the film thickness is incommensurate with the structure period, terraces are formed, as illustrated for a PS-PVP/PDP system in Figure 1-16b.[60,72] The orientation within the terraces can vary as the film thickness and substrate roughness are other factors influencing the film morphology.[60] The case of ultrathin films, which are characterized by a thickness comparable to or less than half the L_0 period,[2] is which are characterized by a thickness comparable to or less than half the L_0 period,[2] is different; their structure is essentially surface-induced,[73] resembling the conditions of block copolymers at the air/water interface (discussed further in Chapter 3).

1.4.3. Diblock Copolymers at the Air/Water Interface

The first block copolymers that were extensively investigated at the air/water interface are based on PS-PVP, where the PVP block is quaternized with alkyl groups (PS-PVP$^+$RX$^-$, Figure 1-17).[74,77–82] Other diblock copolymers investigated in a fair amount of detail are also shown in Figure 1-17. Their LB films morphologies are summarized in the Appendix (Tables 1-3 and 1-4).

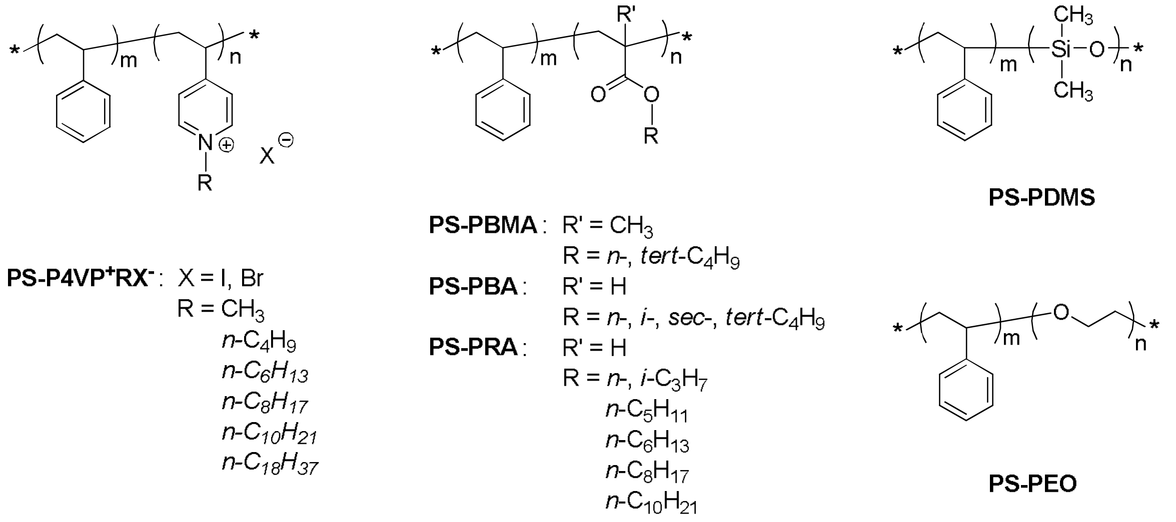

Figure 1-17. Diblock copolymers investigated at the air/water interface in refs. 77–93.

The general sequence of morphologies observed as a function of block composition is illustrated in Figure 1-18. When the hydrophilic block is sufficiently long, surface micelles (“nanodots”) are always observed. With decreasing hydrophilic block length, rod-like and then planar morphologies appear. These 2D morphologies – “starfish”, rod, and planar aggregates – were considered by Eisenberg, Lennox and co-workers to be analogous to the 3D spherical, cylindrical, and lamellar morphologies, respectively.[74] They showed that each below 6 mol% PVP, rod-like structures within the 6–14 mol% PVP range, and starfish morphology above 14 mol% PVP (Appendix, Table 1-3).[74] These are further detailed in the following two sections. It should be noted it is generally assumed that LB monolayers have the same structure as films on the water surface before transfer.[78] This is experimentally supported by the excellent agreement between micelle–micelle distances measured for LB films (imaged by AFM) and *in-situ* synchrotron X-ray reflectivity data of Langmuir films on the water surface.[75]

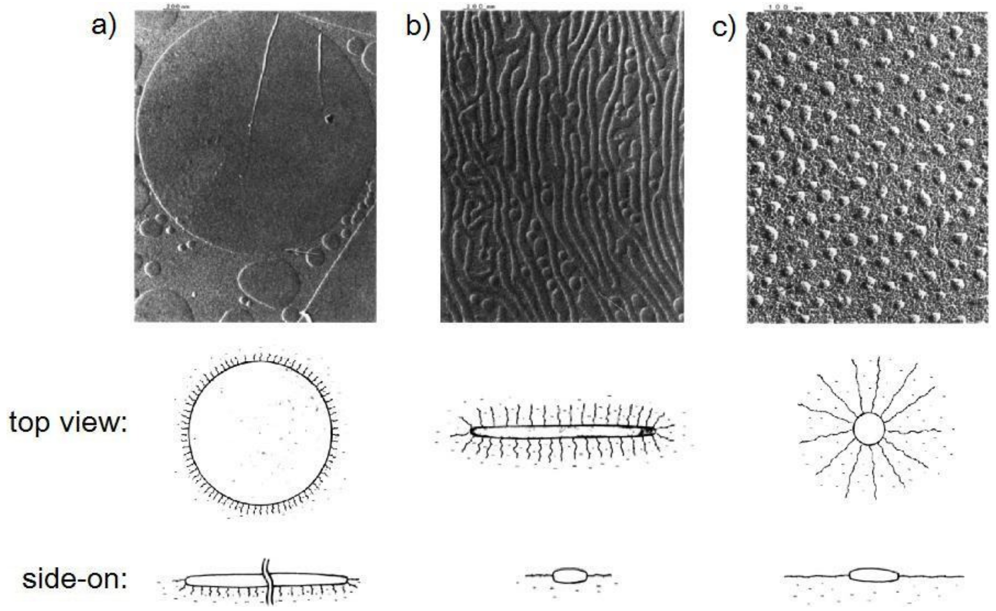

Figure 1-18. TEM images and schematic representations of LB films of PS-PVP$^+$RX$^-$ (where RX$^-$ is $C_{10}H_{21}I^-$): a) planar, b) rod, c) "starfish" structures. (Reproduced with permission from ref. 74. Copyright 1992 American Chemical Society).

1.4.3.1. PS-PVP$^+$RX$^-$ Diblock Polyelectrolytes

<u>*Surface Micelles (Nanodots).*</u>

The vast majority of LB block copolymer films investigated, as also shown in Figure 1-17, have PS as the hydrophobic block. In this connection, the more than two-decade-old study of Kumaki on the Langmuir monolayers and LB films of PS monomolecular particles[76] is highly pertinent. The monomolecular particles (forming isolated unimer surface micelles) were obtained by spreading very dilute solutions of PS. Using PS of many different molecular weights, Kumaki demonstrated that the limiting area (A_{lim}, expressed as Å^2/molecule, obtained by extrapolation of the isotherm to zero surface pressure) is proportional to the molecular weight of PS (M) according to the following expression:

$$\boldsymbol{A_{lim} = 0.04\ M}$$

This equation has been used by various researchers in the analysis of block copolymer isotherms and LB films. For example, Eisenberg, Lennox and co-workers used the Kumaki equation to estimate the area occupied by the hydrophilic block of PS-PVP$^+$RX$^-$ on the water surface.[77] An early picture of surface micelles for PS-PVP$^+$RX$^-$ LB films is shown in Figure 1-19. It was assumed that, when spread, hydrophobic PS immediately takes on a conformation that minimizes its contact area with the water surface, while the hydrophilic block maximizes its contact area. Thus, the aggregates consist of a core of PS blocks and a corona of highly extended vinylpyridinium arms.[78] When the barriers are compressed, this morphology shows a Langmuir isotherm with a plateau (Figure 1-20), indicative of a transition. This was related to a change in the PVP conformation, assuming that the area occupied by PS remains constant. Specifically, the authors proposed that the plateau corresponds to a “starfish → jellyfish” transition, *i.e.* the transformation from 2D into quasi-2D micelles (Figure 1-19). In this transition, barrier compression causes the surface-adsorbed PVP$^+$RX$^-$ blocks (“starfish”), to become submerged in the water subphase (“jellyfish”).[79] The longer the alkyl chain, the greater the energy required for submersion of the PVP$^+$RX$^-$ block into the subphase. This is observed as an increase in the isotherm plateau pressure with increase in alkyl chain length.[75] In fact, PVP$^+$CH$_3$I$^-$ is actually submerged into water even at low surface pressure, being almost perpendicular to the interface.[78] It was also observed that the plateau pressure and limiting area decrease with increasing temperature. This was explained by the increase in water solubility of vinylpyridinium chains at higher temperature, and the correspondingly fewer VP chains submerged in water at lower temperature.[77] The plateau of isotherm was also affected by the total compression time: the slower compression rate, the lower the surface pressure at which the phase transition begins.[79] Therefore, compression/expansion pressure–area isotherms of PS-PVP$^+$RX$^-$ block polyelectrolytes exhibit hysteresis phenomena if the expansion begins after the first-order transition, and no hysteresis if films expansion is initiated before. This indicates that not only chain submersion requires higher energy, but also that chain reorganization is a kinetically slow process.[79]

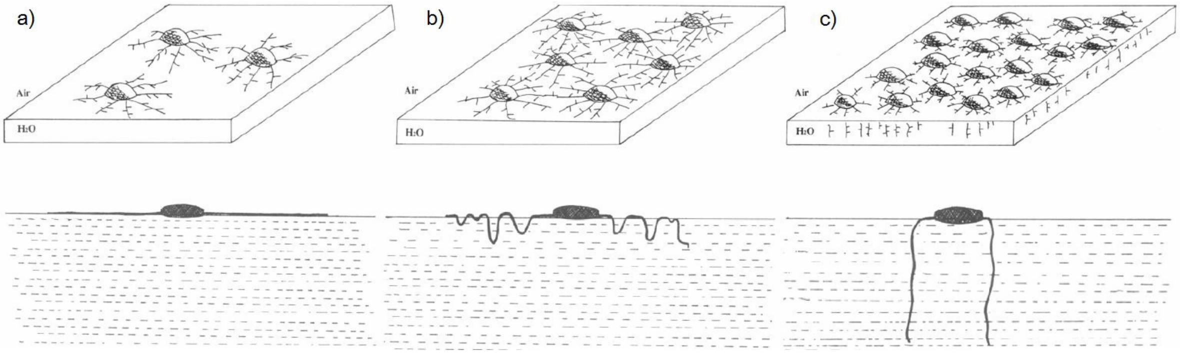

Figure 1-19. Schematic representation of micelle transformation: a) "starfish", b) partially formed "jellyfish", c) "jellyfish". (Adapted with permission from refs. 77 and 78. Copyright 1991, 1992 American Chemical Society).

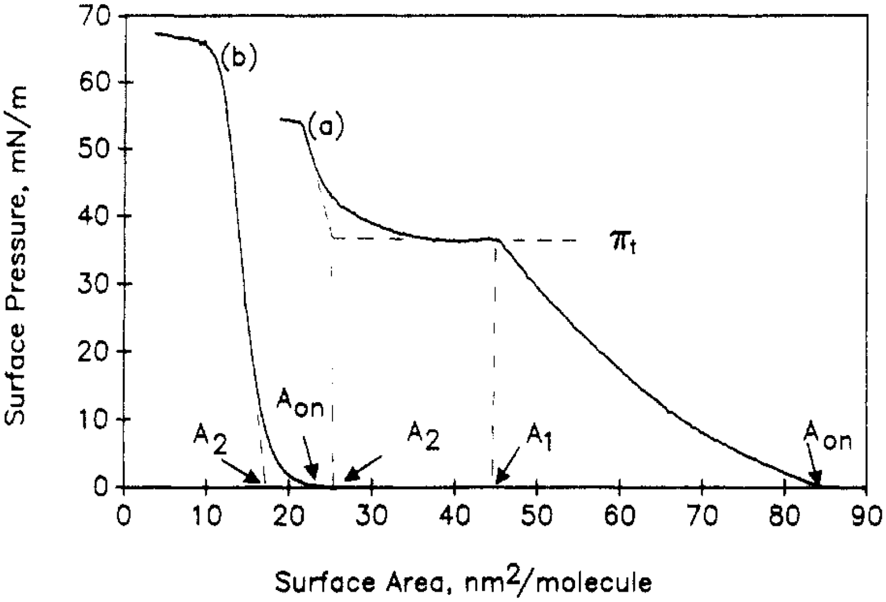

Figure 1-20. Representation of isotherm parameters in Langmuir compression isotherm exhibiting: (a) a plateau, (b) only a monotonic increase. π_t is the surface pressure of the phase transition, A_{on} is the onset area, A_1 is the onset of the transition, and A_2 is the limiting area. (Adapted with permission from ref. 79. Copyright 1991 American Chemical Society).

However, subsequent work argued against the “starfish → jellyfish” transition model. Using *in-situ* FTIR, it was detected that long alkyl chains ($C_{10}H_{21}Br$ and $C_{18}H_{37}Br$) adopt a trans conformation during compression, while short alkyl chain (C_4H_9I) show no ordering.[80] The trans conformation of side chains was established based on the shift of the asymmetric and symmetric CH_2 stretching vibrations from 2924 and 2854 cm^{-1} (for gauche conformation) to 2921 and 2852 cm^{-1} (for trans conformation) for PS_{260}-$PVP_{240}{}^{+}(C_{18}H_{37}Br^{-})_{240}$, and in the same way from 2927 and 2858 cm^{-1} to 2926 and 2857 cm^{-1} for PS_{260}-$PVP_{240}{}^{+}(C_{10}H_{21}Br^{-})_{240}$.[80] In addition, *in-situ* X-Ray and neutron reflectivity showed that the adsorbed monolayer shows no significant thickening at the level of the counterions with compression. In other words, there is no immersion of the polyvinylpyridinium block into the water subphase (except for the short alkyl chains), but the ionic PVP^{+} remains adsorbed on the water surface throughout compression. Instead, the transition in the pressure–area isotherm is due to ordering of the alkyl chains.[80] In contrast, addition of 1–5 vol % *n*-butanol into the water subphase results in a perceptible increase of the corona thickness during film compression, indicating that, under these conditions, the ionic arms can immerse into the subphase.[80]

As in all aggregation phenomena, the aggregation number is of interest. Eisenberg and co-workers presented five independent methods for calculating the aggregation number of the block polyelectrolyte surface “starfish” micelles: stoichiometric method, occupied area method, PS volume method, PS area method, and circumference method.[81] All the methods are independent, though the assumption of distortionless transfer is applied to all methods presented. A comparison of the aggregation numbers of ionic and non-ionic diblock copolymers (*e.g.*, PS-$PVP^{+}RX^{-}$ and PS-PBMA) showed larger values for non-ionic cases, which is explained by electrostatic repulsion between the ionic chains forming the corona, and thus resulting in smaller PS core aggregation.[82] All of the calculation methods gave similar aggregation numbers; however they can be applied only to the circular (“starfish”) morphology, and cannot be used for estimation of the aggregation numbers of other structures.

Other Morphologies.

The structural features of the rod micelles are less clear than the "starfish" morphology, described above.[74] Initially, two possibilities of orientation of the ionic arms on the water surface were considered: they either surround the rod formed by PS or are underneath it. An argument in favour of emerging PVP^+RX^- chains along the air/water interface laterally to the rods is that the closest distance between rods is approximately equal to double the length of the polyvinylpyridinium chains.[74] The width of the rods is about twice as large as the unperturbed PS coil dimensions, which implies high extension of the PS chains in the aggregates.[74] When the ionic arms are very short, they emerge along the underside of the planar aggregates formed by the PS. For all morphologies, the height of the micelles (measured most frequently on "starfish" morphology) depends on the length of PS block, and is roughly the thickness of one collapsed PS random coil.[74]

1.4.3.2. Non-Ionic Diblock Copolymers

PS-PBMA, PS-PBA, and PS-PDMS.

LB films of non-ionic diblock copolymer were observed to exhibit 2D "starfish", rod and planar morphologies, depending on relative block lengths, similarly to the PS-PVP^+RX^- diblock polyelectrolytes. This indicates the generality of the surface micellization phenomenon.[82] The first results for well defined non-ionic diblock copolymer structures were obtained using copolymers with PS as the hydrophobic block and poly(*n*- or *tert*-butyl methacrylate), poly(*tert*-butyl acrylate), or poly(dimethylsiloxane) (PS-PBMA, PS-PBA, PS-PDMS, respectively) as the hydrophilic (polar but non-ionic) block.[82] For instance, decreasing the fraction of the *n*- or *tert*-PBMA block in PS-PBMA from 204–114 to 53 repeat units (for 260 repeat units of PS) leads to a change from nanodot aggregates to rods, followed by large planar lamellae observed for copolymers with 25–18 PBMA repeat units.[83]

Surface pressure–area isotherms of PS-PBMA and PS-PBA with relatively long PBMA and PBA blocks display one or more reversible plateau regions, which were explained as the reorientation of butyl acrylate chains at low surface pressure, and their folding over one another at higher pressure.[82] Temperature experiments enabled an estimation of the thermodynamic parameters of the phase transition, using the 2D Clausius-Clapeyron equation:[83]

$$\Delta H = T\Delta A_t\left(\frac{d\pi_t}{dT} - \frac{d\gamma_0}{dT}\right) = T\Delta S$$

where ΔH is the enthalpy, ΔA_t is the difference in areas between the parallel prone and perpendicular orientations of the BMA chains, $d\gamma_0/dT$ is the rate of change of the pure water surface tension with temperature, π_t is the surface pressure of the phase transition at temperature T, and ΔS is the entropy. Positive and very small (much smaller than for ionic PS-PVP$^+$C$_{10}$H$_{21}$I$^-$) ΔS values for the non-ionic PS-PBMA suggested that the degree of order in the compressed film is similar to that in the "as-cast" film, and no reorganization in the corona chains takes place. It was concluded that the transition occurs due to reorientation of alkyl acrylate at the surface, from a horizontal to a vertical alignment.[83]

A series of experiments on PS-PRA (R = C$_3$–C$_{10}$, Figure 1-17) diblocks with various lengths and structure of side groups of alkyl acrylate block showed that the first transition has a strong relation with isomerization, which, however, has a negligible effect on the second and third transitions, whereas the number of phase transitions depends on the side group length.[84] Specifically, the compression isotherm of PS-poly(propyl acrylate) exhibits only one, low surface pressure, transition, which is absent for PS-poly(octyl acrylate) and PS-poly(decyl acrylate), while isotherms of PS-PBA, PS-poly(pentyl acrylate) and PS-poly(hexyl acrylate) have three transitions (the length of the PRA block is constant, 222 units); the first transition occurs at lower surface pressures for n-alkyls and at higher pressures for branched side groups (PS-P*n*BA < PS-P*i*BA < PS-P*sec*BA < PS-P*tert*BA).[84]

PS-PEO diblock copolymers.

LB films of PS-PEO diblock copolymers have been studied by a number of groups.[85–96] Lennox and co-workers first showed that they have the same general morphology dependence on relative block fractions as the above copolymers.[85]

Many groups consider that the PEO block submerges into the subphase upon barrier compression, as shown in Figure 1-21. This is frequently termed the "pancake → brush" transition, but which might better be termed the “starfish → jellyfish” transition in the Lennox-Eisenberg terminology (to avoid confusion with the term “pancake conformation” sometimes used for the planar morphology). However, no confirmatory evidence of the lateral dimensions of the film structure is available.[85]

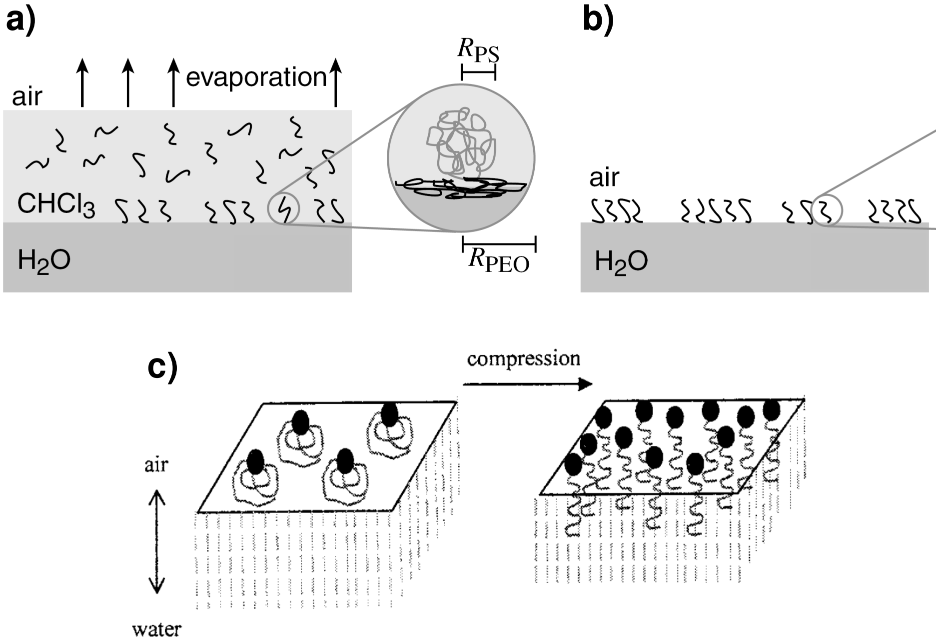

Figure 1-21. *Top*: deposition of PS-PEO on the water surface (a), and polymer film after solvent evaporation (b). *Bottom*: reorganization of PS-PEO molecules on compression (c). (Adapted with permission from refs. 85, 86. Copyright 1999, 2005 American Chemical Society).

The mechanism of surface aggregation has been a subject of controversy. Lennox and co-workers reviewed three different versions of surface aggregate formation of the surface micelle morphology,[85,87] schematically depicted in Figure 1-22. In the first, micelles with PS cores are considered to be present in the spreading solvent before deposition. In the second, they are considered to form as a result of increased surface pressure. The third postulates spontaneous aggregation on the water surface. The first possibility was eliminated by the demonstration that the use of chloroform, which is a good solvent for both blocks, and toluene, which is highly selective for PS, result in the same film morphology.[85] The second possibility was eliminated by the similar results obtained for LB films deposited at $\pi = 0$ and $\pi > 0$, indicating that PS-PEO aggregates are not compression-induced.[85] Therefore, it was concluded that spontaneous surface aggregation is the most likely mechanism for surface micelle formation.

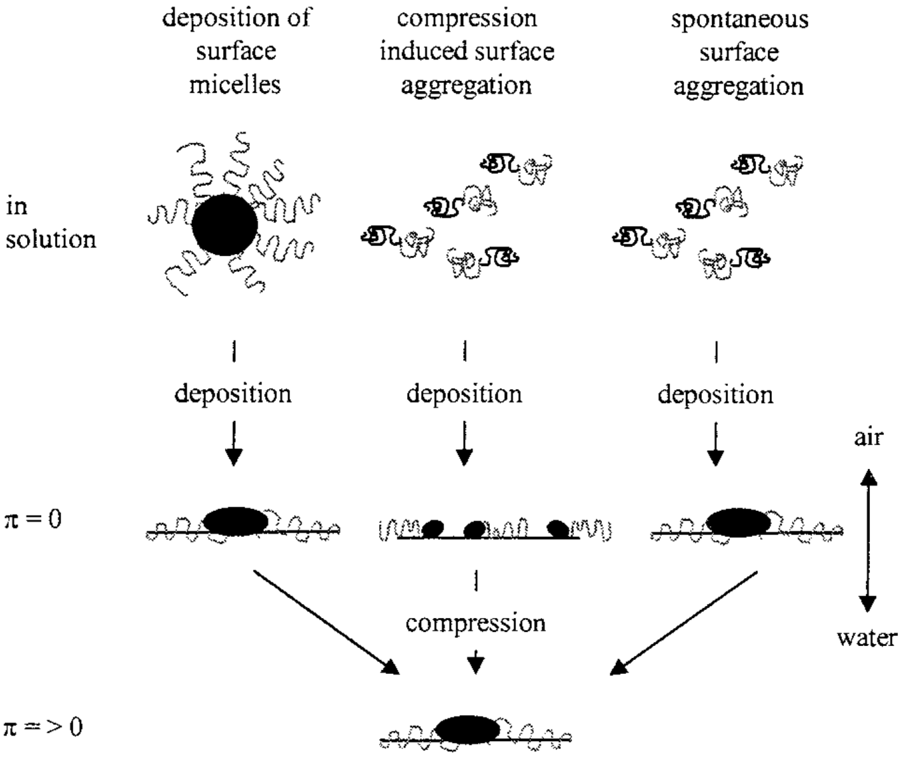

Figure 1-22. Mechanisms of surface micelle formation.
(Reproduced with permission from ref. 85. Copyright 1999 American Chemical Society).

An extension to the third mechanism of 2D structure formation was proposed recently by Moffitt and coll., and is based on the idea of dewetting.[88] This idea considers that a spread drop forms a uniform film of polymer solution, that is subject to rupture due to solvent evaporation and film spreading on the water surface (Figure 1-23). In support of this theory, it was shown that nanoscale aggregates (strands, network, and continents) can also be generated by PS homopolymers of high molecular weight (405,000 g/mol).[89] However, it was found that the presence of a short (2 wt%) PEO block increases the dimensions of well-defined structures, and decreases the polydispersity of the specific surface features.[89]

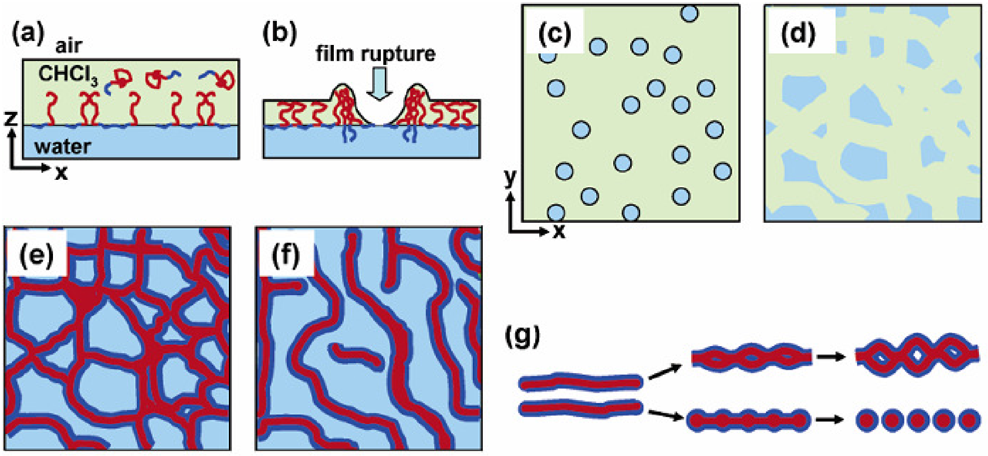

Figure 1-23. Dewetting mechanism: a) formation of a continuous monolayer of a PS(red)-PEO(blue) solution at the air/water interface; b,c) hole formation in various regions of the film as chloroform evaporates; d) growth of holes; e,f) freezing of structure once $CHCl_3$ evaporates completely; g) evolution of spaghetti morphology into chainlike aggregates or dots. (Reproduced with permission from ref. 88. Copyright 2006 American Chemical Society).

The dewetting mechanism was initially proposed in view of the coexistence of different morphological forms.[88] Devereaux and Baker comprehensively studied the relationship of PS-PEO (wt_{PEO} = 7%) morphologies and experimental parameters. For quantitative analysis, they classified the 2D surface micelles observed as follows: *dots*, which are the circular features of less than 300 nm in diameter and have an aspect ratio of 3:1 or less; *spaghetti*, which are features of width less than 150–200 nm and have an aspect ratio of more than 3:1; and *continents*, which are larger than above features and of tremendous variation in size.[90] (Dots, spaghetti, and continents correspond to “starfish” or circular, rod or ribbon, and planar or lamellar structures, respectively). The analysis showed that, although the three types of morphologies are generally present under all experimental conditions investigated, the dot morphology was more dominant for low solution concentrations and continents for high solution concentrations, whereas the surface pressure and compression speed displayed minimal effects on the type of the structure formed.[90] The transition from more dots to more continents, observed by increasing the spreading solution concentration from 0.1 to 4 mg/mL, was thought not to be related to a critical overlap concentration, which is an order of magnitude higher than the highest concentration used.[90] Increasing the surface pressure of film transfer (from 0.3 to 10 mN/m) simply decreased the spacing between the features (most obvious for the dot structure).[90,91] Generally, strands are characterized by flexibility, which is manifested in their ability to turn (up to 180°) without breaking, in contrast to continents that break forming sharp straight cracks.[90] Cheyne and Moffitt observed additional features, termed rings and chains, for low concentration PS-PEO solutions (0.10–0.25 mg/mL, wt_{PEO} = 11.4%).[92] They also pointed out “budding spaghetti” (observed for a 0.50 mg/mL solution), attributed to a transitional morphology between spaghetti and chains.[92] The various morphologies and their dependence on solution concentration were ascribed to kinetic effects, such that different morphologies are “frozen” at different stages as solvent evaporates and the PS becomes glassy.[86,90]

Previously, it was demonstrated that LB films of diblock polyelectrolytes transferred onto mica, silicon or carbon exhibit the same morphology independently of the solid substrate.[82] More recently, it was shown that the use of a chemically patterned hydrophobic/hydrophilic substrate (octadecyltrichlorosilane [OTS] glass) can result an oriented structure deposition, attributed to selective dewetting along the template.[93] To achieve this, however, the film must be transferred at low surface pressure, in which case the aggregates possess sufficient translational freedom to rearrange and accumulate within the hydrophilic regions.[93] At high surface pressure, *i.e.* when the surface micelles exist in a condensed state, transfer to the patterned substrate does not result in selective positioning of the aggregates (Figure 1-24).[93] Another important detail, the patterned substrate must be pulled through the air/water interface with its stripes oriented perpendicular to the water surface, since the presence of heterogeneities in surface energy along the drying front are critical to this process. Withdrawal of the substrate with hydrophilic/hydrophobic stripes oriented parallel to the water surface results in a uniform monolayer like on the unpatterned substrate, because no dewetting-induced segregation of the water subphase occurs at the moving contact line.[93]

The introduction of PS-functionalized Cd nanoparticles (PS-CdS) in PS-PEO system was demonstrated to be a new route to hierarchical 1D hybrid assemblies with potential photonics applications.[94,95] It was shown that, in contrast to other wirelike quantum dots (QDs) assembled at the air/water interface, PS-CdS/PS-PEO aggregates (called cables,

Figure 1-25) are quite uniform and very resistant to compression.[95] By varying the blend composition and spreading concentration, some control over morphology was achieved.[95] For example, the use of higher concentration solutions results in a decrease of circular aggregates (typical for films produced by using low concentration solutions) and the formation of more highly branched cables, while a higher content of PS-CdS causes a more uniform distribution of QDs throughout the cable.[95]

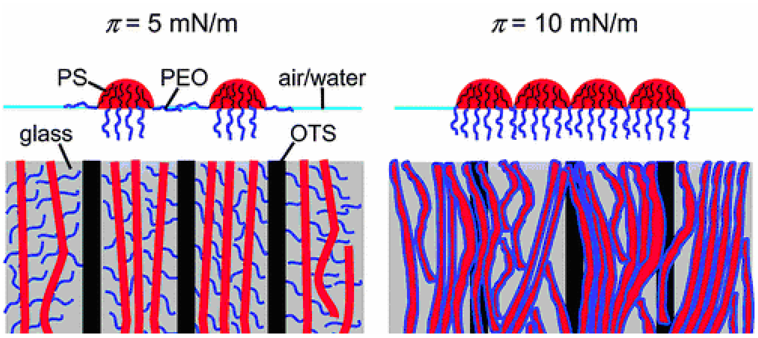

Figure 1-24. Schematic illustrations showing the effect of surface pressure on the transfer of strandlike aggregates onto patterned substrates. (Reproduced with permission from ref. 93. Copyright 2010 American Chemical Society).

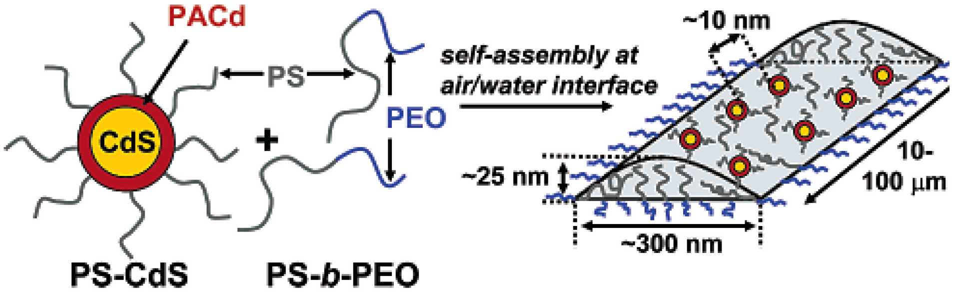

Figure 1-25. Self-assembled cable of quantum dots/polymers blend at the air/water interface. (Reprinted with permission from ref. 94. Copyright 2005 American Chemical Society).

Finally, an example of similar self-assembly into mesoscale strands, but with internal nanoscale cylinders of polybutadiene (PB), was observed for a blend of PS-PEO and PS-PB diblock copolymers.[96] Potentially, this strategy can be used for producing thin films with unique structural complexity possessing diverse functionalities.[96]

1.5. OBJECTIVES AND STRUCTURE OF THE THESIS

The basis for the current work was the discovery in our group of the LB nanostrand network formed from PS-PVP/PDP by an uncommon, “solvent-assisted” method.[97] As will be described in more detail in the introductions to Chapters 2 and 3, this method relies on compressing the barriers as soon as possible after drop spreading on the water surface, and thus it is quite user-dependent. In the light of this, the first **objective** of this work was to study molecular parameters and experimental conditions that allow the optimal formation of this morphology using standard LB technique.

Then, given the above-mentioned controversies regarding block copolymer self-assembly and the influence of solution concentration, it was decided to profit from the ready availability of many PS-PVP block copolymers and their easy modification by small molecules to obtain a deeper understanding of their self-assembly at the air-water interface. This knowledge will allow the building of desired nanopatterns with known properties.

The thesis is divided into five chapters:

Chapter 1 presented a general introduction to self-assembled block copolymers and Langmuir monolayers. A significant part of this chapter was devoted to overview of PS-based amphiphilic block copolymers described in the literature, particularly those based on PS-PVP.

Chapter 2 is a verbatim copy of the full paper recently published in the journal, ACS Nano (2010, Vol. 4, Iss. 11, pp. 6825–6835). It describes the conditions that control the nanostrand network formation; particularly, the spreading solution concentration. The influence of various spreading solvents and temperature on the morphology was also explored. The various data obtained led to the proposal of a new mechanism of nanostrand formation.

Chapter 3 is a wide-ranging series of investigations that focuses on how the isotherms and LB monolayer morphology of PS-PVP and PS-PVP/PDP depend on block composition, solution concentration, molar ratio of VP:PDP, *etc*. Comparison of the results of this chapter with relevant literature results allowed an extended discussion concerning the mechanisms of morphology formation. This fundamental research led to a deeper and broader understanding of the molecular and experimental factors affecting the LB properties of this system.

Chapter 4 presents additional experiments that provide still more insights into the self-assembly phenomena. It first describes what is observed for the nanodot morphology at high surface pressures that leads to a reinterpretation of the transition associated with the isotherm plateau. A new form of the PS-PVP/PDP nanostrand morphology, obtained by rinsing in acetone, is then described and the possible light that it sheds on early stages of polymer association after drop spreading is discussed. The replacement of PDP by other hydrogen-bonding small molecules is also explored, and, finally the effect of very high and very low total molecular weight on the nanostrand network-forming system is investigated.

Chapter 5 presents an overview of the main conclusions. Here, the significant contributions to original knowledge are indicated, and ideas for continued research are proposed.

References to Chapter 1:

1. Li, M.; Coenjarts, C.A.; Ober, C. K. Patternable Block Copolymers. *Adv. Polym. Sci.* **2005**, *190*, 183–226; *and references therein.*
2. Kim, H.-C.; Park, S.-M.; Hinsberg, W. D. Block copolymer based nanostructures: Materials, processes, and applications to electronics. *Chem. Rev.* **2010**, *110*, 146–177.
3. Förster, S.; Plantenberg, T. From self-organizing polymers to nanohybrid and biomaterials. *Angew. Chim. Int. Ed.* **2002**, *41*, 688–714.
4. Matsen, M. W.; Bates, F. S. Unifying weak- and strong-segregation block copolymer theories. *Macromolecules*, **1996**, *29*, 1091–1098.
5. Laforgue, A.; Bazuin, C. G.; Prud'homme, R. E. A study of the supramolecular approach in controlling diblock copolymer nanopatterning and nanoporosity on surfaces. *Macromolecules* **2006**, *39*, 6473–6482.
6. Carter, C. B.; Norton, M. G. *Ceramic materials: Science and Engineering.* Springer: New York, 2007; Chapter 28. Thin films and vapour deposition.
7. Sohn, K. E.; Kojio, K.; Berry, B. C.; Karim, A.; Coffin, R. C.; Bazan, G. C.; Kramer, E. J.; Sprung, M.; Wang, J. Surface effects on the thin film morphology of block copolymers with bulk order–order transitions. *Macromolecules* **2010**, *43*, 3406–3414.
8. Li, Z.; Zhao, W.; Liu, Y.; Rafailovich, M. H.; Sokolov, J.; Khougaz, K.; Eisenberg, A.; Lennox, R. B.; Krausch, G. Self-ordering of diblock copolymers from solution. *J. Am. Chem. Soc.* **1996**, *118*, 10892–10893.
9. Meli, M.-V.; Lennox, R. B. Preparation of nanoscale Au islands in patterned arrays. *Langmuir* **2003**, *19*, 9097–9100.
10. Spatz, J. P.; Eibeck, P.; Möβmer, S.; Möller, M.; Herzog, T.; Ziemann, P. Ultrathin diblock copolymer/titanium laminates – a tool for nanolithography. *Adv. Mater.* **1998**, *10*, 849–852.
11. Yang, S. Y.; Park, J.; Yoon, J.; Ree, M.; Jang, S. K.; Kim, J. K. Virus filtration membranes prepared from nanoporous block copolymers with good dimensional stability under high pressures and excellent solvent resistance. *Adv. Funct. Mater.* **2008**, *18*, 1371–1377.
12. Jackson, E. A.; Hillmyer, M. A. Nanoporous membranes derived from block copolymers: From drug delivery to water filtration. *ACS Nano* **2010**, *4*, 3548–3553.
13. Langmuir, I. Surface Chemistry. *Nobel Lecture* **1932**, 287–325.
14. Ozin, G. A.; Arsenault, A. C.; Cademartiri, L. *Nanochemistry. A chemical approach to nanomaterials*, 2nd ed.; Royal Society of Chemistry: Cambridge, 2009; Chapter 1.19. Two-dimensional assemblies.
15. Pockels, A. Surface tension. *Nature* **1891**, *43*, 437–439.
16. Langmuir, I. Two-Dimensional Gases, Liquids, and Solids. *Science* **1936**, *84*, 379–400.

17. Taylor, H. Irving Langmuir. *Biogr. Mems Fell. R. Soc.* **1958**, *4*, 167–184.
18. Petty, M. C. *Langmuir–Blodgett films: An introduction*. Cambridge University Press: Cambridge, 1996; Chapter 2. Monolayers: two-dimensional phases.
19. Damodaran, S. Water activity at interfaces and its role in regulation of interfacial enzymes: a hypothesis. *Colloids Surf. B: Biointerfaces* **1998**, *11*, 231–237.
20. Levine, M. J.; Schwarz, J. A. Experimental guidelines for producing molecular assemblies by Langmuir-Blodgett techniques. *J. Chem. Educ.* **1988**, *65*, 638–641.
21. de Gennes, P. G. Deposition of Langmuir-Blodgett layers. *Colloid Polym. Sci.* **1986**, *264*, 463–465.
22. Okahata, Y.; Ariga, K.; Tanaka, K. Evaluation of a horizontal lifting method of Langmuir-Blodgett films using a quartz-crystal microbalance. *Thin Solid Films* **1992**, *210/211*, 702–706.
23. Langmuir, I.; Schaefer, V. J. Activities of urease and pepsin monolayers. *J. Am. Chem. Soc.* **1938**, *60*, 1351–1360.
24. Li, M.; Li, X.-H.; Huang, L.; Jia, Q.-L.; Zheng, W.-L.; Mai, Z.-H. Incomplete transfer-induced interfacial roughening of Langmuir-Blodgett films. *Europhys. Lett.* **2003**, *64*, 385–391.
25. KSV-Nima website: http://www.ksvnima.com/langmuir-and-langmuir-blodgett-troughs
26. Giancarlo, L. C.; Fang, H.; Avila, L.; Fine, L. W.; Flynn, G. W. Molecular photography in the undergraduate laboratory: Identification of functional groups using scanning tunneling microscopy. *J. Chem. Educ.* **2000**, *77*, 66–71.
27. Vollhardt, D.; Fainerman, V. B. Characterisation of phase transition in adsorbed monolayers at the air/water interface. *Adv. Coll. Int. Sci.* **2010**, *154*, 1–19.
28. Berthomieu, C.; Hienerwadel, R. Fourier transform infrared (FTIR) spectroscopy. *Photosynth. Res.* **2009**, *101*, 157–170.
29. Dluhy, R. A. Infrared spectroscopy of biophysical monomolecular films at interfaces: Theory and applications. *Appl. Spectrosc. Rev.* **2000**, *35*, 315–351.
30. Autschbach, J.; le Guennic, B. Analyzing and interpreting NMR spin–spin coupling constants using molecular orbital calculations. *J. Chem. Educ.* **2007**, *84*, 156–171.
31. (a) De Souza, R. A.; Martin, M. Secondary ion mass spectrometry (SIMS) – a powerful tool for studying mass transport over various length scales. *Phys. Stat. Sol. C* **2007**, *4*, 1785–1801. (b) Griffiths, J. Secondary ion mass spectrometry. *Anal. Chem.* **2008**, *80*, 7194–7197.
32. Heinz, W. H.; Hoh, J. H. Getting physical with your chemistry: Mechanically investigating local structure and properties of surfaces with the atomic force microscope. *J. Chem. Educ.* **2005**, *82*, 695–703.
33. Jalili, N.; Laxminarayana, K. A review of atomic force microscopy imaging systems: Application to molecular metrology and biological sciences. *Mechatronics* **2004**, *4*, 907–945.

34. Brandys, F. A.; Bazuin, C. G. Mixtures of an acid-functionalized mesogen with poly(4-vinylpyridine). *Chem. Mater.* **1996**, *8*, 83–92.
35. Bossé, F.; Schreiber, H. P.; Eisenberg, A. Specific adsorption of some styrene/vinylpyridine diblocks from selective solvents onto solid substrates – An NMR study. *Macromolecules* **1993**, *26*, 6447–6454.
36. Bossé, F.; Eisenberg, A.; El-Kindi, M.; Deng, Z.; Schreiber, H. P. Surface properties of some styrene/vinyl pyridine diblock co-polymers. *J. Adhesion Sci. Technol.* **1992**, *6*, 455–465.
37. Fiege, H.; Voges, H.-W.; Hamamoto, T.; Umemura, S.; Iwata, T.; Miki, H.; Fujita, Y.; Buysch, H.-J.; Garbe, D.; Paulus, W. *Ullmann's Encyclopedia of Industrial Chemistry*. Wiley-VCH: Weinheim, 2000; Vol. 25, p 65. Phenol derivatives.
38. Yang, F.; Li, G.; Qi, J.; Zhang, S.-M.; Liu, R. Synthesis and surface activity properties of alkylphenol polyoxyethylene nonionic trimeric surfactants. *Appl. Surf. Sci.* **2010**, *257*, 312–318.
39. Attanasi, O. A.; Mele, G.; Filippone, P.; Mazzetto, S. E.; Vasapollo, G. Synthesis and characterization of novel cardanol based fulleropyrrolidines. *ARKIVOC* **2009**, *8*, 69–84.
40. Nagabhushana, K. S.; Ravindranath, B. Efficient medium-scale chromatographic group separation of nacardic acids from solvent-extracted cashew nut (Anacardium occidentale) shell liquid. *J. Agric. Food Chem.* **1995**, *43*, 2381–2383.
41. Ruokolainen, J.; Saariaho, M.; Ikkala, O.; ten Brinke, G.; Thomas, E. L.; Torkkeli, M.; Serimaa, R. Supramolecular routes to hierarchical structures: Comb-coil diblock copolymers organized with two length scales. *Macromolecules* **1999**, *32*, 1152–1158.
42. Mäki-Ontto, R.; de Moel, K,; de Odorico, W.; Ruokolainen, J.; Stamm, M.; ten Brinke, G.; Ikkala, O. “Hairy tubes”: Mesoporous materials containing hollow self-organized cylinders with polymer brushes at the walls. *Adv. Mater.* **2001**, *13*, 117–120.
43. Polushkin, E.; Alberda van Ekenstein, G. O. R.; Knaapila, M.; Ruokolainen, J.; Torkkeli, M.; Serimaa, R.; Bras, W.; Dolbnya, I.; Ikkala, O.; ten Brinke, G. Intermediate segregation type chain length dependence of the long period of lamellar microdomain structures of supramolecular comb-coil diblocks. *Macromolecules* **2001**, *34*, 4917–4922.
44. de Moel, K.; Alberda van Ekenstein, G. O. R.; Nijland, H.; Polushkin, E.; ten Brinke, G.; Mäki-Ontto, R.; Ikkala, O. Polymeric nanofibers prepared from self-organized supramolecules. *Chem. Mater.* **2001**, *13*, 4580–4583.
45. Valkama, S.; Ruotsalainen, T.; Nykänen, A.; Laiho, A.; Kosonen, H.; ten Brinke, G.; Ikkala, O.; Ruokolainen, J. Self-assembled structures in diblock copolymers with hydrogen-bonded amphiphilic plasticizing compounds. *Macromolecules* **2006**, *39*, 9327–9336.
46. Ruotsalainen, T.; Turku, J.; Hiekkataipale, P.; Vainio, U.; Serimaa, R.; ten Brinke, G.; Harlin, A.; Ruokolainen, J.; Ikkala, O. Tailoring of the hierarchical structure within electrospun fibers due to supramolecular comb–coil block copolymers: Polystyrene-block-poly(4-vinylpyridine)

plasticized by hydrogen bonded pentadecylphenol. *Soft Matter* **2007**, *3*, 978–985.

47. Ruokolainen, J.; Mäkinen, R.; Torkkeli, M.; Mäkelä, T.; Serimaa, R.; ten Brinke, G.; Ikkala, O. Switching supramolecular polymeric materials with multiple length scales. *Science* **1998**, *280*, 557–560.
48. Ikkala, O.; Ruokolainen, J.; Mäkinen, R.; Torkkeli, M.; Serimaa, R.; Mäkelä, T.; ten Brinke, G. Electrical switching based on dimensional transitions in nanostructured polymers. *Synthetic Metals* **1999**, *102*, 1498–1501.
49. Ruokolainen, J.; ten Brinke, G.; Ikkala, O. Supramolecular polymeric materials with hierarchical structure-within-structure morphologies. *Adv. Mater.* **1999**, *11*, 777–780.
50. Kosonen, H.; Valkama, S.; Hartikainen, J,; Eerikäinen, H.; Torkkeli, M.; Jokela, K.; Serimaa, R.; Sundholm, F.; ten Brinke, G.; Ikkala, O. Mesomorphic structure of poly(styrene)-block-poly(4-vinylpyridine) with oligo(ethylene oxide)sulfonic acid side chains as a model for molecularly reinforced polymer electrolyte. *Macromolecules* **2002**, *35*, 10149–10154.
51. Kosonen, H.; Valkama, S.; Ruokolainen, J.; Torkkeli, M.; Serimaa, R.; ten Brinke, G.; Ikkala, O. One-dimensional optical reflectors based on self-organization of polymeric comb-shaped supramolecules. *Eur. Phys. J. E.* **2003**, *10*, 69–75.
52. Valkama, S.; Ruotsalainen, T.; Kosonen, H.; Ruokolainen, J.; Torkkeli, M.; Serimaa, R.; ten Brinke, G.; Ikkala, O. Amphiphiles coordinated to block copolymers as a template for mesoporous materials. *Macromolecules* **2003**, *36*, 3986–3991.
53. Ruotsalainen, T.; Torkkeli, M.; Serimaa, R.; Mäkelä, T.; Mäki-Ontto, R.; Ruokolainen, J.; ten Brinke, G.; Ikkala, O. Structural hierarchy in flow-aligned hexagonally self-organized microphases with parallel polyelectrolytic structures. *Macromolecules* **2003**, *36*, 9437–9442.
54. Tiitu, M.; Torkkeli, M.; Serimaa, R.; Mäkelä, T.; Ikkala, O. T. Self-assembly and flow alignment of protonically conducting complexes of polysterene-block-poly(4-vinylpyridine) diblock copolymer with phosphoric acid. *Solid State Ionics* **2005**, *176*, 1291–1299.
55. van Zoelen, W.; Alberda van Ekenstein, G.; Polushkin, E.; Ikkala, O.; ten Brinke, G. Nanorod engineering by reinforcing hexagonally self-assembled PS-b-PVP(DDP) with PPE. *Soft Matter* **2005**, *1*, 280–283.
56. van Zoelen, W.; Alberda van Ekenstein, G.; Ikkala, O.; ten Brinke, G. Incorporation of PPE in lamellar self-assembled PS-b-PVP(PDP) supramolecules and PS-b-PVP diblock copolymers. *Macromolecules* **2006**, *39*, 6574–6579.
57. Laiho, A.; Ras, R. H.; Valkama, S.; Ruokolainen, J.; Österbacka, R.; Ikkala, O. Control of self-assembly by charge-transfer complexation between C60 fullerene and electron donating units of block copolymers. *Macromolecules* **2006**, *39*, 7648–7653.
58. Valkama, S.; Nykänen, A.; Kosonen, H.; Ramani, R.; Tuomisto, F.; Engelhardt, P.; ten Brinke, G.; Ikkala, O.; Ruokolainen, J. Hierarchical porosity in self-assembled polymers: Post-

modification of block copolymer – phenolic resin complexes by pyrolysis allows the control of micro- and mesoporosity. *Adv. Funct. Mater.* **2007***, 17,* 183–190.

59. Korhonen, J. T.; Verho, T.; Rannou, P.; Ikkala, O. Self-assembly and hierarchies in pyridine-containing homopolymers and block copolymers with hydrogen-bonded cholesteric side-chains. *Macromolecules* **2010**, *43*, 1507–1514.
60. van Zoelen, W.; Asumaa, T.; Ruokolainen, J.; Ikkala, O.; ten Brinke, G. Phase behavior of solvent vapor annealed thin films of PS-b-PVP(PDP) supramolecules. *Macromolecules* **2008**, *41*, 3199–3208.
61. Takahashi, H.; Mamola, K.; Plyler, E. K. Effects of hydrogen bond formation on vibrations of pyridine, pyrazine, pyrimidine, and pyridazine. *J. Mol. Spectrosc.* **1966**, *21*, 217–230.
62. Ruokolainen, J.; ten Brinke, G.; Ikkala, O.; Torkkeli, M.; Serimaa, R. Mesomorphic structures in flexible polymer–surfactant systems due to hydrogen bonding: poly(4-vinylpyridine)–pentadecylphenol. *Macromolecules* **1996**, *29*, 3409–3415.
63. Ruokolainen, J.; Tanner, J.; Ikkala, O.; ten Brinke, G.; Thomas, E. L. Direct imaging of self-organized comb copolymer-like systems obtained by hydrogen bonding: poly(4-vinylpyridine)–4-nonadecylphenol. *Macromolecules* **1998**, *31*, 3532–3536.
64. Ruokolainen, J.; Torkkeli, M.; Serimaa, R.; Vahvaselkä, S.; Saariaho, M.; ten Brinke, G.; Ikkala, O. Critical interaction strength for surfactant–induced mesomorphic structures in polymer–surfactant systems. *Macromolecules* **1996**, *29*, 6621–6628.
65. Ikkala, O.; ten Brinke, G. Hierarchical self-assembly in polymeric complexes: Towards functional materials. *Chem. Commun.* **2004**, *19*, 2131–2137.
66. Ruokolainen, J.; Torkkeli, M.; Serimaa, R.; Komanschek, E.; Ikkala, O.; ten Brinke, G. Order-disorder transitions in polymer-surfactant systems. *Phys. Rev. E* **1996**, *54*, 6646–6649.
67. Ruokolainen, J.; Torkkeli, M.; Serimaa, R.; Komanschek, E.; ten Brinke, G.; Ikkala, O. Order-disorder transition in comblike block copolymers obtained by hydrogen bonding between homopolymers and end-functionalized oligomers: poly(4-vinylpyridine)-pentadecylphenol. *Macromolecules* **1997**, *30*, 2002–2007.
68. Ruokolainen, J.; Tanner, J.; Ikkala, O.; ten Brinke, G.; Thomas, E. L. Direct imaging of self-organized comb copolymer-like systems obtained by hydrogen bonding: poly(4-vinylpyridine)-4-nonadecylphenol. *Macromolecules* **1998**, *31*, 3532–3536.
69. Spatz, J. P.; Sheiko, S.; Möller, M. Substrate-induced lateral micro-phase separation of a diblock copolymer. *Adv. Mater.* **1996**, *8*, 513–517; *and references therein.*
70. Albert, J. N. L.; Epps, T. H. Self-assembly of block copolymer thin films. *Materials Today* **2010**, *13*, 24–33.
71. Spatz, J. P.; Möller, M; Noeske,M.; Behm, R. J.; Pietralla, M. Nanomosaic surfaces by lateral phase separation of a diblock copolymer. *Macromolecules* **1997**, *30*, 3874–3880.

72. van Zoelen, W.; Polushkin, E.; ten Brinke, G. Hierarchical Terrace Formation in PS-*b*-PVP(PDP) Supramolecular Thin Films. *Macromolecules* **2008**, *41*, 8807–8814.
73. Spatz, J. P.; Eibeck, P.; Mössmer, S.; Möller, M.; Kramarenko, E. Y.; Khalatur, P. G.; Potemkin, I. I.; Khokhlov, A. R.; Winkler, R. G.; Reineker, P. Order-disorder transition in surface-induced nanopattern of diblock copolymer films. *Macromolecules* **2000**, *33*, 150–157.
74. Zhu, J.; Lennox, R. B.; Eisenberg, A. Polymorphism of (quasi) two-dimensional micelles. *J. Phys. Chem.* **1992**, *96*, 4727–4730.
75. Li, Z.; Zhao, W.; Quinn, J.; Rafailovich, M. H.; Sokolov, J.; Lennox, R. B.; Eisenberg, A.; Wu, X. Z.; Kim, M. W.; Sinha, S. K.; Tolan, M. X-ray reflectivity of diblock copolymer monolayers at the air/water interface. *Langmuir* **1995**, *11*, 4785–4792.
76. Kumaki, J. Monolayer of polystyrene monomolecular particles on a water surface studied by Langmuir-type film balance and transmission electron microscopy. *Macromolecules* **1988**, *21*, 749–755.
77. Zhu, J.; Eisenberg, A.; Lennox, R. B. Interfacial behavior of block polyelectrolytes. 1. Evidence for novel surface micelle formation. *J. Am. Chem. Soc.* **1991**, *113*, 5583–5588.
78. Zhu, J.; Eisenberg, A.; Lennox, R. B. Interfacial behavior of block polyelectrolytes. 6. Properties of surface micelles as a function of R and X in P(S260-b-VP240/RX). *Macromolecules* **1992**, *25*, 6556–6562.
79. Zhu, J.; Eisenberg, A.; Lennox, R. B. Interfacial behavior of block polyelectrolytes. 5. Effect of varying block lengths on the properties of surface micelles. *Macromolecules* **1992**, *25*, 6547–6555.
80. Shin, K.; Rafailovich, M. H.; Sokolov, J.; Chang, D. M. Cox, J. K.; Lennox, R. B.; Eisenberg, A.; Gibaud, A.; Huang, J.; Hsu, S. L.; Satija, S. K. Observation of surface ordering of alkyl side chains in polystyrene/polyelectrolytes diblock copolymer Langmuir films, *Langmuir* **2001**, *17*, 4955–4961.
81. Zhu, J.; Lennox, R. B.; Eisenberg, A. Interfacial behavior of block polyelectrolytes. 2. Aggregation numbers of surface micelles. *Langmuir* **1991**, *7*, 1579–1584.
82. Li, S.; Hanley, S.; Khan, I.; Varshney, S. K.; Eisenberg, A.; Lennox, R. B. Surface micelle formation at the air/water interface from non-ionic diblock copolymers. *Langmuir* **1993**, *9*, 2243–2246.
83. Li, S.; Clarke, C. J.; Lennox, R. B.; Eisenberg. A. Two-dimensional self assembly of polystyrene-b-poly(butyl-methacrylate) diblock copolymers. *Colloids Surfaces A* **1998**, *133*, 191–203.
84. Li, S.; Clarke, C. J.; Eisenberg, A.; Lennox, R. B. Langmuir films of polystyrene-b-poly(alkyl acrylate) diblock copolymers. *Thin Solid Films* **1999**, *354*, 136–141.

85. Cox. J. K.; Yu, K.; Constantine, B.; Eisenberg, A.; Lennox, R. B. Polystyrene–poly(ethylene oxide) diblock copolymers form well-defined surface aggregates at the air/water interface. *Langmuir* **1999**, *15*, 7714–7718; *and references therein.*
86. Hosoi, A. E.; Kogan, D.; Devereaux, C. E.; Bernoff, A. J.; Baker, S. M. Two-dimensional self-assembly in diblock copolymers. *Phys. Rev. Lett.* **2005**, *95*, 037801 (1–4).
87. Cox, J. K.; Eisenberg, A.; Lennox, R. B. Patterned surfaces via self-assembly. *Curr. Opin. Colloid Interface Sci.* **1999**, *4*, 52–59.
88. Cheyne, R. B.; Moffitt, M. G. Self-assembly of polystyrene-block-poly(ethylene oxide copolymers at the air–water interface: Is dewetting the genesis of surface aggregate formation? *Langmuir* **2006**, *22*, 8387–8396.
89. Price, E. W.; Harirchian-Saei, S.; Moffitt, M. G. Strands, network, and continents from homopolystyrene dewetting at the air/water interface: Implications for amphiphilic block copolymer self-assembly. *Langmuir* **2011**, *27*, 1364–1372.
90. Devereaux, C. A.; Baker, S. M. Surface features in Langmuir-Blodgett monolayers of predominantly hydrophobic poly(styrene)–poly(ethylene oxide) diblock copolymer. *Macromolecules* **2002**, *35*, 1921–1927.
91. Baker, S. M.; Leach, K. A.; Devereaux, C. E.; Gragson, D. E. Controlled patterning of diblock copolymers by monolayer Langmuir-Blodgett deposition. *Macromolecules* **2000**, *33*, 5432–5436.
92. Cheyne, R. B.; Moffitt, M. G. Novel two-dimensional "ring and chain" morphologies in Langmuir-Blodgett monolayers of PS-b-PEO block copolymers: Effect of spreading solution concentration on self-assembly at the air/water interface. *Langmuir* **2005**, *21*, 5453–5460.
93. Harirchian-Saei, S.; Wang, M. C. P.; Gates, B. D.; Moffitt, M. G. Patterning block copolymer aggregates via Langmuir-Blodgett transfer to microcontact-printed substrates. *Langmuir* **2010**, *26*, 5998–6008; *and references therein.*
94. Cheyne, R. B.; Moffitt, M. G. Hierarchical nanoparticles/block copolymer surface features via synergistic self-assembly at the air–water interface. *Langmuir* **2005**, *21*, 10297–10300.
95. Cheyne, R. B.; Moffitt, M. G. Controllable organization of quantum dots into mesoscale wires and cables via interfacial block copolymer self-assembly. *Macromolecules* **2007**, *40*, 2046–2057; *and references therein.*
96. Price, E. W.; Guo, Y.; Wang, C.-W.; Moffitt, M. G. Block copolymer strands with internal microphase separation structure via self-assembly at the air–water interface. *Langmuir* **2009**, *25*, 6398–6406.
97. Lu, Q.; Bazuin, C. G. Solvent-assisted formation of nanostrand networks from supramolecular diblock copolymer/surfactant complexes at the air/water interface. *Nano Lett.* **2005**, *5*, 1309–1314.

Appendix to Chapter 1

The appendix contains tables that summarize information about 3D (bulk) and 2D (LB films) morphologies of PS-based amphiphilic diblock copolymers studied in the literature. (For a graphical representation of the data, see Figure 1-15).

Table 1-2. PS-PVP/small molecules. Composition dependence on their morphologies in the bulk.

Sample	Molecular weight, g/mol		Fraction of hydrophilic block		Structure**
	M_n(PS)	M_n(PVP)	mol_{PVP}, %	wt_{comb}*, %	
PS-PVP	40,000	5,600	12	12	S[41]
PS-PVP/**PDP**$_{0.5}$	40,000	5,600	12	25	C[41]
PS-PVP/**PDP**$_{1.0}$	240,000	2,000	1	3	disordered[45]
	41,400	1,900	4	15	S[41]
	301,000	19,600	6	20	LwS[45]
	365,300	29,400	7	24	LwS[45]
	34,000	2,900	8	25	C,[41]LwC[42,45,65]
	35,500	3,600	9	28	LwC[45]
	35,500	3,680	9	29	C[41]
	40,000	5,600	12	35	L,[41] LwL[45]
	42,100	8,100	16	43	LwL[45]
	238,100	49,500	17	45	L[41]

(*Continued on the next page*)

---

* Comb fraction consists of PVP block and small molecules.

** S, C, L denote spherical, cylindrical, lamellar morphologies, correspondingly. LwS and LwC abbreviations are used to designate structure with short length scale lamellar order within a long length scale order consisting of spherical and cylindrical PVP-containing domains in PS matrix, respectively. In LwL, a short length scale lamellar order is represented by alternating small molecules and PVP layers, while PS and PVP form a long length scale lamellar. GwL, CwL, SwL denote gyroid, PS cylinders and PS spheres, respectively, at a long scale within a matrix with short-length lamellar order of alternating layers of PVP and small molecules.

(*Continuation of Table 1-2*)

Sample	M_n(PS)	M_n(PVP)	mol$_{PVP}$, %	wt$_{comb}$, %	Structure
PS-PVP/**PDP**$_{\mathbf{1.0}}$	32,900	8,100	20	49	L[41], LwL[45]
	19,600	5,100	21	50	LwL[56]
	128,400	33,500	21	50	LwL[45]
	78,900	30,300	28	60	LwL[45]
	31,900	13,200	29	62	C*,[41] GwL[45]
	57,300	24,700	30	63	LwL[45]
	47,600	20,900	31	63	LwL[45]
	130,300	83,100	39	71	CwL[45]
	56,300	43,500	44	75	CwL[45]
	21,400	20,700	49	79	C*,[41] CwL[44,45]
	19,900	29,400	60	85	SwL[45]
	18,600	55,800	75	92	S*,[41] SwL[45]
PS-PVP/**MSA**$_{\mathbf{1.0}}$**/PDP**$_{\mathbf{1.0}}$	34,000	2,900	8	29	LwC[45]
	35,500	3,600	9	33	LwC[45]
	193,700	21,400	10	35	LwS[45]
	40,000	5,600	12	40	LwL[45,47]
	42,100	8,100	16	48	LwL[45]
	32,900	8,100	20	54	LwL[45]
	19,600	5,100	21	56	LwL[45]
	78,900	30,300	28	65	LwL[45]
	31,900	13,200	29	67	LwL[45]
	71,900	30,200	30	67	LwL[45]
	57,300	24,700	30	67	LwL[45]
	47,600	20,900	31	68	CwL[45]
	21,400	20,700	49	82	CwL[45]
	19,900	29,400	60	88	CwL[45]

(*Ended on the next page*)

(*Ending of Table 1-2*)

Sample	M$_n$(PS)	M$_n$(PVP)	mol$_{PVP}$, %	wt$_{comb}$, %	Structure
PS-PVP/**TSA$_{0.9}$/PDP$_{1.0}$**	41,400	1,900	4	19	C[53]
PS-PVP/**NDP$_{1.0}$**	41,400	1,900	4	17	LwS (S)[49]
	301,000	19,600	6	22	LwS (S)[49]
	34,000	2,900	8	27	LwC (C)[49]
	35,500	3,680	9	31	LwL (L)[49]
	40,000	5,600	12	38	LwL (L)[49]
	238,100	49,500	17	48	LwL (L)[49]
	31,900	13,200	29	65	CwL (C*)[49]
	21,400	20,700	49	81	CwL (C*)[49]
	18,600	55,800	75	93	SwL (S*)[49]
PS-PVP/**DDP$_{1.0}$**	21,400	20,700	49	77	C*(CwL)[55]
PS-PVP/**(H$_3$PO$_4$)$_{2.2}$**	35,500	3,600	9	24	LwL[54]
PS-PVP/**DBSA$_{1.0; 1.5; 2.0}$**	42,100	8,100	16	44; 52; 58	L[51]
	238,100	49,500	17	46; 54; 60	L[51]
PS-PVP/**(Zn[DBSA]$_2$)$_{0.9}$**	238,100	49,500	17	60	LwL[52]
	41,400	1,900	4	25	L[52]
PS-PVP/**EO8-SA$_{1.0}$**	40,000	5,600	12	43	LwL[50]
PS-PVP/**EO8-SA$_{1.0}$/(LiClO$_4$)$_8$**	40,000	5,600	12	47	LwL[50]
PS-PVP/**EO13-SA$_{1.0}$**	40,000	5,600	12	51	LwL[50]
PS-PVP/**EO13-SA$_{1.0}$/ (LiClO$_4$)$_{13}$**	40,000	5,600	12	54	LwL[50]
PS/**(PPE)$_{0.09}$**-PVP/**EO8-SA$_{1.0}$ /(LiClO$_4$)$_8$**	21,400	20,700	49	76	C*(CwL)[55]
PS/**PPE$_{0.1; 0.2; 0.3; 0.35}$**-PVP	20,000	19,000	49	46; 43; 40; 38	LwL[56]
PS/**PPE$_{0.17; 0.23; 0.28}$**-PVP/**DDP$_{1.0}$**	21,400	20,700	49	74; 73; 73	C*(CwL)[55]
PS/**PPE$_{0.1; 0.2; 0.3; 0.4}$**-PVP/**PDP$_{1.0}$**	19,600	5,100	21	48; 45; 42; 38	LwL[56]
PS-PVP/**C60**	47,600	20,900	31	n/a	S (*for aged solution*)[57]

Table 1-3. PS-PVP$^+$RX$^-$ polyelectrolytes. Composition dependence on the LB films morphology.

Sample	Molecular weight, g/mol		Fraction of hydrophilic block		Structure
	M_n(PS)	M_n(PVP)	mol$_{PVP}$, %	wt$_{PVP/RX}$, %	
PS-PVP$^+$ $C_{10}H_{21}I^-$	49,900	1,300	3	9	planar[74,79]
	27,000	1,300	5	15	planar[74,79]
	5,600	300	5	17	planar[74,79]
	18,700	1,100	6	18	planar[74,79]
	49,900	3,500	7	20	rod[74]
	27,000	3,000	10	29	rod[74,79]
	5,600	1,000	14	37	rod[74,79]
	18,700	3,000	14	37	rod[74,79]
	49,900	8,300	14	37	“starfish”[74,79]
	27,000	7,400	21	49	“starfish”[74]
	18,700	7,600	29	59	“starfish”[74,79]
	49,900	21,000	29	60	“starfish”[74,79]
	27,000	12,600	32	62	“starfish”[79]
	27,000	25,200	48	77	“starfish”[77,79]
	18,700	19,900	51	79	“starfish”[74,79]
PS-PVP$^+$ CH_3I^-	27,000	25,200	48	69	“starfish”[78]
PS-PVP$^+$ $C_4H_9I^-$	27,000	25,200	48	72	“starfish”[78]
PS-PVP$^+$ $C_6H_{13}I^-$	27,000	25,200	48	74	“starfish”[78]
PS-PVP$^+$ $C_{18}H_{37}I^-$	27,000	25,200	48	81	“starfish”[78]

Table 1-4. PS-based non-ionic diblock copolymers.
Composition dependence on the LB films morphologies.

Sample	Molecular weight (M_n), g/mol		Fraction of hydrophilic block		Structure (called as in original papers)
	hydrophobic block	hydrophilic block	mol, %	wt, %	
PS-P*n*BMA	27,000	2,500	6	9	planar [83]
	27,000	7,500	17	22	ribbon [83]
	27,000	29,000	44	52	“starfish” [82]
PS-P*t*BMA	17,200	3,500	13	17	“starfish” [83]
	18,700	9,900	28	35	“starfish” [82]
	17,200	14,500	38	46	“starfish” [83]
PS-P*t*BA	31,700	1,500	4	5	planar [84]
	31,700	6,000	13	17	rod [84]
	31,700	10,800	22	26	“starfish” [84]
	31,700	17,600	31	36	“starfish” [84]
	31,800	28,400	42	47	“starfish” [82]
PS-PDMS	85,200	44,400	42	34	rod [82]
PS-PEO	22,300	1,600	15	7	planar + rod [85]
	47,700	3,600	15	7	dots, spaghetti, continents [90]
	13,000	1,300	19	9	planar + rod [85]
	125,000	16,100	23	11	dots, spaghetti, rings/chains [88,92]
	211,500	39,000	30	16	dots [91]
	22,300	5,000	34	18	“starfish” [85]
	14,500	3,500	36	19	“starfish” [85]
	150,000	35,000	36	19	mainly dots, a few strands (disordered) [88]
	13,000	4,100	43	24	“starfish” [85]
	80,000	120,000	78	60	dots [91]
	30,000	345,000	96	92	dots [91]

Chapter 2

Nanostrand Formation of Block Copolymers at the Air/Water Interface[*]

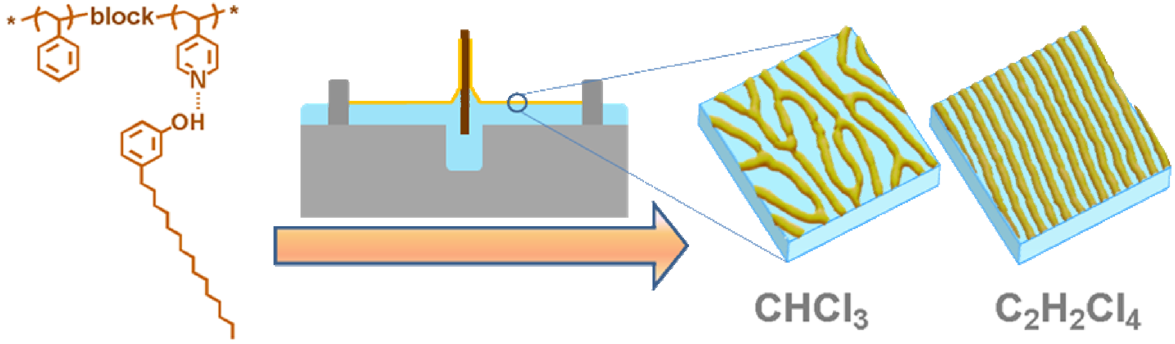

---

[*] This is the full reprint of the article by I. I. Perepichka, A. Badia, and C. G. Bazuin published in *ACS Nano* **2010**, Vol. 4, Iss. 11, pp. 6825–6835. (Reproduced with permission. Copyright 2010 American Chemical Society).

2.1. INTRODUCTION

Nanotechnology relies on the ability to construct very precise nanostructures or nano-objects with well-defined shapes, sizes, and long-range order.[1,2] One of the most important methods to achieve this is the self-assembly of suitably designed molecules. This approach is privileged by nature to produce very complex but exquisitely designed biological structures. For materials scientists, block copolymers are a material of choice for achieving nanostructures based on phase separation between dissimilar blocks.[3–6] The size, shape, and order of the nanostructures can be tuned by changing the absolute and relative block lengths, by adding other substances that selectively associate with or modify the nature of one of the blocks, or by manipulating preparation conditions.[3–6]

Many nanotechnological applications of nanostructured polymers – ranging from nanoporous membranes to components in active nanodevices – require the polymer to be in the form of thin films with well-ordered nanopatterns.[6] One way to obtain solid-supported (ultra-)thin nanopatterned films is by the Langmuir-Blodgett (LB) technique. This involves spreading a polymer solution at the air/water interface in a Langmuir trough, laterally compressing the available surface in a controlled manner with movable barriers, and transferring the monolayer film to a solid substrate. A common pattern obtained in this way, generally from amphiphilic diblock copolymers with relatively large hydrophilic block sizes, is composed of nanodots (also called spherical surface micelles) that tend to have two-dimensional hexagonal order.[7–14] The elevated core of these nanodots is formed from the condensed hydrophobic block that avoids the aqueous surface; it is surrounded laterally (and underneath) by the hydrophilic block that is spread as a monolayer on the water surface. When the hydrophilic block is much smaller than the hydrophobic block, elongated or cylindrical-type nanostructures (also termed spaghetti, ribbons, rods, worms, strands, stripes, wires) with various length-to-width aspect ratios can be obtained. Here, the elevated hydrophobic block in elongated form is surrounded on both sides (and underneath) by the flat hydrophilic block, as shown in Figure 2-1.[8–12] For still smaller hydrophilic blocks, variably sized planar aggregates (also termed pancakes, continents, islands), where the hydrophilic block resides mainly between the hydrophobic block and the water surface, usually form.[8–12] In contrast to the nanodot aggregates, which are relatively uniform in size, the latter two types of aggregates not only tend to have extensive size variability but also frequently occur together and/or mixed with nanodots and/or other nanoforms such as rings and chains.[8–11,15–18] Besides block composition and block ratio variation (which can include the addition of block-selective substances), strategies based on preparative conditions can be used to generate various nanostructures in LB films; for example, "nano-donuts" were formed by spreading a vesicular solution of an amphiphilic triblock copolymer onto a high pH subphase.[19]

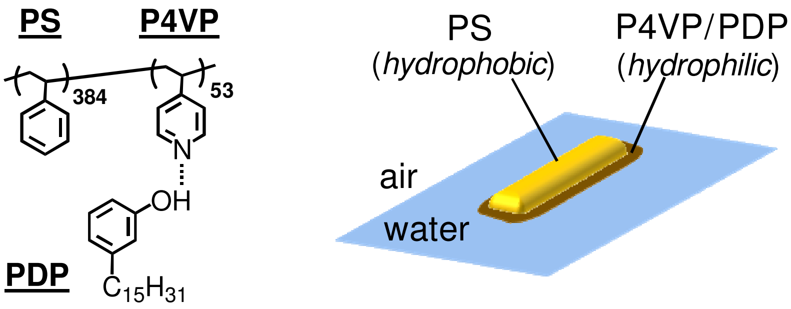

Figure 2-1. Molecular structure of PS-PVP/PDP (left) and schematic representation of a segment of an elongated aggregate at the air/water interface (right).

Among the elongated nanostructures, those with very high aspect ratios have particular interest. They have potential use, for example, for forming long nanowires by templating the deposition of metals[20–22] or, as an alternative to electrospinning techniques, for producing nanofibers for various applications including medical.[23] A network or mesh of nanostrands (dubbed "nanostrand network morphology"[24]), composed of interconnected strands with relatively few ends, may be envisaged for, *e.g.* constructing novel nanoseparation membranes by multilayer LB transfers of monolayers with this pattern. However, these nanostructures can be useful only if they are highly reproducible and "pure".

In this work, we focus on the optimization of experimental conditions that favour reproducible patterns of long nanostrands or nanostrand networks with high surface coverage. This pattern and, more generally, related patterns containing high aspect ratio strands obtained at the air/water interface have been reported in the literature much less frequently than have surface micelles or nanodots. They have been observed in diblock copolymers including blends,[10,11,15–18,24–28] as well as in triblock[29,30] and starblock[31–33] polymers. In part, this relative infrequency is in line with the fact that strand- or rod-like patterns of any kind occur over a relatively narrow range of block copolymer composition.[9–12] When it is reported, it is often mixed with one or more additional morphologies, whether intimately or in the form of partial surface coverage.

We previously reported that the nanostrand network pattern can be obtained with high surface coverage using a polystyrene-*b*-poly(4-vinyl pyridine) (PS-PVP) block copolymer (12 mol % VP content) mixed with 3-*n*-pentadecylphenol (PDP),[24] which hydrogen bonds to the VP block to form a “supramolecular complex”[34] (Figure 2-1). This pattern was obtained under conditions dubbed the “solvent-assisted” procedure where the PS-PVP/PDP solution was spread very rapidly on the water surface, followed immediately by surface compression (typically to 10 mN/m) without waiting for the spreading solvent to evaporate. If the barriers were compressed after waiting for complete solvent evaporation or if the LB monolayer transfer took place at low surface pressure (typically less than 5 mN/m), a morphology composed primarily of nanodots mixed with planar aggregates was obtained. That the “solvent-assisted” procedure worked to produce the nanostrand network pattern was attributed to sufficient mobility maintained in the system, due to the presence of spreading solvent, that it could respond to changing surface pressure conditions and adopt the nanostrand network morphology that appeared to be the preferred morphology at higher surface pressure. This concords with the similar explanation given by Seo *et al.*[25] for a blend of polystyrene-*b*-poly(ferrocenyl silane) (PS-PFS) and polystyrene-*b*-poly(2-vinyl pyridine) (PS-P2VP) (4:1 FS:VP molar ratio), which also showed a transition from predominantly spherical to nanostrand network morphology on increasing the surface pressure. Mobility allowing the change in morphology in this case was attributed to the plasticizing action of the low-T_g majority component PS-PFS.

A disadvantage of the "solvent-assisted" procedure is its reliance on rapid action that is prone to be user-dependent and thus susceptible to irreproducibility. Therefore, it is desirable to seek alternative conditions that allow the target morphology to be obtained using easily controlled standard procedures. This paper describes experimental conditions that optimize the nanostrand morphology at the air/water interface, using the same PS-PVP/PDP system as for the solvent-assisted procedure (12 mol % VP, equimolar or near-equimolar VP:PDP molar ratio).[24] The main variables investigated are solution concentration, choice of spreading solvent, and subphase temperature. We will show not only that the nanostrand network can be obtained almost exclusively over very large surface areas, but also that nanostrands with very little branching and high mutual alignment are achievable. Furthermore, the observation of a fingerprint morphology when using poorly spreading solvents suggests a novel mechanism for the formation of the nanostrand network.

2.2. EXPERIMENTAL SECTION

2.2.1. Materials

Polystyrene-*b*-poly(4-vinyl pyridine) (PS-PVP) with M_n(PS)=40,000 g/mol, M_n(PVP) = 5,600 g/mol (384 S repeat units, 53 VP repeat units, 12 mol % VP content), and M_n/M_w = 1.09, was obtained from Polymer Source (Montreal, Canada), and used as received. 3-n-Pentadecylphenol (PDP) (Sigma-Aldrich, 90%) was recrystallized twice from hexane before use. Chloroform (HPLC grade, ≥99.8%; b.p. 61°C), 1,2-dichloroethane (HPLC grade, 99.8%; b.p. 84°C), nitrobenzene (ACS reagent grade, ≥99.0%; b.p. 210–211°C), and hexachloropropene (96%; b.p. 209–210°C), all obtained from Sigma-Aldrich, and 1,1,2,2-tetrachloroethane (GC, ≥98.0%; b.p. 144–146°C) from Fluka, were used to prepare solutions for monolayer spreading. Ultrapure water (18.2 MΩ cm), used as the subphase in the Langmuir-Blodgett trough, was obtained by purification of distilled water with a Millipore Milli-Q Gradient system. Muscovite ruby mica (ASTM Grade 2, B&M Mica, Flushing, NY, USA) was cleaved immediately before its immersion into the subphase.

2.2.2. Langmuir Isotherms and Monolayer Deposition

PS-PVP and PDP, dissolved separately in the desired solvent, were mixed in the desired proportion (between 1.0:1.0 and 1.0:1.3 molar ratio VP:PDP), and left to stir overnight at room temperature in sealed volumetric flasks. It was noted that $C_2H_2Cl_4$ solutions, in contrast to the other solutions, were unstable over time, with more aged solutions giving very different morphologies compared to solutions that were freshly prepared up to a day old. Hydrogen-bonding of PDP to VP in $CDCl_3$ and $C_2D_2Cl_4$ solutions was confirmed by ^{1}H-NMR spectroscopy, which shows that the sharp OH proton for pure PDP (located at 4.59 ppm in $CDCl_3$ and 4.65 ppm in $C_2D_2Cl_4$) undergoes extensive broadening with accompanying intensity decrease and a downfield shift (centered at *ca.* 5.15 and 4.80 ppm, respectively) in the presence of PS-PVP, as shown in the Appendix to Chapter 2 (Figures SI-2-4 and SI-2-5).

A computer-controlled KSV 3000 Langmuir-Blodgett system with a platinum Wilhelmy plate sensing device (KSV Instruments, Helsinki, Finland) was used. The subphase temperature in the trough (150 x 518 mm) was maintained at 20–21°C unless otherwise specified, using a refrigerated circulator (Isotemp 3016, Fisher Scientific). Solution was spread dropwise in a checkerboard pattern, using Hamilton microliter syringes: 50–200 μL for 0.35–2.05 mg/mL concentrations, 1 mL for 0.10 mg/mL concentration, where concentration is expressed in terms of block copolymer weight per volume of solvent. At least one drop was deposited within about 3–4 cm from the area above the submerged substrate(s). This was found to be important for the reproducibility of the observed film morphology for the more highly concentrated solutions for which as few as 8 drops were necessary to reach the required total mass of material to spread on the water surface.

Following solvent evaporation (30–60 min for $CHCl_3$, 60–90 min for the other spreading solvents), surface pressure (π) *vs.* mean molecular area (A) isotherms were obtained by symmetrical compression of the barriers at a speed of 10 mm/min (15 cm^2/min). All isotherms were run at least 2–3 times, and showed good reproducibility.

Under the same conditions as for the isotherms and following a 20–30 min wait at the desired surface pressure (usually, 5 or 10 mN/m) for barrier stabilization, LB films were deposited on mica substrates (sizes varying from 1×1.5 to 2.5×5 cm^2) that were vertically withdrawn from the subphase at a controlled speed (5 or 10 mm/min). The films were found to show good stability during the barrier stabilization step, with about a decrease in pressure of about 0.5 nm^2/molecule recorded. The transfer ratio was generally 1.0±0.2. Other substrates besides mica [silicon wafer, quartz and glass microscope slides, indium tin oxide (ITO) glass, gold, and highly ordered pyrolytic graphite (HOPG)] were also tested, and did not modify the basic morphology compared to that observed with mica (Appendix, Figure SI-2-6).

Occasionally, Langmuir-Schaefer (LS) films, where transfer was performed on a horizontally lying substrate, were also obtained. In another experiment, single-drop deposition[15] was combined with the LS technique. First, a mica substrate, whose length (*ca.* 14.5 cm) was close to the width of the trough, was placed on the trough floor, midway between and in parallel with the movable barriers. Then, the surface area was compressed to give zero surface pressure slightly below the onset of measurable pressure for the solution to be deposited as calculated from the π–A isotherm (159 cm^2, or 150 x 106 mm), and a single drop (*ca.* 10 µl) of 2.05 mg/mL PS-PVP/PDP solution in $CHCl_3$ was deposited above one end of the substrate. After 60 min, the water was removed carefully by aspiration using the water pump.

2.2.3. AFM Imaging

The deposited films were dried in a clean box overnight at room temperature and then imaged in air by atomic force microscopy (AFM) in tapping mode using a Multimode AFM with a Nanoscope IIIa controller (Digital Instruments/Veeco, Santa-Barbara, USA) and silicon probes (MikroMasch USA: rectangular, no aluminum coating on tip and backside, resonance frequency 265–400 kHz, tip curvature radius less than 10 nm; or Nanosensors: type PPP-NCH, nominal spring constant of 42 Nm-1, resonance frequency 330 kHz, tip radius of curvature <10 nm). Nanofeature dimensions were determined from height profiles across the strands. Widths were measured at half-height of sufficiently isolated strand segments. Heights were determined from the nanostrand summits relative to the flat areas between them. At least two separate experiments per condition were performed, and each LB film obtained was imaged (typically as 10×10 µm images) at a minimum of 10 different places scattered over the film but avoiding the substrate edges. Generally, at least 90% of the images for a given experimental condition ("image set") show the same morphology. When a second (or, rarely, third) morphology is observed in 20% or more of the image set, this is stated in the text and, in some cases, illustrated. All transferred films are stable in air at ambient temperature (*i.e.* no changes were observed in one-year old films compared to their freshly prepared state).

2.3. RESULTS AND DISCUSSION

2.3.1. Copolymer Solution Concentration Using Chloroform As the Spreading Solvent

One obvious change that occurs during barrier compression in the solvent-assisted technique used previously by us[24] is an effective increase in the surface concentration (density) of the polymer. This led us to investigate, first of all, the effect of the concentration of the spread copolymer solution on the morphology of the monolayer films when using the standard Langmuir technique that includes waiting for complete solvent evaporation before barrier compression.

Figure 2-2a–f presents AFM images of monolayer films of PS-PVP/PDP (1.0:1.0 VP:PDP molar ratio) prepared from chloroform solutions having copolymer concentrations that range from 0.10 to 1.75 mg/mL for identical total mass of material spread, and transferred to mica at a surface pressure (π) of 10 mN/m. These images show that nanodots and planar aggregates (up to 500 nm in diameter) are predominant at lower concentrations (0.10 and 0.35 mg/mL), in agreement with what we found previously for the 0.35 mg/mL solution using the standard Langmuir procedure (the same concentration that produced the nanostrand network using the "solvent-assisted" procedure).[24] At intermediate concentrations (0.75 and 1.00 mg/mL), elongated or rod-like structures (along with some nanostrand network for the higher concentration) appear, but they tend to be short and are mixed with nanodots and other small (irregular) aggregates. At the highest concentrations

(1.35 and 1.75 mg/mL), the nanostrand network, composed of strands [6±1 nm in height, 60±10 nm in width at half-height (Figure 2-2h), and up to more than 10 μm in length] that are more or less laterally disordered and interconnected by three-branch junction points, is the almost exclusive morphology observed. Dangling strand ends are also visible, especially for the lower concentration solution. The same copolymer without PDP does not lead to nanostrand formation, but to variably sized rounded aggregates at low spreading solution concentration and to very large platelets at high concentration. It is noteworthy that the Langmuir isotherms (Figure 2-2g), discussed previously in comparison with those for PS-PVP and PDP,[24] are very similar for low and high concentrations, especially at the pressures of 5 and 10 mN/m typically employed for film transfer. This indicates that the morphological differences in the films do not significantly impact the surface pressure evolution with molecular area for the concentration range investigated.

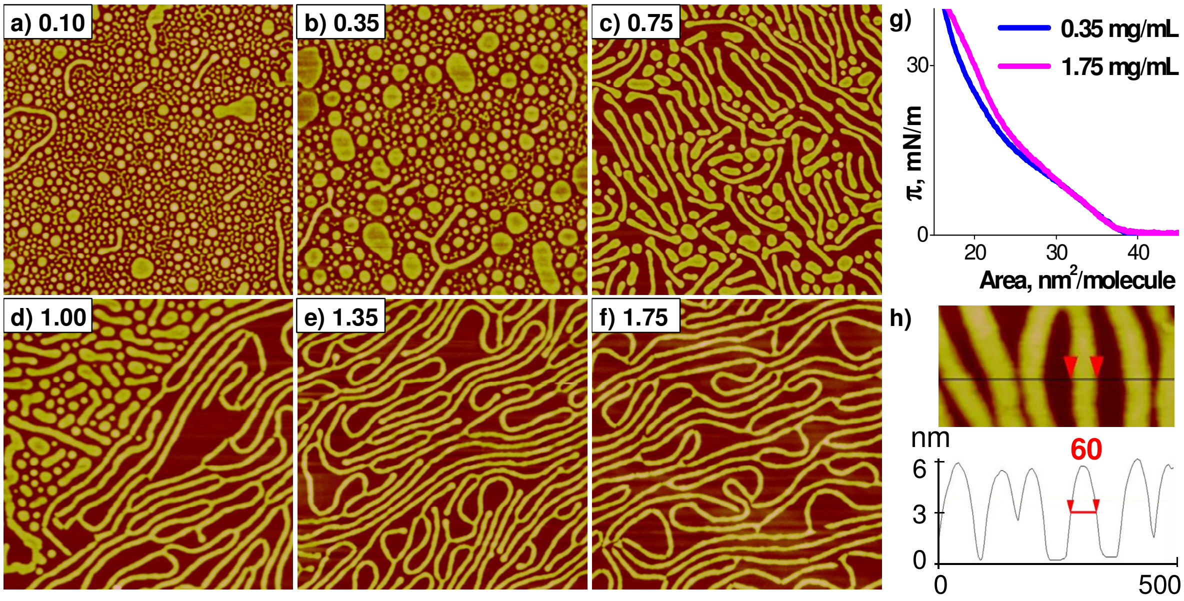

Figure 2-2. a–f) AFM height images (3×3 μm) of LB monolayers of PS-PVP/PDP$_{1.0}$ formed at 20°C from chloroform solutions of the copolymer concentrations (in mg/mL) indicated, and transferred to mica at π=10 mN/m. g) Langmuir compression isotherms of PS-PVP/PDP. h) Cross-section of height image (250x500 nm).

Clearly, use of a sufficiently high spreading solution concentration is a key parameter for obtaining the nanostrand network morphology. The importance of concentration is illustrated also by another experiment involving a modified Langmuir-Schaefer (LS) technique, where a single drop (*ca.* 10 μL) of a PS-PVP/PDP (1.0:1.3) solution of high concentration (2.05 mg/mL) was deposited on the water surface above one end of a submerged substrate. After removal of the water, AFM images, shown in Figure 2-3, were taken at defined distances from the spot above which the drop was deposited. This series of images shows optimal nanostrand network formation within a few centimeters of the deposition spot and short nanostrands mixed with nanodots, along with poor surface coverage, in the areas furthest from the deposition spot. This morphology evolution can be correlated with a decrease in local polymer concentration (density) in moving away from the deposition spot. The LS film morphology also shows that the nanostrands are not induced by the LB (vertical) transfer. Given that this LS experiment (and some others described below) was conducted with solutions having a small excess of PDP relative to VP, it must be specified that LB experiments at various VP:PDP molar ratios, to be described in detail in a subsequent paper, show that there is no difference in morphology obtained for 1.0:1.0 to 1.0:1.3 molar ratios.

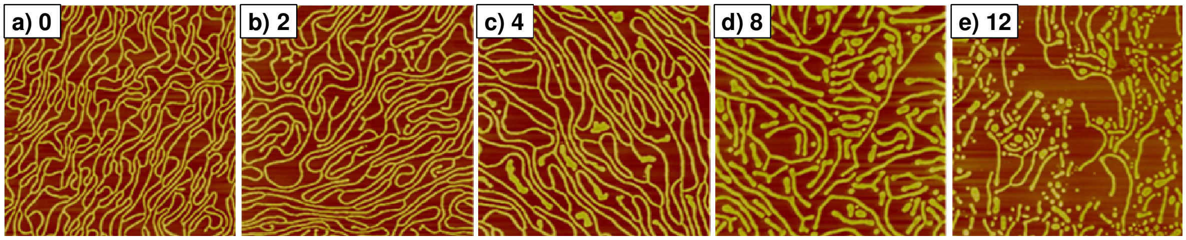

Figure 2-3. AFM images (5×5 μm) of a Langmuir-Schaefer film of PS-PVP/PDP$_{1.3}$ obtained from a single drop of $CHCl_3$ copolymer solution having a concentration of 2.05 mg/mL. The numbers indicate the position in centimeters of the area imaged relative to the area where the drop was deposited.

The influence of the concentration of the spreading solution on the LB film morphology was observed previously by Devereaux and Baker[15] and by Cheyne and Moffitt[16,17] for PS-PEO [PEO: poly(ethylene oxide)] diblock copolymers. In the first case,[15] where PEO constitutes 7 wt% of the polymer, low concentration favours nanodot formation and high concentration favours planar aggregates ("continents"), although both morphologies are generally coexistent. Nanostrands ("spaghetti") are also present for most concentrations, but cover less than half, often only a small fraction, of the film area. In the second case,[16,17] involving 11.4 wt% PEO, mixed morphologies of nano-dots and -strands were observed at most concentrations studied, along with a high proportion of rings and chains at the lowest concentration and a network of what were interpreted as dewetted rims at the highest concentration.

2.3.2. Other Spreading Solvents

Chloroform is the most common spreading solvent used to prepare Langmuir monolayers. However, solvent can be used as a tool to maintain mobility in the system for longer times by turning to ones that evaporate more slowly. To this end, we investigated the use of 1,2-dichloroethane ($C_2H_4Cl_2$) and 1,1,2,2-tetrachloroethane ($C_2H_2Cl_4$), chemically similar to chloroform but with lower vapour pressures (v.p. = 160, 87, and 8 mm Hg at 20°C for $CHCl_3$, $C_2H_4Cl_2$ and $C_2H_2Cl_4$, respectively), as well as hexachloropropene (C_3Cl_6; v.p. = 4 mm Hg at 100°C) and nitrobenzene ($PhNO_2$; v.p. = 0.15 mm Hg at 20°C). It was noted that $C_2H_2Cl_4$ solution appears to spread more slowly than $CHCl_3$ and $C_2H_4Cl_2$ solutions; *i.e.*, the spreading $C_2H_2Cl_4$ drops were visible by eye for a few seconds, in contrast to drops of the other two solvents. $PhNO_2$ spreads relatively little (and is malodorous), whereas C_3Cl_6 does not spread at all and was therefore mixed with $C_2H_2Cl_4$ (50/50 v/v), which allowed limited spreading. Langmuir isotherms using these solvents, given in the Supporting Information, are all similar in form to that using $CHCl_3$, with the shift to somewhat lower molecular areas for $C_3Cl_6/C_2H_2Cl_4$ probably a consequence of its very incomplete spreading. Overall, these isotherms again indicate relatively little sensitivity to the morphological differences described below.

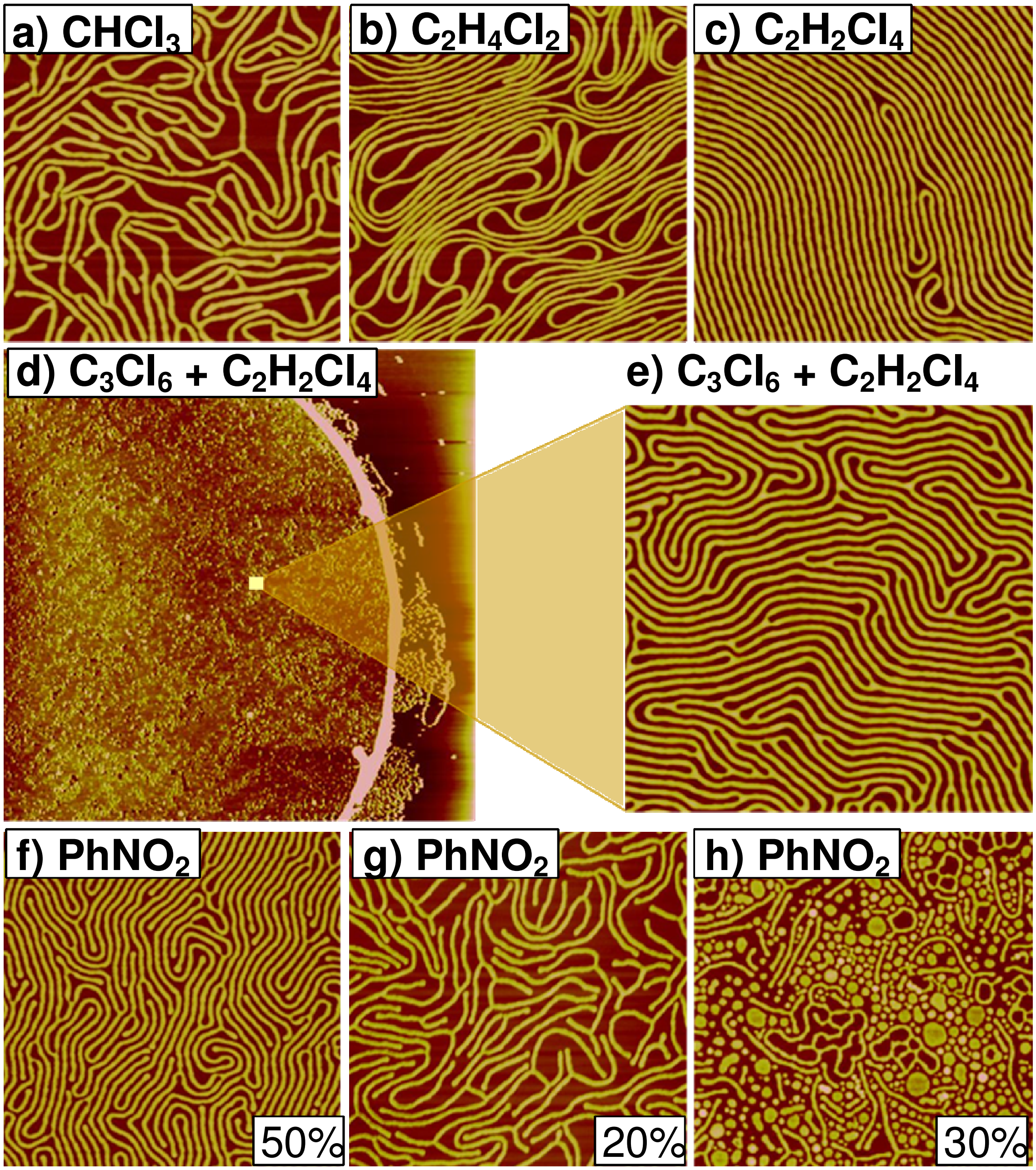

Figure 2-4. AFM height images of PS-PVP/PDP (1.0:1.2) monolayers deposited from 1.80–1.90 mg/mL solutions for the spreading solvents indicated (T=20–21°C, π=5 mN/m). Scan size: a–c, e–h) 3×3 μm; d) 100×100 μm. Numbers refer to % area covered by the morphology shown (>80% if not indicated).

AFM images of PS-PVP/PDP (1.0:1.3) LB films obtained at low surface pressure (5 mN/m) using the different spreading solvents with high copolymer concentration (1.80–1.90 mg/mL) are compared in Figure 2-4a–c. The nanostrand morphology is obtained from both $C_2H_4Cl_2$ and $C_2H_2Cl_4$ solutions, but with differing density and alignment of the strands. The morphology obtained using $C_2H_4Cl_2$ is similar to that using $CHCl_3$, with the nanostrands in significant lateral disorder in both cases, with only a mildly greater degree of strand alignment and density for $C_2H_4Cl_2$. In addition, almost no interjection of other morphological features was observed for $C_2H_4Cl_2$ (based on two trials) compared with 5 to 20% for $CHCl_3$ (considering many different trials). In contrast, when using $C_2H_2Cl_4$, which has a much lower vapor pressure than the other two solvents and thus evaporates significantly more slowly from the water surface, strand density is generally close to maximal due to a very high degree of nanostrand alignment along with few branching points and strand ends. This results in smooth and uniform strands – composed of elevated PS stripes (light regions in the AFM phase image) separated by monolayer-thin PVP/PDP stripes (dark regions in the phase image) – that are extremely long, more than 30 microns. There are also spaces (often large) with no material on the mica substrate, indicating incomplete spreading, as well as a few places with more disordered strands. It may be added that no correlation was found between strand alignment and substrate withdrawal direction.

The reduced spreading ability of $PhNO_2$ and especially $C_3Cl_6/C_2H_2Cl_4$ results in large circumscribed areas of material (visible by optical microscopy and also observed using the LS technique), as illustrated in Figure 2-4d. Within these areas, a dense form of the nanostrand network – *i.e.* highly mutually aligned nanostrands – is observed (Figure 2-4e,f). This pattern actually resembles the "fingerprint" texture often observed in thin block copolymer films obtained by spin- and dip-coating, including in films of similar thickness to LB monolayers.[21,22,35–41] For $C_3Cl_6/C_2H_2Cl_4$, there is little interjection of other morphologies, whereas for $PhNO_2$ (Figure 2-4f–h), the dense fingerprint texture (*ca.* 50%) is the main texture observed, but there are also areas of the more disordered nanostrand network (*ca.* 20%) and areas of a mixed morphology (*ca.* 30%) of nanodots / short nanostrands / planar aggregates (when large, the latter sometimes contain holes as in “nanofoams”[42] and occasionally appear in the form of interconnected “dewetted rims”[17]).

2.3.3. Subphase Temperature

Reducing the temperature of the subphase, which reduces the evaporation rate of the spreading solvent, is another way to prolong the presence of solvent and therefore the time period of polymer mobility. The effect of a low subphase temperature on the morphology using $C_2H_2Cl_4$ as the spreading solvent is shown in Figure 2-5b,c. In comparison with the morphology obtained at 20–21°C, that obtained at 8–9°C shows highly mutually aligned strands with far fewer loops and turns. Furthermore, the densely aligned nanostrand pattern extends over areas that are much larger, as shown in Figure 2-5b for an 8×8 μm^2 region and in the Appendix to Chapter 2 for a 30×30 μm^2 region (Figure SI-2-2). No areas with the disordered nanostrand network morphology were observed, but there were more and larger empty areas, in line with the greater packing density of the areas with material. In contrast, when using $CHCl_3$, lowering the temperature to 8–9°C has only a minor effect on the morphology (Figure 2-5a): here, the nanostrands, while also extending over large areas, remain disordered on the 2D surface, with many loops, turns, branching points and loose packing, and essentially only the number of strand ends is reduced. Use of a dilute (0.37 mg/mL) $C_2H_2Cl_4$ solution does not yield the dense nanostrand pattern, either at ambient or low temperature (instead, short nanostrands mixed with nanodots and planar aggregates are observed, as shown in the Appendix, Figure SI-2-3), indicating again the key role of spreading solution concentration.

The 10×10 μm image shown in Figure 2-5c, where the edge of a densely aligned nanostrand domain was captured, is also of interest. First, it shows that the aligned strands are highly parallel to the domain edge, which suggests that the nanostrand pattern is susceptible to macroscopic alignment. Indeed, it has recently been shown that macroscopic alignment is achievable on chemically patterned substrates,[43] although this was for LB transfer of the already-formed nanostrand network, whereas the alignment shown in Figure 5c presumably occurred in the course of morphology formation on the water surface. Second, only three defects, two single-loop ones and one double-loop one (which can also be considered as two neighboring defects, since each isolated single-loop defect is in the same strand as one loop in the paired defect), are visible in the area shown. Third, there are a few isolated nanostrands in the area outside of the dense nanostrand domain, which will be commented on in the discussion below.

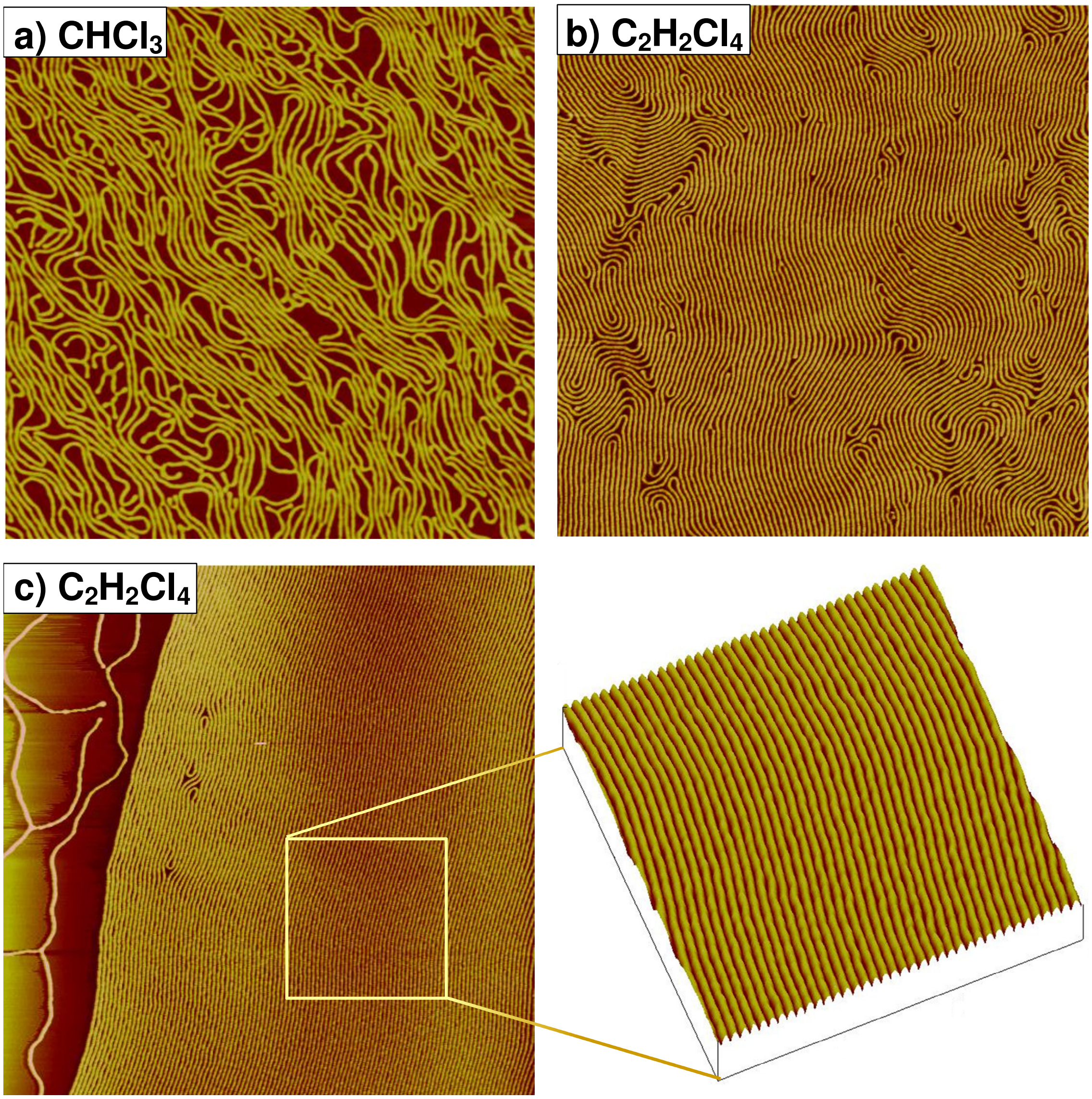

Figure 2-5. AFM height images of PS-PVP/PDP (1.0:1.3) monolayers spread at 8°C, using the solvents indicated and a copolymer solution concentration of 1.85 mg/mL, and transferred to mica at π=5 mN/m. Scan size: a,b) 8×8 μm; c) 10×10 μm (zoom: 3×3 μm).

The widths and heights of the nanostrands obtained using the different solvents and at the two different temperatures appear relatively constant within experimental uncertainty. Considering various measurements of sufficiently isolated strand segments, heights are generally 6±1 nm and the widths at half-height 70±20 nm (where the higher numbers are most likely due to imaging with blunter AFM tips). These dimensions are comparable to those found for other PS-based block copolymers showing cylindrical type morphology in LB films,[8,9,15,16] with the height being similar to the (collapsed) random coil radius of the PS block segment as in ref. 8 and reflecting the hydrophobicity of PS, and the width more than ten times larger, reflecting laterally stretched PS chains[8] and/or the overlapping of several PS chains[16] across the strand. Periodicities of parallel, closely spaced strand segments are generally in the 70-100 nm range (78 nm for the zoomed image in Figure 2-5c, where the large number of parallel strands allows a particularly accurate measurement). This corresponds to closest approach spacings between the strands of roughly 30 nm, similar to twice the extended length of the PVP block segment (13 nm). This is consistent with PVP being located as a surface-adsorbed monolayer alongside the strands (and therefore too thin to distinguish from the bare surface in AFM images of isolated strand segments), again in accordance with previous studies, particularly on a system based on n-alkylated PS-PVP block polyelectrolytes where the alkyl chains are covalently bonded to the PVP block, therefore with a molecular architecture like that of the present PS-PVP/PDP system (albeit ionic).[8,9] Presumably, PDP hydrogen-bonded to PVP lies more or less parallel to the water surface at low pressures, as determined by X-ray and neutron reflectivity for the alkyl chains of n-alkylated PS-PVP (with nanodot morphology).[44,45]

2.3.4. Surface Pressure

All of the LB films imaged above were transferred at relatively low surface pressure (≤ 10 mN/m). It is of interest to examine possible effects of this parameter on the film morphology, shown in Figures 2-6 and 2-7 for spreading solvents, $CHCl_3$ and $C_2H_2Cl_4$, respectively.

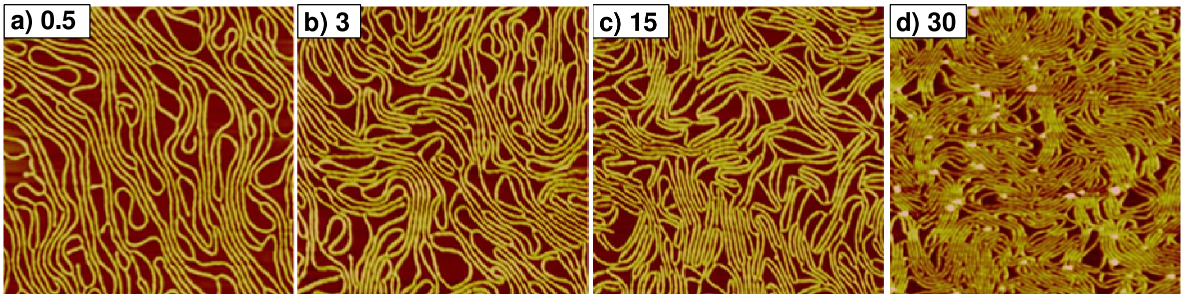

Figure 2-6. AFM height images (5×5 μm) of PS-PVP/PDP$_{1.0}$ monolayers spread from a 1.80 mg/mL $CHCl_3$ solution (subphase temperature 20°C), an transferred to mica at the surface pressures (in mN/m) indicated.

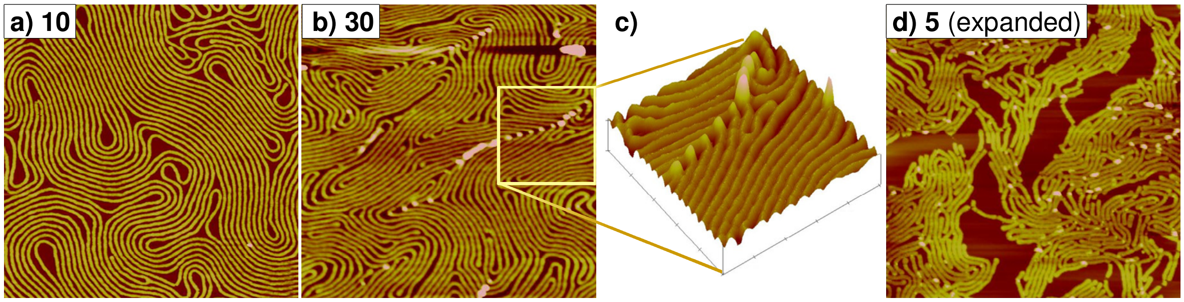

Figure 2-7. AFM height images (a,d: 5×5 μm, b: 3×3 μm, c: 1×1 μm) of PS-PVP/PDP$_{1.3}$ monolayers spread from a 1.90 mg/mL $C_2H_2Cl_4$ solution (subphase temperature 9°C), and transferred to mica at the surface pressures (in mN/m) indicated; a–c) in compression cycle, d) after expansion from 30 mN/m.

First, it must be emphasized that low concentration solutions (0.35 mg/mL) do not yield the nanostrand network morphology even at high transfer surface pressure, in accordance with what we reported previously.[24] On the other hand, as shown in Figure 6, spreading from a high concentration solution (1.75–1.80 mg/mL) gives nanostrands from very low (0.5 mN/m) up to high (at least 40 mN/m) surface pressure. Only strand density tends to increase with surface pressure (most obvious when comparing very different surface pressures), with separated strand widths and heights unaffected. This indicates that the nanostrand network forms soon after solution deposition and that barrier compression simply pushes the network strands closer together. At 30–40 mN/m, the transferred film appears buckled in some places, especially where the nanostrands make sharp turns (observed as bright spots in the AFM height images, indicating greater heights; see Figures 2-6d and 2-7b–d). These buckled films remain buckled after barrier expansion to low surface pressure and open cracks appear within the dense nanostructured areas throughout the film, illustrated by the image in Figure 2-7d, indicating significant irreversible interstrand “sticking”.

2.3.5. General Discussion and Proposed Mechanism of Nanostrand Network Formation

The above results show that it is possible, under suitable conditions, to obtain the nanostrand morphology from PS-PVP/PDP block copolymers over large surface areas quite uniformly and reproducibly. One of these conditions, not investigated here, is the proper choice of block ratio that favours elongated nanostructures (12 mol% PVP/PDP content worked very well in the present case), just as found for other systems investigated as a function of block copolymer composition.[8–12] In particular, LB monolayers of architecturally similar n-decylated PS-PVP show cylindrical-like morphology (*i.e.* relatively short nanostrands) in the 6-14 mol% VP range.[9] (The morphology evolution in LB films of PS-PVP with change in block ratio both with and without PDP present, showing the restricted composition range in which nanostrand morphology is found, will be addressed in a forthcoming paper.) The nanostrand morphology is thus considered to be a special case of the general class of elongated morphologies observed in LB block copolymer monolayers (see 2.1. Introduction), where the illustration in Figure 2-1 represents a nanostrand segment; that is, an elevated PS core forms the backbone of the nanostrands and this backbone is lined alongside (and probably underneath) by a PVP/PDP monolayer adsorbed to the water surface.

The present work has shown, using the standard Langmuir technique, that the concentration of the spreading solution is a key parameter for obtaining the nanostrand morphology with PS-PVP/PDP(12 mol%) (discussed further below). In addition, use of a less volatile spreading solvent and lowering of the subphase temperature are favourable to nanostrand formation as well as to high mutual alignment of the strands. The latter can be attributed, at least in part, to the increased residence time of the spreading solvent on the water surface, which increases the period of polymer mobility during which self-assembly and morphology development can take place. Furthermore, the presence of PDP plays a role, since without it nanostrands are not found. First, it no doubt contributes to the total volume of the hydrophilic block and thus to the appropriate block composition favouring this morphology. In addition, its low molecular weight, amphiphilic, and liquid crystal character may be important for the high surface coverage of the nanostrand morphology. As a small molecule that is presumably largely hydrogen-bonded to VP as an effective side chain throughout the process, it can behave as an internal plasticizer for PVP and thus contribute to mobility in the system (recognizing, however, that the hydrophilic PVP itself maintains significant mobility on the water surface). As a liquid crystal when H-bonded to PVP[34] and/or as an amphiphilic surfactant, it may also directly aid in the surface organization. An analogous effect was reported for the addition of a polar liquid crystal, 4'-pentyl-4-cyanobiphenyl, to a solution of an approximately symmetric PS-PVP diblock copolymer, which was shown to facilitate the development of a highly regular nanodot array in LB films.[46]

In considering the complex monolayer-forming process during which the surface conditions continuously evolve, it must be kept in mind that the solution concentrations used are an order of magnitude smaller than the critical overlap concentration (greater than 50 mg/mL), as analyzed in ref. 15 for a similar PS block molecular weight (7,700 g/mol higher than in the present case), indicating the absence of entanglements initially. Then, as the drops spread and as solvent evaporates, the block copolymer chains tend to aggregate and possibly entangle at the level of the hydrophobic PS blocks, while undergoing morphological reorganization in response to their changing local concentration, to their increasing exposure to water and air, and to their increasingly ultrathin film confinement, until they are vitrified (partially or completely, or in distinct stages) or until final equilibrium is reached, whichever comes first.[47] Possibly, during a certain initial period of the solvent spreading/evaporation process, the system is in equilibrium with the instantaneous thermodynamic conditions until at some point it begins to lag behind, then increasingly so until parts or all of the system become frozen in. Only systems that maintain sufficient mobility throughout the entire process are at equilibrium at the final conditions of complete surface coverage, which is undoubtedly rare for polymers.

Baker and coll. and Moffitt and coll. have discussed previously how various morphologies including nanostrands are kinetic structures trapped by vitrification at different stages in the complex process.[15–17] This was supported by numerical simulations that showed that a sufficiently concentrated solution can go through a stage of (short) strand-like structures during drop spreading that, if vitrified before further evolution, compose the final morphology of the Langmuir film, but, if still mobile, break up into dots.[47] Applied to the present case, this picture indicates that drops of more concentrated PS-PVP/PDP solution, implying initially high polymer density at the water surface, are more likely to achieve the strand morphology and, because less solvent is present, can become vitrified in this form before breakup into nanodots can occur. In contrast, many drops of more dilute solution (for the same total mass on the surface), implying lower polymer density at the water surface from the start, may not even go through the nanostrand stage,[47] or, if they do, there is enough solvent left to allow breakup into nanodots before vitrification sets in. Moffitt and coll. proposed another mechanism where the various morphologies in LB films are a consequence of dewetting phenomena that occur during the continuously evolving process following drop deposition, and that nanostrands, in particular, are formed from the breakup of dewetted rim networks at their junction points.[17] On the other hand, Chang and coll. suggested that isolated surface micelles can be induced under special conditions (in their case by reducing the subphase pH, which ionizes the P2VP block) to aggregate into a necklace-type network[48] that may further coalesce[27] into a nanostrand network if sufficient mobility remains. This latter mechanism might perhaps apply to the morphology transition from nanodots to nanostrand network with increase in surface pressure that was observed for the PS-PFS/PS-P2VP blend reported in ref. 25 (see 2.1. Introduction).

The observation, in the present work, of the fingerprint morphology using poorly spreading solvents ($PhNO_2$ and $C_3Cl_6/C_2H_2Cl_4$) suggests still another possible mechanism of nanostrand formation. First, to comment on the fingerprint morphology itself, it should be pointed out that in poorly spreading solvents, the polymer density within the spreading drop remains high as the solvent evaporates and spreading is far from complete before immobility sets in. It is reasonable that, in these concentrated drops, the block copolymer can self-assemble into the same fingerprint morphology as observed under certain conditions for spin- or dip-coated films on hard polar surfaces (only partially understood for asymmetric diblock copolymers[21,39]). This fingerprint morphology (Figure 2-4d,e and 2-4f–h) is composed of meandering stripes of alternating PS and PVP/PDP domains in a locally coherent film, probably also with a “wetting layer”[37] (a monolayer adsorbed to the polar substrate) of the hydrophilic block below the PS parts. (It should be noted that, because the film thickness is much smaller than the lateral periodicity, the fingerprint pattern can be viewed indifferently as a thin slice through either end-on stacked lamellae or horizontally lying cylinders of the microphase-separated block copolymer.[8,35]) For $C_2H_2Cl_4$ as solvent, which spreads faster than $PhNO_2$ and $C_3Cl_6/C_2H_2Cl_4$ but not as fast as $CHCl_3$, and which has a relatively long residence time on the water surface compared to $CHCl_3$, the morphology obtained (Figure 2-4c) can be considered to be a more perfected version of the fingerprint morphology with fewer defects in the form of strand ends, forks and loops, allowing extensive mutual alignment of extremely long strands, especially at lower subphase temperature (Figure 2-5b,c) where the solvent resides for an even longer time. The greater spreading of $C_2H_2Cl_4$ compared to $PhNO_2$ and $C_3Cl_6/C_2H_2Cl_4$ may also allow more space for what can be considered as effective solvent annealing to take place, while still maintaining high polymer density during the self-assembly process.

What we now propose is the following mechanism for nanostrand formation, illustrated in Figure 2-8. First, spreading drops of sufficiently concentrated $CHCl_3$ solutions are considered to pass through a fingerprint morphology stage, the PS stripes become vitrified in this stage, then, as the drops continue to spread, the fingerprints break up (*i.e.* disassemble) at the level of the hydrophilic PVP/PDP stripes, which remain mobile (and unentangled, being relatively short) on the water surface. This allows the strands to separate from one another to float more or less individually on the water surface – within the constraints of the allowed space and of the interconnectivity at the level of the PS stripes (the latter leading to the network aspect) – as drop spreading continues until completion, thus forming the loosely structured (*i.e.* disordered) nanostrand network morphology. The few such free strands observed in Figure 2-5c for $C_2H_2Cl_4$ at low subphase temperature can be interpreted as having separated in this way from the rest of the structure shown.

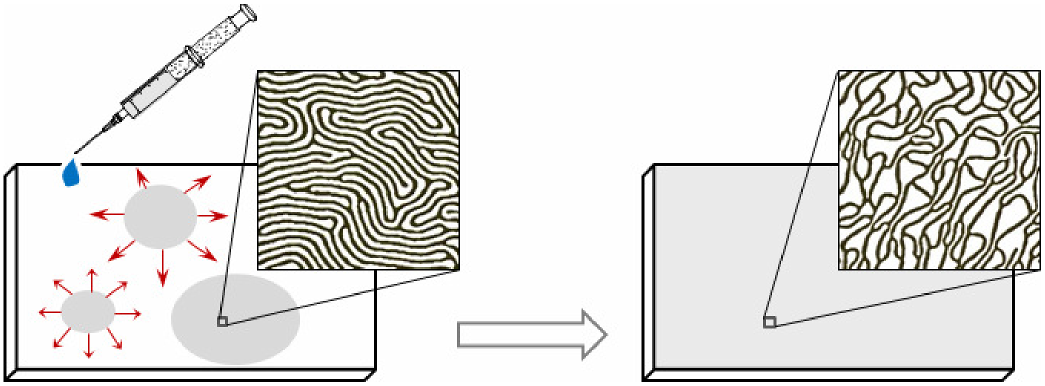

Figure 2-8. Model illustrating fingerprint to nanostrand network formation: the fingerprint morphology (left, with black and white stripes representing phase-separated PS and PVP/PDP domains, respectively) forms in concentrated drops of PS-PVP/PDP solution spreading on the water surface, with immobilization occurring in the hydrophobic PS stripes, then upon further spreading this fingerprint pattern disassembles at the level of the hydrophilic and mobile PVP/PDP stripes to form the nanostrand network (right, with black lines representing floating, interconnected PVP/PDP-lined PS nanostrands).

This mechanism is analogous to what was obtained in bulk (3D) films of PS-PVP/PDP having cylindrical PS domains in a PVP/PDP matrix, where a selective solvent for PDP caused the disassembly of the cylindrical bulk structure into PVP-coated nanofibers with PS cores (interestingly, with a PS core diameter of 25 nm, which compares well with the nanostrand widths taking into account the PS molecular weight, which is half that used in the present work).[49] Furthermore, the uniformity in width and height of the nanostrands is consistent with the characteristic lateral spacing of the fingerprint pattern. The interconnection of strands *via* triple-strand junctions and the random presence of dangling strands in the nanostrand network, as well as the great lengths and smooth twists and turns of the nanostrands, are also consistent with what is observed in the fingerprint texture. Finally, the extensive coverage of the nanostrand network over the surface would reflect the uniformity of the fingerprint texture in essentially all of the spreading drops.

The fingerprint-to-nanostrand network mechanism is not necessarily to be construed as a replacement for the other mechanisms proposed in the literature. In other words, there may be more than one way to arrive at the nanostrand morphology: by direct polymer self-organization from a sufficiently concentrated and initially homogeneous solution spread on the air/water interface,[8,47] by the assembly of nanodots upon increasing the surface density of polymer when appropriate mobility is maintained in the system,[25,48] by the disassembly of a coherent film having a fingerprint morphology within spreading droplets of concentrated solution (this work), or from the breakup of a dewetted rim structure where the rims effectively concentrate the polymer material.[17] Future work should provide additional understanding of these different possibilities at the air/water interface.

2.4. CONCLUSIONS

Using the PS-PVP/PDP block copolymer system with 12 mol% VP content, where the PDP small molecule hydrogen bonds to the PVP block, we have shown that the disordered nanostrand network morphology with relatively few strand ends can be obtained reproducibly and uniformly over large surface areas using the standard Langmuir-Blodgett technique. A key condition for obtaining this morphology is the use of spreading solutions of relatively high polymer concentration, so that self-organization at the air/water interface takes place under conditions of high polymer density. The use of tetrachloroethane instead of chloroform as the spreading solvent and a low subphase temperature, both of which retard solvent evaporation and thus maintain polymer mobility at the water surface for longer periods, result in a pattern of densely packed, highly aligned nanostrands. This pattern may be considered as a perfected version of the nanostrand network due to solvent annealing. The poorly spreading solvents used, nitrobenzene and hexachloropropene / tetrachloroethane (50/50), produce the well-known fingerprint pattern observed in spin- and dip-coated thin films of block copolymers. The latter pattern leads to the proposal that a possible mechanism for nanostrand network formation, besides others proposed in the literature, is *via* the fingerprint morphology that may form in the course of spreading of concentrated drops. The hydrophobic PS stripes become vitrified in this morphology, whereas the hydrophilic PVP/PDP stripes remain mobile, such that, as drop spreading continues, the stripes disassemble at the level of these hydrophilic stripes, leaving PVP-lined PS nanostrands free to float into the form of a disordered network on the water surface.

References to Chapter 2:

1. Hamley, I. W. Nanotechnology with Soft Materials. *Angew. Chem. Int. Ed.* **2003**, *42*, 1692–1712.
2. Mendes, P. M.; Preece, J. A. Precision Chemical Engineering: Integrating Nanolithography and Nanoassembly. *Curr. Opin. Colloid Interface Sci.* **2004**, *9*, 236–248.
3. Hamley, I. W. Nanostructure Fabrication Using Block Copolymers. *Nanotechnology* **2003**, *14*, R39–R54.
4. Park, C.; Yoon, J.; Thomas, E. L. Enabling Nanotechnology with Self Assembled Block Copolymer Patterns. *Polymer* **2003**, *44*, 6725–6760.
5. Lazzari, M.; López-Quintela, M. A. Block Copolymers As a Tool for Nanomaterial Fabrication. *Adv. Mater.* **2003**, *15*, 1583–1594.
6. Li, M.; Coenjarts, C. A.; Ober, C. K. Patternable Block Copolymers. *Adv. Polym. Sci.* **2005**, *190*, 183–226.
7. Zhu, J.; Eisenberg, A.; Lennox, R. B. Interfacial Behavior of Block Polyelectrolytes. 1. Evidence for Novel Surface Micelle Formation. *J. Am. Chem. Soc.* **1991**, *113*, 5583–5588.
8. Zhu, J.; Lennox, R. B.; Eisenberg, A. Interfacial Behavior of Block Polyelectrolytes. 4. Polymorphism of (Quasi) Two-Dimensional Micelles. *J. Phys. Chem.* **1992**, *96*, 4727–4730.
9. Zhu, J.; Eisenberg, A.; Lennox, R. B. Interfacial Behavior of Block Polyelectrolytes. 5. Effect of Varying Block Lengths on the Properties of Surface Micelles. *Macromolecules* **1992**, *25*, 6547–6555.
10. Li, S.; Hanley, S.; Khan, I.; Varshney, S. K.; Eisenberg, A.; Lennox, R. B. Surface Micelle Formation at the Air/Water Interface from Nonionic Diblock Copolymers. *Langmuir* **1993**, *9*, 2243–2246.
11. Li, S.; Clarke, C. J.; Lennox, R. B.; Eisenberg, A. Two-Dimensional Self Assembly of Polystyrene-b-Poly(butyl-methacrylate) Diblock Copolymers. *Colloids Surf. A* **1998**, *133*, 191–203.
12. Cox, J. K.; Yu, K.; Constantine, B.; Eisenberg, A.; Lennox, R. B. Polystyrene–Poly(ethylene oxide) Diblock Copolymers Form Well-Defined Surface Aggregates at the Air/Water Interface. *Langmuir* **1999**, *15*, 7714–7718.
13. Baker, S. M.; Leach, K. A.; Devereaux, C. E.; Gragson, D. E. Controlled Patterning of Diblock Copolymers By Monolayer Langmuir–Blodgett Deposition. *Macromolecules* **2000**, *33*, 5432–5436.

14. Seo, Y.; Im, J.-H.; Lee, J.-S.; Kim, J.-H. Aggregation Behaviors of a Polystyrene-b-Poly(methyl methacrylate) Diblock Copolymer at the Air/Water Interface. *Macromolecules* **2001**, *34*, 4842–4851.
15. Devereaux, C. A.; Baker, S. M. Surface Features in Langmuir–Blodgett Monolayers of Predominantly Hydrophobic Poly(styrene)–Poly(ethylene oxide) Diblock Copolymer. *Macromolecules* **2002**, *35*, 1921–1927.
16. Cheyne, R. B.; Moffitt, M. G. Novel Two-Dimensional "Ring and Chain" Morphologies in Langmuir–Blodgett Monolayers of PS-b-PEO Block Copolymers: Effect of Spreading Solution Concentration on Self-Assembly at the Air–Water Interface. *Langmuir* **2005**, *21*, 5453–5460.
17. Cheyne, R. B.; Moffitt, M. G. Self-Assembly of Polystyrene-block-Poly(ethylene oxide) Copolymers at the Air–Water Interface: Is Dewetting the Genesis of Surface Aggregate Formation? *Langmuir* **2006**, *22*, 8387–8396.
18. Kumaki, J.; Hashimoto, T. Two-Dimensional Microphase Separation of a Block Copolymer in a Langmuir–Blodgett Film. *J. Am. Chem. Soc.* **1998**, *120*, 423–424.
19. Park, J. Y.; Liu, M.; Mays, J.; Dadmun, M.; Advincula, R. Nano-Donuts From pH-dependent Block Restructuring in Amphiphilic ABA Triblock Copolymers Vesicles at the Air/Water Interface. *Soft Matter* **2009**, *5*, 747–749.
20. Lopes, W.A. Nonequilibrium Self-Assembly of Metals on Diblock Copolymer Templates. *Phys. Rev. E* **2002**, *65*, 031606 (1–14).
21. van Zoelen, W.; ten Brinke, G. Thin Films of Complexed Block Copolymers. *Soft Matter.* **2009**, *5*, 1568–1582.
22. Nandan, B.; Gowd, E. B.; Bigall, N. C.; Eychmüller, A.; Formanek, P.; Simon, P.; Stamm, M. Arrays of Inorganic Nanodots and Nanowires Using Nanotemplates Based on Switchable Block Copolymer Supramolecular Assemblies. *Adv. Funct. Mater.* **2009**, *19*, 2805–2811.
23. Greiner, A.; Wendorff, G. H. Electrospinning: A Fascinating Method for the Preparation of Ultrathin Fibers. *Angew. Chem. Int. Ed.* **2007**, *46*, 5670–5703.
24. Lu, Q.; Bazuin, C. G. Solvent-Assisted Formation of Nanostrand Networks from Supramolecular Diblock Copolymer/Surfactant Complexes at the Air/Water Interface. *Nano Lett.* **2005**, *5*, 1309–1314.
25. Seo, Y.-S.; Kim, K. S.; Galambos, A.; Lammertink, R. G. H.; Vancso, G. J.; Sokolov, J.; Rafailovich, M. Nanowire and Mesh Conformations of Diblock Copolymer Blends at the Air/Water Interface. *Nano Lett.* **2004**, *4*, 483–486.

26. Kim, Y.; Pyun, J.; Fréchet, J. M. J.; Hawker, C. J.; Frank, C. W. The Dramatic Effect of Architecture on the Self-Assembly of Block Copolymers at Interfaces. *Langmuir* **2005**, *21*, 10444–10458.
27. Chung, B.; Park, S.; Chang, T. HPLC Fractionation and Surface Micellization Behavior of Polystyrene-b-Poly(methyl methacrylate). *Macromolecules* **2005**, *38*, 6122–6127.
28. Price, E. W.; Guo, Y.; Wang, C.-W.; Moffitt, M. G. Block Copolymer Strands with Internal Microphase Separation Structure *via* Self-Assembly at the Air−Water Interface. *Langmuir* **2009**, *25*, 6398–6406.
29. Kadota, S.; Aoki, K.; Nagano, S.; Seki, T. Morphological Conversions of Nanostructures in Monolayers of an ABA Triblock Copolymer Having Azobenzene Moiety. *Colloid Surface A* **2006**, *284–285*, 535–541.
30. Deschênes, L.; Bousmina, M.; Ritcey, A. M. Micellization of PEO/PS Block Copolymers at the Air/Water Interface: A Simple Model for Predicting the Size and Aggregation Number of Circular Surface Micelles. *Langmuir* **2008**, *24*, 3699–3708.
31. Xu, H.; Erhardt, R.; Abetz, V.; Müller, A. H. E.; Goedel, W.A. Janus Micelles at the Air/Water Interface. *Langmuir* **2001**, *17*, 6787–6793.
32. Peleshanko, S.; Jeong, J.; Gunawidjaja, R.; Tsukruk, V. V. Amphiphilic Heteroarm PEO-b-PS*m* Star Polymers at the Air−Water Interface: Aggregation and Surface Morphology. *Macromolecules* **2004**, *37*, 6511–6522.
33. Matmour, R.; Francis, R.; Duran, R. S.; Gnanou, Y. Interfacial Behavior of Anionically Synthesized Amphiphilic Star Block Copolymers Based on Polybutadiene and Poly(ethylene oxide) at the Air/Water Interface. *Macromolecules* **2005**, *38*, 7754–7767.
34. Ruokolainen, J.; Saariaho, M.; Ikkala, O.; ten Brinke, G.; Thomas, E. L.; Torkkeli, M.; Serimaa, R. Supramolecular Routes to Hierarchical Structures: Comb-Coil Diblock Copolymers Organized with Two Length Scales. *Macromolecules* **1999**, *32*, 1152–1158.
35. Fasolka, M. J.; Mayes, A. M. Block Copolymer Thin Films: Physics and Applications. *Annu. Rev. Mater. Res.* **2001**, *31*, 323–355.
36. Hamley, I. W. Ordering in Thin Films of Block Copolymers: Fundamentals to Potential Applications. *Prog. Polym. Sci.* **2009**, *34*, 1161–1210.
37. Tokarev, I.; Krenek, R.; Burkov, Y; Schmeisser, D.; Sidorenko, A.; Minko, S.; Stamm, M. Microphase Separation in Thin Films of Poly(styrene-block-4-vinylpyridine) Copolymer–2-(4'-Hydroxybenzeneazo)benzoic Acid Assembly. *Macromolecules* **2005**, *38*, 507–516.

38. Laforgue, A.; Gaspard, D.; Bazuin, C. G.; Prud'homme, R. E. Controlling Diblock Copolymer Nanopatterning and Nanoporosity on Surfaces Using Small Molecules. *Amer. Chem. Soc. Polym. Prepr.* **2007**, *48(1)*, 670–671.

39. van Zoelen, W.; Asumaa, T.; Ruokolainen, J.; Ikkala, O.; ten Brinke, G. Phase Behavior of Solvent Vapor Annealed Thin Films of PS-*b*-PVP(PDP) Supramolecules. *Macromolecules* **2008**, *41*, 3199–3208.

40. van Zoelen, W.; Polushkin, E.; ten Brinke, G. Hierarchical Terrace Formation in PS-*b*-PVP(PDP) Supramolecular Thin Films. *Macromolecules* **2008**, *41*, 8807–8814.

41. Tung, S.-H.; Kalarickal, N. C.; Mays, J. W.; Xu, T. Hierarchical Assemblies of Block-Copolymer-Based Supramolecules in Thin Films. *Macromolecules* **2008**, *41*, 6453–6462.

42. Meszaros, M.; Eisenberg, A.; Lennox, R. B. Block Copolymer Self-Assembly in Two Dimensions: Nanoscale Emulsions and Foams. *Faraday Discuss.* **1994**, *98*, 283–294.

43. Harirchian-Saei, S.; Wang, M. C. P.; Gates, B. D.; Moffitt, M. G. Patterning Block Copolymer Aggregates *via* Langmuir-Blodgett Transfer to Microcontact-Printed Substrates. *Langmuir* **2010**, *26*, 5998–6008.

44. Li, Z.; Zhao, W.; Quinn, J.; Rafailovich, M. H.; Sokolov, J.; Lennox, R. B.; Eisenberg, A.; Wu, X. Z.; Kim, M. W.; Sinha, S. K.; *et al.* X-ray Reflectivity of Diblock Copolymer Monolayers at the Air/Water Interface. *Langmuir* **1995**, *11*, 4785–4792.

45. Shin, K.; Rafailovich, M. H.; Sokolov, J.; Chang, D. M.; Cox, J. K.; Lennox, R. B.; Eisenberg, A.; Gibaud, A.; Huang, J.; Hsu, S. L.; *et al.* Observation of Surface Ordering of Alkyl Side Chains in Polystyrene/Polyelectrolytes Diblock Copolymer Langmuir Films. *Langmuir* **2001**, *17*, 4955–4961.

46. Nagano, S.; Matsushita, Y.; Ohnuma, Y.; Shinma, S.; Seki, T. Formation of a Highly Ordered Dot Array of Surface Micelles of a Block Copolymer *via* Liquid-Crystal-Hybridized Self-Assembly. *Langmuir* **2006**, *22*, 5233–5236.

47. Hosoi, A. E.; Kogan, D.; Devereaux, C. E.; Bernoff, A. J.; Baker, S. M. Two-Dimensional Self-Assembly in Diblock Copolymers. *Phys. Rev. Lett.* **2005**, *95*, 037801(1–4).

48. Chung, B.; Choi, M.; Ree, M.; Jung, J. C.; Zin, W. C.; Chang, T. Subphase pH Effect on Surface Micelle of Polystyrene-*b*-Poly(2-vinylpyridine) Diblock Copolymers at the Air-Water Interface. *Macromolecules* **2006**, *39*, 684–689.

49. Fahmi, A. W.; Braun, H.-G.; Stamm, M. Fabrication of Metallized Nanowires from Self-Assembled Diblock Copolymer Templates. *Adv. Mater.* **2003**, *15*, 1201–1204.

Appendix to Chapter 2

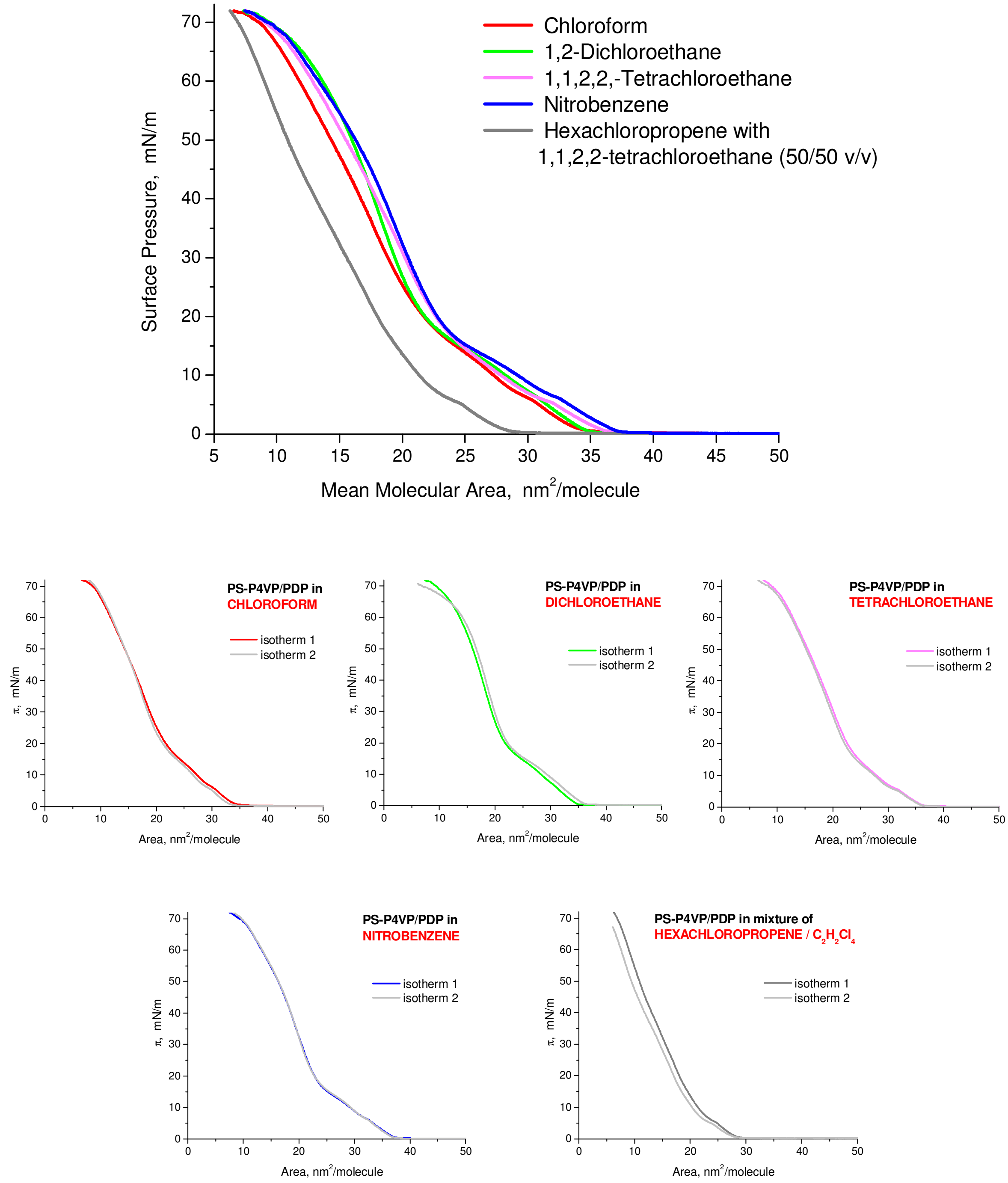

Figure SI-2-1. Langmuir compression isotherms of PS(40,000)-PVP(5,600)/PDP (VP:PDP=1.0:1.0) spread at 22±0.5°C water subphase using various solvents (copolymer concentration 1.80 mg/mL), reproduced twice each.

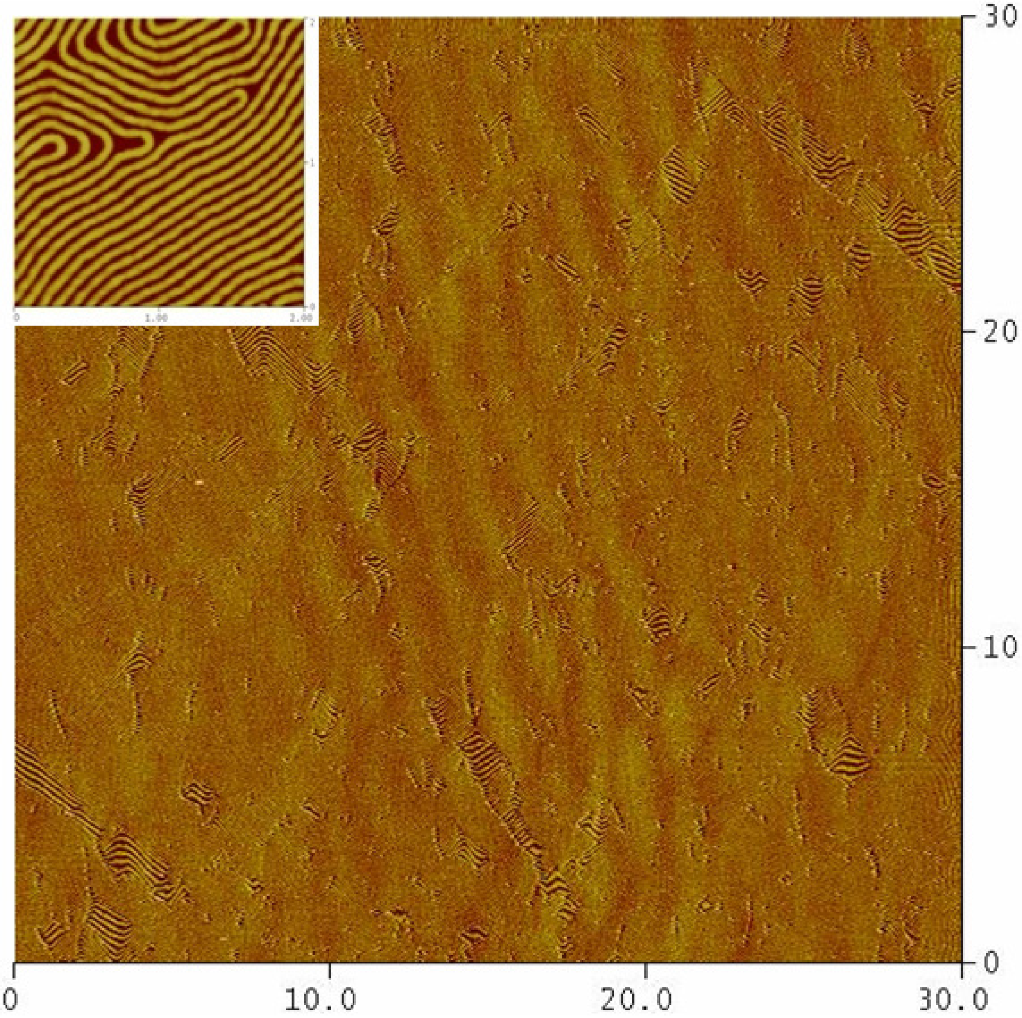

Figure SI-2-2. AFM height image (with close-up image in inset) of a PS-PVP/PDP (1.0:1.3) monolayer spread from a $C_2H_2Cl_4$ solution (subphase temperature 8°C), and transferred to mica at π=5 mN/m. Concentration of copolymer solution 1.87 mg/mL. Scale in µm.

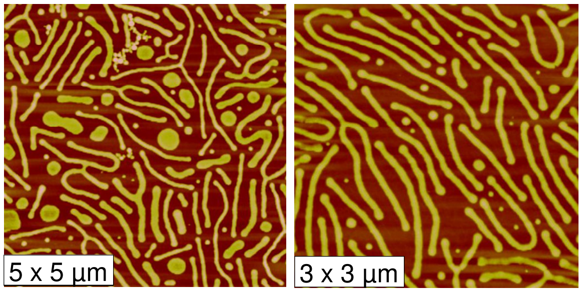

Figure SI-2-3. AFM height images of PS-PVP/PDP (1.0:1.0) spread from a dilute $C_2H_2Cl_4$ solution (subphase temperature 8°C), and transferred to mica at π=5 mN/m. Concentration of copolymer solution 0.37 mg/mL.

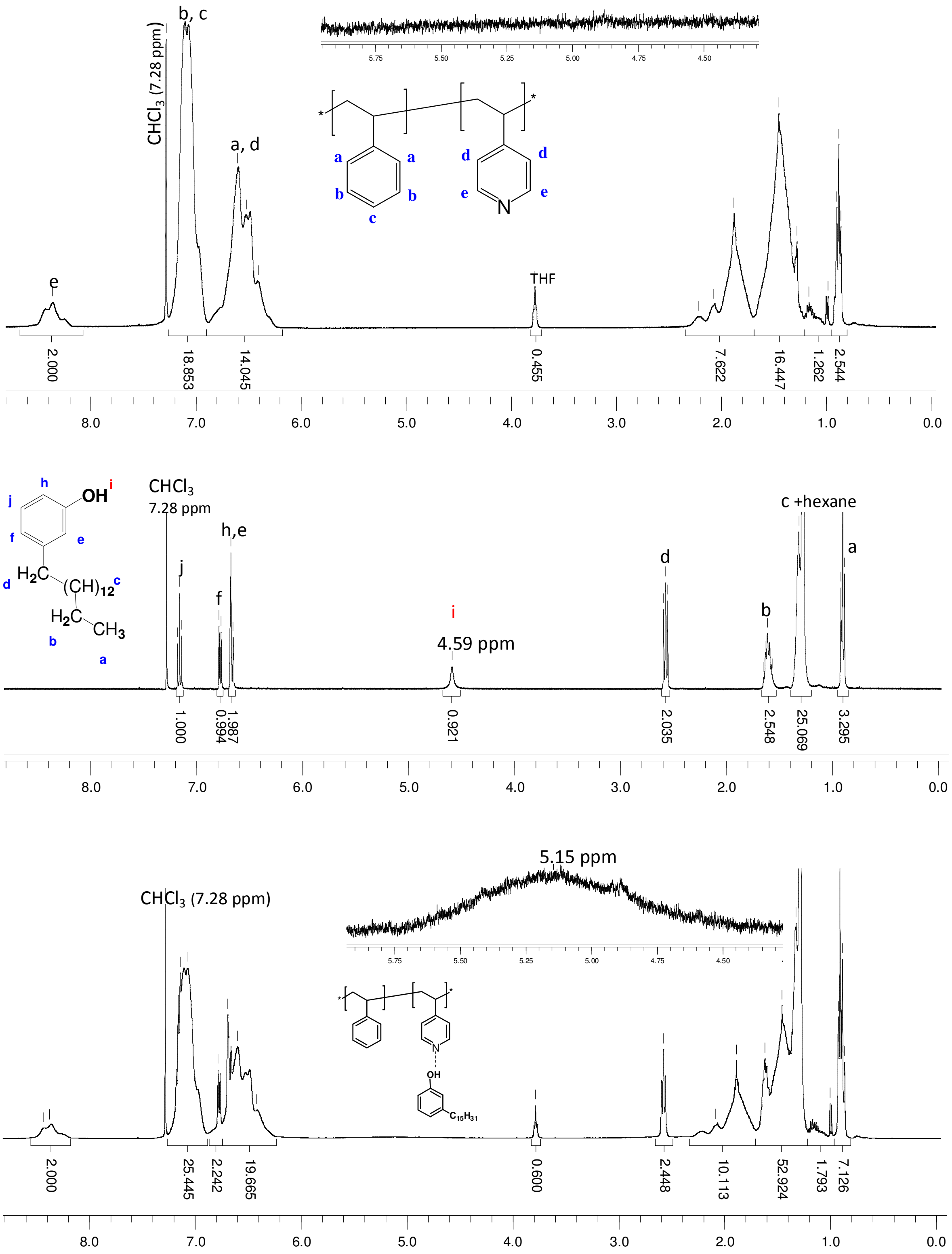

Figure SI-2-4. ^{1}H NMR spectra of PS$_{384}$-PVP$_{53}$ (*top*), PDP (*center*), and PS$_{384}$-PVP$_{53}$/PDP (1:1) (*bottom*) in CDCl$_3$.

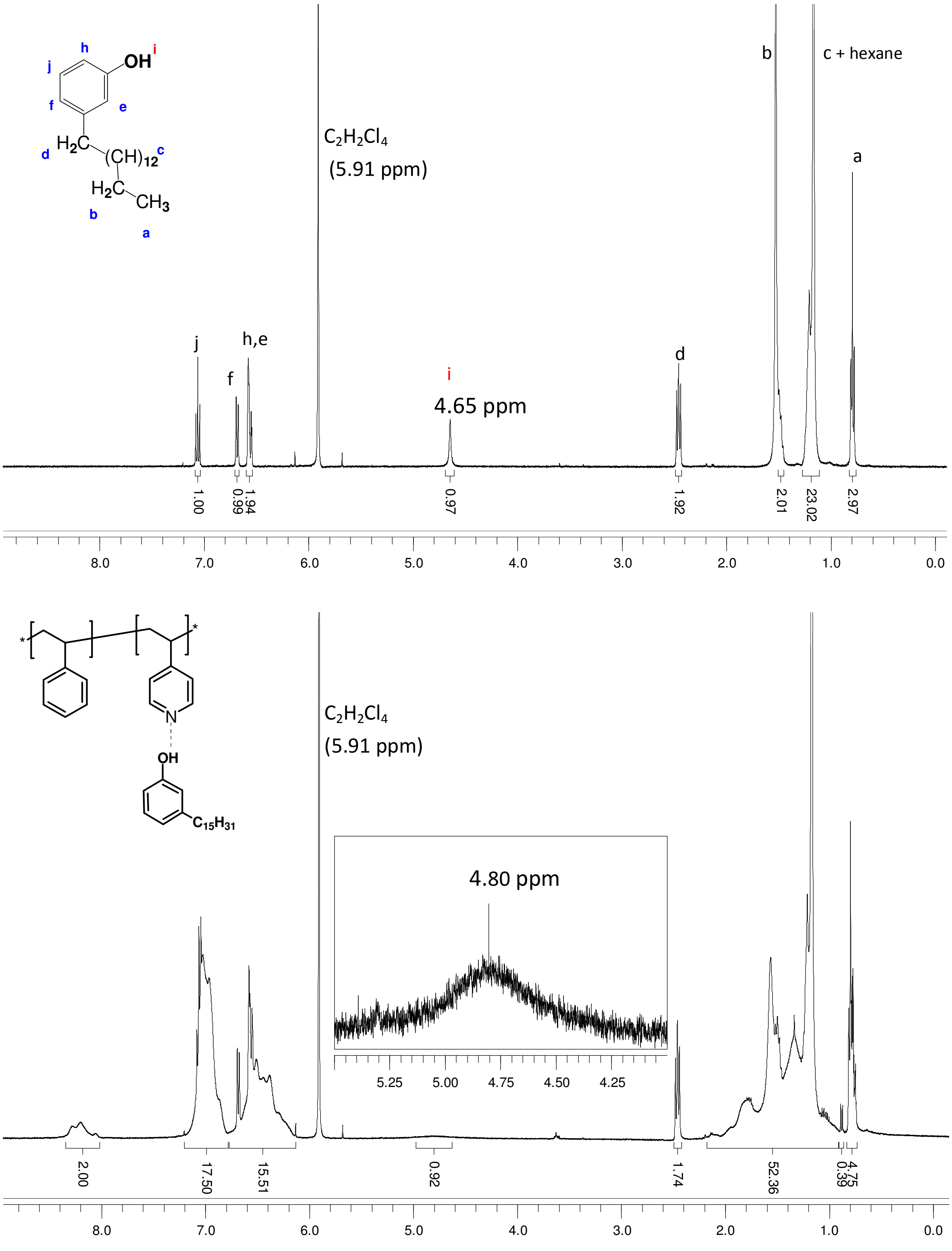

Figure SI-2-5. ^{1}H NMR spectra of PDP (*top*) and PS$_{384}$-PVP$_{53}$/PDP (1:1) (*bottom*) in $C_2D_2Cl_4$.

Characteristics of Solid Substrates

Mica was usually used as the substrate since it can be cleaved easily to produce a very flat clean surface. However, many applications require transparent or conducting surfaces. We observed that monolayers of the nanostrand network (obtained by using concentrated $CHCl_3$ solution) can be transferred onto any hydrophilic substrate, as tested on mica, silicon, quartz, glass, ITO glass, and gold, both by the LB (Figure SI-5a-i) and LS methods. It may be added that the flatter the substrate surface, the closer the transfer ratio was to unity. Since AFM imaging is better on flatter surfaces, it is preferable to use superwite flat glass (Schott; Figure SI-2-5d) rather than simple microscope glass (VWR) when depositions are made on glass microscope slides. In the case of ITO glass (Delta Technologies), two substrates of different resistivities (and different roughness) were tested (Figure SI-2-5g and SI-2-5i). The one with greater roughness prevented obtaining good height images (Figure SI-2-5g); however, the nanostrand network morphology is clearly distinguishable in the phase image (Figure SI-2-5h). The height images of the nanostrand network on the gold surfaces are also affected by surface roughness due to the cleaning procedures (Figure SI-2-5e–f). The nanostrand network could not be deposited by LB onto bare hydrophobic surfaces (HOPG) by withdrawing previously submerged substrates, but only by lowering the vertically suspended substrate into the water subphase after monolayer spreading. In this case, a bilayer is obtained, since a second layer is deposited during substrate withdrawal from the water (Figure SI-2-5j). A monolayer can be deposited onto HOPG using the LS method (Figure SI-2-5k).

Various substrates used:

- silicon (University Wafer),
- glass (VWR or Schott) and quartz (Technical Glass Products) microscope slides
- indium tin oxide (ITO) glass (Delta Technologies),
- gold (prepared in our lab by deposition of 80–85 nm gold onto glass and Si wafers),
- highly ordered pyrolytic graphite (HOPG) (SPI Supplies).

Description of Substrate Cleaning Processes

- Mica and HOPG were freshly cleaved;
- Silicon wafers were cleaned by the standard RCA-1 procedure[*]
  (5 parts H_2O and 1 part 27% NH_4OH were heated to 70 °C, then 1 part 30% H_2O_2 was added; the Si wafers were soaked in this solution for 15 min, followed by washing with flowing Milli-Q water);
- Glass and quartz microscope slides were cleaned using a Piranha solution (3:1 v/v mixture of concentrated H_2SO_4 and 30% H_2O_2);
- ITO glass was cleaned by sonication in different solvents (HPLC acetone, methanol, isopropanol) followed by plasma cleaning;
- Gold substrates were freshly prepared and stored in ethanol.

---

[*] Kern, W. *Handbook of Semiconductor Cleaning Technology. Science, Technology, and Applications*. Noyes Publications: Westwood (NJ, U.S.A.), 1993; Chapter 1.

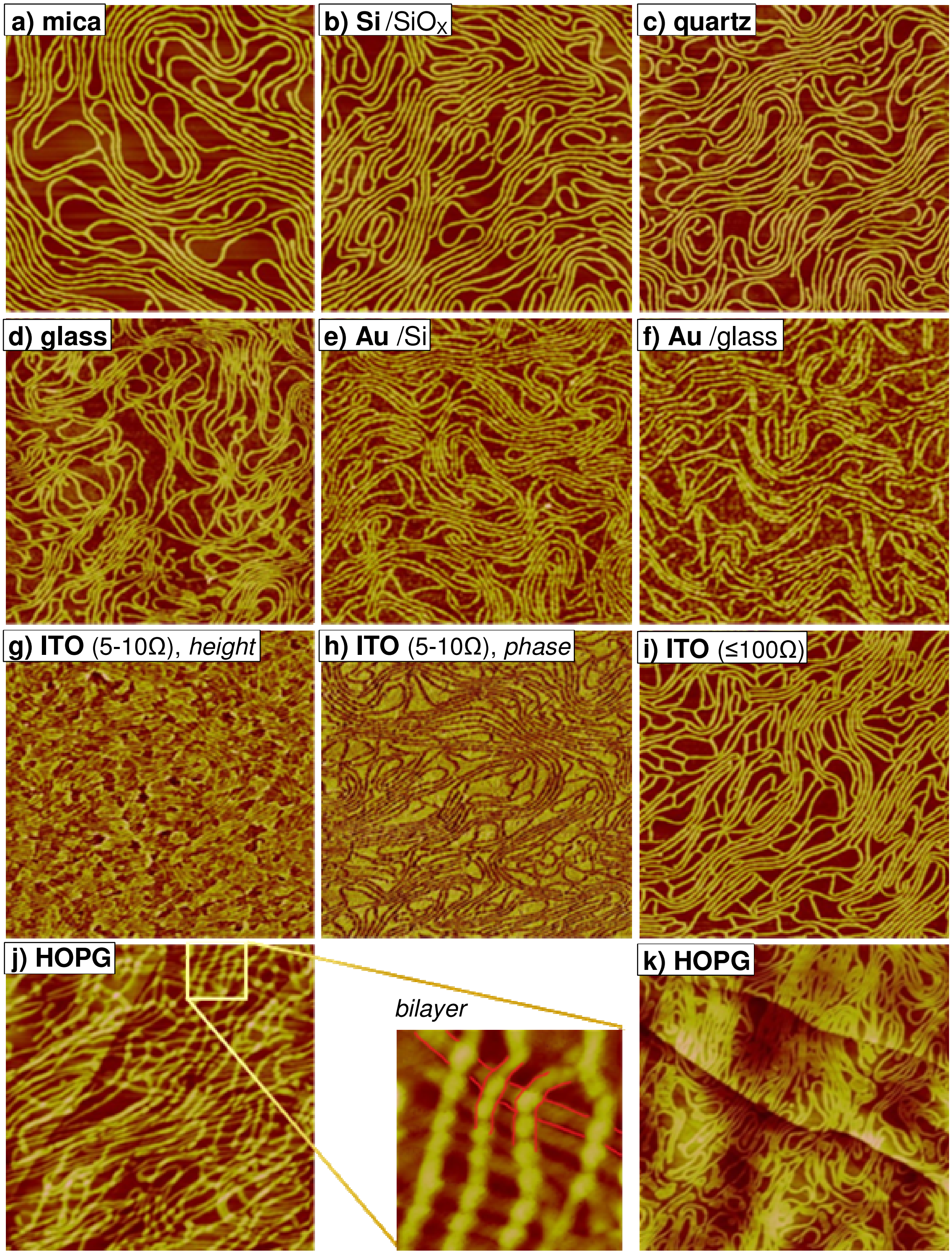

Figure SI-2-6. AFM 5×5 μm height images (except **h** – phase image) of PS-PVP/PDP (1.0:1.2) films spread from a $CHCl_3$ solution of copolymer concentration 1.71 mg/mL, and transferred to the substrates indicated at π=10 mN/m; a–i) monolayers produced by LB; j) bilayer (with 1×1 μm expansion) produced by LB; k) monolayer produced by LS.

Brewster Angle Microscopy (BAM) images presented below demonstrate that films obtained from chloroform (Figure SI-2-7) are more uniform than those spread from 1,1,2,2-tetrachloroethane solution (Figure SI-2-8).

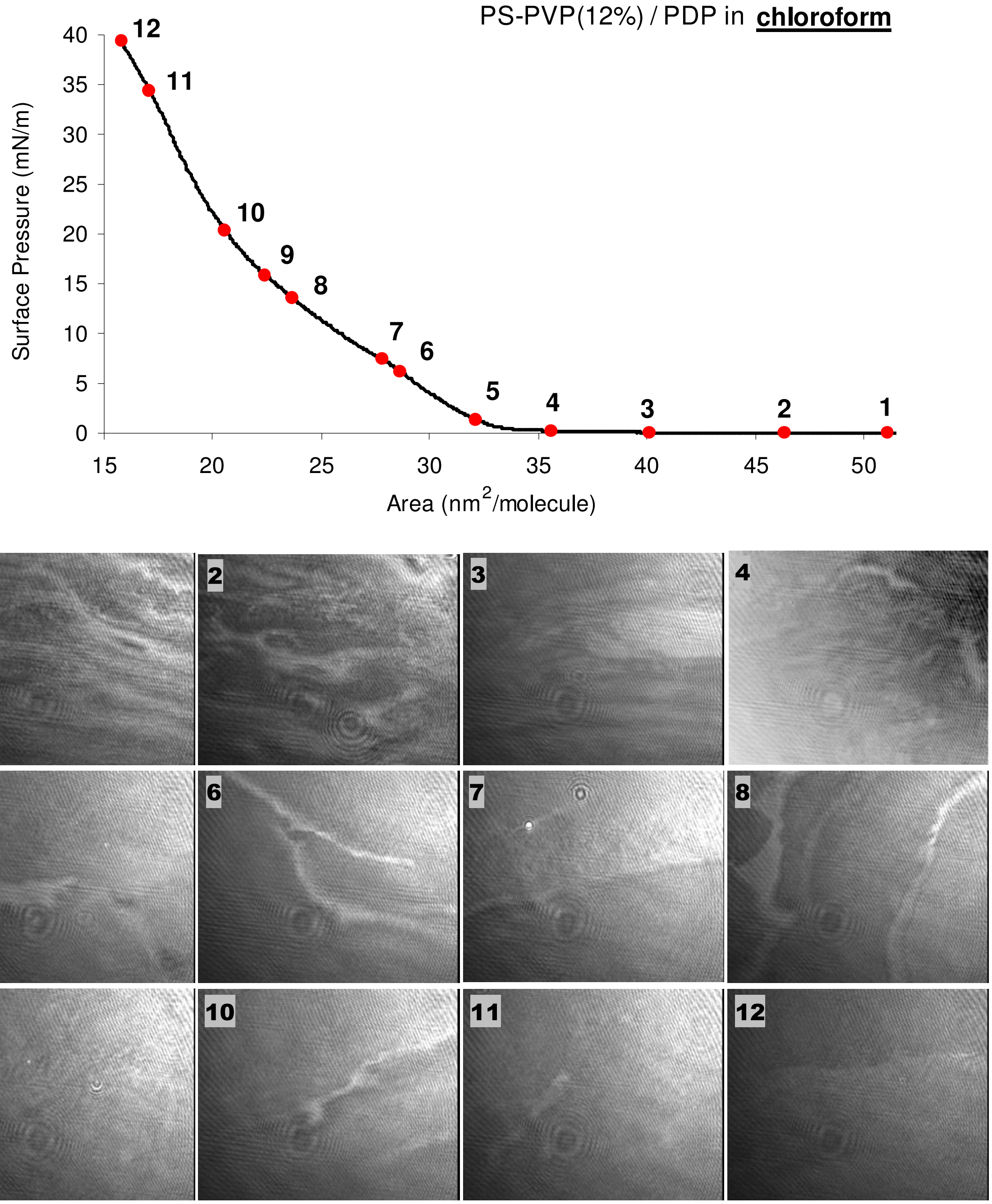

Figure SI-2-7. Pressure–area isotherm and BAM images (220 x 275 µm; resolution: 1 µm) of PS-PVP/PDP$_{1.0}$ spread from concentrated $CHCl_3$ solution on water surface (T = 20°C). All images were done during compression cycle followed 30 min. wait for solvent evaporation.

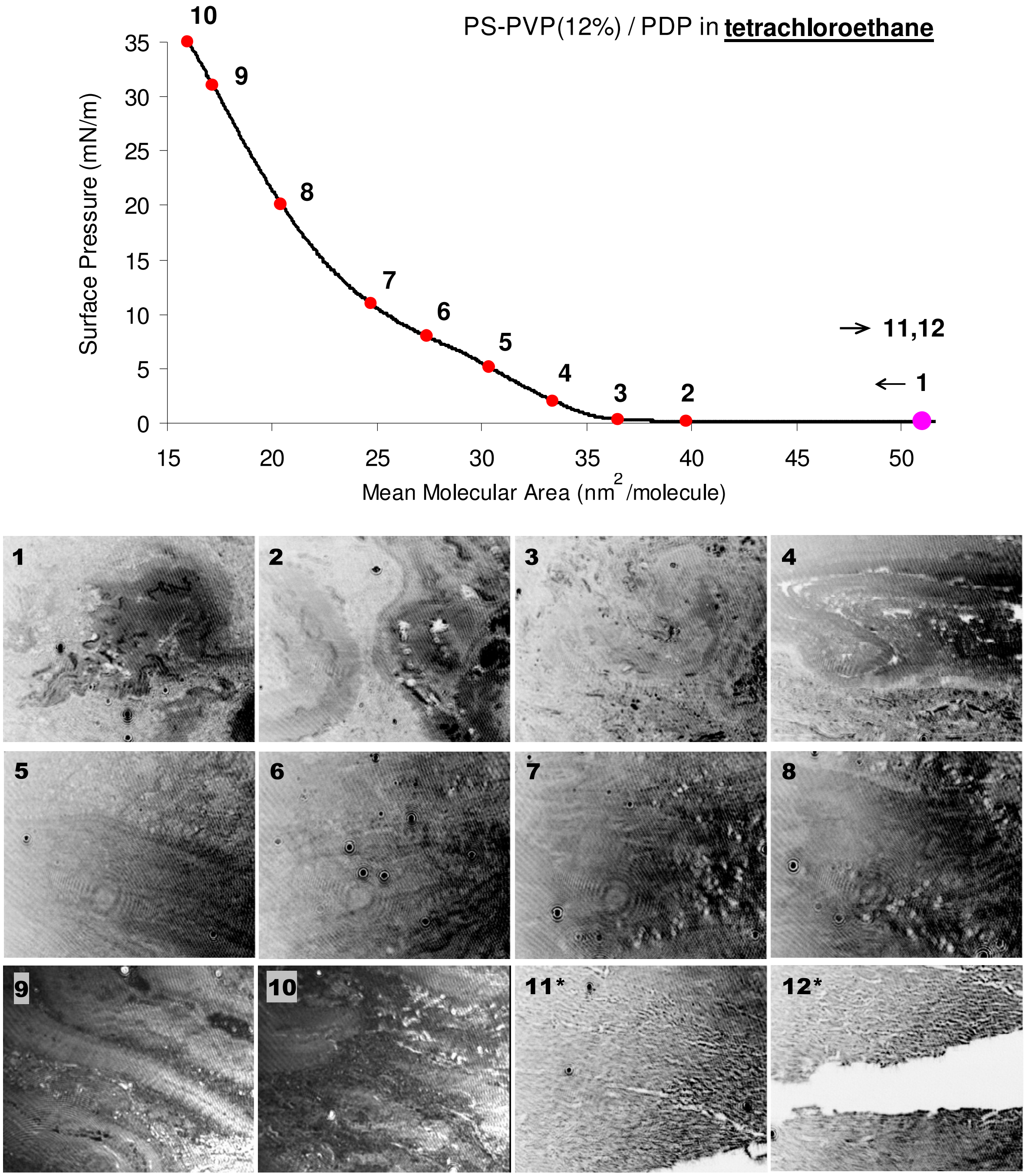

Figure SI-2-8. Pressure–area isotherm and BAM images (220 x 275 μm; resolution: 1 μm) of PS-PVP/PDP$_{1.0}$ spread from concentrated $C_2H_2Cl_4$ solution on water surface (T = 20°C). Images 1–10 were done during compression cycle followed 50 min. wait for solvent evaporation; images 11,12 were done after complete barriers expansion followed compression to π = 35 mN/m.

Chapter 3

Controlling and Understanding Self-Assembly Evolution in Langmuir-Blodgett Block Copolymer Films Using PS-PVP and PS-PVP/PDP

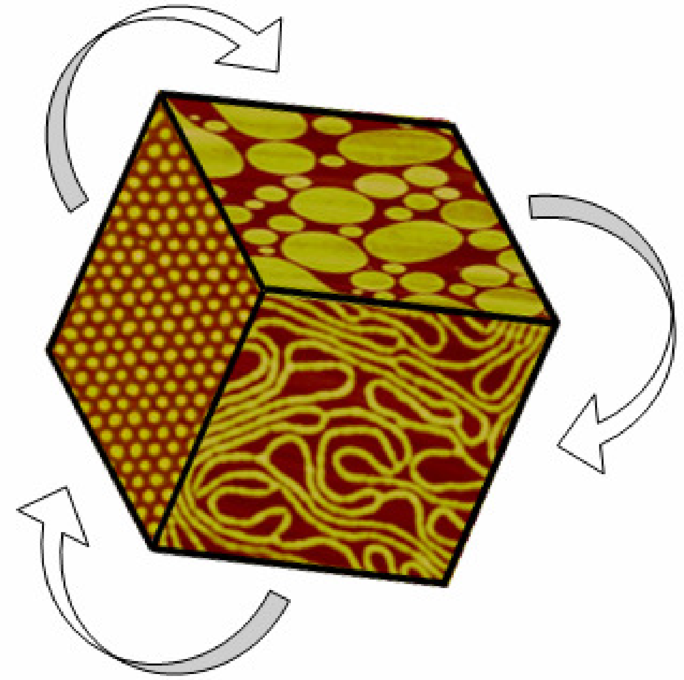

3.1. INTRODUCTION

It is well known that block copolymers in the bulk self-organize into various morphologies (most commonly cubic, cylindrical, gyroid and lamellar for diblock copolymers), depending on the block copolymer composition (relative block lengths), the χ parameter between the blocks, and the total molecular weight of the polymer.[1–3] It is equally well known that thin film morphologies are determined by interfacial energies (substrate, air) and film thickness in addition to the above parameters.[4–7] In the latter, the relationships between the different parameters and the resulting morphologies are quite well understood for lamellar-forming block copolymers,[4] and partially understood for cylinder-forming and sphere-forming, block copolymers.[7] Equilibrium or pseudo-equilibrium morphologies in these materials are achieved by thermal annealing in the bulk (limited mainly by the degradation temperature) and by thermal or solvent vapor annealing in thin films (although the solvent itself adds additional factors affecting equilibrium conditions, and thus it is more accurate to speak of changes in order induced by solvent annealing[8]).

In ultrathin films of (generally amphiphilic) block copolymers prepared by the Langmuir-Blodgett (LB) technique, various morphologies are also observed, but the processes leading to these morphologies are particularly complex, due to the influence of complex kinetic effects during film formation and solvent evaporation, to the soft aqueous interface on which they form, and to the difficulty if not impossibility of ensuring the attainment of equilibrium conditions (at least in the later stages of film formation). In early work on LB block copolymer films, it was shown that the block composition (relative block lengths) is, unsurprisingly, one determining factor in the morphology obtained.[9–12] Three main types of morphologies were observed: variably sized, including very large, planar-type aggregates (also called continents, pancakes, islands, *etc.*) at low hydrophilic block content; nanostrands (also called spaghetti, rods, strands, stripes, worms, *etc.*) of relatively constant width but often highly variable lengths, sometimes highly interconnected in the form of a nanostrand network,[13–15] at somewhat higher hydrophilic block content; and nanodots (also called surface micelles) that are much more uniform in size and generally tend to 2D hexagonal packing at still higher hydrophilic block content. The picture that is generally held of these structures is the following: the nanodots (*i.e.* elevated core of the surface micelles) are composed of the condensed hydrophobic block that avoids the aqueous surface and are surrounded laterally (and probably below) by the relatively long hydrophilic block that is spread as a cohesive monolayer on the water surface; the rod-like aggregates are composed of the elevated hydrophobic block in elongated form, surrounded on both sides (and probably below) by the significantly shorter hydrophilic block in monolayer form; planar aggregates consist of an upper layer of the hydrophobic block that is protected from the water surface by the very short hydrophilic block acting as a wetting monolayer.[9–12]

It was later observed with diblock copolymers (generally of relatively low hydrophilic block content)[16–19] and even polystyrene homopolymers[20] that these kinds of morphologies, often mixed together and with variable shapes and sizes, can also be observed for one and the same composition, and that they are influenced by spreading solvent concentration and total block copolymer molecular weight. Other morphologies, such as planar aggregates with holes (“nanofoams”),[18,21] linearly interconnected nanodots (“necklaces”, “chains”),[17,18,22] and nanorings (“nanodonuts”),[17,23] have also been observed under different experimental conditions. The dependence of the morphologies on experimental conditions and the observation of mixed morphologies in the same film have generally been attributed to various kinetic effects operating during the film forming process, leading to frozen-in morphologies.[16,17,22,24] Most recently, Moffitt and coll. have interpreted the various morphologies as resulting from different frozen-in stages of a dewetting process of an initially uniform film of spreading polymer solution.[18,20] On the other hand, the possibilities that block copolymer association into domains might also be frozen in at various stages and that the coherent film itself may have a particular morphology at some stage should also be considered. The latter possibility was postulated by us recently to explain the formation of the highly uniform nanostrand network morphology.[15] The ordered nanodot morphology is, in fact, a nanopatterned cohesive film held together by the hydrophilic block monolayer. Such a monolayer has also been obtained by spin-casting an ultradilute chloroform solution of PS-P2VP onto a mica substrate.[25]

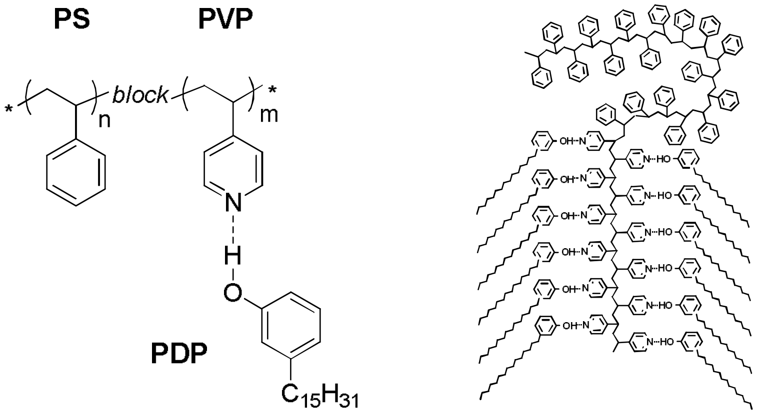

Figure 3-1. Schematic structure of PS-PVP/PDP.

The supramolecular coil-comb diblock copolymer system based on polystyrene-poly(4-vinyl pyridine) (PS-PVP) mixed with 3-*n*-pentadecylphenol (PDP), which hydrogen-bonds via the phenol moiety to the pyridine moiety in PVP, as shown in Figure 3-1, has been widely studied in the bulk[26–32] and, more recently, in the form of thin films (usually obtained by spin-coating techniques).[7,8,33,34] Because PS-PVP is commercially available in a wide variety of block compositions and because it is a relatively simple matter to modulate the characteristics of the polymer by addition of a block selective small molecule, this system is ideal for developing greater understanding of ultrathin LB film morphologies, their relationship to molecular and experimental parameters, and their mechanisms of formation. Thus, the present contribution compares LB morphologies obtained at various block compositions, both with and without PDP present, for low and high spreading solution concentration, including use of the so-called "solvent-assisted" LB technique,[14] for varying PDP content, and, to a limited extent, for different total molecular weights. The importance of spreading solution concentration on the LB film morphologies has been highlighted in several recent publications, but for limited block compositions.[15–17] The "solvent-assisted" technique, which consists of the suppression of the waiting period following solution spreading and before barrier compression (such that the presence of spreading solvent can maintain sufficient polymer mobility to allow a potential morphology transformation during compression to take place), was shown to lead to an extensive nanostrand network pattern formed from a dilute spreading solution of a PS-PVP copolymer with 12 wt % PVP.[14] The extensive results of the present contribution, along with recent and less recent insights in the literature, will enable a wide-ranging discussion of the processes leading to different morphologies.

It is noteworthy that there are actually few block copolymer systems reported in the literature whose LB morphologies have been investigated systematically as a function of relative block length. The first such study, mentioned above, involves a diblock polyelectrolyte series composed of PS-PVP where the PVP block is quaternized by an *n*-decyl chain (PS-PVP$^+$RX$^-$). This series also constitutes a particularly relevant comparison for the PS-PVP/PDP system of the present study, since they have the same molecular architecture in principle, both combining a linear block with a comb-like block. The two systems differ by the type of attachment of the alkyl chain to PVP, which is via non-covalent hydrogen-bonding in PS-PVP/PDP (in this case, the possibility of incomplete hydrogen-bonding must be considered) and by covalent bonding in PS-PVP$^+$RX$^-$. They also differ in that PVP$^+$RX$^-$ is an ionic block, whereas PS-PVP/PDP is not. Other copolymer systems whose LB behavior were investigated at various block compositions are PS-PEO [PEO: poly(ethylene oxide)][12] including a linear triblock[35] and star diblocks,[36] and some poly[alkyl (meth)acrylates],[10,11,37] all nonionic block copolymers. In general, they tend to show the same three basic LB morphologies as PS-PVP$^+$RX$^-$ – planar, nanorod-like, nanodots – dependent on the block composition. The mixed morphologies dependent on experimental parameters referred to above were observed mainly using PS-PEO block copolymers of relatively low PEO content.[16–19]

3.2. EXPERIMENTAL SECTION

3.2.1. *Materials*

Diblock copolymers of poly(styrene)-*b*-poly(4-vinyl pyridine) (PS-PVP) with PVP content ranging from 4 to 49 mol % were obtained from Polymer Source (Dorval, QC, Canada), and used as received. They are listed in Table 3-1, along with their molecular weight characteristics, and will frequently be referred to by their mol % PVP content, as indicated by the nomenclature given. Before use, 3-*n*-pentadecylphenol (PDP) (Sigma-Aldrich, 90%) was recrystallized twice from hexane. Chloroform (HPLC grade, ≥99.8%;

Sigma-Aldrich) was used for solution preparation and in all cleaning processes, with anhydrous ethanol (Commercial Alcohols) used also for trough cleaning. Ultrapure water (18.2 MΩ cm), used as the subphase in the Langmuir-Blodgett trough, was obtained by purification of distilled water with a Millipore Milli-Q Gradient system. Muscovite ruby mica (ASTM Grade 2, B&M Mica, Flushing, NY, USA), used as a solid substrate for film transfer, was cleaved immediately before its immersion into the subphase.

Table 3-1. Nomenclature and characteristics of the PS-PVP diblock copolymers studied.

Nomenclature*	Molecular weight, g/mol		M_w/M_n	Number of repeat units		mol % PVP
	M_n (PS)	M_n (PVP)		N_{PS}	N_{PVP}	
4%	41,400	1,900	1.07	398	18	4.3
8%	34,000	2,900	1.07	326	28	7.9
9%	35,500	3,600	1.06	341	34	9.1
12%	40,000	5,600	1.09	384	53	12.1
14_H%	252,000	43,000	1.09	2,420	409	14.4
16%	42,100	8,100	1.08	404	77	16.0
19%	32,900	8,000	1.06	316	76	19.4
29_2%	31,900	13,200	1.08	306	126	29.2
29_4%	41,500	17,500	1.07	398	166	29.4
33_H%	72,000	35,000	1.09	691	333	32.5
46%	20,000	17,000	1.08	192	162	45.8
49%	20,000	19,000	1.09	192	181	48.5

* The letter “H” in 14_H% and 33_H% nomenclatures designate PS-PVP’s of high molecular weight to distinguish them from those of “normal” (35–60 kg/mol) molecular weight. The subscripts in 29_2% and 29_4% designate the decimal precision of PVP mol%, used to distinguish the two 29% samples.

3.2.2. Langmuir-Blodgett Films

The block copolymers and recrystallized PDP were dried under vacuum at room temperature for a week before use. Then, the PS-PVP and PS-PVP/PDP were dissolved in chloroform, and left to stir overnight at room temperature in sealed volumetric flasks. The concentration of the block copolymer in the final solution was 1.8 (concentrated solutions) or 0.3 (dilute solutions) mg/mL.

A computer-controlled KSV 3000 Langmuir-Blodgett system with a platinum Wilhelmy plate sensing device (KSV Instruments, Helsinki, Finland) was used. The subphase temperature in the trough (150 x 518 mm) was maintained at 20–21°C, using a refrigerated circulator (Isotemp 3016, Fisher Scientific). Solution was spread dropwise in a checkerboard pattern using Hamilton microliter syringes (20–100 μL for concentrated solutions, 40–400 μL for dilute solutions; generally, the lower the VP content, the higher the volume spread (thus, qualitatively tending to include the PDP weight in the total amount of material spread).

Following a 20–30 min wait after solution deposition to ensure chloroform evaporation, Langmuir compression isotherms (surface pressure *vs.* mean molecular area isotherms) were obtained by symmetrical compression of the barriers at a speed of 10 mm/min (15 cm^2/min). All isotherms were run at least three times.

Under the same conditions as for the isotherms and following a 15–25 min wait at the desired surface pressure (3–15 mN/m) for barrier stabilization, Langmuir-Blodgett (LB) monolayers were transferred onto mica substrates during vertical withdrawal from the subphase at a rate of 5 or 10 mm/min (no differences were observed between these two speeds). In the "solvent-assisted" method,[13] used with dilute solutions only, the waiting step for chloroform evaporation after solution deposition was omitted; instead, barrier compression was implemented as soon as practically possible after solution deposition. To minimize the time required for barrier compression, the Langmuir bath area was first decreased by about half (to approximately 340 cm^2), giving an initial surface pressure of *ca.* 1–2 mN/m.

3.2.3. Atomic Force Microscopy

The deposited films were dried in a clean box overnight at room temperature and then imaged in air by atomic force microscopy (AFM) in tapping mode using a Multimode AFM with a Nanoscope IIIa controller (Digital Instruments/Veeco, Santa Barbara, USA) and silicon probes (MikroMasch USA: rectangular, no aluminum coating on tip and backside, resonance frequency 265–400 kHz, tip curvature radius < 10 nm; or Nanosensors: type PPP-NCH, nominal spring constant of 42 N/m, resonance frequency 330 kHz, tip radius of curvature <10 nm). Nanofeature dimensions were determined from height profiles, and the width was measured at half-height. Usually, 5–10 well-spaced locations per sample (excluding near the edges) and 2–4 samples (with a minimum of 2 separate dips per condition) were scanned. One type of morphology is shown when it covers at least 80% of the images; otherwise, the next most common morphology is also shown.

3.3. RESULTS AND DISCUSSION

3.3.1. Langmuir-Blodgett Monolayer Morphologies

For reference, the Langmuir isotherms obtained in various conditions relevant to the transfer of LB films to solid substrates can be found in a later section. It is preferable to present the morphologies of the transferred LB monolayers before the isotherms, because the latter are best interpretable in the light of these morphologies. Suffice it to mention at this point that the type of morphology was not observed to depend on the transfer pressure (until the collapse region was reached), but mainly the surface features were pushed closer to one another and some deformation could occur (see ref. 15 for the case of the 12% PVP copolymer). To minimize deformation, the LB transfers were done at low surface pressure (3–15 mN/m).

LB films of PS-PVP with a wide range of relative block contents, both in pure form and with equimolar PDP present, for both high and low spreading solution concentrations, and using both the conventional and the “solvent-assisted” procedures, were analyzed and compared. The results for the high solution concentrations will be presented first. It was observed in these experiments that the transfer ratios were generally 0.4±0.2 for the pure copolymers and 1.0±0.1 for PS-PVP/PDP. In addition, it was noticed that the transfer was more uniform for the PDP-containing films than the pure copolymer films (as observed by the generally linear increase in barrier compression during the transfer process for the former compared to a variable increase for the latter). In accordance with this, the PS-PVP/PDP films were observed to be more uniform than the PS-PVP films, noticed in particular by more frequent empty areas found in the latter during scanning of images in different parts of each film. It was also noted that, when barriers were compressed to their maximum, the collapsed nature of the PS-PVP films could be observed visually, whereas the PS-PVP/PDP films remained visually transparent, indicative of optically uniform films.

3.3.1.1. Effect of Relative Block Fraction and PDP (High Concentration Solutions)

AFM height images of LB films of PS-PVP of varying block fractions but similar total molecular weights for one series without and one series with equimolar PDP present, obtained from high concentration spreading solutions, are illustrated in Figures 3-2 and 3-3. The images shown are for LB films obtained at a transfer pressure of 3 mN/m; they were also obtained at 15 mN/m, giving images (see the Appendix to Chapter 3, Figure SI-3-1 and SI-3-2) that are essentially identical to those for 3 mN/m (except for some places of apparent buckling in the planar, and occasionally, rod-like morphologies; never observed in the nanodot morphologies).

In following the structural evolution of the pure PS-PVP films first (Figure 3-2), the three basic types of morphologies reported in the literature can be identified. In the lower PVP content range (4–16%), planar aggregates, which are in the form of long and relatively wide ribbon-like structures, are observed. For the 4–16% PVP films, the ribbon edges tend to be smooth and quite straight, and the ends often square-like. The morphology of the 19% PVP film is completely different and is dominated by a nanostrand network morphology, but the network also shows some fused regions of small ribbon-like or planar-type areas. Thus, this composition can be taken as the transition composition between the planar and nanostrand morphologies. Nanostrands are still predominant in the 29_2% PVP film, but many more strand ends are visible and some nanodots are dispersed among the strands. In the 29_4% PVP film, there are many more nanodots that are interspersed with fewer and less interconnected nanostrands of variable length (including some as short as the equivalent of 2–3 nanodots), sometimes with the appearance of being a sequence of partially fused nanodots. Despite their very close composition, the difference in morphology of these two block copolymers is striking and reproducible. This indicates that 29–30% PVP is the compositional transition between the nanostrand morphology and the nanodot morphology that is observed for higher PVP contents (studied up to 49% PVP). The nanodots in the latter clearly tend to pack in 2D hexagonal order, even in the 29_4% PVP film; however, it is noteworthy that their shape is generally asymmetric.

In the presence of equimolar PDP (Figure 3-3), the same three basic morphologies – planar aggregates, nanostrand network, and nanodots in order of increasing PVP content – are observed, but with the transitional compositions shifted to lower PVP contents, namely 8–9% and 16–19% PVP/PDP (compared to *ca.* 19% and 29–30% PVP, respectively; *i.e.* in the absence of PDP). Planar structures are found for the 4 and 8% PVP/PDP compositions, but they differ significantly from those for pure PS-PVP. For 4% PVP/PDP, ribbon-like features are still present, but they are generally much thinner than for pure PS-PVP and often have rounded ends. There are also many shorter objects, to the extreme of being disk-like. The latter are more prevalent for 8% PVP/PDP, coexisting with much thinner ribbons that now begin to resemble nanostrands, except that they have more variable widths. It should also be noted that the circular or nearly circular aggregates are of variable sizes and usually much larger than nanodots. The 9 and 12% PVP/PDP films show the "true" nanostrand network morphology almost exclusively, with just a few thicker areas in the 9% film (Figure 3-3c). (This morphology in the 12% PVP/PDP film was investigated and described extensively in the previous chapter[15]) Nanostrands still predominate in the 16% PVP/PDP film, but are shorter and much less interconnected, as well as interspersed by some nanodots and nanorings. The 19% PVP/PDP film contains, in roughly equal proportion, regions of only nanodots in quasi-hexagonal packing order and regions where variable length nanostrands are interspersed by a few nanodots, and is therefore taken as the approximate transition composition. The films with higher PVP compositions all show the quasi-hexagonal nanodot morphology.

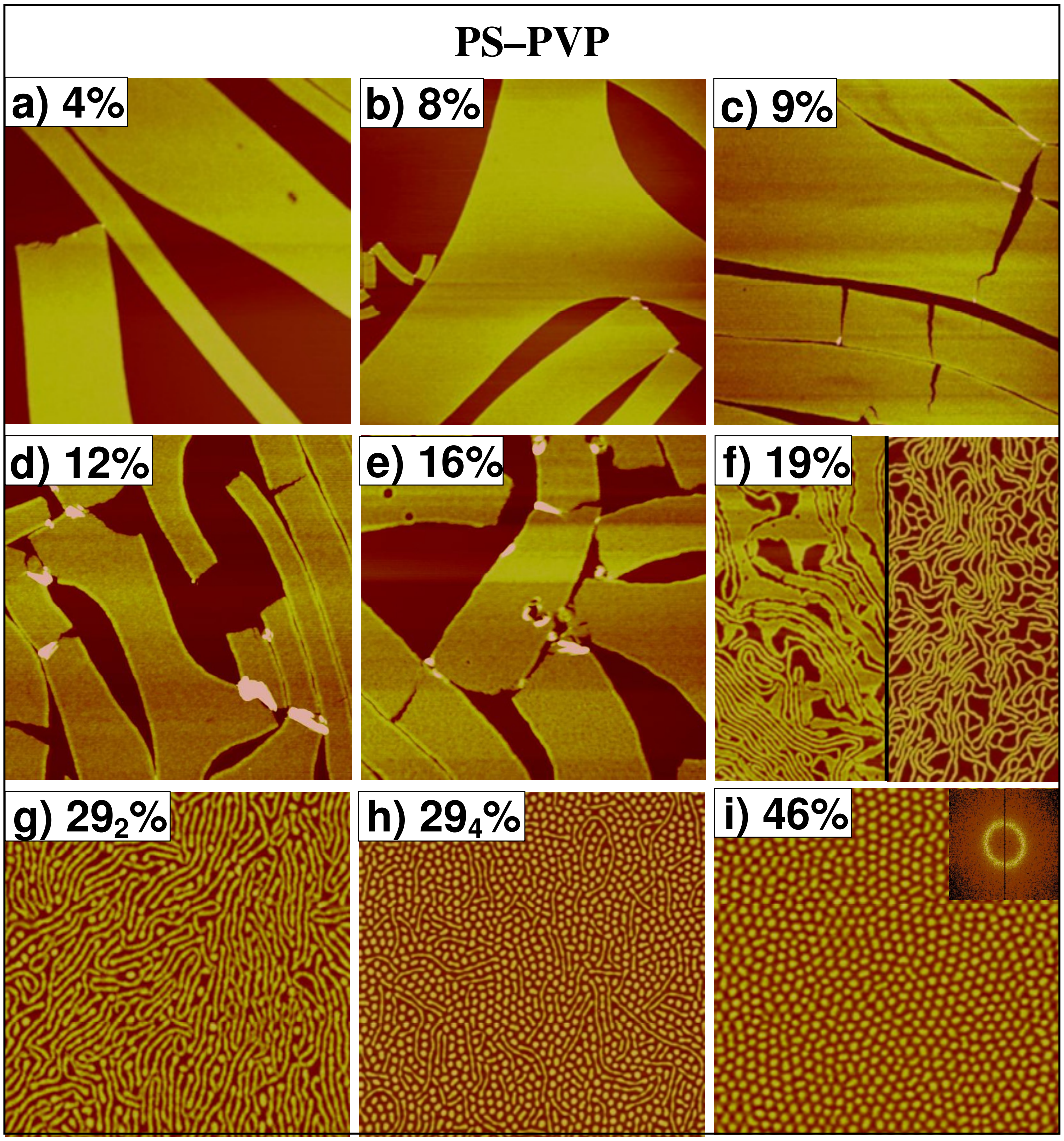

Figure 3-2. AFM height images of PS-PVP LB films spread from concentrated solutions and transferred at $\pi = 3$ mN/m. The numbers indicate mol % PVP content Image scan: a–e, h) 5×5 μm; f) 5×2.5 μm (two images); g, i) 3×3 μm.

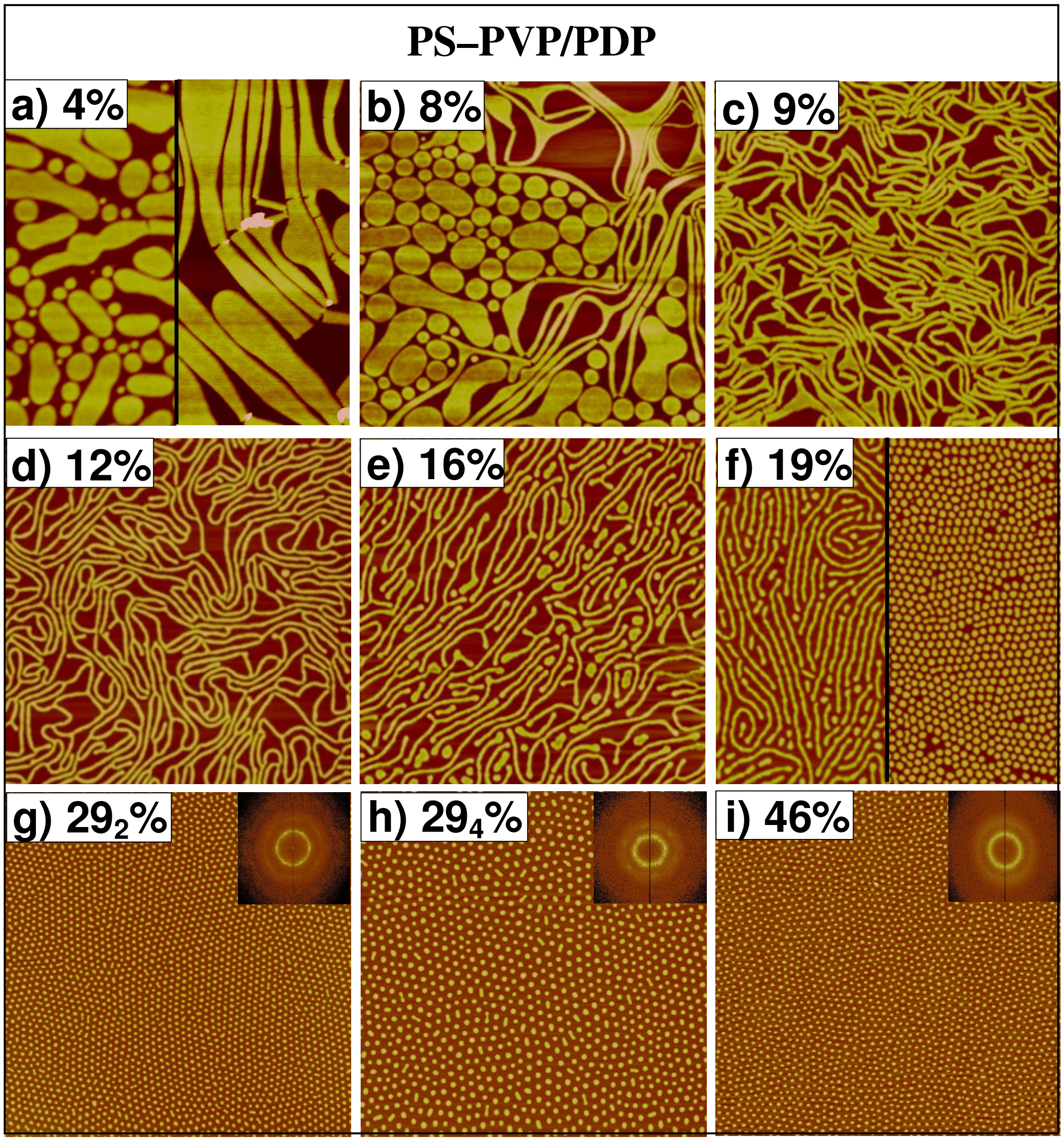

Figure 3-3. AFM height images of PS-PVP/PDP$_{1.0}$ LB films spread from concentrated solutions and transferred at $\pi = 3$ mN/m. The numbers indicate mol % PVP content. Image scan: 5×5 μm (a,f: two places, 5×2.5 μm each).

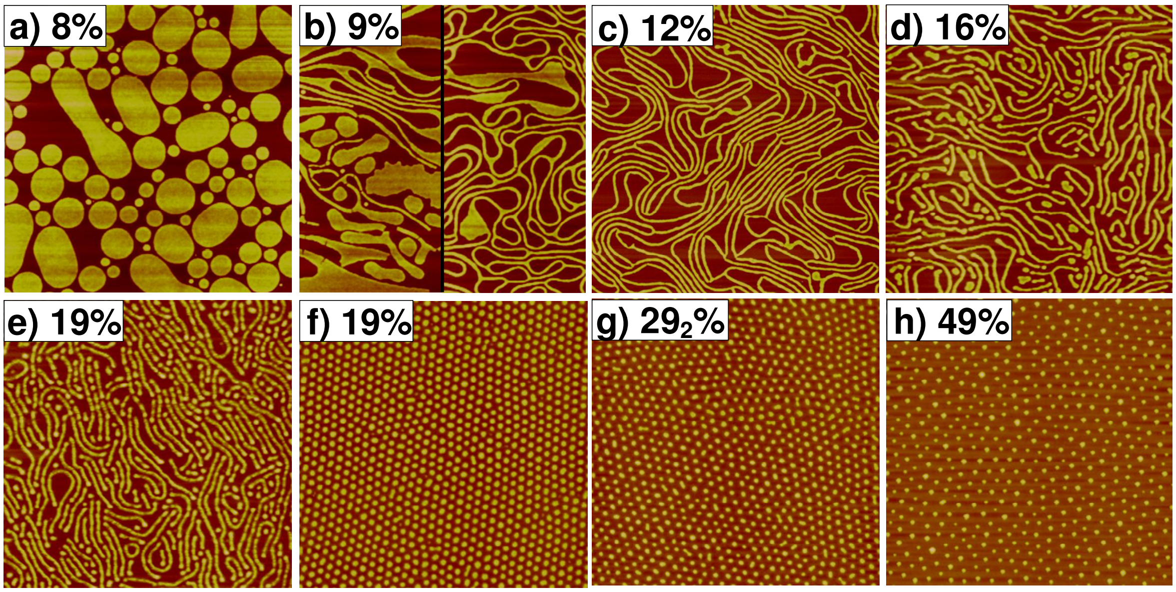

Figure 3-4. AFM height images of PS-PVP/$PDP_{1.3}$ LB films spread from concentrated solutions. π = 3 mN/m (a, b, d, h), 4 mN/m (g), 5 mN/m (c, e, f). The numbers indicate mol % PVP content. Image scan: a–d) 5×5 μm (b: two places, 5×2.5 μm each); e–h) 3×3 μm.

The choice of preparing PS-PVP/PDP films where PDP is equimolar to VP assumes the ideal situation of one-to-one PDP–VP hydrogen bonding. This may not be the case if there is equilibrium between free and hydrogen-bonded PDP on the water surface and if some PDP might be solubilized in the PS phase (shown to be *ca.* 5% w/w PDP/PS in bulk PS-PVP/PDP of total copolymer molecular weight 24,700 and 20.5 mol % PVP content[38]). Considering this possibility, a number of the block copolymers were also mixed with a small excess of PDP (1.0:1.3 VP:PDP; Figure 3-4). In general, the morphologies obtained for this molar ratio are the same as for the equimolar ratio, with just a slight tendency for the morphological transition to be displaced to higher PVP content – *i.e.* 8% PVP/PDP shows no strands and 9% PVP/PDP contains some planar structures in addition to nanostrands.

LB films of two copolymers of higher molecular weight, in the presence of PDP (1.0:1.3 VP:PDP) only, were also investigated. Their compositions, 14 and 33 mol % PVP, lie within the nanostrand and nanodot regimes, respectively, for the molecular weights described above. The latter, 33_H% PVP/PDP, has a total molecular weight that is more than twice that of the above series. As shown in Figure 3-5, there is no change in the type of morphology; however, it is significantly more disordered compared to those in Figure 3-3 having this morphology. In contrast, the $14_H\%$ PVP/PDP polymer, whose total molecular weight is about five times that of the above series, shows a very different morphology from its lower molecular weight analog, one that is in the form of variably sized and irregularly spaced circular micelles.

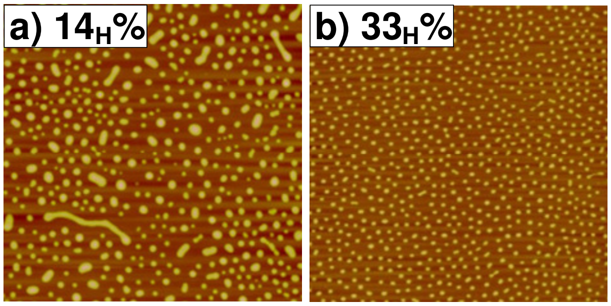

Figure 3-5. AFM height images (5×5 μm) of high molecular weight PS-PVP/$PDP_{1.3}$ LB films spread from concentrated solutions (π = 3 mN/m). The numbers indicate mol % PVP content.

3.3.1.2. Comparison With Low Concentration Spreading Solutions and the “Solvent-Assisted” Technique

Representative AFM height images of PS-PVP films of various PVP contents, both with and without PDP present, this time obtained from low concentration solutions, along with those obtained from the same solutions by the “solvent-assisted” method,[13] are shown in Figure 3-6. For pure PS-PVP, three morphology regimes are again observed, with transitional compositions corresponding to those for the high concentration solutions. One major difference between the two concentrations is observed; notably, the large ribbon-like structures obtained from high spreading concentrations for the low PVP content regime are completely replaced by smaller (on average) and usually circular or near-circular structures of variable sizes and in total disorder. Otherwise, similar to the high concentration solutions, nanostrands are the dominant morphology for 19% PVP content (some are present also for 16% PVP) and quasi-hexagonally ordered nanodots for higher PVP content (investigated at 46 and 49% PVP).

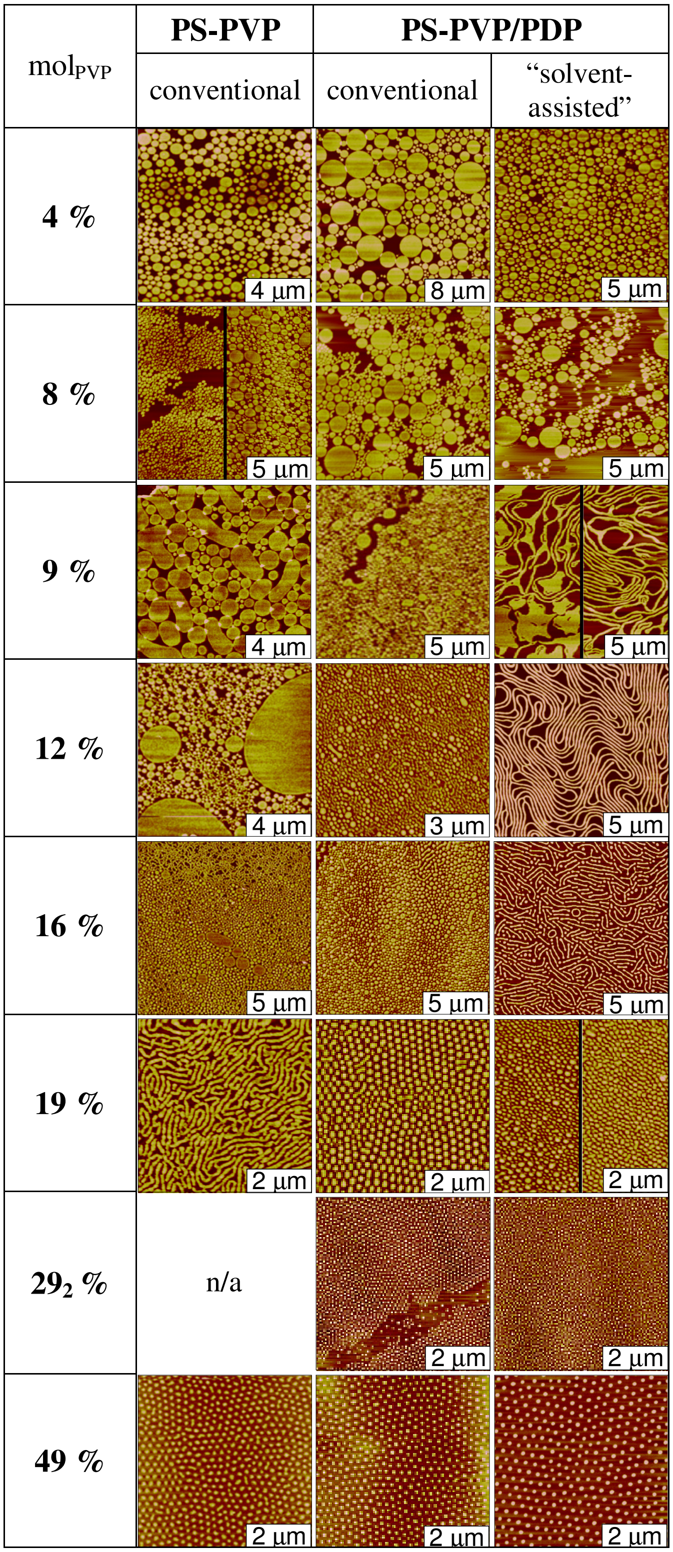

Figure 3-6. AFM height images of PS-PVP and PS-PVP/PDP$_{1.0}$ LB films spread from dilute solutions by conventional and "solvent-assisted" methods.

(Unpublished results obtained by Qing Lu.)

With equimolar PDP present, the nanostrand regime appears suppressed or occurs in a narrow range not covered by the copolymer compositions investigated. For low PVP contents, there are variably sized circular aggregates (they appear to be particularly perfect disks for the 4% PVP/PDP film), which remain the dominant morphology up to 16% PVP/PDP. In the latter film, there are, in addition, a minor amount of short strands dispersed among the circular aggregates, and there are no large circular aggregates; however, despite the latter being quasi-nanodots, they are still of sufficiently variable size that their packing remains disordered. In contrast, the 19% PVP/PDP film shows predominantly quasi-hexagonally ordered nanodots of relatively uniform size (with a small amount of short, dispersed nanostrands) and, as for all other higher PVP contents, the 29 and 49% PVP/PDP films display the quasi-hexagonal nanodot morphology exclusively. Thus, there appear to be just two morphology regimes in this series, with the transitional composition lying in the 16–19% PVP/PDP range.

When using the “solvent-assisted” technique, where the barriers are compressed to the desired transfer pressure as soon as possible after deposition of the spreading solvent, the nanostrand regime reappears. This morphology can most easily be obtained, and is by far the dominant morphology, for the 12% PVP/PDP content, as described previously.[13] It is also dominant in the 9% PVP/PDP film, but with a few thickened nanostrand regions, and in the 16% PVP/PDP film, where they appear broken-up into many short, unconnected strand segments among which a few nanodots are dispersed. A very small number of strand segments are still visible in the 19% PVP/PDP film, which otherwise shows nanodot morphology. Thus the nanostrand composition regime, using the “solvent-assisted” technique with dilute spreading solutions, is similar to that using high concentration spreading solutions, that is *ca.* 9–16% PVP/PDP. This was explained by barrier compression increasing the surface density of polymer to that obtained in high concentration solutions while the system is still sufficiently mobile, due to the presence of spreading solvent, so that aggregation leading to nanostrand formation can take place.[15] For the planar and nanodot morphology regimes, the “solvent-assisted” technique does not change the morphology significantly from those observed using the standard technique (dilute solutions). Only in one case, for 8% PVP/PDP, was a ribbon-like morphology observed. This indicates that, for the planar morphology regime, the “solvent-assisted” technique did not lead to the necessary polymer surface concentration during the mobile period to allow ribbon-forming aggregation, except for that one time, presumably as a result of working particularly quickly. For the nanodot morphology, there is no dependence on solution concentration, so it is reasonable that there is also no effect of the "solvent-assisted" technique.

The ordering of the nanodots in the region of the fissure in Figure 3-6 for the 29_2% PVP/PDP is of interest to note. There are a number of isolated, non-organized dots, along with one isolated hexagon of seven nanodots, within the fissure space. The organized dots in the film alongside the fissure are linearly ordered in parallel with the breakage line in some places, at angles that meet one another in others, and generally look as if they have self-organized in hexagonal order to the extent possible given the various meeting points of those already incorporated, the space available, and whether they are isolated or in the form of small aggregates at the point of their assembling into the rest of the film. All this can easily account for the many defects to perfect hexagonal order in the films (considering that the diffusion of nanodots that are already assembled in film form, required to perfect the order, most likely requires much longer times than available).

3.3.1.3. Comparison with Published LB Block Copolymer Systems

The morphologies observed in the moderate molecular weight PS-PVP and PS-PVP/PDP systems above correlate well overall with those described in the literature for similar systems, in that the three main types of morphologies – disordered planar-type objects of variable sizes (and often shapes), rod-like objects of variable lengths (usually much shorter and with relatively few interconnections compared to the nanostrand network), and relatively ordered and uniformly sized nanodots, in order of increasing hydrophilic block content – are observed in the other systems for which a sufficient range of compositions were investigated.[9–12] Thus, it can be concluded that this sequence of morphologies and their dependence on block composition is general.

It is of particular interest that the architecturally similar PS-PVP/PDP and PS-$PVP^+C_{10}H_{21}I^-$ systems have similar morphological transition compositions in terms of mol % hydrophilic block: 8–9 and 16–19 mol % for the former and 6 and 14 mol % for the latter (Table 3-2). This suggests that the nonionic *vs.* ionic character and the difference in alkyl chain length (15 *vs.* 10 carbons), despite possibly incomplete PDP complexation to VP, do not strongly influence these transitions (they appear to be just a little lower for PS-PVP$^+$C$_{10}$H$_{21}$I$^-$ than for PS-PVP/PDP). The relative unimportance of alkyl chain length (considering the limited number of compositions investigated in each block copolymer system) is supported by studies of block copolymers of PS and poly(meth)acrylates with short alkyl chains (*n*- or *tert*-butyl),[10,11,37] for which the transition compositions also appear similar to those for PS-PVP$^+$C$_{10}$H$_{21}$I$^-$ and PS-PVP/PDP (see Table 3-2). On the other hand, without the presence of alkyl chains, the transition compositions clearly occur at significantly higher mol % hydrophilic block content, as shown by our results for PS-PVP (19 and 29 mol %) and literature results for PS-PEO (about 20 and 30 mol %[12]). It should be added that there appears to be no systematic dependence on composition in terms of weight fraction (wt %) that includes the side chain (PDP in our case) when comparing these systems (contrary to what occurs in bulk block copolymer systems[27]). Furthermore, high molecular weight systems often appear to have more complex behavior,[17,18] as observed above for the 14$_H$% PVP/PDP copolymer. Nevertheless, it is striking that the morphology variants observed for PS-PEO of 24 mol% PEO (total M$_n$ 141k)[17,18] can be qualified as predominantly strand-like and those observed for PS-PEO of 36 mol% PEO (total M$_n$ 185k)[18] as predominantly dot-like (albeit very disordered).

In the transition composition regions, mixed morphologies are generally observed. This may be related, in part, to the variable length of polymer chains, even if the polydispersity is quite low. An example that supports this is the study of Chung *et al.* on LB films of fractionated samples of a PS-PMMA [PMMA: poly(methyl methacrylate] diblock copolymer with unfractionated polydispersity of 1.08 and in the composition range (21 mol % PMMA) of the rod-dot transition.[39] They showed that the fractionated samples have more uniform morphologies than the original sample, and display a trend to greater rod-like content with increase in PS content, although with no sharp phase boundary.

Table 3-2. LB film morphology dependence on the hydrophilic block content in various diblock copolymer systems.

Copolymer	Planar–rod transition (mol %)	Rod–dot transition (mol %)
PS-PVP/PDP	8–9	16–20
PS-PVP$^+$C$_{10}$H$_{21}$I$^-$ [9]	6	14
PS-PnBMA [10,11]	10–15	~ 20[a]
PS-PtBMA [10,11]	> 5[b]	< 13[b]
PS-PtBA [10,37]	5–10	15–20
PS-PVP	19	29
PS-PEO [12,22]	~ 20	~ 30

[a] No compositions between 17 and 30 mol% were investigated.

[b] No compositions between 5 and 13 mol% were investigated (thus, it is not known if this system has a rod regime).

The wide ribbon-like form of the planar morphology has been reported previously for PS-PEO block copolymers in particular, first in ref. 12, where it was reported that LB films prepared with 15 and 19 mol % PEO (total M_w 24k and 14k, respectively) compositions from $CHCl_3$ solution concentrations of *ca.* 1 mg/mL (intermediate to our "low" and "high" concentration solutions) give a mixed morphology of ribbon-like aggregates, strands (often appearing to be partially fused), and circular aggregates. This was investigated in greater detail by Devereaux and Baker[16] using a 15 mol % (7 wt %) PEO copolymer (total M_w 51k). They showed that the proportion of the three aggregates (where the edges of the ribbon-like aggregates were more irregular than observed in the PS-PVP above) depends on the spreading solution concentration, with the ribbon-like structures, considered to be cracked "continents", being predominant for high concentration solutions (typically 2–4 mg/mL) and circular aggregates being predominant for low concentration solutions (typically < 0.5 mg/mL). (Nanostrands were never observed to be present to more than 50% and often much less in this copolymer.) Similarly, for the 141k PS-PEO copolymer of 24 mol% PEO (in the strand regime), the strand morphology is much better defined when obtained from higher concentration solutions (1.0 mg/mL) than for lower concentration solutions (0.25 mg/mL), the latter showing a predominance of looped structures (including rings).[18] These tendencies are clearly in agreement with our results, to the effect that high concentrations favour large planar aggregates or nanostrands (depending on the composition) and low concentrations favour generally smaller and (more) circular aggregates (typically of variable sizes).

3.3.1.4. Dimensions of Nanofeatures

It is of interest to measure the heights of the various nanofeatures as well as the diameters and center-to-center distances of nearest approach of the nanostrands and nanodots, and compare these values with relevant molecular parameters. Nanofeature dimensions for PS-PVP and equimolar PS-PVP/PDP are summarized Table 3-3.

Table 3-3. Heights and widths of the PS-PVP and PS-PVP/PDP$_{1.0}$ nanofeatures, and center-to-center distances between them using concentrated solutions and the conventional LB method.

Sample	Height, (±0.5) nm				Width, (±10) nm				Distance, (±15) nm			
	PS-PVP		PS-PVP/PDP		PS-PVP		PS-PVP/PDP		PS-PVP		PS-PVP/PDP	
	π=3	π=15	π=3	π=15	π=3	π=15	π=3	π=15	π=3	π=15	π=3	π=15
4%	11.3	11.4	11.5	10.0	varied	varied	varied	varied	varied	varied	varied	varied
8%	7.0	4.9	8.0	7.5	varied	varied	50-250	50-250	varied	varied	varied	varied
9%	5.0	4.3	6.0	6.2	varied	varied	70	70	varied	varied	70	65
12%	n/a	4.4	6.7	6.9	varied	varied	60	60	varied	varied	80	75
16%	3.3	3.8	4.0	2.7	varied	varied	55	40	varied	varied	95	70
19%	3.0	3.1	3.5	4.2	55	58	35	35	60	60	65	50
29_2%	2.6	2.9	5.4	5.4	47	40	50	60	40	60	85	75
29_4%	3.1	n/a	7.0	7.5	45	n/a	65	65	80	n/a	155	150
46%	3.2	n/a	3.9	4.1	70	n/a	45	45	90	n/a	120	110

Two trends, considering similar PS block lengths only, are especially noteworthy. One, the heights are clearly greatest for the lowest VP content, and rapidly decrease with increasing VP content to reach an approximately constant value. Second, this constant value is typically higher for PS-PVP/PDP than for PS-PVP. Since the PVP block is considered to exist as an adsorbed monolayer, the main contribution to the nanofeature heights must come from the PS block.[40] Thus, the heights can be compared to calculated dimensions related to the root mean square (rms) end-to-end distance of PS chains in a theta solvent (*R*) using equation (1):[41]

$$R = 0.274\sqrt{n}\ \ (nm) \qquad \textbf{(1)}^{*}$$

where *n* is the number of repeat units in the PS block. They were also calculated from the Kumaki equation, taking the diameter (*d*) of a sphere with area $\mathbf{A_{lim} = 0.04M}$,[42] which give lower values than equation (1), as shown when cast in the same form:

$$d = 0.230\sqrt{n}\ \ (nm) \qquad \textbf{(2)}^{\dagger}$$

Both values are tabulated in Table 3-4.

For the majority of compositions in the PS-PVP/PDP series, the measured heights are closer to the rms end-to-end distances of PS in a theta solvent than to the Kumaki values, whereas in the PS-PVP series the measured heights tend to be lower than even the Kumaki values. The lowest VP contents, especially 4% PVP and PVP/PDP, give measured heights that are much greater than the calculated values. This might be attributed to the very short VP block providing less adsorbed surface area above which the PS block can reside, thus causing greater accumulation of the PS chains.

---

[*] This equation is adapted from: $R_{g-\Theta} = 0.269\sqrt{M_W}$ where $R_{g-\Theta}$ is the rms end-to-end distance of PS in Å, M_W is the weight average molecular weight of PS. Substituting molecular weight of PS repeat unit gives: $R = 0.274\sqrt{n_{PS} \times PDI}$ where *R* is in nm now. Assuming $M_w/M_n \approx 1$ results in eq.1.

[†] Assuming a spherical PS particle, which occupies (on the water surface) an area (*A*) proportional to the molecular weight of PS, its diameter (and therefore, height of the surface micelle) can be derived as follows:

$$A = \pi \times \left(\frac{d}{2}\right)^2; \quad d = 2\sqrt{\frac{A/100}{\pi}} = 2\sqrt{\frac{0.04 \times (104.15 \times n_{PS})}{100 \times \pi}} = 0.230\sqrt{n_{PS}}\ \text{(nm)}$$

Table 3-4. Calculated values of the rms end-to-end distance of PS in a theta solvent (R, eq. 1) and the diameter of a PS sphere using the Kumaki equation (d, eq. 2), and comparison with the experimental heights of the surface micelles (π = 3 mN/m).

Sample	Calculated height of PS features (nm)		Experimental height of features (measured by AFM) (±0.5 nm)	
	R	d	for PS-PVP	for PS-PVP/PDP
4%	5.5	4.6	11.3	11.5
8%	4.9	4.2	7.0	8.0
9%	5.1	4.2	5.0	6.0
12%	5.4	4.5	4.4 ($\pi = 15$)	6.7
14_H%	13.5	11.3	–	11.5 (±1.5)
16%	5.5	4.6	3.3	4.0
19%	4.9	4.1	3.0	3.5
29_2%	4.8	4.0	2.6	5.4
29_4%	5.5	4.6	3.1	7.0
33_H%	7.2	6.0	–	10.5 (±1.5)
46%	3.8	3.2	3.2	3.9
49%	3.8	3.2	–	5.2

It is noteworthy that the planar aggregates often show ridges at their edges, as also observed by other groups.[9,16,18] They are barely if at all visible for 4 and 8% PS-PVP, are less than 0.5 nm high (relative to the inside part of the aggregate) for 4% PS-PVP/PDP, roughly 0.5 nm for 9 and 12 % PS-PVP, and 1 nm for 8% PS-PVP/PDP. The ridges were interpreted in ref. 9 as reflecting greater repulsion of the PS from the water surface at the edges of the aggregates, in ref. 18 as resulting from dewetting. The smallest aggregates in the planar morphology regime, *i.e.* those similar to nanodot sizes, have heights corresponding to those of the ridges. Generally, when mixed morphologies are present, the nanostrand heights are similar to those of the planar aggregate ridges, and nanodots are a little higher than nanostrands (noting that nanostrand ends often look as if they are capped with a nanodot), again as observed by others.[13,18]

Aggregation numbers of surface micelles, calculated by using the stoichiometric total area method[‡] described in ref. 43, are independent of the deposition pressures (the same as for PS-PEO[22]), and are 287±7 molecules per micelle for 29_4% PS-PVP/PDP$_{1.0}$, and 80±2 for 46 % PS-PVP/PDP$_{1.0}$. Other nanodot self-assemblies are characterized by either mixed structures incorporated or irregularity in the feature periodicities, thus calculation of aggregation numbers for those samples is considered not to be feasible. Previously, Devereaux and Baker reported an inverse linear relationship between the aggregation number and PEO content in PS-PEO (235±13, 95±18, and 35±5 molecules per micelle for 886, 2720, and 7841 PEO repeat units, respectively).[16,22] Our results do not follow this trend; the 29_2% and 46% PVP/PDP samples are of equal PVP block length (166 and 162 repeat units), but the aggregation numbers vary substantially. we can consider instead a direct dependence of the aggregation number on PS content, observing that when the number of PS repeat units decreases by half [29_2%: $n_{PS} = 398$; 46%: $n_{PS} = 192$], the aggregation number decreases in 3.6 times. Assuming a linear relationship, a simple calculation for $n_{PS} = 260$ gives 148 molecules per micelle, which is in good agreement with experimental data reporting an aggregation number of 122±3 for PS(27k)-PVP(25.2k)$^{+}$C$_{10}$H$_{21}$I^{-}.[43] In spite of additional experiments required to determine the limits of the above linear relationship, it seems evident that the aggregation number has a dependence on the molecular weight of the PS block. In ref. 22, when M_n(PEO) increases, M_n(PS) decreases, so the statement of *inverse* linear relationship between PEO and aggregation number can also be taken as a *direct* linear relationship between the latter and PS. The relationship is shown in Figure SI-3-3 of the Appendix, indicating that it is linear, although with a slope that is an order of magnitude less than that for PS-PVP/PDP.

[‡] The aggregation number (or the number of molecules per micelle) is calculated by dividing the area per micelle (which is obtained by dividing the area of the topography image by the number of micelles in it) by the area per molecule (which is determined from the deposition conditions and π/A measurements).

3.3.1.5. Effect of PDP Content

Since the nanostrand network morphology appears to be the most sensitive of the different morphologies to molecular and experimental conditions, and since it can be obtained reproducibly and almost purely for the 12% VP copolymer, this latter was chosen to investigate the effect of varying PDP content on the resulting LB monolayer morphology. As shown in Figure 3-7 for high concentration spreading solutions (transfer ratios 0.9–1.2), reducing the PDP content causes the morphology to tend towards that for pure PS-PVP. That is, for 1.5:1.0 VP:PDP, the nanostrand network is modified by the presence of short and thicker elongated structures as well as nodules, and for 2.0:1.0 VP:PDP, there are many quite large merged or planar-like areas interconnected with the nanostrands. A small excess of PDP, at least up to 1.0:1.3 VP:PDP, has no effect on the nanostrand network morphology (nor on the other morphologies as observed for all of the copolymers mentioned above for which both 1.0:1.0 and 1.0:1.3 VP:PDP compositions were investigated). However, with double the amount of PDP relative to VP, only short nanostrands remain, along with nanodots and circular and elongated nanorings (both isolated and at the end of nanostrands). The latter objects are spaced much further apart and are generally isolated for the 1.0:10.0 composition, indicating dilution of the PS-PVP copolymer aggregates. Presumably, given the transfer ratio, the large excess of PDP (lying flat on the substrate) surrounds those objects. Strands are still present (albeit short) with much higher PDP content (and using a somewhat more dilute spreading solution), as shown by the image for 1:10 VP:PDP. The main effect of dilution appears to be that the strands are very short and unconnected, to the extreme of being nanodots. The nanorings and a few other objects with loops may be viewed as strands with their two ends joined together, favoured by their extreme dilution in a PDP matrix. It is noteworthy that rings and looped strands were also observed in the PS-PEO copolymer of 23 mol % PEO (strand regime), obtained from dilute spreading solutions, mentioned above.

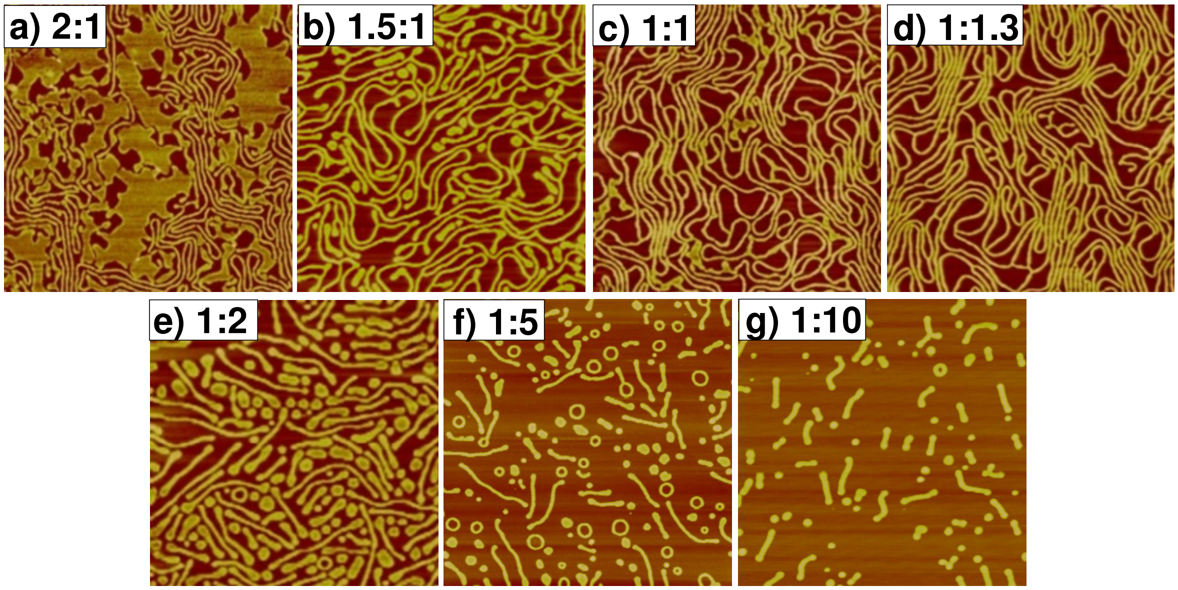

Figure 3-7. AFM height images of PS-PVP(12%)/PDP LB films spread from 1.8 mg/mL solutions (*g*: 1.1 mg/mL) with the different VP:PDP ratios indicated (π = 10 mN/m for b–f; 5 mN/m for a, g). Image scan: 5×5 μm.

3.3.2. Langmuir Compression Isotherms

Figure 3-8 shows Langmuir isotherms of PS-PVP copolymers of similar total molecular weights (37–59 kg/mol) but varying block fractions (4–46% VP), both alone and mixed with PDP (equimolar to VP), all spread from concentrated $CHCl_3$ solutions. (The isotherms for dilute solutions are generally essentially the same as for concentrated solutions, whereas those for 1.0:1.3 VP:PDP ratio show somewhat more expanded isotherms, shown in the Appendix, Figure SI-3-5) The isotherms for the polymers with lower PVP block fractions (without and with PDP) show only a monotonic, relatively featureless, increase in surface pressure. With increasing PVP block fraction, these isotherms first move to higher molecular areas, and then, at a critical PVP fraction, which corresponds to the appearance of nanodots in the AFM images, a plateau indicative of a transition develops. Accordingly, a hint of this plateau is detectable for 29_2% PVP (where nanodots are a minority morphology) and clearly visible for 29_4% PVP. The correlation between the appearance of a plateau and the nanodot morphology was observed previously by Zhu *et al.*[40]

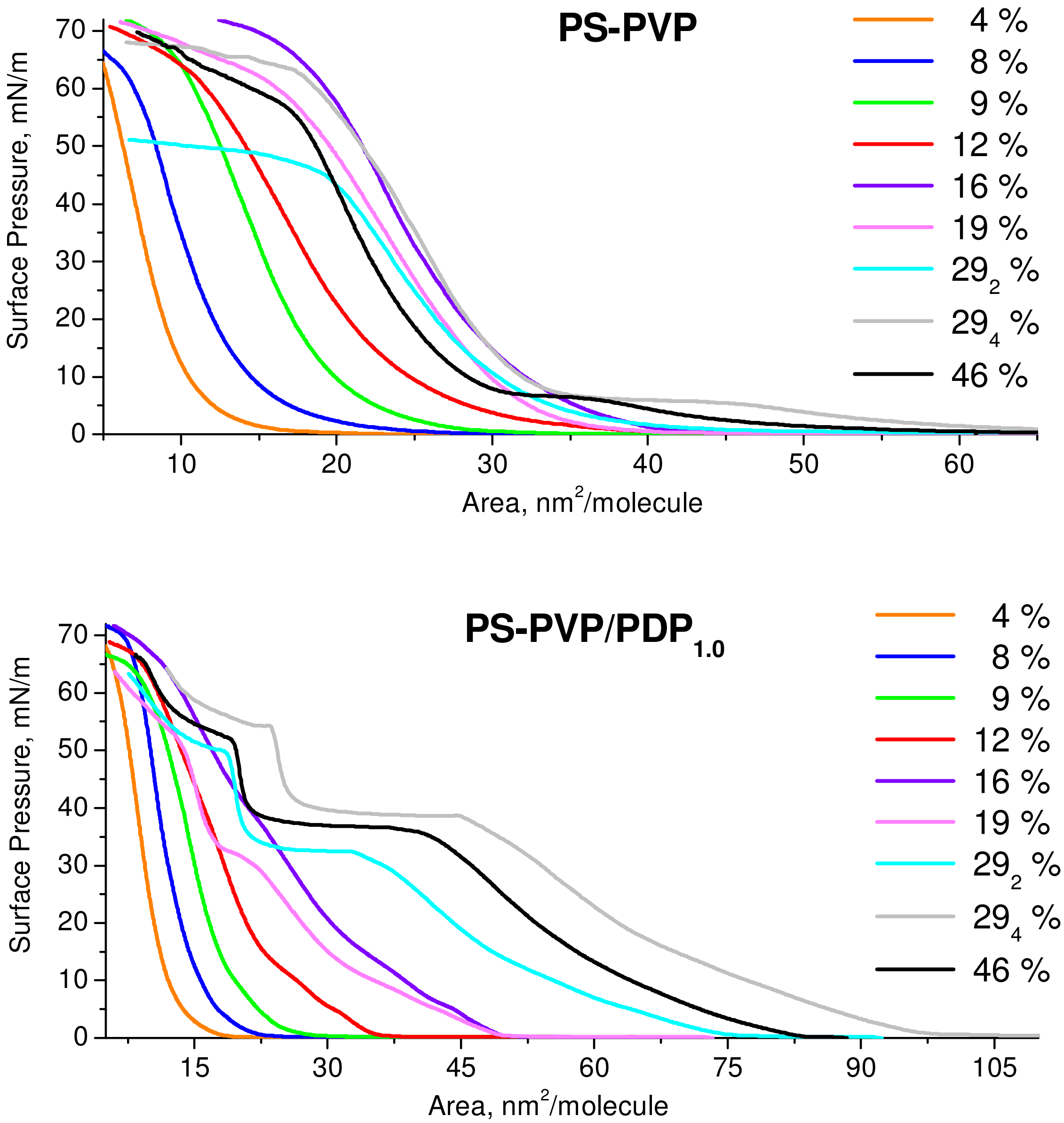

Figure 3-8. Langmuir compression isotherms of PS-PVP diblock copolymers (top) and their equimolar complexes with PDP (bottom) spread from $CHCl_3$ solution (1.8 mg/mL) at 21 ±0.5 °C. The nomenclature gives the mol % PVP content. The area is presented per polymer molecule. (In Figure SI-3-4, the area of above isotherms is presented per VP repeat unit).

For pure PS-PVP, the plateau appears at a low surface pressure of *ca.* 4 mN/m for VP contents of 29$_4$% and above. In comparison, PS-PEO diblock copolymers display a plateau at 5–10 mN/m for PEO contents above *ca.* 29 mol % (15 wt %), interpreted as a transition from surface-adsorbed to surface-solubilized PEO ("pancake→brush" transition)[44] or as a dehydration/conformational change of surface-adsorbed PEO[45] like for spread films of PEO homopolymer.[46] For PS-PVP/PDP (1.0:1.0), the plateau appears at a much higher surface pressure, 33–37 mN/m and a much lower VP content, 16 mol% (where it is very slightly visible, whether using the low or the high concentration spreading solutions, corresponding to the appearance of a minority nanodot morphology). This is comparable to the plateau pressure of 29–38 mN/m in the isotherms of the PS-PVP$^+$RX$^-$ diblock copolymers above *ca.* 14 mol% VP content.[9] In the latter, this plateau was initially interpreted as a transition from surface-adsorbed to subphase-solubilized PVP$^+$RX$^-$, also called the "starfish → jellyfish" transition.[9] However, later it was interpreted, based on *in-situ* X-ray and neutron reflectivity and infrared analysis, as arising from a disorder–order transition of the alkyl side chains; that is, the PVP block does not desorb from the water surface to solubilize into the water phase, but instead, it is the alkyl chains that become more ordered into a trans conformation.[47]

The much higher plateau pressure for the copolymers mixed with PDP compared to PS-PVP alone and its similarity to the plateau pressure for PS-PVP$^+$RX$^-$ can be attributed to the stabilizing effect of the alkyl sidechains. This is supported by the decrease in plateau height with decrease in alkyl chain length observed in surface micelle-forming PS-PVP$^+$RX$^-$ copolymers of varying alkyl chain length (R). It is noteworthy that the isotherm of pure PDP also displays a plateau at *ca.* 43 mN/m, but which is attributed to collapse; the lower plateau near 6 mN/m is thought to be related to the alkyl chain reorientation from prone to vertical.[48] In the isotherms of the 12% PVP copolymer with varying VP:PDP ratio, shown in Figure 3-9, this plateau increases in length with increasing PDP content, as might be expected.

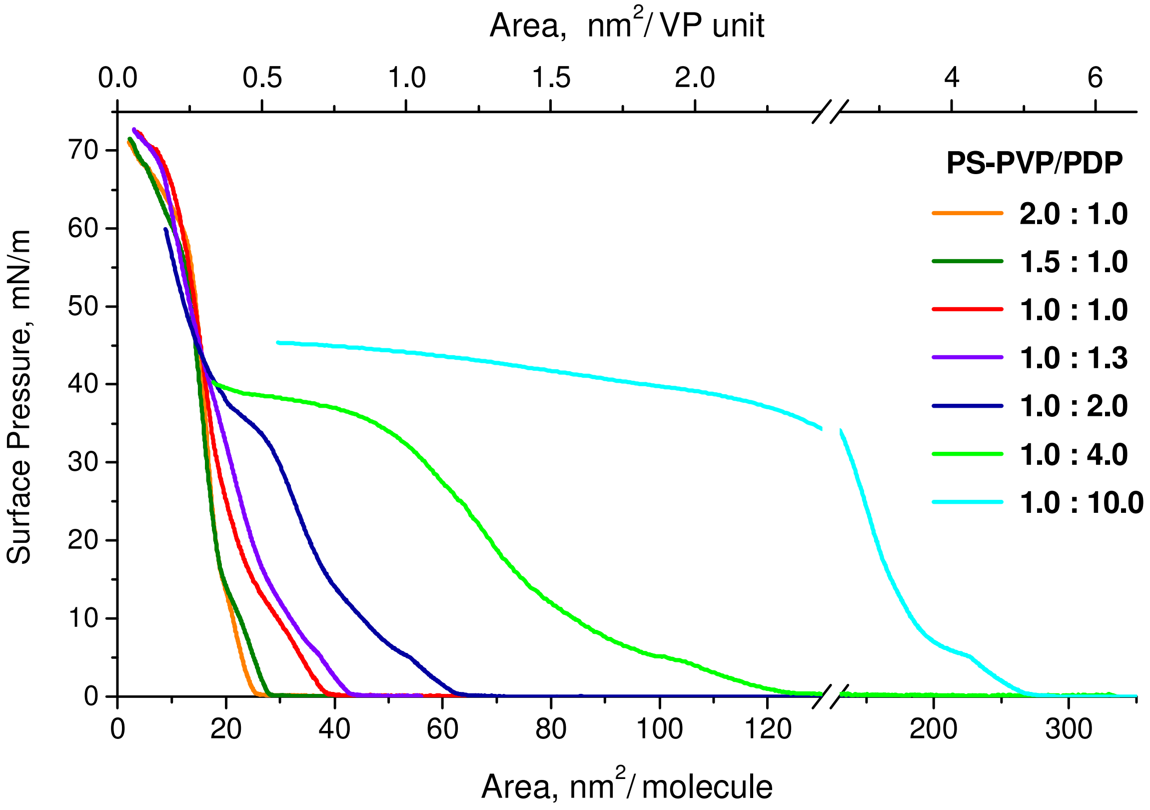

Figure 3-9. Langmuir compression isotherms of 12% PS-PVP/PDP spread from $CHCl_3$ solutions (concentration of copolymer 0.35 mg/mL) at 21 ±1°C. The numbers indicate VP:PDP molar ratios. (The isotherm of pure PDP is presented in Figure SI-3-6).

The plateau length per molecule for the copolymers, with and without equimolar PDP present, tends to increase with increase in content of the hydrophilic block (Figure 3-8), as observed previously for PS-PVP$^+$RX$^-$ [9,49,50] and PS-PEO.[22] In addition, it appears to depend to some extent on molecular weight; for example, it is significantly longer for the higher molecular weight 14_H% PVP/PDP copolymer, 252k-43k, than for the 16% PVP/PDP copolymer,

42k-8k, where both have a small excess of PDP (1.0:1.3 VP:PDP) present (Appendix, Figure SI-3-5). However, this might be related more directly to the majority nanodot morphology (even if variable in size) found for the former compared to the minority nanodot morphology for the latter.

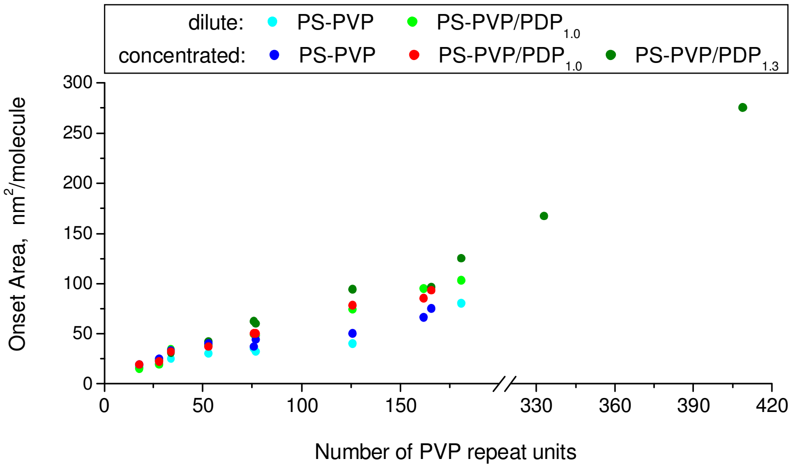

Figure 3-10. Onset area per polymer molecule in PS-PVP and PS-PVP/PDP Langmuir compression isotherm as a function of length of PVP block.

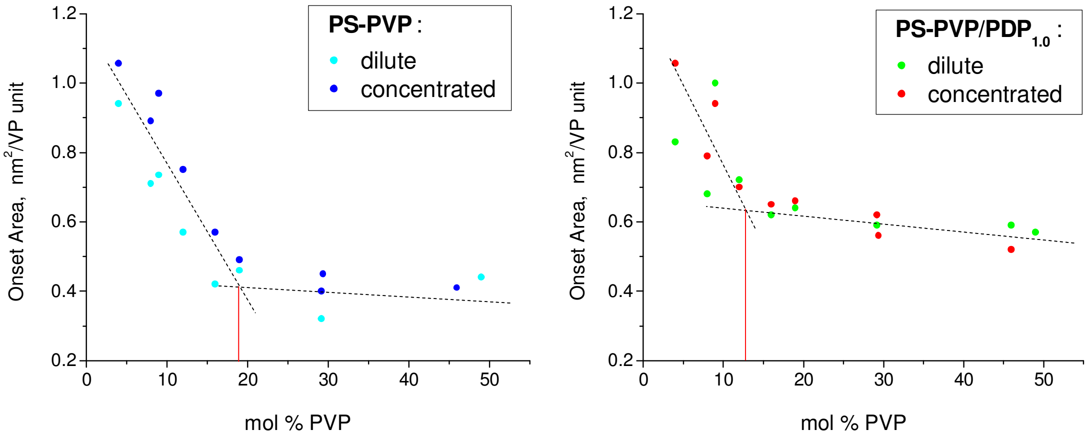

Figure 3-11. Onset area per VP repeat unit in PS-PVP (left) and PS-PVP/PDP$_{1.0}$ (right) Langmuir compression isotherms as a function of molar fraction of PVP block.

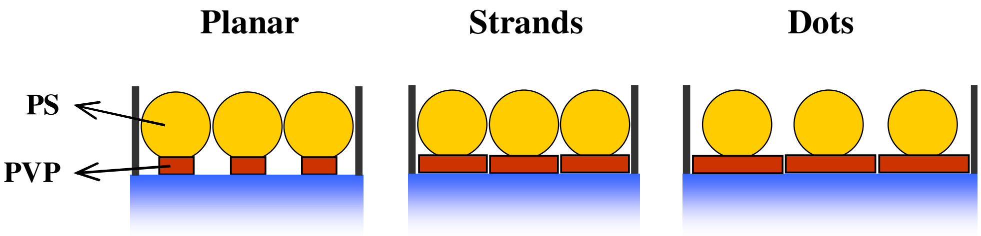

Figure 3-12. Schematic representation of the contributions of the hydrophilic and hydrophobic blocks to the onset areas for films of different morphologies.

It is of interest to compare the onset areas of the various isotherms. When the onset area per molecule is plotted as a function of number of repeat units in the PVP block, including the data from low and high concentration solutions, an essentially linear relationship is observed for both PS-PVP and PS-PVP/PDP (Figure 3-10). However, it is more instructive, under the assumption that the polar PVP is spread as a monolayer on the water surface including beneath hydrophobic PS, to plot the values of onset area per VP against mol % VP. This is shown in Figure 3-11 for the copolymers with and without equimolar PDP present, including various total molecular weights and including for high (1.8 mg/mL) and low (*ca.* 0.3 mg/mL) concentration solutions. A first observation is that there is no significant difference within experimental uncertainty between the two spreading solution concentrations. In fact, the isotherms for the two concentrations are generally very similar to each other in each case, as was found also by Moffitt and coll. for limiting areas of a PS-PEO block copolymer in this concentration range.[17] Second, the onset areas per VP repeat unit tend to decrease quite sharply with increasing mol % VP to then tend to a constant value, particularly in the range of mol % VP for which a plateau is found in the isotherms. If limiting values [defined by extrapolation to zero surface pressure of the linear portion of the surface pressure rise – unambiguous in the isotherms without plateaus, taken as the linear part immediately after the plateau in the isotherms with plateaus (usually, but not always, reasonably well defined)] are plotted instead (Appendix, Figure SI-3-7), the overall trend is the same.

As shown above, the morphologies of the LB films corresponding to the Langmuir isotherms with plateaus are in the form of nanodots, which lead to quite uniform and well-defined films, whereas those corresponding to the isotherms without plateaus have irregular structures that do not allow optimal packing, leaving many empty places in the film. From this point of view, the rise in onset area per VP with decreasing PVP content can be attributed, at least in part, to an artifact caused by the non-uniformity of the film, and is therefore not necessarily molecularly meaningful. (This also can account for the rather large scatter in the values.) One might also speculate that the PVP monolayer in the lower PVP content films may become increasingly stretched on the water surface with decreasing PVP content, to accommodate the much larger hydrophobic PS fraction. In other words, its coverage beneath the aggregates may become increasingly less dense. This would also be consistent with the greater height of the planar structures for low PVP content, as noted above, in that less coverage by PVP implies lesser shielding of PS from the water surface, which may cause it to extend away from the water surface to a greater extent.

The constants to which the onset values tend should be interpretable on a molecular level. The value for PS-PVP alone is somewhat lower, at 0.4±0.1 nm/VP, than for PS-PVP/PDP, at *ca*. 0.55–0.60 nm/VP. If the limiting area relative to the total number of VP repeat units is examined, they similarly show a decrease in value to a constant with increasing mol % VP. In this case, the constant is *ca*. 0.35±0.05 and 0.45±0.05 nm/VP for PS-PVP without and with PDP, respectively (Appendix, Figure SI-3-7). This is comparable to the value of 0.34 nm/VP determined for a PVP homopolymer monolayer[51] and 0.48 nm/VP for alkylated PVP homopolymer monolayers,[52] respectively. Similarly, a value of 0.45 nm/VP was observed for the nanodot-forming PS-PVP$^+$RX$^-$ copolymer in ref. 40 (when PS is not subtracted), with more variable values obtained for a larger series of PS-PVP$^+$RX$^-$ in ref. 9. The higher value when PDP is present seems reasonable, considering that H-bonding of PDP to PVP might be expected to cause greater extension of the PVP chains for steric reasons, especially if it tends to lie prone to the surface. The value for alkylated PVP was attributed to ionic repulsion of the polyelectrolyte chains, but the similar result for PS-PVP/PDP suggests that the alkyl chain is equally responsible.

An additional observation can be made for the plots of onset area per VP unit *vs*. mol% PVP (Figure 3-11). If the low and high mol% VP ranges are approximated by two lines, these lines intersect at a composition that corresponds to that for the strand morphology for both the pure diblock copolymer and complex series. This suggests the following interpretation. When planar aggregates are formed, the PVP block is very short and lies under the PS. In this case, the PS contribution to the molecular area outweights the PVP contribution, thus giving onset areas per VP unit that are exaggeratedly high (Figure 3-12a). In this case, the smaller the relative PVP block length, the greater the overestimation in terms of mol% VP, thus explaining its linear increase with decrease in mol% VP. For the strand and dot morphologies, the molecular area is defined correctly by the contribution of hydrophilic block, as illustrated in Figure 3-12b,c, and thus, the onset area per VP unit becomes almost constant with VP content. The strand morphology is where the PS and PVP contributions are similar.

3.3.3. General Discussion and Mechanisms of Morphology Formation

This discussion, in its references to the literature on LB block copolymer films, is limited to systems for which the initial spreading solutions are not micellar or otherwise structured. We also consider only a pure H_2O subphase, which is not manipulated in any way (*e.g.* by changing pH or by adding a complexing substance) to influence the monolayer on its surface. Within this framework, the wide-ranging results presented above allow a more complete understanding of the likely processes occurring at the air/water interface that determine the final morphologies observed in the LB films. What follows brings together, refines and extends ideas previously exposed in the literature.

First of all, this work reinforces previous studies[9–12] on LB films of block copolymers showing that the relative block length is a primary factor in determining the type of surface aggregation that occurs at the air/water interface. It also confirms that spreading solution concentration, as well as molecular weight, can quite strongly influence the LB film morphology,[16–18,24] especially the nanostrand (rod-like) and planar types. Well-developed and (almost) pure nanostrand morphology is generally favoured within the appropriate composition range by sufficiently concentrated solutions and for moderate molecular weights. Planar-type aggregates tend to vary greatly in form depending on solution concentration, and often several forms coexist (including dots and strands, albeit generally with much greater variability in diameter/width compared to the "true" nanostrand and nanodot morphologies). Coexistence of morphologies is, of course, inevitable in the vicinity of morphological transition compositions (which, furthermore, are relatively broad).

The basic principles underlying morphology formation in relation to the relative block copolymer chain lengths, and which give rise to different morphologies in different composition ranges,[9–12] can be viewed as the result of a competition between the tendency of the hydrophilic block to spread as a monolayer adsorbed to the water surface, thereby maximizing its lateral area, and the tendency for the hydrophobic block to coil away from both the water surface and the hydrophilic monolayer, thereby minimizing its lateral area. When the hydrophilic block is very short, extensive association of the hydrophobic blocks is allowed, and is favoured, furthermore, by the resulting reduction in the interfacial energy of this phase with the air surface. In this case, practically the entire hydrophilic block is located as a monolayer between the water surface and the hydrophobic block. When the hydrophilic block is much longer, its monolayer form simultaneously maintains significant distance between the hydrophobic aggregates to prevent further association and limits the number of hydrophobic chains ("aggregation number") that can actually associate into each aggregate, thereby resulting in the formation of relatively uniformly sized hydrophobic nanodots or circular surface micelles. Rod- or strand-like structures are perceived as an intermediate regime, somewhat analogous to cylindrical structures in the bulk.

This same picture was given for the ultrathin PS-P(2 or 4)VP films spin-cast (or dip-coated) onto a solid hydrophilic surface from ultradilute $CHCl_3$ solutions, as mentioned earlier, and supported by extensive theoretical modeling.[25,53–57] The nanodot morphology was shown to be an equilibrium morphology by the observation that thermal annealing did not destroy the structure, but perfected it.[25] Further analysis as a function of the relative block lengths led to an equilibrium phase diagram for the three major regimes of surface patterns: planar ("brush"), strands ("stripes") and micelles (along with a fourth regime of single chains for very short hydrophobic blocks).[55] This analysis also showed that the stability of the "stripe" regime can be reduced and even eliminated for a certain range of block lengths and interfacial energies, which may be one reason for the apparent absence of this morphology in some systems mentioned above. In these morphologies, the hydrophilic block is considered as a strongly adsorbed integral monolayer film, whereas the hydrophobic block in the planar regime is considered to cover the adsorbed hydrophilic monolayer and in the stripe and micellar regimes is considered to be "dewetted" on top of the adsorbed hydrophilic monolayer. The nanostrands observed by us and others are, however, mainly separated from one another. We previously postulated that they actually result from disassembly, at the level of the hydrophilic stripes during continued spreading, of a stripe ("fingerprint") pattern that developed in the course of the spreading/evaporation process on the water surface.[15] This explanation reconciles the theoretical analysis involving the stripe regime and the experimental observation of separated nanostrands.

Given the consistency of the morphological dependence on relative block length observed in our LB systems and those in the literature, as shown above, we believe that the picture and theoretical analysis of ultrathin amphiphilic block copolymer films on hydrophilic solid surfaces[25,53–57] is directly applicable to these films spread on a water surface. In other words, the variety of morphological forms observed in LB diblock copolymer films, where one block is strongly adsorbing on the water surface (hydrophilic) and the other non-adsorbing (hydrophobic), should fall within the same three basic morphology regimes (or possibly four if considering also very short hydrophobic blocks, not yet investigated on a water surface to our knowledge) identified for the ultrathin films on the solid surface, and shown to be determined by the relative block lengths in conjunction with the various interfacial and chain stretching energies involved.

On the other hand, an important difference observed between the two surfaces is that spreading on water generally involves a maximal area that is so large that even the hydrophilic film is subject to some kind of dewetting that contributes to the final morphology. Furthermore, the interplay between spreading over this surface and solvent evaporation renders the system susceptible to kinetically frozen-in structures before spreading is completed. This is especially true when the hydrophobic block is a high T_g polymer, as is the case with the majority of LB block copolymer films investigated to date, which most often involve a PS block. In addition, the hydrophilic (water-loving) block is likely to maintain mobility throughout the morphology formation process, due to its effective plasticization by H_2O. This is where the discussions of Baker and coll. and Moffitt and coll., and the dependence of morphological forms on solution concentration (which is contrary to an equilibrium process), are relevant.

For this, the complexity of the spreading process combined with simultaneous solvent evaporation that follows drop deposition on the water surface must be taken into account.[15–17,24] On the one hand, it is necessary to consider the association or coalescence of individual chains that must occur in the course of the spreading/evaporation process, since, as pointed out elsewhere,[15,16,22] the spreading solutions generally have concentrations that are well below that of the critical concentration for entanglements (c*). In our case, we estimate that, using the same equation[§] as in ref. 16, these critical concentrations are 16 and 56 mg/mL for the $14_{H}\%$ and $33_{H}\%$ copolymers, respectively, the two highest molecular weight polymers of those investigated here (for copolymers of lower molecular weight, c^* is further increased). Thus, the polymer solutions used cannot be considered as being near the critical entanglement concentration. This means that the chains are initially individually solvated, and aggregate in the course of the spreading/evaporation process.[24] (It may be noted that aggregation may or may not include entanglement; since entanglement should occur on a longer time-scale than simple association, it might be disfavoured if the system becomes freezes in before significant entanglement occurs.) This, in turn, implies that the extent of association and reorganization in response to changing local polymer concentration and film thinning as spreading continues and solvent evaporates, can also be subject to kinetic limitations and become frozen in. On the other hand, the spreading drop itself, initially a uniform film of solution, becomes subject to dewetting during the spreading/evaporation process.[18] This can occur as an equilibrium process on the level of the hydrophobic block relative to the hydrophilic monolayer, as posited for the nanodot and nanostrand morphologies,[25,53–55] or as a kinetically controlled process on the level of the entire film relative to the water surface.[18]

With the above considerations in mind, the film-forming process, with reference to PS-PVP, can be viewed as follows. As any given drop hits the surface and begins to spread, the individual polymer chains in the drop position themselves almost instantaneously such that (a) the hydrophilic (PVP) block adsorbs to the water surface to decrease the interfacial energy of H_2O with the hydrophobic (PS) block and the H_2O-immiscible spreading solvent

---

[§] $c^* = \dfrac{3MW}{4\pi N_A\sqrt{(R_g^2)^3}}$ where c^* is the critical overlap concentration, *MW* is the molecular weight of the entire polymer, N_A is Avogadro's number, $(R_g^2)^{1/2}$ is the radius of gyration of a polymer chain in a good solvent. $(R_g^2)^{1/2} = a \times n_{PS}{}^{0.6}$, where a is the effective monomer length (and equal to 1.8 Å, as determined by light-scattering for PS in toluene) and n_{PS} is the number of PS units in the polymer. Hence it follows: $c^* = \dfrac{68 \times MW}{n_{PS}{}^{1.8}}$, mg/mL.

($CHCl_3$), and (b) the PS block bathed in the spreading solvent resides above the nascent PVP monolayer. (It should be pointed out here that $CHCl_3$ is a better solvent for PS than for PVP,[8] so that the underlying PVP monolayer is likely to lose solvating $CHCl_3$ much earlier than the PS layer for this reason in addition to its being driven off to minimize $H_2O/CHCl_3$ contact.) As solvent evaporates, thus increasing the local polymer concentration, polymer chain association occurs, driven by the decrease in interfacial energy with H_2O by its coverage with PVP and with air by PS association. However, eventually this association is limited either because the equilibrium extent of association has been reached or because chain immobilization sets in due to solvent evaporation increasing the T_g of at least the hydrophobic block to above the working temperature. In addition, depletion of polymer chains may occur around growing aggregates, due to relatively slow chain kinetics, which, if polymer immobilization sets in, will stop further growth. This is where both spreading solution concentration and molecular weight can have an influence. The lower the solution concentration, the lower the local polymer concentration in the spreading drop, and the earlier polymer depletion around growing aggregates may occur. Similarly, the higher the molecular weight, the slower the chain kinetics, which can also induce earlier depletion. These kinetic effects can be expected to be present in particular for morphologies for which the equilibrium extent of association is high. Subsequent film dewetting will, in turn, be influenced by the extent and type of aggregation. These principles will now be explained in further detail with reference to the specific morphology types.

The nanodot or surface micelle morphology, where the extent of aggregation (as given by the aggregation number) is finite, undoubtedly develops during the spreading process and is the closest to an equilibrium morphology (the greater the nanodot order, the closer it is to equilibrium). This rationalizes our experimental observations to the effect that the nanodot morphology is essentially independent of the initial spreading solution concentration. In this morphology, the PVP monolayer retains mobility on the water surface. Therefore, as spreading continues to a surface area greater than that occupied by a continuous PVP monolayer, the film can be expected to dewet essentially anywhere along the micelle peripheries where the extended PVP chains from neighboring micelles meet. This may result in disordered individual micelles or groups of ordered micelles in variably sized integral films (*i.e.* integral at the level of the PVP monolayer). Any dewetting of a still mobile film of solution will have a similar result. However, upon barrier compression to positive surface pressure, the PVP mobility allows re-association into a uniform monolayer (at the PVP level). Therefore, under usual conditions of LB film transfer (at positive surface pressure) and for a transfer ratio near unity, film dewetting at the level of the PVP monolayer is not observed. Kinetic effects may enter in for very high molecular weight copolymers, reducing only the extent of nanostructure order, not its type, as observed in 33_H% PVP/PDP. This can be attributed to the slower kinetics of such long chains to associate into relatively uniform and circular nanodots.

At the other extreme, in the planar-type morphologies found for short PVP blocks and comparatively much longer PS blocks, the PS phase is a continuous layer above a PVP wetting layer that, at equilibrium, is a result of unlimited chain aggregation (thus with an effectively infinite aggregation number). In this case, slow chain kinetics creating depletion zones around growing aggregates can be expected to significantly limit aggregate growth. Clearly, these dynamics will be influenced by the initial solution concentration. In particular, lower local polymer concentration on the water surface will result in earlier formation of depletion zones and therefore less aggregation, thus leading to smaller final aggregates. [A counter-argument that more concentrated polymer solutions should have slower polymer kinetics (higher viscosity) is considered to be less significant, since the solutions are below the critical entanglement concentration, and, even as local concentration increases due to solvent evaporation, little entanglement may ensue if the timescale for entanglement is too slow.] This is essentially what our results (and, it can be argued, those in ref. 16) generally show when comparing the planar-type morphologies obtained from low and high concentration solutions.

Moreover, it is striking that the planar aggregates tend to be more rounded, even disk-like, for low concentration solutions and in the form of often wide ribbons for high concentration solutions, particularly evident for PS-PVP without PDP (and for PS-PEO[16]). This can be explained on the basis that the PS layer in the planar morphology completely covers the PVP monolayer and it is glassy when aggregate growth ceases. This means that, on further spreading, the already formed aggregates simply float around on the surface and that, with barrier compression, they are simply pushed more closely together. For low-concentration solutions, the depletion zones circumscribe the aggregates and therefore also the places where dewetting happens. The high-concentration morphology in the planar regime is, in contrast, a consequence of the break-up or cracking of very large planar aggregates (glassy films). It is interesting that partial linear cracks are also sometimes visible across ribbon-like structures (*e.g.*, 9% PVP in Figure 2). These cracks might occur during the last stages of spreading as a kind of dewetting, or during barrier compression, due to the propagation of cracks initiated from sites of imperfection; but we believe that it is even more likely to occur during LB film transfer, due to the bending of a glassy film in going from a horizontal to a vertical surface. In the case of limited aggregate growth, it may be expected that the 2D planar morphology should give rise to disk-like aggregates in the absence of any surface perturbation. However, surface perturbation of any kind (*e.g.*, slight temperature gradients, impurities, air movement) may give rise to a wide variety of 2D forms, including strand-like objects[**] (as observed for oil slicks on water surfaces). In addition, dewetting of (still mobile) polymer solution film relative to the water surface may take place simultaneously with aggregation, also leading to variably sized and shaped aggregate forms, as discussed in ref. 18. This is most likely to be prevalent in the planar aggregate regime, since the polymers with short PVP blocks have a much smaller surface coverage compared to those with longer PVP blocks (for similar total molecular weights).

Nanostrand network formation has been amply discussed in ref. 15, and summarized above. Basically, we proposed that it is formed via a stripe (fingerprint) morphology, where PS is dewetted in stripes above a PVP monolayer, followed by dewetting, this time at the level of the PVP stripes, upon further spreading to the entire available water surface. This can account not only for the extensive surface coverage possible with the nanostrand morphology (see ref. 15), but also the high uniformity of the nanostrand widths, in contrast to the strand-like forms sometimes observed in the planar morphology regime, where they are usually mixed with various other forms and where the widths show significant variability not only from strand to strand but also along a single strand (see, *e.g.*, refs. 16 and 20). Like for the planar morphology, the equilibrium extent of aggregation is

---

[**] Some of the strand-like morphologies observed for PS in ref. 20 may be called "Chee Chee" morphologies due to their strong resemblance to some paintings of Canadian native artist, Benjamin Chee Chee.

effectively indeterminate, with the difference that it is one-dimensional rather than two-dimensional. If the extent of aggregation is limited due to depletion (as in dilute spreading solutions) or slow kinetics (as for high molecular weight polymers, *e.g.* $14_H\%$), then, as for the planar aggregates, the aggregates formed will be much smaller (shorter strands, which may also favour looped or ringed structures through end-to-end association, or dot-like), and the subsequent dewetting (relative to the water surface) will occur around these smaller aggregates at the level of the mobile PVP located in these regions. The re-association into an integral stripe texture upon barrier compression does not occur because the floating about of the separated strands on the expanded surface has randomized their relative positions too much. For this morphology, dewetting of the spreading drops relative to the water surface that might occur in competition with polymer chain association is expected to have a less major effect on the nanostrand morphology compared to planar morphology, since this morphology, like the nanodot morphology, is based essentially on the internal lateral nanostructure of the spreading film (in contrast to the planar morphology, for which the spreading film has no internal lateral nanostructure).

Finally, a few comments concerning the role of PDP should be made. Although no direct proof is given, the distinct differences between PS-PVP/PDP and pure PS-PVP LB films and the striking similarities of the former with the PS-PVP$^+$RX$^-$ system is strong indirect evidence that PDP is actually present in the films obtained from PS-PVP/PDP solutions (this question is revisited in the next chapter). It was shown that the presence of PDP modifies the composition ranges of the three main morphology regimes, provides more uniform transferred films (fewer bare areas in accordance with higher transfer ratios and more extensive morphological uniformity in transferred LB films), and raises the plateau pressure of nanodot-forming films to that observed for PS-PVP$^+$C$_{10}$H$_{21}$I$^-$. The effect on the transition compositions and plateau pressure can be ascribed to its role as hydrogen-bonded PVP side chains, in parallel with the alkyl side chains of PS-PVP$^+$RX$^-$[9,49] and the PS-poly[alkyl(meth)acrylate] polymers mentioned above.[10,11,37] The difference in onset/limiting areas for PS-PVP versus PS-PVP/PDP (similar to PS-PVP$^+$RX$^-$), at least for higher VP content, indicates that the alkyl side chains exert an expansion effect on the PVP chains on the water surface. This will modify the ratio between the lateral areas taken up by PVP compared to PS for a given composition. It seems reasonable that the morphological transitions are determined by this ratio, which increases in order of planar to nanostrand to nanodot morphologies. In this case, it is logical that the addition of PDP decreases the transition compositions. The greater morphological uniformity obtained in the presence of PDP may be compared to a similar effect observed by the addition of 4'-pentyl-4-cyanobiphenyl (5CB, a well-known liquid crystal in the bulk) to an approximately symmetrical PS-PVP giving the nanodot morphology.[58] The effect might be related, in part, to a plasticizing role of the PDP as a side chain to PVP (5CB may also associate via its cyano terminal group with PVP), or to some surfactant role as a mobile small molecule. As mentioned earlier, it has been shown that the PS phase (in the bulk) can solubilize a small amount of PDP;[38] if true in the LB film, then the PS phase, which is the crucial one that becomes immobile, will also be plasticized (have a reduced T_g). Any, or a combination of, these effects will maintain mobility in the system for a significantly longer time during the spreading/evaporation process, which may be enough to enable improved order.

3.4. CONCLUSIONS

Using PS-PVP block copolymers with a wide range of block fractions, spread from both low and high concentration solutions, with and without the presence of equimolar PDP as well as various VP:PDP molar ratios, we have reached a more complete understanding of their morphology formation at the air/water interface. The study has reinforced the importance of composition in determining the type of morphology, classed into three main regimes (planar, rod/nanostrand, micelle/nanodot), as shown in just a few previous publications for other systems. In comparing the transition compositions in our systems with those previously published, it seems that they depend primarily on the presence or not of an alkyl chain (not its length) attached to the hydrophilic block. This dependence may actually be related to the lateral area per hydrophilic repeat unit [affected by the presence or not of PDP (and therefore alkyl chain), as shown by the onset and limiting areas of the Langmuir isotherms] and/or to the resulting modification of the different interfacial energies involved. It has been shown that the spreading solution concentration can strongly influence the planar and nanostrand morphology regimes. This was related to more limited polymer chain association for low concentration solutions due to diffusion limitations in combination with the cessation of mobility of the hydrophobic block when its T_g rises above the subphase temperature as solvent evaporates; this, in turn, influences the dewetting that occurs relative to the water surface. High total molecular weight tends to have similar effects as low concentration solutions, due to the slower chain kinetics. High concentration solutions enable more extensive chain association before diffusion and mobility limitations, combined with dewetting, set in. In the planar regime, this implies the possibility of much larger planar aggregates, which, however, because they are glassy, can crack due to dewetting in the final stages of spreading, and/or during barrier compression, and/or (particularly likely) during film transfer. In the nanostrand regime, we already proposed in the previous chapter that large-scale aggregation in the form of a periodic stripe or fingerprint morphology takes place during spreading; it then dewets (disassembles) on the level of the hydrophilic stripes on continued spreading to form the nanostrand network. Similarly, in the nanodot regime, the film during spreading becomes nanostructured as observed in the LB films, due to having finite aggregation numbers; these might dewet during final spreading on the water surface, but can reform into a continuous film due to the mobility of the hydrophilic block during barrier compression.

References to Chapter 3:

1. (a) Bates, F. S.; Fredrickson, G. H. Block copolymer thermodynamics: Theory and experiment. *Annu. Rev. Phys. Chem.* **1990**, *41*, 525–557. (b) Bates, F. S.; Fredrickson, G. H. Block copolymers – Designer soft materials. *Phys. Today* **1999**, *52*, 32–38.
2. Hamley, I. *The Physics of Block Copolymers*. Oxford University Press: Oxford, 1998.
3. Abetz, V.; Simon, P. F. W. Phase behaviour and morphologies of block copolymers. *Adv. Polym. Sci.* **2005**, *189*, 125–212.
4. Fasolka, M. J.; Mayes, A. M. Block copolymer thin films: Physics and applications. *Annu. Rev. Mater. Res.* **2001**, *31*, 323–355.
5. Hamley, I. W. Ordering in Thin Films of Block Copolymers: Fundamentals to potential applications. *Prog. Polym. Sci.* **2009**, *34*, 1161–1210.
6. Li, M.; Coenjarts, C.A.; Ober, C. K. Patternable block copolymers. *Adv. Polym. Sci.* **2005**, *190*, 183–226.
7. van Zoelen, W.; ten Brinke, G. Thin films of complexed block copolymers. *Soft Matter.* **2009**, *5*, 1568–1582.
8. van Zoelen, W.; Asumaa, T.; Ruokolainen, J.; Ikkala, O.; ten Brinke, G. Phase behavior of solvent vapor annealed thin films of PS-b-PVP(PDP) supramolecules. *Macromolecules* **2008**, *41*, 3199–3208.
9. Zhu, J.; Eisenberg, A.; Lennox, R. B. Interfacial behavior of block polyelectrolytes. 5. Effect of varying block lengths on the properties of surface micelles. *Macromolecules* **1992**, *25*, 6547–6555.
10. Li, S.; Hanley, S.; Khan, I.; Varshney, S. K.; Eisenberg, A.; Lennox, R. B. Surface micelle formation at the air/water interface from non-ionic diblock copolymers. *Langmuir* **1993**, *9*, 2243–2246.
11. Li, S.; Clarke, C. J.; Lennox, R. B.; Eisenberg. A. Two-dimensional self assembly of polystyrene-b-poly(butyl-methacrylate) diblock copolymers. *Colloids Surfaces A* **1998**, *133*, 191–203.
12. Cox. J. K.; Yu, K.; Constantine, B.; Eisenberg, A.; Lennox, R. B. Polystyrene–poly(ethylene oxide) diblock copolymers form well-defined surface aggregates at the air/water interface. *Langmuir* **1999**, *15*, 7714–7718.
13. Seo, Y.-S.; Kim, K. S.; Galambos, A.; Lammertink, R. G. H.; Vancso, G. J.; Sokolov, J.; Rafailovich, M. Nanowire and mesh conformations of diblock copolymer blends at the air/water interface. *Nano Lett.* **2004**, *4*, 483–486.

14. Lu. Q.; Bazuin, C. G. Solvent-assisted formation of nanostrand networks from supramolecular diblock copolymer/surfactant complexes at the air/water interface. *Nano Lett.* **2005**, *5*, 1309–1314.
15. Perepichka, I. I.; Badia, A.; Bazuin, C. G. Nanostrand formation of block copolymers at the air/water interface. *ACS Nano*, **2010**, *4*, 6825–6835.
16. Devereaux, C. A.; Baker, S. M. Surface features in Langmuir-Blodgett monolayers of predominantly hydrophobic poly(styrene)–poly(ethylene oxide) diblock copolymer. *Macromolecules* **2002**, *35*, 1921–1927.
17. Cheyne, R. B.; Moffitt, M. G. Novel two-dimensional "ring and chain" morphologies in Langmuir-Blodgett monolayers of PS-b-PEO block copolymers: Effect of spreading solution concentration on self-assembly at the air/water interface. *Langmuir* **2005**, *21*, 5453–5460.
18. Cheyne, R. B.; Moffitt, M. G. Self-assembly of polystyrene-block-poly(ethylene oxide copolymers at the air–water interface: Is dewetting the genesis of surface aggregate formation? *Langmuir* **2006**, *22*, 8387–8396.
19. Cheyne, R. B.; Moffitt, M. G. Controllable organization of quantum dots into mesoscale wires and cables via interfacial block copolymer self-assembly. *Macromolecules* **2007**, *40*, 2046–2057.
20. Price, E. W.; Harirchian-Saei, S.; Moffitt, M. G. Strands, network, and continents from homopolystyrene dewetting at the air/water interface: Implications for amphiphilic block copolymer self-assembly. *Langmuir* **2011**, *27*, 1364–1372.
21. Meszaros, M.; Eisenberg, A.; Lennox, R. B. Block copolymer self-assembly in two dimensions: Nanoscale emulsions and foams. *Faraday Discuss.* **1994**, *98*, 283-294.
22. Baker, S. M.; Leach, K. A.; Devereaux, C. E.; Gragson, D. E. Controlled patterning of diblock copolymers by monolayer Langmuir-Blodgett deposition. *Macromolecules* **2000**, *33*, 5432–5436.
23. Park, J. Y.; Liu, M.; Mays, J.; Dadmun, M.; Advincula, R. Nano-donuts from pH-dependent block restructuring in amphiphilic ABA triblock copolymers vesicles at the air/water interface. *Soft Matter* **2009**, *5*, 747–749.
24. Hosoi, A. E.; Kogan, D.; Devereaux, C. E.; Bernoff, A. J.; Baker, S. M. Two-dimensional self-assembly in diblock copolymers. *Phys. Rev. Lett.* **2005**, *95*, 037801 (1–4).
25. Spatz, J. P.; Sheiko, S.; Möller, M. Substrate-induced lateral micro-phase separation of a diblock copolymer. *Adv. Mater.* **1996**, *8*, 513–517.

26. Ruokolainen, J.; Mäkinen, R.; Torkkeli, M.; Mäkelä, T.; Serimaa, R.; ten Brinke, G.; Ikkala, O. Switching supramolecular polymeric materials with multiple length scales. *Science* **1998**, *280*, 557–560.
27. Ruokolainen, J.; Saariaho, M.; Ikkala, O.; ten Brinke, G.; Thomas, E. L.; Torkkeli, M.; Serimaa, R. Supramolecular routes to hierarchical structures: Comb-coil diblock copolymers organized with two length scales. *Macromolecules* **1999**, *32*, 1152–1158.
28. Ruokolainen, J.; ten Brinke, G.; Ikkala, O. Supramolecular polymeric materials with hierarchical structure-within-structure morphologies. *Adv. Mater.* **1999**, *11*, 777–780.
29. Mäkinen, R.; Ruokolainen, J.; Ikkala, O.; de Moel, K.; ten Brinke, G.; De Odorico, W.; Stamm, M. Orientation of supramolecular self-organized polymeric nanostructures by oscillatory shear flow. *Macromolecules* **2000**, *33*, 3441–3446.
30. de Moel, K.; Alberda van Ekenstein, G. O. R.; Nijland, H.; Polushkin, E.; ten Brinke, G.; Mäki-Ontto, R.; Ikkala, O. Polymeric nanofibers prepared from self-organized supramolecules. *Chem. Mater.* **2001**, *13*, 4580–4583.
31. Alberda van Ekenstein, G.; Polushkin, E.; Nijland, H.; Ikkala, O.; ten Brinke, G. Shear alignment at two length scales: Comb-shaped supramolecules self-organized as cylinders-within-lamellar hierarchy. *Macromolecules* **2003**, *36*, 3684–3688.
32. Valkama, S.; Ruotsalainen, T.; Nykänen, A.; Laiho, A.; Kosonen, H.; ten Brinke, G.; Ikkala, O.; Ruokolainen, J. Self-assembled structures in diblock copolymers with hydrogen-bonded amphiphilic plasticizing compounds. *Macromolecules* **2006**, *39*, 9327–9336.
33. Tung, S.-H.; Kalarickal, N. C.; Mays, J. W.; Xu, T. Hierarchical assemblies of block-copolymer-based supramolecules in thin films. *Macromolecules* **2008**, *41*, 6453–6462.
34. van Zoelen, W.; Polushkin, E.; ten Brinke, G. Hierarchical terrace formation in PS-*b*-PVP(PDP) supramolecular thin films. *Macromolecules* **2008**, *41*, 8807–8814.
35. Deschênes, L.; Bousmina, M.; Ritcey, A. M. Micellization of PEO/PS block copolymers at the air/water interface: A simple model for predicting the size and aggregation number of circular surface micelles. *Langmuir* **2008**, *24*, 3699–3708.
36. Logan, J. L.; Masse, P.; Gnanou, Y.; Taton, D.; Duran, R. S. Polystyrene-block-poly(ethylene oxide) stars as surface films at the ar/wter iterface. *Langmuir* **2005**, *21*, 7380–7389.
37. Li, S.; Clarke, C. J.; Eisenberg, A.; Lennox, R. B. Langmuir films of polystyrene-b-poly(alkyl acrylate) diblock copolymers. *Thin Solid Films* **1999**, *354*, 136–141.
38. van Zoelen, W.; Alberda van Ekenstein, G.; Ikkala, O.; ten Brinke, G. Incorporation of PPE in lamellar self-assembled PS-b-PVP(PDP) supramolecules and PS-b-PVP diblock copolymers. *Macromolecules* **2006**, *39*, 6574–6579.

39. Chung, B.; Park, S.; Chang, T. HPLC fractionation and surface micellization behavior of polystyrene-b-poly(methyl methacrylate). *Macromolecules* **2005**, *38*, 6122–6127.
40. Zhu, J.; Eisenberg, A.; Lennox, R. B. Interfacial behavior of block polyelectrolytes. 1. Evidence for novel surface micelle formation. *J. Am. Chem. Soc.* **1991**, *113*, 5583–5588.
41. Zhang, J.; Liu, D.; Yang, G.; Han, B.; Wu, Z. Effect of ultrasound on the microstructure of polystyrene in cyclohexane: a synchrotron small-angle X-ray scattering study. *Colloid Polym. Sci.* **2007**, *285*, 1275–1279.
42. Kumaki, J. Monolayer of polystyrene monomolecular particles on a water surface studied by Langmuir-type film balance and transmission electron microscopy. *Macromolecules* **1988**, *21*, 749–755.
43. Zhu, J.; Lennox, R. B.; Eisenberg, A. Interfacial behavior of block polyelectrolytes. 2. Aggregation numbers of surface micelles. *Langmuir* **1991**, *7*, 1579–1584.
44. Gonçalves da Silva, A. M.; Filipe, E. J. M.; d'Oliveira, J. M. R.; Martinho, J. M. G. Interfacial behavior of poly(styrene)–poly(ethylene oxide) diblock copolymer monolayers at the air−water interface. Hydrophilic block chain length and temperature influence. *Langmuir* **1996**, *12*, 6547–6553.
45. Cox, J. K.; Yu, K.; Eisenberg, A.; Lennox, R. B. Compression of polystyrene–poly(ethylene oxide) surface aggregates at the air/water interface. *Phys,. Chem. Chem. Phys.* **1999**, *18*, 4417–4421.
46. Shuler, R. L.; Zisman, W. A. Study of the behavior of polyoxyethylene at the air-water interface by wave damping and other methods. *J. Phys. Chem.* **1970**, *74*, 1523–1534.
47. Shin, K.; Rafailovich, M. H.; Sokolov, J.; Chang, D. M. Cox, J. K.; Lennox, R. B.; Eisenberg, A.; Gibaud, A.; Huang, J.; Hsu, S. L.; Satija, S. K. Observation of surface ordering of alkyl side chains in polystyrene/polyelectrolytes diblock copolymer Langmuir films. *Langmuir* **2001**, *17*, 4955–4961.
48. Gaines, G. L. J. *Insoluble monolayers at liquid-gas interfaces*. John Wiley & Sons: New York, 1966.
49. Zhu, J.; Lennox, R. B.; Eisenberg, A. Polymorphism of (quasi) two-dimensional micelles. *J. Phys. Chem.* **1992**, *96*, 4727–4730.
50. Li, Z.; Zhao, W.; Quinn, J.; Rafailovich, M. H.; Sokolov, J.; Lennox, R. B.; Eisenberg, A.; Wu, X. Z.; Kim, M. W.; Sinha, S. K.; Tolan, M. X-ray reflectivity of diblock copolymer monolayers at the air/water interface. *Langmuir* **1995**, *11*, 4785–4792.
51. Miller, I. R. Properties of polyelectrolyte monolayers. *Colloid Interface Sci.* **1954**, *9*, 579–590.

52. Kawaguchi, M.; Itoh, S.; Takahashi, A. Liquid-expanded to liquid-condensed phase transition in polyelectrolyte monolayers on the aqueous potassium bromide solution. 1. Salt concentration dependence. *Macromolecules* **1987**, *20*, 1052–1056.
53. Spatz, J. P.; Möller, M; Noeske,M.; Behm, R. J.; Pietralla, M. Nanomosaic surfaces by lateral phase separation of a diblock copolymer. *Macromolecules* **1997**, *30*, 3874–3880.
54. Kramarenko, E. Y.; Potemkin, I. I.; Khokhlov, A. R.; Winkler, R. G.; Reineker, P. Surface micellar nanopattern formation of adsorbed diblock copolymer systems. *Macromolecules* **1999**, *32*, 3495–3501.
55. Potemkin, I. I.; Kramarenko, E. Y.; Khokhlov, A. R.; Winkler, R. G.; Reineker, P.; Eibeck, P.; Spatz, J. P.; Möller, M. Nanopattern of diblock copolymers selectively adsorbed on a plane surface. *Langmuir* **1999**, *15*, 7290–7298.
56. Spatz, J. P.; Eibeck, P.; Mössmer, S.; Möller, M.; Kramarenko, E. Y.; Khalatur, P. G.; Potemkin, I. I.; Khokhlov, A. R.; Winkler, R. G.; Reineker, P. Order-disorder transition in surface-induced nanopattern of diblock copolymer films. *Macromolecules* **2000**, *33*, 150–157.
57. Potemkin, I. I.; Möller, M. Microphase separation in ultrathin films of diblock copolymers with variable stickiness of one of the blocks to the surface. *Macromolecules* **2005**, *38*, 2999–3006.
58. Nagano, S.; Matsushita, Y.; Ohnuma, Y.; Shinma, S.; Seki, T. Formation of a highly ordered dot array of surface micelles of a block copolymer *via* liquid-crystal-hybridized self-assembly. *Langmuir* **2006**, *22*, 5233–5236.

Appendix to Chapter 3

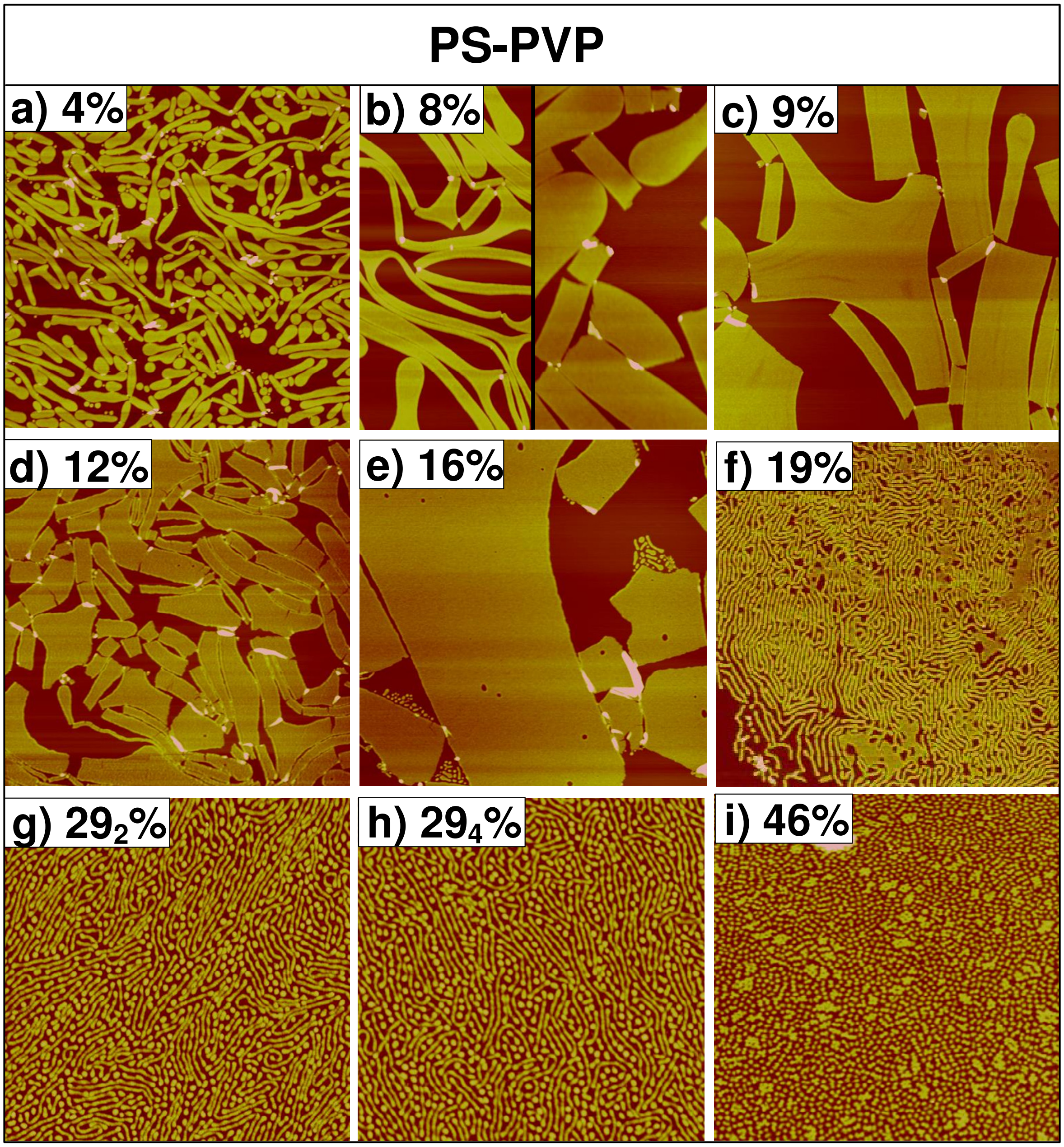

Figure SI-3-1. AFM height images of PS-PVP LB films spread from concentrated solutions and transferred at $\pi = 15$ mN/m. The numbers indicate mol % PVP content Image scan: a–e) 10×10 µm; f–i) 5×5 µm.

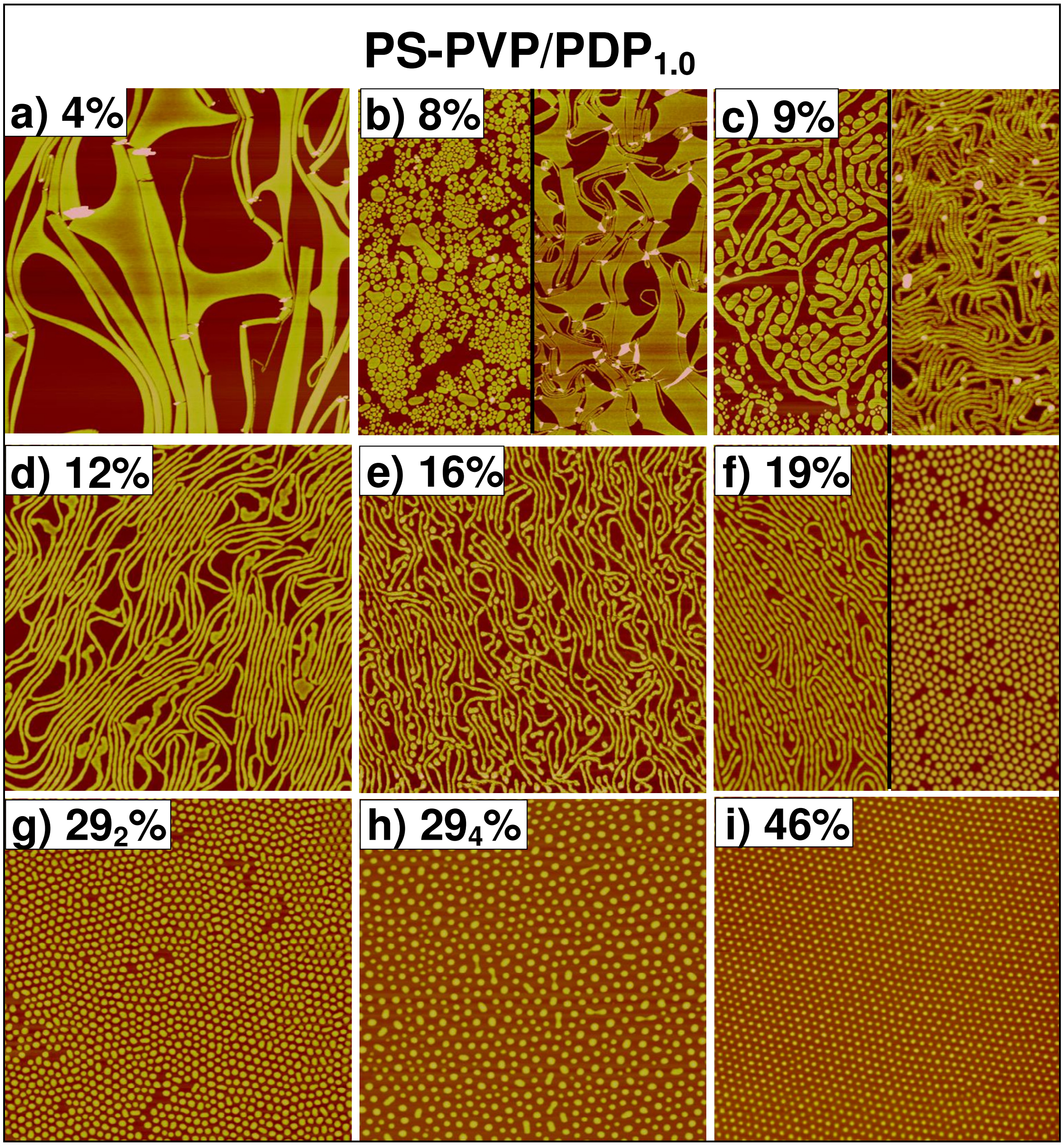

Figure SI-3-2. AFM height images of PS-PVP/PDP$_{1.0}$ LB films spread from concentrated solutions and transferred at $\pi = 15$ mN/m. The numbers indicate mol % PVP content. Image scan: a,b) 10×10 μm ; c–e) 5×5 μm; f–i) 3×3 μm.

PS-PVP/PDP and PS-PVP$^+$RX$^-$ (f_{PVP} = 29–48 mol%)

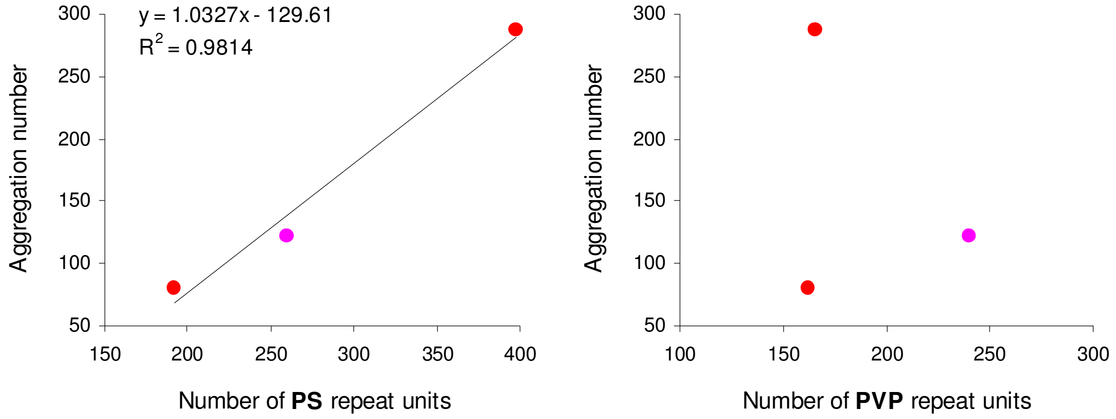

PS-PEO (f_{PEO} = 30–96 mol%)

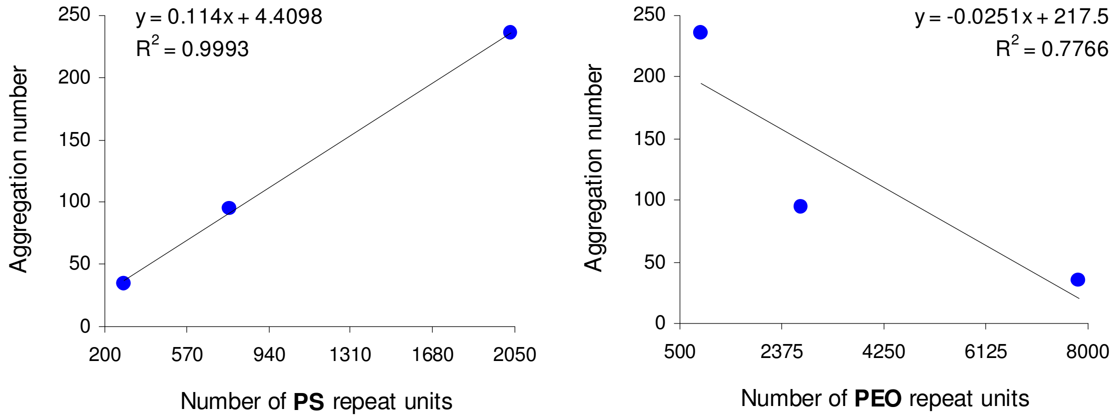

Figure SI-3-3. Aggregation number as a function of hydrophobic (left) or hydrophilic (right) blocks in:

- ● PS(41.0k)-PVP(17.5k)/PDP$_{1.0}$
- ● PS(20.0k)-PVP(17.0k)/PDP$_{1.0}$
- ● PS(27.0k)-PVP(25.2k)$^+$C$_{10}$H$_{21}$I$^-$
- ● PS(211.5k)-PEO(39.0k)
- ● PS(80.0k)-PEO(120.0k)
- ● PS(30.0k)-PEO(345.0k)

(The data for PS-PVP$^+$C$_{10}$I$^-$ and PS-PEO were taken from refs. 43 and 22, respectively).

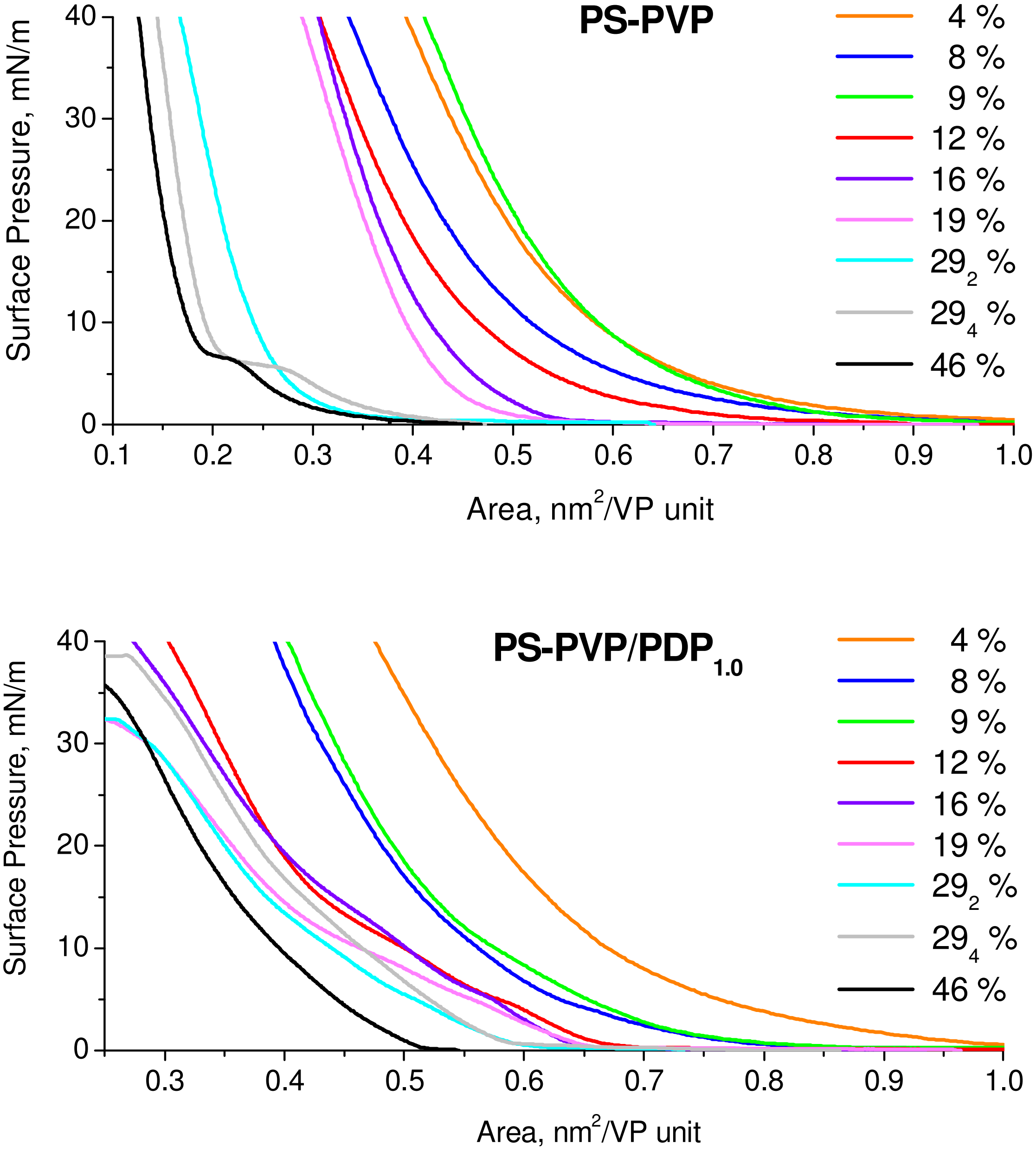

Figure SI-3-4. Langmuir compression isotherms of PS-PVP block copolymers (top) and their equimolar complexes with PDP (bottom) spread from $CHCl_3$ solution (1.8 mg/mL) at 21 ±0.5 °C. The nomenclature gives the mol % PVP content. The area is presented per VP repeat unit (in contrast to Figure 3-8, which presents area per molecule).

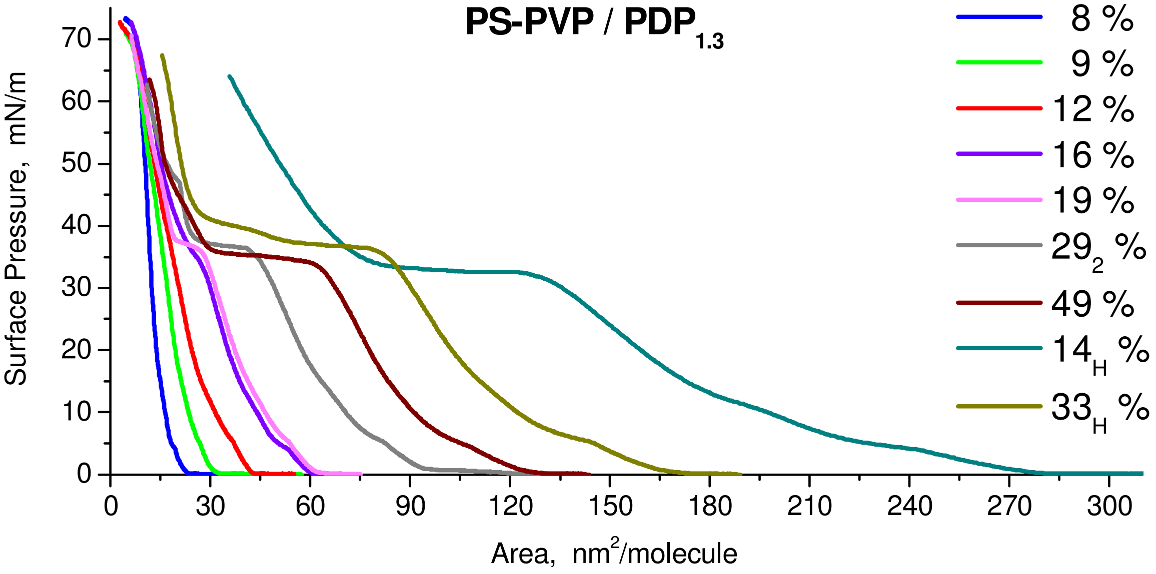

Figure SI-3-5. Langmuir compression isotherms of PS-PVP/PDP (1:1.3 VP:PDP molar ratio) spread from $CHCl_3$ solution (concentratcion of copolymer 1.75 mg/mL) at 21 ±1 ºC. The nomenclature gives the mol % PVP content. The area is presented per polymer molecule.

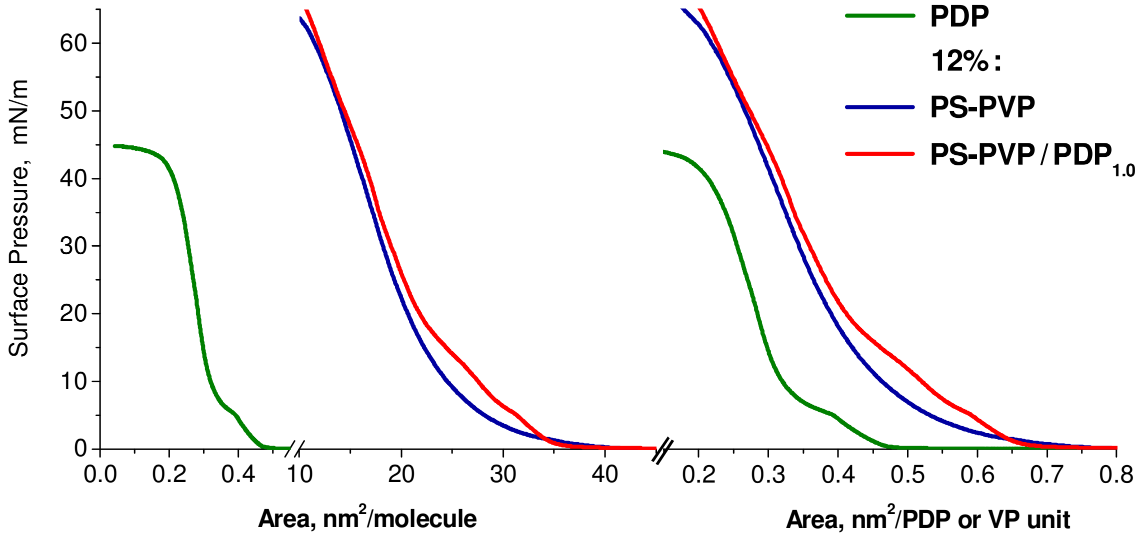

Figure SI-3-6. Langmuir compression isotherms of 12% PS-PVP, PDP and their equimolar (VP:PDP = 1.0:1.0) complex, all spread from $CHCl_3$ solutions at 21 ±1 ºC.

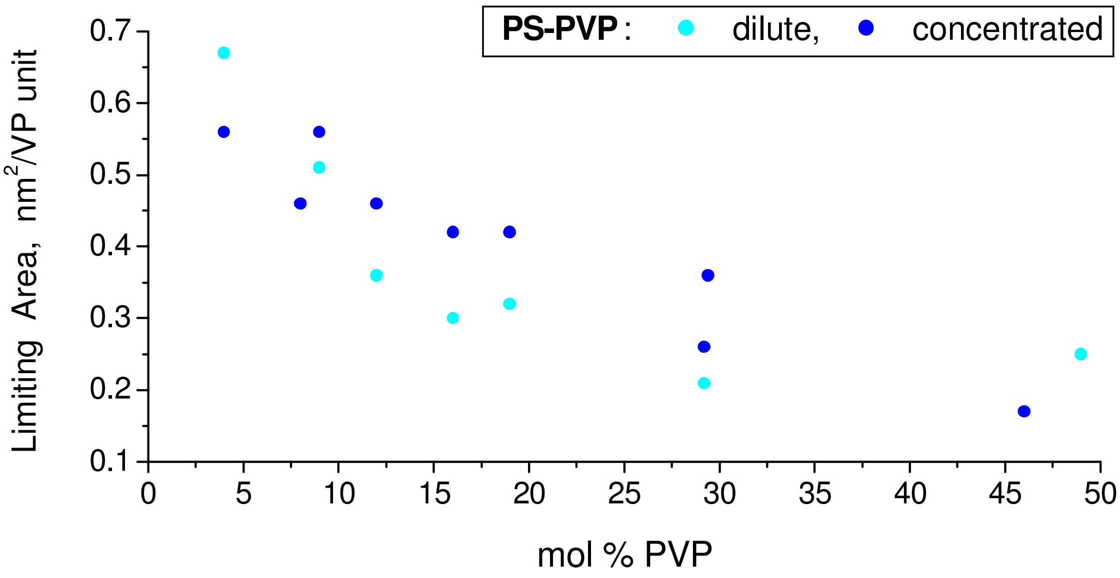

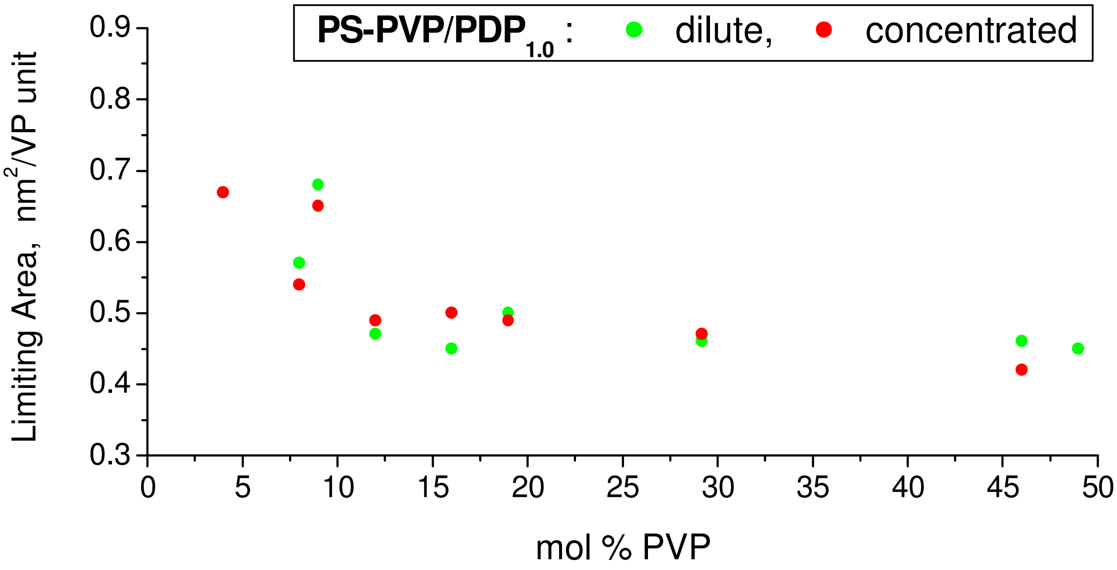

Figure SI-3-7. Limiting area (after the long plateau, if those are present) per VP repeat unit in PS-PVP (top) and PS-PVP/PDP$_{1.0}$ langmuir compression isotherm as a function of molar fraction of PVP block.

Chapter 4

New Insights into the Self-Assembly of PS-PVP Supramolecular Complexes at the Air/Water Interface

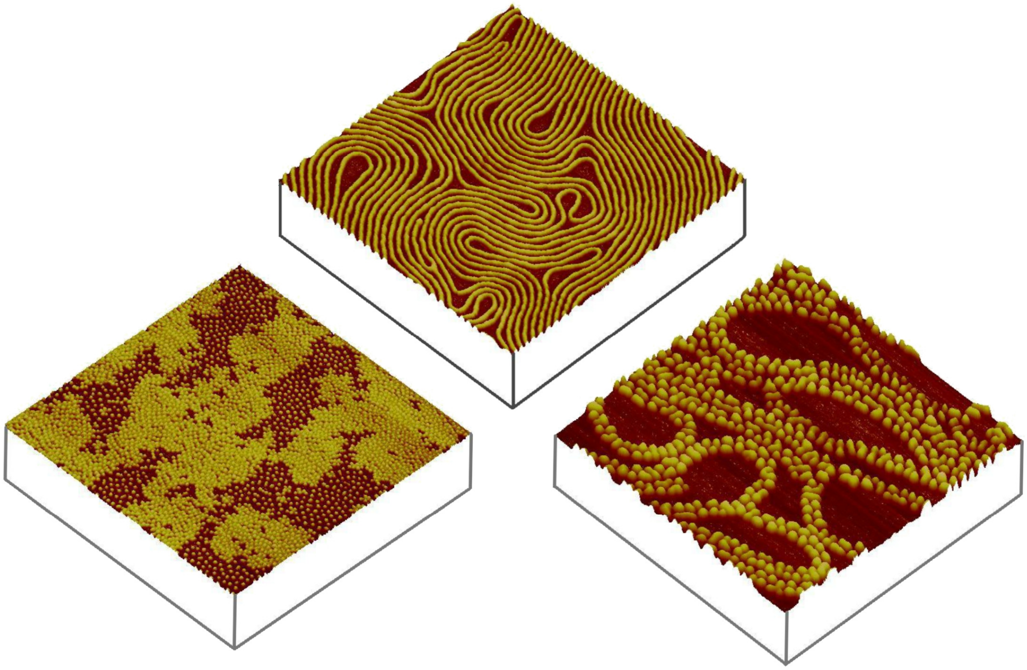

4.1. INTRODUCTION

This chapter presents additional experiments that have been conducted on LB films of the block copolymers and that provide new insights into the self-assembly process. It is divided into four distinct parts. The first part shows new and important data regarding the nanodot morphology in LB films of PS-PVP/PDP, obtained below and above the high pressure isotherm plateau, that allow a new interpretation of the nature of the transition involved. The second part illustrates an interesting modification of the nanostrand morphology induced by soaking in acetone, and that allows a discussion concerning the early stages of aggregate formation at the air/water interface. The third part explores the effects on the nanostrand network morphology of replacing PDP with other hydrogen-bonding molecules. Finally, the fourth part compares the morphologies obtained for the 12% VP copolymer with much higher and much lower total molecular weights, where the results are interpreted in the light of the discussion in Chapter 3 and additional considerations are introduced. Since the four parts have quite different goals, the relevant background to each part is given at the beginning of each section rather than in this Introduction.

4.2. EXPERIMENTAL SECTION

4.2.1. Materials

Poly(styrene)-*b*-poly(4-vinyl pyridine) diblock copolymers, listed in Table 4-1, were obtained from Polymer Source (Dorval, QC, Canada), and used as received. 3-*n*-Pentadecylphenol (Sigma-Aldrich, 90%) was recrystallized twice from hexane. 4-*n*-Octylphenol (Sigma-Aldrich, 99%), 4-*n*-octylbenzoic acid (Sigma-Aldrich, 99%), 1-octanol (Sigma-Aldrich, ~99%), 1H,1H,2H,2H-perfluoro-1-octanol (Sigma-Aldrich, 97%), 1-naphthol (Sigma-Aldrich, ≥99%), 10,12-pentacosadiynoic acid (Sigma-Aldrich, ≥97%), and 4-dodecylbenzenesulfonic acid (TCI America, >90%, mixture of isomers) were used as received. 1,16-Hexadecanediol was previously synthesized in our lab. A polystryrene homopolymer of low molecular weight, 800 g/mol (referred as oligostyrene, OS) was purchased from Pressure Chemical Company (special PS standard) and used as received.

Chloroform (HPLC grade, ≥99.8%; Sigma-Aldrich) was used for solution preparation. Solvents used for cleaning processes, MilliQ water used as the subphase in the Langmuir trough, and solid substrates (mica and silicon wafers) used for monolayer deposition have been described previously in Chapters 2 and 3.

For sample treatment, HPLC grade acetone (Sigma-Aldrich, ≥99.9%) was used.

Table 4-1. Nomenclature and characteristics of the PS-PVP diblock copolymers studied.

Nomenclature*	Molecular weight, g/mol		M_w/M_n	Number of repeat units		mol % PVP
	M_n (PS)	M_n (PVP)		N_{PS}	N_{PVP}	
12_L%	12,000	1,700	1.09	115	16	12.2
12% (or 12_M%)	40,000	5,600	1.09	384	53	12.1
12_H%	535,000	75,000	1.20	5,137	713	12.2
29_4%	41,500	17,500	1.07	398	166	29.4
46%	20,000	17,000	1.08	192	162	45.8

* The letters “L”, “M”, “H” are used to distinguish the 12% PS-PVP’s of low, medium, and high molecular weights, respectively; 29_4% follows the nomenclature used in Chapter 3.

4.2.2. Methods and Instruments

The Langmuir and Langmuir-Blodgett methods used have been described previously in Chapters 2 and 3. Here, only $CHCl_3$ solutions were used. Block copolymer concentrations in solution varied from 0.35 to 4.06 mg/mL, and are usually mentioned in the text title or figure caption; the word “concentrated” is used for solutions of 1.8 mg/mL concentration. All complexes are equimolar unless specified otherwise. All LB films for AFM imaging were transferred onto mica substrate.

Most of the AFM images were acquired in tapping mode using a Multimode AFM with a Nanoscope IIIa controller (Digital Instruments/Veeco, Santa-Barbara, USA) and silicon probes (Nanosensors) as described in previous chapters. Figures 4-3, SI-4-2, SI-4-3, and SI-4-7 were obtained with AIST-NT's Smart SPM under ambient conditions without acoustic and vibration protection in semicontact mode using silicon probes (NanoWorld, Arrow NCR, force constant 42 mN/m, tip radius <10 nm). When "hard tapping" and "soft tapping" parameters are mentioned, they mean free amplitudes of 22 and 12 nm, respectively, and setpoints of 68 and 80%, respectively.

FTIR Spectroscopy.

Attenuated total reflection infrared (ATR-IR) spectra using Ge crystal (GATR, Harrick) were recorded on a Tensor 27 (Bruker Optics) spectrometer equipped with a liquid-nitrogen-cooled HgCdTe detector. Samples for ATR-IR were prepared by two methods: either by the conventional LB method with films transferred at $\pi \geq 20$ mN/m onto silicon wafer or gold substrate (prepared in our lab as follows: 100 nm of Au were thermally evaporated on glass slide covered by 5 nm Ti, at a speed of 0.5 Å/sec), or by deposition of concentrated solution onto the crystal followed by solvent evaporation (referred to as bulk). All the spectra were acquired with the acquisition 1024 scans at 4 cm^{-1} resolution.

In-situ polarization modulation infrared reflection–adsorption (PM-IRRAS) spectra were recorded using a Magna 850 (Nicolet, Madison, WI; Figure 4-1) spectrometer with 8 cm^{-1} resolution. The experimental setup was as follows: 30 μL of 0.3 mg/mL solution of 46% PS-PVP/PDP$_{1.0}$ in $CHCl_3$ was spread on a Langmuir trough (50x350 mm); after 20 min (required for solvent evaporation), the barriers were compressed at a speed of 0.08 mm/sec and spectra were recorded at $\pi = 0$, 3, 10, 15, 25, and 35 mN/m (each time after a 5-min wait for film stabilization). The angle of incidence of the infrared beam with respect to the normal to the water surface was 76°. Normalized PM-IRRAS signals were obtained using the following expression: $\Delta S / S = S(d) - S(0) / S(0)$, where $S(d)$ and $S(0)$ are the PM-IRRAS signals of the covered and uncovered subphase, respectively.

Sample treatment.

LB films prepared using concentrated $CHCl_3$ solution of 12% PS-PVP/PDP$_{1.0\text{–}1.3}$ were immersed in vigorously stirred acetone for 10 min to 3 h, followed by drying in air overnight, and imaging by AFM.

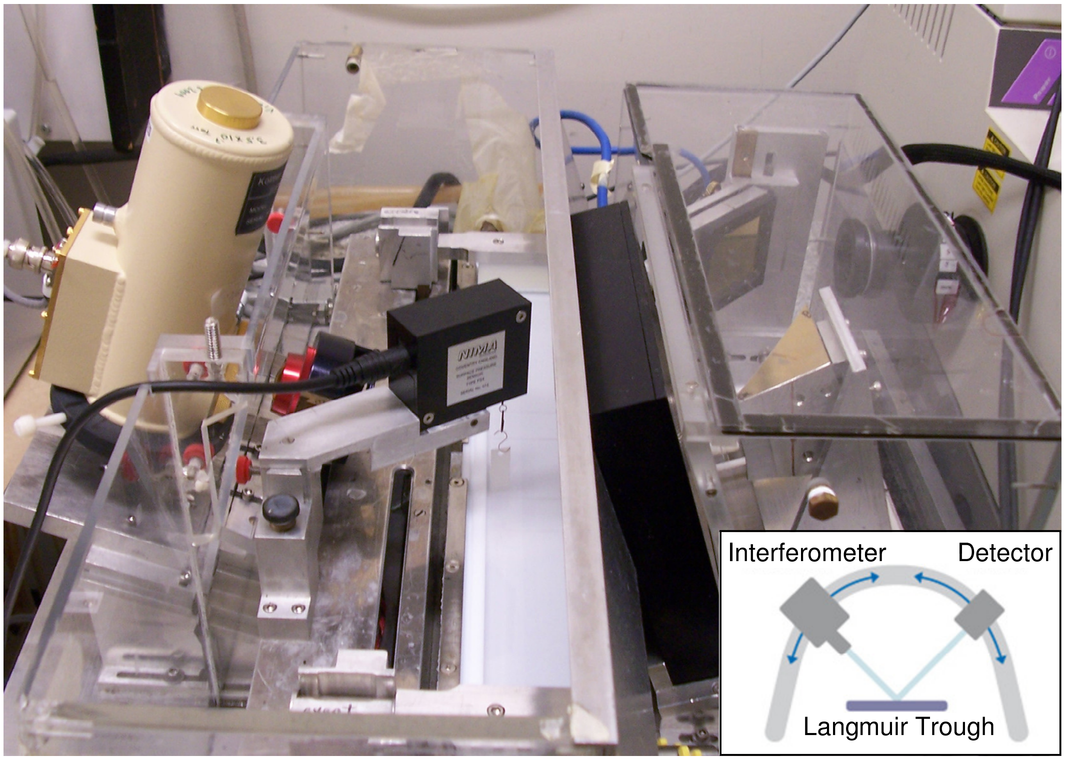

Figure 4-1. Photo and schematic representation (inset) of PM-IRRAS and Langmuir trough for *in-situ* analysis of monolayers floating on an aqueous subphase.

4.3. RESULTS AND DISCUSSION

4.3.1. Quasi-2D Surface Micelles and Mechanism of High Surface Pressure Transition

A quasi-2D spherical surface micelle morphology, also called the nanodot morphology, is generally observed in LB films of amphiphilic diblock copolymers when their composition exceeds a certain critical block fraction, which is *ca*. 29 mol% PVP for pure PS-PVP diblock copolymer,[1] 16–20 mol% PVP for its equimolar complex with PDP,[1] and 14 mol% for quaternized PS-PVP$^+$C$_{10}$H$_{21}$I$^-$.[2] The core of the surface micelles is composed of the hydrophobic (PS) block, often arranged in a quasi-hexagonal order above the hydrophilic (PVP) monolayer adsorbed to the water surface. This hydrophilic monolayer is most likely a continuous film, residing both beneath (as a wetting layer) and around the PS nodules, very much like the picture retained for ultrathin diblock films obtained by spin- or dip-coating of mica substrates using ultradilute $CHCl_3$ solutions.[3–5] At lower hydrophilic block contents, a nanostrand morphology is often observed, consisting of hydrophobic (PS) strands, below and alongside which lies the hydrophilic (PVP) monolayer, attributed by us to disassembly of a continuous strand morphology at the level of the mobile PVP stripes separating the PS stripes.[1,6] At very low hydrophilic block contents (*ca.* 8 mol% and less), a third morphology type – in the form of often large but variably sized and shaped planar aggregates – is observed, where the hydrophilic block lies essentially only beneath the hydrophobic layer.

In our systems, it has been observed that surface pressure–area isotherms of block copolymer films with the nanodot morphology, and none of the other morphologies, always display a plateau (or pseudo-plateau) indicative of a transition. This plateau lies at surface pressures of *ca.* 4, 33–37, and 29–38 mN/m for PS-PVP,[1] PS-PVP/$PDP_{1.0}$,[1] and PS-$PVP^+C_{10}H_{21}I^-$,[9] respectively. In the latter, this plateau was initially interpreted as a transition from surface-adsorbed to subphase-solubilized $PVP^+C_{10}H_{21}I^-$, also called the "starfish–jellyfish" transition.[9] The ionic nature of the quaternized PVP was considered to favour solubilization into the subphase under high pressure. However later, the plateau was interpreted as arising from a disorder–order transition of the alkyl side chains, where the alkyl chains become more ordered into a trans conformation.[7] This interpretation was based on *in-situ* X-ray and neutron reflectivity, which showed insufficient thickening of the polyelectrolyte layer during compression compared to what would be expected if the $PVP^+C_{10}H_{21}I^-$ chains became submerged into the subphase, and on infrared analysis, which showed greater trans character of the alkyl chains with increasing surface pressure.[7,8] In this section, further insight into the film morphology and plateau transition is sought, focusing on PS-PVP/PDP copolymers.

First, the question of the thickness of the hydrophilic monolayer, and its lateral extension relative to the PS core, will be addressed, where it will be shown that this can be estimated directly by AFM. In fact, it can be questioned whether the background of the topography images of the nanodot and nanostrand morphologies is the thin hydrophilic block or the pure substrate. The picture of the nanodot morphology (Figure 4-2) indicates that it is the hydrophilic block. However, in the case of the nanostrand morphology (*e.g.* Figure 4-3) or planar aggregates, the distance between aggregates is usually much too big (up to a few hundreds of nanometers), so it is evident that the background is the bare surface of the solid substrate, and yet, the AFM images in the literature to date show no evidence of a hydrophilic monolayer lying alongside the strands, presumably because its thickness is of the same order of magnitude as the background noise. Indeed, the hydrophilic monolayer of the ultrathin PS-P2VP film obtained by spin-coating was estimated, by removal of polymer by rubbing with AFM tips in hard contact mode, to be 0.8 nm.[3]

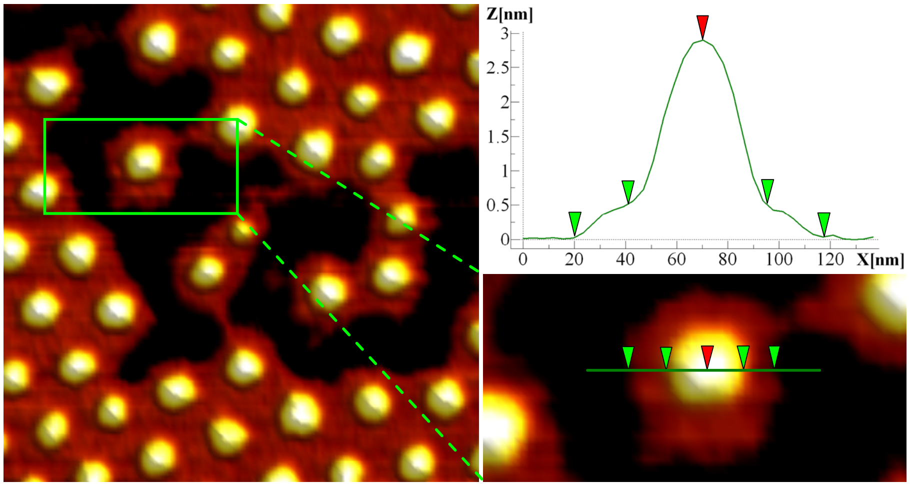

Figure 4-2. AFM height images (left: 515×515 nm, right: 218×109 nm) with a section profile (along the green line in the right image) of the 46% PS–PVP/PDP$_{1.0.}$ LB film. The images were flattened, filtered using a Gaussian 1x3 filter, corrected to remove horizontal streaks, and rendered 3D. (The original image is shown in the Appendix, Figure SI-4-1).

The image in Figure 4-2 (see additional images in the Appendix to Chapter 4, Figures SI-4-1, SI-4-2) of a defect area of the nanodot morphology is revealing. It clearly shows that the areas between the nanodots in the hexagonally ordered region and immediately around the more isolated nanodots in the defect region have greater height than the rest of the area, which is necessarily bare surface, in the defect region. The expanded region in Figure 4-2 shows the topography AFM image and the height profile of an individual spherical surface micelle, directly illustrating its elevated core surrounded by a thin corona.

The height profile indicates that the corona has a vertical thickness of *ca*. 0.5 nm. [It is of interest to mention here that the height of the elevated core is 5–7 nm if soft tapping is applied and 3–4 nm if hard tapping is used; *i.e.*, when the main forces are attractive and repulsive, respectively (see Figure SI-4-2 in Appendix).] A closer look at the strand morphology similarly shows evidence of thin stripes alongside the strands, which are also *ca*. 0.5 nm in height (Figures 4-3).

It is of interest to compare the lateral width of the corona with the length of the PVP block. Since the accuracy depends on the AFM tip radius, and thus cannot be controlled precisely, these values were obtained by measuring the center-to-center distance between two closely spaced features (or periodicity) from which the measured width of the elevated micelles was subtracted. For the nanostrand morphology, we previously showed that the separation distance between closely spaced strand segments is similar to double the length of the PVP block in extended conformation.[6] As indicated in Table 4-2, which shows good agreement between the theoretical and experimental micelle separations, this is the same for the hexagonally close-packed nanodot structure. This relationship was found also by Zhu *et al*. for PS-PVP^{+}C$_{10}$H$_{21}$I^{-}.[9]

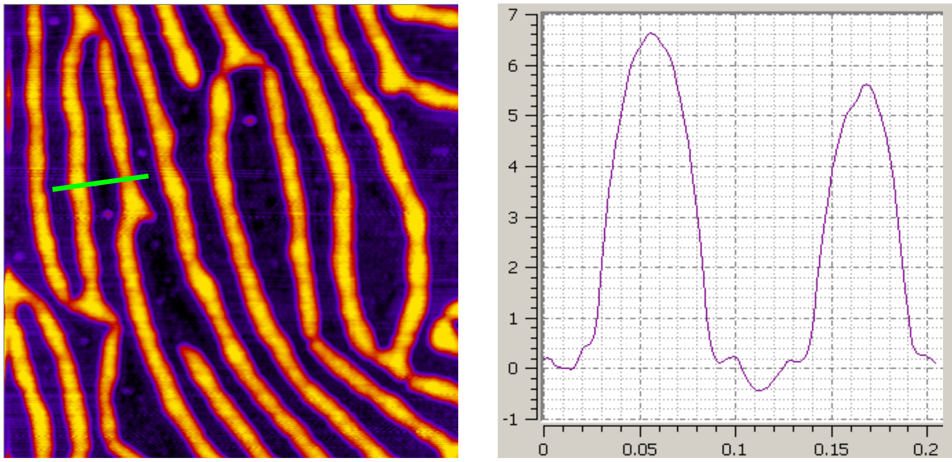

Figure 4-3. AFM height image (1×1 µm) and a section profile (along the green line in the left image) of the 12% PS–PVP/PDP$_{1.0}$ LB film.

(See Figure SI-4-3 in Appendix for 3×3 and 0.3×0.3 µm images).

Table 4-2. Correlation between the length of PVP chains in PS-PVP/$PDP_{1.0}$ and separation of surface micelles at π=3 mN/m.

Sample	n(PVP)	Calculated PVP length[a] (nm)	Center-to-center micelle distance (nm)	Micelle width (nm)	Micelle separation (nm)	
					theoretical[b]	experimental[c]
12 %	53	13	80 ± 10	60 ±10	26	*ca.* 20
29_4%	166	42	155 ± 15	65 ±5	84	*ca.* 90
46 %	162	41	120 ±10	45 ±5	82	*ca.* 75

[a] Calculated assuming a fully extended PVP block starting at the micelle edge.

[b] Twice the calculated PVP length.

[c] Difference between the center-to-center distance and width of strand or dot segments.

With such thin coronae, which can only be the hydrophilic monolayer, it may be questioned whether PDP is actually associated with the PVP there. Infrared investigations were undertaken to try to answer this. Figure 4-4 compares the ATR-IR spectra of bulk PS-PVP/PDP with those of pure PS-PVP and of PDP. The absorbance bands of particular interest are the phenyl ring vibrations at 1591 cm^{-1} for PDP (phenol group) and 1600 cm^{-1} for PS-PVP (composite band of the PS phenyl ring and the PVP pyridyl group). In PS-PVP/PDP, both bands are shifted, the PVP band to 1603 cm^{-1} and the phenol band to 1588 cm^{-1}, which is indicative of phenol-pyridyl H-bonding. (Similarly, the pyridyl band at 1417 cm^{-1} in PS-PVP shifts to 1421 cm^{-1} in PS-PVP/PDP.) In the grazing angle FTIR spectrum of an LB monolayer of PS-PVP/PDP, the phenyl bands of both PVP and PDP are also present, at 1605 and 1590 cm^{-1}, respectively (Figures SI-4-5 in Appendix). This clearly indicates that PDP is present in the LB monolayer, and the position of the maxima suggests that PDP is indeed H-bonded to PVP. Fragments of spectra of the equimolar complex, presented in Figure 4-5, show a good agreement in ratio between the peak intensities corresponding to PVP and PDP in the complex in bulk form and as an LB film, 1.0:0.9 and 1.0:0.7, respectively. *In-situ* PM-IRRAS of the monolayer for the detection of H-bonding on the water surface was also attempted; however, the bands affected by H-bonding were too weak to be conclusive.

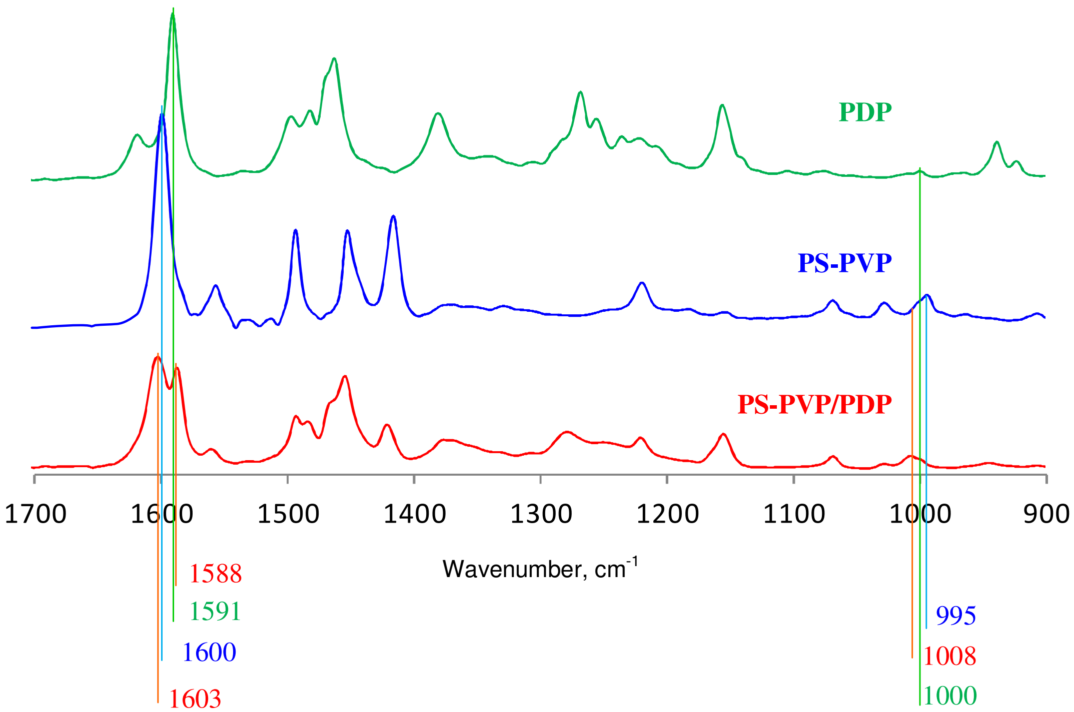

Figure 4-4. ATR-IR spectra of 12% PS-PVP, PDP, and 12% PS-PVP/PDP$_{1.0}$ in bulk. (Full spectra is available in Appendix, Figure SI-4-4).

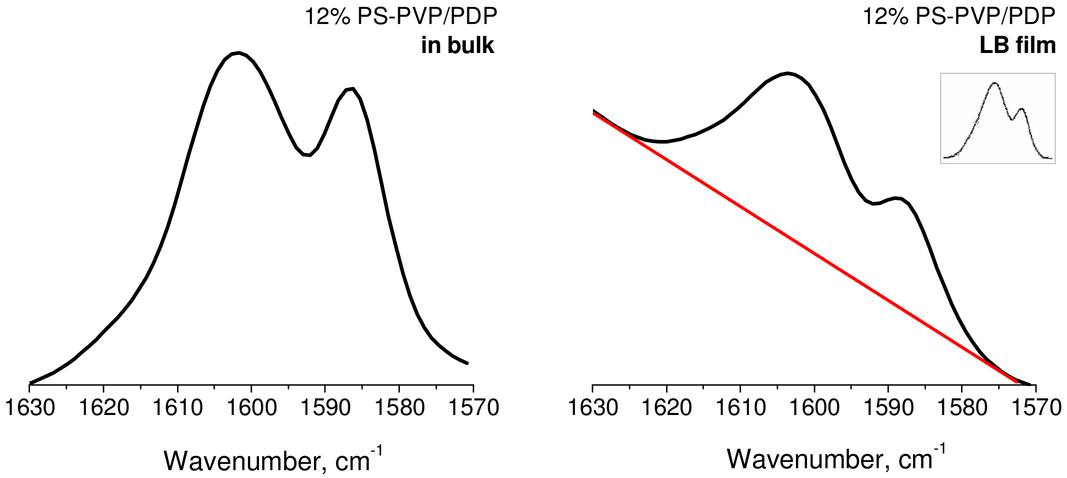

Figure 4-5. Fragments of ATR-IR spectra of 12% PS-PVP/PDP$_{1.0}$ in bulk. (left) and LB film transferred onto Au substrate at π = 30 mN/m (right). To compare the ratio between peaks corresponding to VP and PDP in the complex, the baseline (marked as a red line on the right image) was set up. In inset (at the right image), spectrum after baseline subtraction is shown.

Assuming then that PDP is indeed associated with the PVP monolayer between the hydrophobic cores, we next tried to observe what might be observed by AFM in the nanodot morphology of LB films transferred at different surface pressures below and above the plateau pressure. Figure 4-6 compares the morphology of 30% PS-PVP/PDP$_{1.0}$ LB films at the four different pressures indicated on the Langmuir compression isotherm (Figure 4-6a) for this sample. Detailed analysis of PS-PVP/PDP Langmuir compression isotherms is described in the previous chapter; here, we will concentrate on the film morphology. LB monolayers deposited at surface pressures before the long plateau region of the pressure–area isotherm are characterized by a uniform morphology of hexagonally ordered nanodots (Figure 4-6b–d) of relatively constant width, slightly increasing height, and gradually decreasing distance with increasing surface pressure (Table 4-3). In contrast, the topography of the LB film transferred just above the plateau (π = 40 mN/m, Figure 4-6e) displays two surface regions, one (termed "oceans") that is the same as those in films transferred below the plateau pressure and one (termed "continents") where the areas between the nanodots have clearly become more elevated in a rather uniform manner. The difference between the two regions is highlighted by the expanded image and height profile in Figure 4-6g. It shows that the nanodots themselves do not change in height (relative to the ocean "background"), remaining close to that for the film transferred at π = 30 mN/m (Figure 4-6f). The step-change in height between the ocean and the continent "backgrounds" is *ca.* 3 nm. In comparison, the van der Waals length of the PDP molecule with the alkyl tail in its most extended (all-trans) form is 2.6 nm.[*] This is evidence that the increase in height is due mainly to the PDP molecules going from a prone (flat) to almost-perpendicular position relative to the surface (see Figure 4-7). This change is accompanied by decomposition of the hexagonal order in the continent regions, leading to two, essentially orthogonal, characteristic periodicities, one that is similar to that of the ocean regions (and similar to the periodicity at π = 30 mN/m) and one that is much smaller. In other words, the order of the nanodots in the continental regions tends to a rectangular rather than hexagonal 2D lattice.

---

[*] The length from O to the farthest H is 2.32 nm; with van der Waals radii of O (0.152 nm) and H (0.12 nm), this results in total length of 2.6 nm.

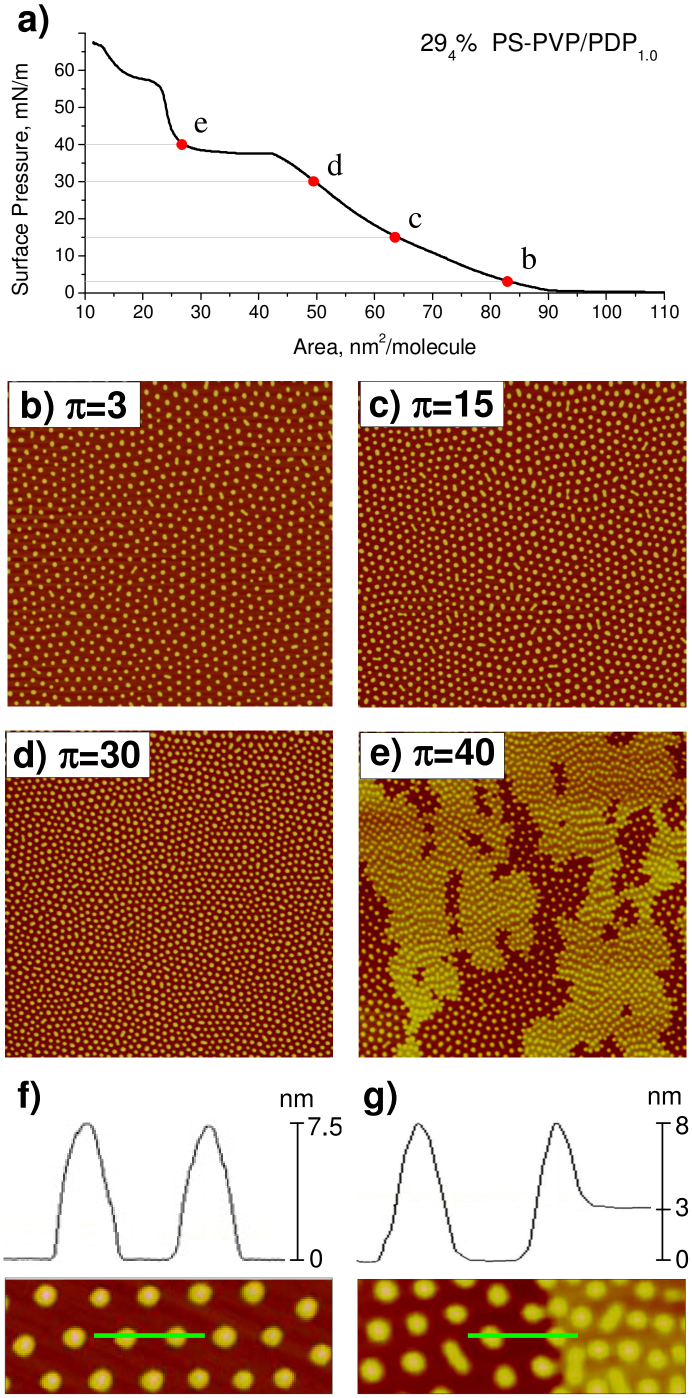

Figure 4-6. (a) Langmuir compression isotherm of 29_4% PS-PVP/PDP$_{1.0}$ in CHCl$_3$ at 21°C, and AFM topography images (5×5 μm) of LB films transferred at: (b) 3 mN/m, (c) 15 mN/m, (d) 30 mN/m, and (e) 40 mN/m, and their height profiles for: (f) π = 30 mN/m, (g) π = 40 mN/m. [Dimensions of the above nanodots have been summarized in Table 4-3].

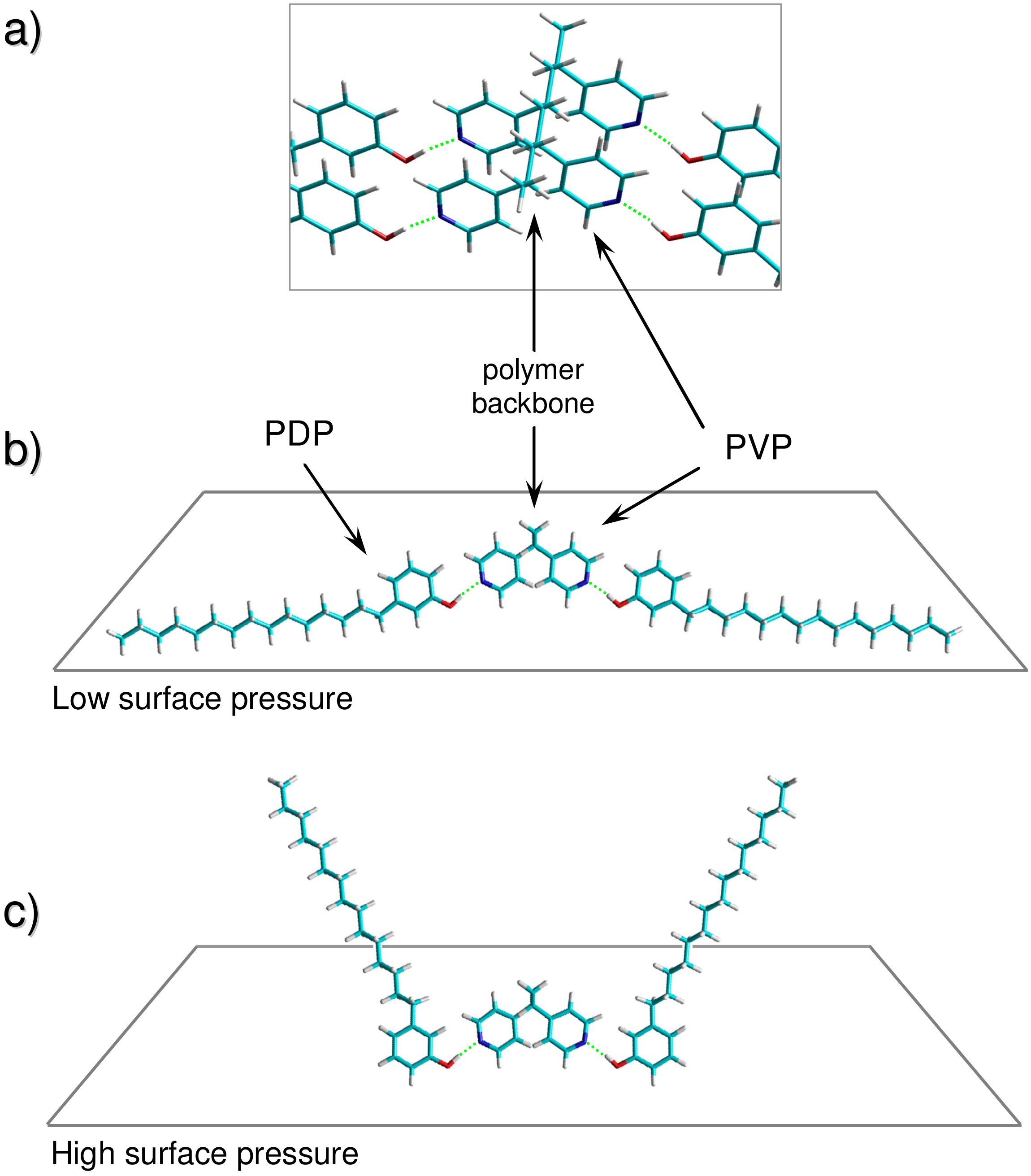

Figure 4-7. Proposed supramolecular arrangements of PDP-PVP self-assembly in nanodots at low (b) and high (c) surface pressures. The geometry of PDP and its binding to pyridine were calculated at DFT level of theory (B3LYP 6-31G) in Gaussian 03.[10] Images of the structural models were rendered in HyperChem.[11] For the sake of clarity, small fragment of syndiotactic PVP was used in both models (a). Color assignment of elements: H – white, C – cyan, N – blue, O- red. H-bonding is shown by green dotted lines.

Table 4-3. Average dimensions of the nanodots in the morphologies of 29_4 % PS-PVP/PDP$_{1.0}$ LB films transferred at various surface pressures (π).

π, mN/m	Height, (±0.5) nm	Width, nm	Center-to-center distance, nm
3	7.0	65 ±5	155 ±15
15	7.5	65 ±5	150 ±10
30	7.5	65 ±10	115 ±5
40	8.0; 5.0	65 ±10	110 ±10; 80 ±10

The elevated areas and the reordering of the nanodots in these areas are shown also in Figure 4-8. In the 50×50 μm image shown, the elevated areas are predominant, so that the continent regions appear to be studded by lakes rather than coexisting with oceans. The tendency to rectangular order is limpid in the smaller-scale images. Furthermore, it is striking that the smallest rectangular side tends to be perpendicular to the direction of compression (parallel to the compressed barriers). This indicates that the rectangular lattice results from the squeezing together of the hexagonal lattice by barrier compression. That this order is not perfect can be ascribed to the imperfections in the initial hexagonal order and/or to release of pressure during transfer of the film to the solid substrate provoking some disorder.

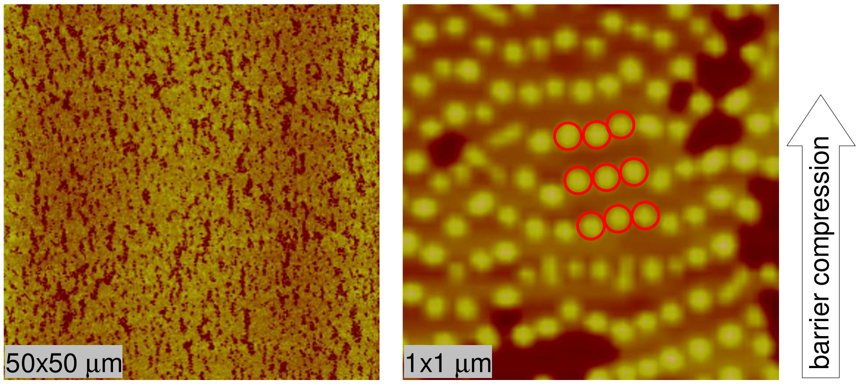

Figure 4-8. AFM topography images of 29_4% PS-PVP/PDP$_{1.0}$ LB films transferred at π = 40 mN/m. The arrow indicates the direction of barrier compression, which is the same as vertical substrate removal.

These data clearly show that the plateau transition must be ascribed not only to a change in alkyl chain orientation, as concluded in ref. 7, but also to a change in the nanodot order. The nanodots at the apices of hexagonal order (relative to the barriers) are forced to insert themselves in line with the next-nearest nanodots. To do this, PDP must be displaced into the regions between the aligned dots, with the consequence that the limited area available forces the PDP to adopt a perpendicular conformation. Thus, the two phenomena – the change in order and alkyl chain reorientation – must occur together. To our knowledge, this is the first time that clear evidence for the complexed alkyl chain reorientation in LB block copolymer films has been shown by AFM and, even more important, the first time that the isotherm plateau has been shown to be associated with an order–order transition of the nanodots.

Preliminary PM-IRRAS (*in-situ* FTIR) spectra on a Langmuir monolayer of 46% PS-PVP/PDP$_{1.0}$ at low and high surface pressures (Figure 4-9) show the shift of antisymmetric and symmetric CH_2 stretching bands from 2921 to 2919 cm^{-1} and from 2851 to 2850 cm^{-1}, respectively, confirming the change of *gauche*-to-*trans* conformation with decrease in surface area.[7,12] For lower surface pressures, the bands were too weak to give reliable maxima. It should be mentioned that, in the 46% PS-PVP/PDP equimolar complex, the ratio between methylene groups in the copolymer (PS and PVP) and in PDP is 1:6.4 per supramolecular chain. Thus, the conformational changes are mainly associated with the alkyl chains of PDP. The wavenumber shift observed in Figure 4-9 is closer to that observed for PS-PVP$^+C_{10}H_{21}Br$ than for PS-PVP$^+C_{18}H_{37}Br$ in ref. 7. This might suggest that PDP, with 15 carbons, is associated with PVP in slightly less than equimolar stoichiometry, leaving room for slightly greater disorder, possibly due to dissolution of a small fraction in the PS phase, as found in ref. 13 for PS-PVP/PDP in the bulk.

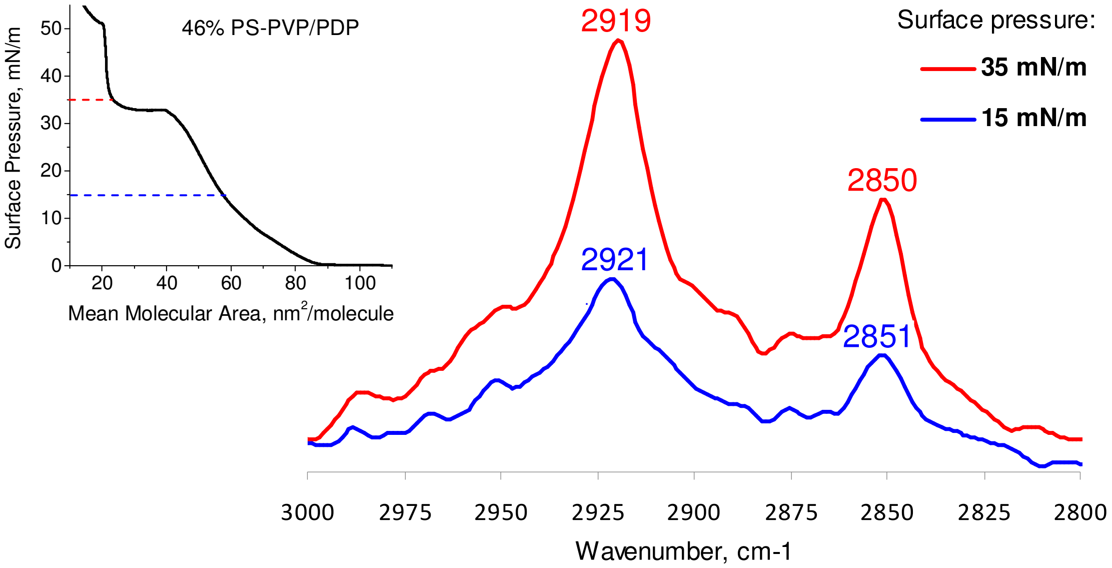

Figure 4-9. PM-IRRAS spectra of 46% PS-PVP/PDP$_{1.0}$ monolayer at the air/water interface, and in the inset (left), Langmuir compression isotherm.

Figure 4-10 illustrates a mechanism of transformation at the air/water interface as a result of surface area compression. When the surface area is large (below the onset area), the PS cores are embedded in highly extended PVP chains to which PDP of disordered conformation and mainly in prone orientation is hydrogen-bonded, forming surface micelles that may be contiguous to some extent as a continuous film at the PVP level and/or as individual disordered surface micelles. With decrease in surface area to very low surface pressure, the film may be essentially continuous with quasi-hexagonally ordered nanodots. This situation corresponds most closely to that in the ultrathin spin- and dip-coated films with this morphology mentioned above.[3–5] Further increase in surface pressure probably results initially in decreased stretching of the PVP blocks and/or some interpenetration of PVP chains emanating from neighboring nanodots, with essentially no change in PDP orientation. Then, when the plateau pressure is reached, the transition to rectangularly ordered nanodots and vertically oriented PDP occurs.

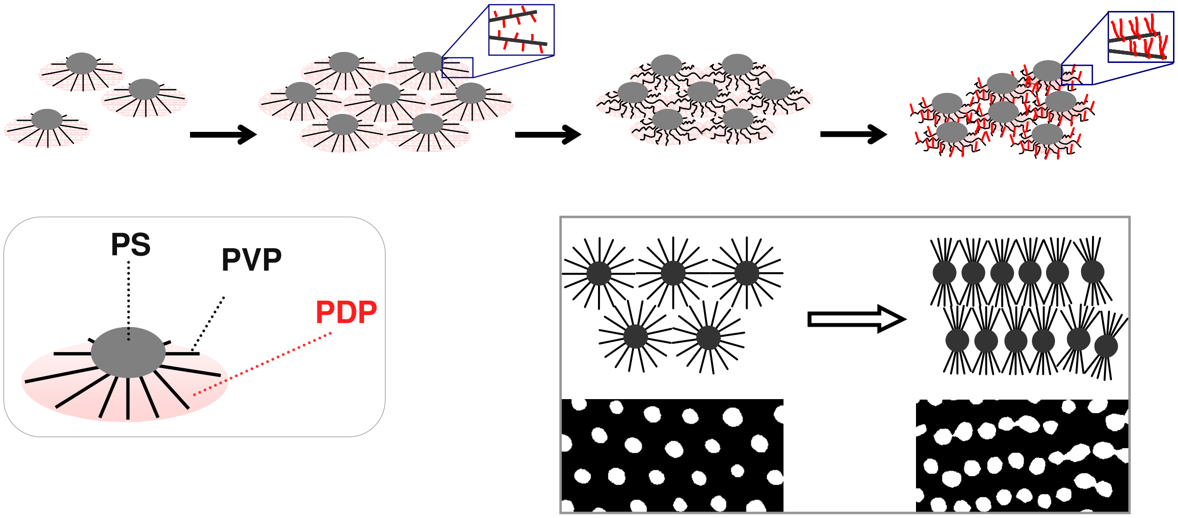

Figure 4-10. Model of PS-PVP/PDP nanodot behaviour on water when surface area decreases. The top image (3D-view) illustrates a sequential compression between features followed by reorientation of alkyl tails of PDP (from almost-parallel to all-perpendicular to the surface) when PVP chains reach their maximum compression. The bottom right image (2D-view) illustrates the change in nanodot order combined with alkyl chain above the plateau region.

4.3.2. Removal of PDP and Modification of Nanostrand Morphology

One of the potential applications of highly-ordered patterned LB films is their use as a template; but for this, access to the functional group and/or alternation of hydrophilic/hydrophobic surfaces is required. As was shown above, the surface of the PS-PVP/PDP monolayer is mostly hydrophobic because PS alternates with alkyl chains of PDP that cover the PVP matrix. Removal of PDP (thus, opening an access to PVP) would make feasible the use of the film as a template for the deposition of metals to obtain metallic nanowires, monomers for electropolymerization for organically conductive nanowires, initiators for graft-from polymerization, reactive small molecules for biosensing, *etc*. Because our initial interest concentrated on the nanostrand network morphology and in view of potential nanowire-type materials, our investigation of PDP removal from films is focused here on this structure.

To wash out PDP from bulk (3D) 12% PS-PVP/PDP structures, Ikkala, ten Brinke and coll. dialyzed the material against ethanol, a selective solvent for PVP and PDP, for 2 weeks.[14] In our case, we first soaked the transferred film in methanol for 30 min (as used by Laforgue *et al.* to obtain nanoporous dip-coated films of PS-PVP mixed with another hydrogen-bonding small molecule[15]), but found that it partially washed away the monolayer. Hexane, which is a non-solvent for both PS[16] and PVP, but dissolves PDP [it was used for recrystallization of PDP (300 mg/mL)] was tried next. After soaking in hexane for a few hours, the film topography showed no change. Presumably, PDP was effectively removed; however, its flat orientation on the PVP monolayer, and the inertness of both blocks to hexane, would leave no significant impact on the observed morphology after PDP removal. Contact angle measurements are inconclusive in this case because the initial obtuse contact angle (measured on film of nanostrand network before any treatment) gradually decreases during the experiment (*i.e.* less than half a minute). This is explained by the fact that hydrophobic strands do not cover the entire hydrophilic substrate (there are spaces between strands), thus when the drop of water is placed, it "feels" the hydrophobic surface first (*i.e.* elevated strands) but within time, the drop spreads because the monolayer is "holey" (perforated).

Finally, we experimented with acetone, which is an excellent solvent for PDP and a non-solvent for PVP.[17] PS is also not soluble in acetone, but swelling takes place.[16,18,19] In this case, significant morphological changes were observed, as shown in Figure 4-11 (and SI-4-7 in Appendix) for a film soaked in acetone for 10 min. Soaking for longer times (up to 3 hours) did not cause any further change in the morphology. Interestingly, it was found that soaking without stirring, including overnight, caused little change; instead, vigorous stirring was necessary to provoke the change, suggesting that mechanical and/or diffusive forces play a role to greatly accelerate, or even enable, the effect of acetone.

The new morphology remains in the form of strands, but the appearance of the strands was drastically modified. Each strand now consists of essentially two parallel rows of triangularly arranged nodules similar to nanodots. Although we have no direct proof at this time, it is probable that the acetone treatment has completely removed the PDP, not only from the PVP surface, but also any PDP dissolved in the PS phase (and possibly any PDP located or "trapped" between PS and the PVP monolayer). At the same time, and perhaps aided by the removal of PDP from PS, some kind of reconstruction of the PS strands has occurred. The strand morphology itself is not perturbed, due to being held in place by the PVP monolayer, which is not affected by acetone. There is little modification in height (from 6 ±1 nm to 8 ±2 nm) of the elevated (PS) parts of the modified (double-rowed) strands, but the total width has increased by *ca.* 30 nm (from 60 ±10 nm to 90 ±15 nm). This increase is the same as the width of the part of the PVP monolayer that, before acetone treatment, lay laterally along both sides of the strands. Correspondingly, the double row of quasi-nanodots are spaced apart to about the same extent as two neighboring rows, one from each of two neighboring strand segments when these segments were initially as closely spaced as possible. This indicates that the PS stripes have reorganized in the form of more distinct aggregates over the entire width of the fixed PVP monolayer underlying each strand. Furthermore, the PS aggregates are relatively uniform in size and tend to be ordered in a close-packed (triangular) manner along the PVP strand.

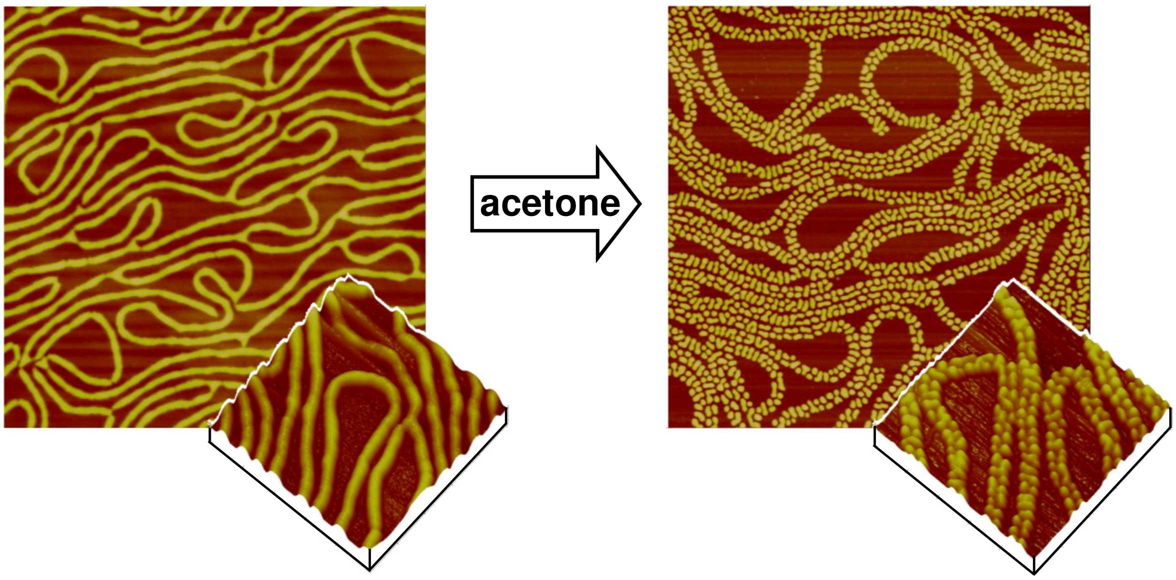

Figure 4-11. AFM topography images of 12% PS-PVP/PDP$_{1.0}$ LB films before (left) and after (right) stirring in acetone for 10 min (with no further change after treatment for longer times). Scan size: 3×3 μm (2D images) and 1×1 μm (3D images).

The relatively uniformly sized and ordered nature of the reconstructed PS aggregates along the original strands may simply be the result of the limited mobility of the PS chains in the presence of acetone due to their anchorage by the immobile PVP monolayer and due to the fact that PS only swells in acetone, followed by PS contraction due to acetone evaporation. However, it might also be taken as indicative of how aggregation takes place during the spreading/evaporation process at the air/water interface, particularly in the early stages. As explained in the previous chapter, the spreading solution is initially well below the critical entanglement concentration. This implies that polymer chain association must take place as solvent evaporates, in competition with further separation of chains and/or initial aggregates as the film of polymer solution continues to spread. The latter may be expected to lead to depletion zones due to diffusion limitation around growing aggregates, restricting their size and/or slowing their growth. The extent of entanglement may similarly be kinetically limited; *i.e.* polymer chain association can occur without significant entanglement, considering that the latter occurs on a longer timescale than simple association.

Within this context, the following mechanism underlying the aggregation process can be considered, shown schematically in Figure 4-12 as applied to nanostrand formation. In the initial stages of aggregation, the aggregates formed are necessarily small and likely to be in the form of spherical nanodots (termed hereafter quasi-nanodots to distinguish from the true nanodot morphology where aggregation is limited thermodynamically rather than kinetically). They may be hampered kinetically due to diffusion limitations early on in their growth (which might be expected to be influenced by initial solution concentration). At this stage, there might be enough time for the PS segments in these quasi-nanodots to entangle to some extent, since the solution is then the least concentrated and therefore the PS has the greatest mobility. The initially formed aggregates continue to grow as solvent evaporation continues, either more slowly due to the diffusion limitations and/or in steps by further association of the already formed initial aggregates, thereby tending towards the final morphologies (planar, stripe, nanodot) dictated by the block copolymer composition but impinged upon by kinetic restraints (see previous chapter). The schematic shown in Figure 4-12 considers only the further aggregation of already formed quasi-nanodots. Being in the regime where the cylindrical or stripe morphology is favoured, the quasi-nanodots tend to self-assemble longitudinally. Since the PVP blocks extending laterally around the nanodots are relatively short, the attractive forces between the PS coils favour this type of self-assembly, with the PVP monolayer able to accommodate by some migration to the regions neighboring the contact point, which thus densifies a little the PVP monolayer on the sides near the point of contact. Since the least densification would take place in the region furthest from the point of quasi-nanodot association, it is the preferred location for subsequent quasi-nanodot association, thereby favouring the longitudinal self-assembly. (In the planar morphology, the PVP chains are so short that they exert no spatially preferred repelling effects on association of the initial quasi-nanodots, and in the nanodot morphology, they are too long to favour any further association beyond what the equilibrium aggregation number permits.)

Association in triangular order enables close-packing of the quasi-nanodots in the strands. Defects along a strand occur most commonly as a change in growth direction, which favours division of the strand into two. This corresponds to the experimental observation that the maximum number of strands radiating out from a common point is three. Termination of the strands occurs when the PS blocks become rigid (their T_g rises above the ambient temperature), preventing further growth. With this picture, the acetone rinsed nanostrand morphology may be seen as revealing the originally formed quasi-nanodots, which are held together by their tighter association, possibly in the form of entanglements, which acetone cannot undo.

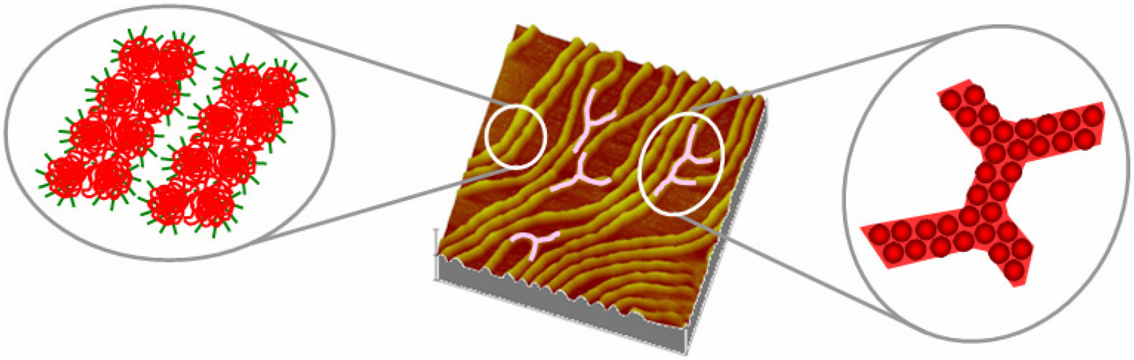

Figure 4-12. Schematic representation of the internal composition of strands, suggesting an early-stage mechanism of strand formation based on initially formed “quasi-nanodots”.

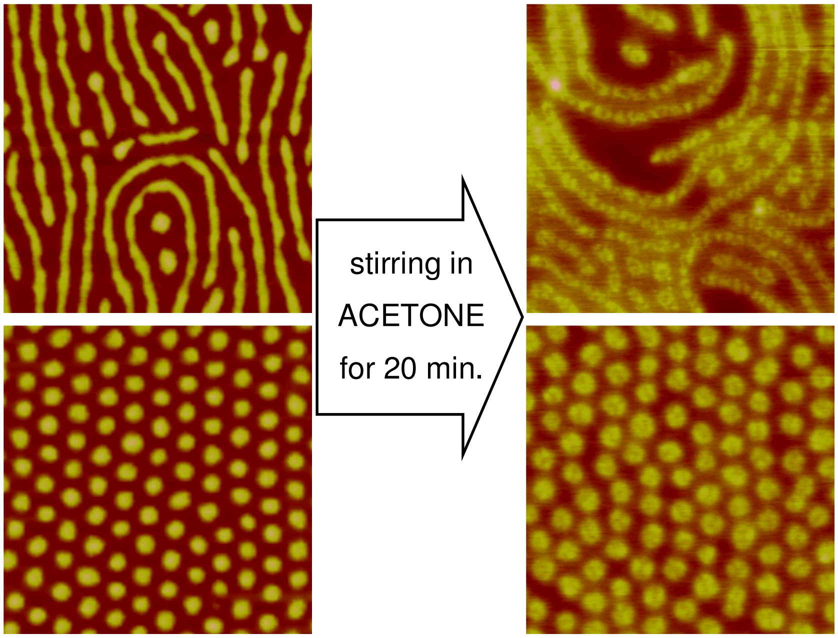

Figure 4-13. AFM topography images of 19% PS-PVP/PDP$_{1.3}$ LB films before and after acetone treatment. Scan size: 1×1 µm.

At first sight, this mechanism may appear to contradict the one proposed in Chapter 2 for nanostrand formation via the fingerprint or stripe morphology. However, the above mechanism does not preclude simultaneous lateral self-assembly into contiguous stripes such that the PVP monolayer becomes a coherent 2D film in the course of spreading, which then disassembles at the level of the exposed PVP stripes upon further spreading, as explained in Chapter 2. It might also be supposed that, if the above mechanism holds, it should hold for all of the morphologies. This needs further investigation; however, one preliminary result for the mixed nanostrand/nanodot morphology for the 19 mol% PS-PVP/PDP film, shown in Figure 4-13, does show some evidence of limited aggregation of the nanodots as well as nanostrands. A close look at the image of nanodots after acetone treatment shows a kind of dimpling of the nanodots that seem to correspond to three smaller aggregates (quasi-nanodots).

As a final remark, we can also consider how these results might be interpreted in the light of the Moffitt proposal that stripes are a product of polymer/water dewetting. In this case, the internal dots must be viewed as a microphase separation structure triggered by the increased concentration of copolymer in rims. One can argue that if the microphase separation structure can develop at the air/water interface (*i.e.* individual dots form and then assemble) *via* a disorder–order transition at high local copolymer concentration as solvent evaporates. Clearly, additional studies are required to prove or refute the above hypotheses.

4.3.3. 12% PS-PVP Complexes with Other Functional Small Molecules

PDP is the only small molecule used for complexation with PVP in the investigations described so far in this thesis. It is of interest to see if other small molecules might alter the morphology, in particular the nanostrand morphology, which occurs over a more restricted block copolymer composition range. For this brief study, we chose a range of small molecules that selectively interact with PVP (Figure 4-14), some involving different H-bonding strengths for the same alkyl chain length, and others with different alkyl chain lengths (including one with no alkyl chain and one with an unsaturated alkyl chain), and one with a sulfonic acid functionality that interacts with PVP via proton transfer, leading to ionic bonds. The surface topographies of the LB films of PS-PVP$_{(12\%)}$ with these molecules are shown in Figure 4-15 (Langmuir compression isotherms are available in the Appendix to Chapter 4, Figure SI-4-8).

Figure 4-15 demonstrates that OctPh and OctBA result in the same well-formed nanostrand network morphology as PDP, but with more apparent breakage points in the nanostrand loops observed. The LB films with these molecules were also all deposited with a good transfer ratio (*ca.* 1). Thus, neither the strength of the hydrogen bond (the OH–pyridine hydrogen bond being considered intermediate in strength and the COOH–pyridine hydrogen bond considered strong[20]) nor the position (meta- *vs.* para-) or length (C_8 *vs.* C_{15}) of the alkyl tail in these molecules influences the morphology significantly. OctOH, NOH, C_{16}diol, and PCDA also give overall nanostrand network morphology, but they are accompanied by much more bare surface, tend to be less well-defined and are accompanied by planar-type regions or have strands with variable thicknesses. The case of OctOH is especially interesting, in that the nanostrands tend to have three typical widths, 40–45, 60–65, and 80–85 nm, which appear to be multiples of a 20-nm base width. The apparent periodicity in the stripe widths for OctOH is intriguing, and it may be speculated, with reference to the previous section, that the pseudo-nanodots are aggregated in the form of 2, 3 and 4 rows per stripe (instead of the 2 rows per stripe observed with PDP). It was also noted that the transfer ratios for the LB films of PS-PVP with OctOH, NOH and C$_{16}$diol are all low (<0.3), as found previously for pure copolymer (Chapter 3). This suggests that complexation of these molecules with PVP is significantly less than for PDP, OctPh and OctBA. This may be attributed to the weaker H-bond formed by aliphatic COOH in PCDA and still weaker hydrogen bond formed by aliphatic OH group in OctOH and C$_{16}$diol, compared to aromatic COOH and OH, with PVP. Incomplete complexation of molecules with aliphatic OH and COOH to PVP was previously observed in the bulk with PVP homopolymer.[21] If there is less complexation, the planar-nanostrand transition composition (explained in Chapter 3) likely occurs at some PVP content intermediate to that observed for PS-PVP with and without PDP; in other words, this composition may be close to 12 mol% PVP, thus accounting for coexistence with some planar aggregates.

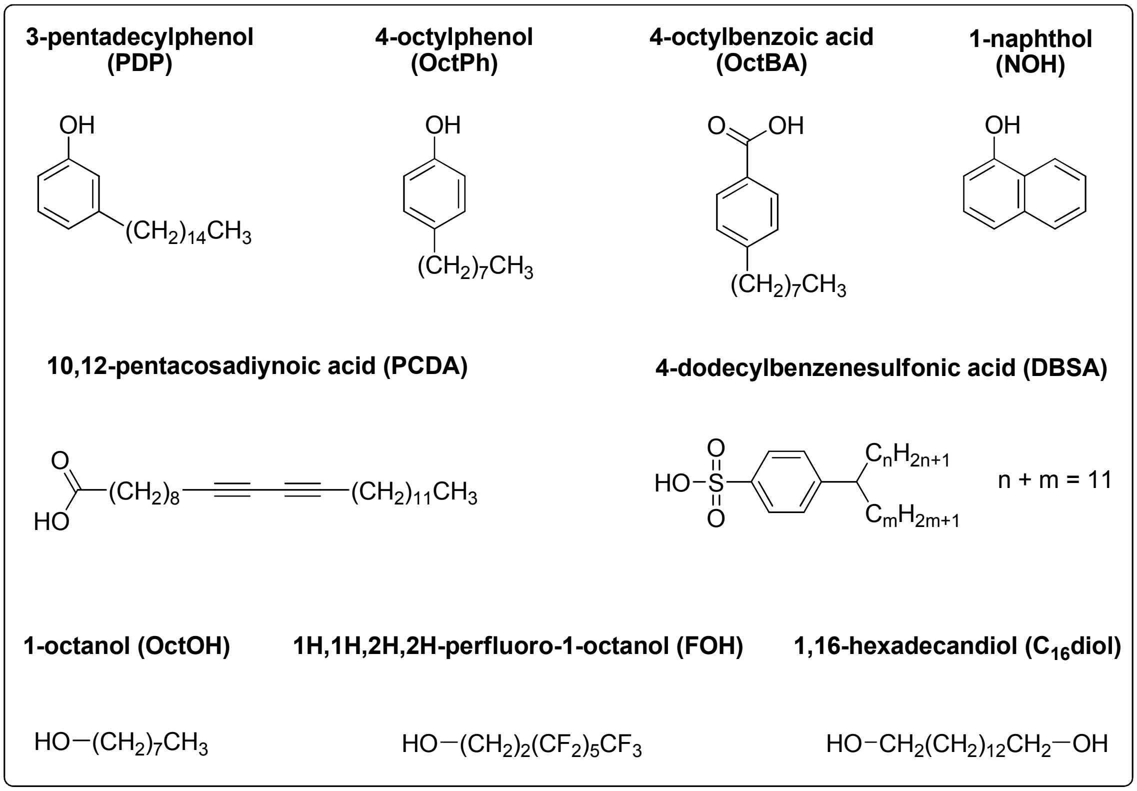

Figure 4-14. The small molecules used for complexation with 12% PS-PVP.

It is reasonable to expect stronger complexation of VP with FOH than that with OctOH, however, the PS-PVP/FOH morphology looks very similar to the morphology of pure PS-PVP. This can be due to immiscibility of perfluorocarbons and hydrocarbons, and thus it is unlikely that FOH is solubilized in PS as in the case of PDP,[13] and this additional repulsion between chains can also prevent regular structure formation. In the case of NOH, the H-bond strength should be similar to that for the molecules with the other aromatic OH groups, but complexation may be reduced for steric reasons due to the bulkiness of the aromatic part. It is also noteworthy that NOH results in a less flexible nanostrand structure that is subject to collapse at low surface pressures, observed in Figure 4-15 by the bright-colored spots. The complex with DBSA forms a film with mixed morphologies. Since the molecular weight of DBSA is similar to that of PDP (326.5 and 304.5 g/mol, respectively), the tendency towards a nanodot is not due to a morphology transition (as represented in the classical morphology diagram, Chapter 1). The ionic bond is also unlikely to be the reason because quaternized PS-PVP$^+$RX$^-$ of 6–14 mol% results in strand morphology.[2] In so far as DBSA is a mixture of isomers, we think that the change in structure can be associated with a steric effect. Besides, the aging of DBSA should not be ignored.

In addition to functional small molecules, we also explored if the addition of oligostyrene (OS, MW = 800 g/mol) in 12% PS-PVP/PDP system results in strand plasticization and improvement in their length and order. Addition of a small amount of OS, in a molar ratio OS:PS repeat units 1:20 does not change the morphology at all, but a large amount, 1:2 ratio, results in thickening of the intersection between strands. This new structure, presented in Figure 4-16, can be a sequence of morphology shift towards planar aggregates (since the molar ratio of PVP in the OS/PS-PVP system decreases to 8.4%).

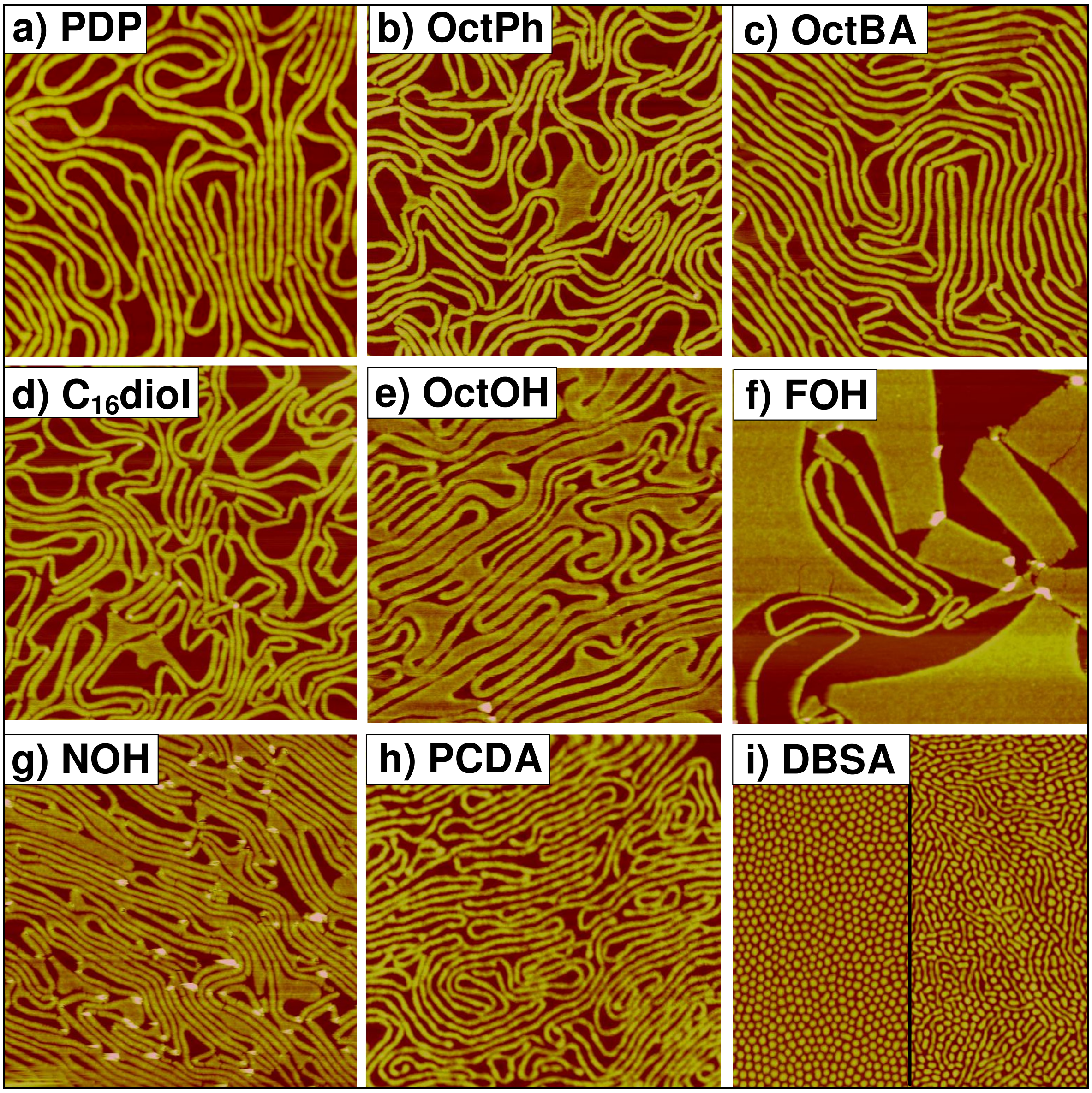

Figure 4-15. AFM topography images (3×3 μm) of LB films of 12% PS-PVP with various small molecules. The molar ratio of PVP to small molecule functional group is 1.0:1.0–1.3 (*i.e.* 2.0:1.0 molecular molar ratio for hexadecanediol). Copolymer concentration: 1.8–2.0 mg/mL; π = 5–10 mN/m. a) 3-pentadecylphenol; b) 4-octylphenol; c) 4-octylbenzoic acid; d) 1,16-hexadecandiol; e) 1-octanol; f) 1H,1H,2H,2H-perfluoro-1-octanol; g) 1-naphthol; h) 10,12-pentacosadiynoic acid; i) 4-dodecylbenzenesulfonic acid.

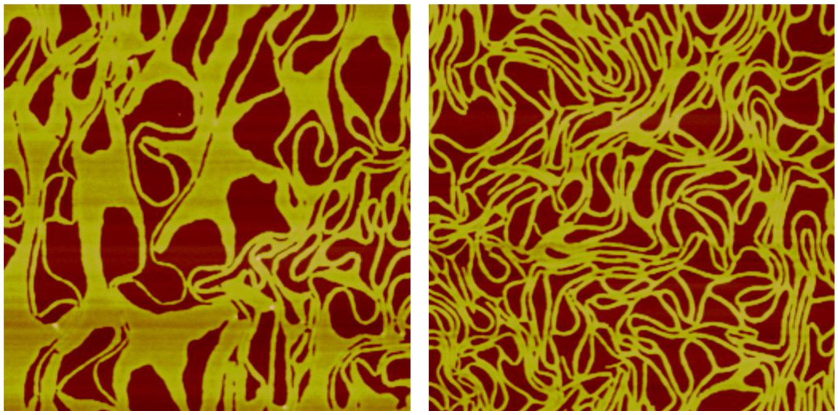

Figure 4-16. AFM height images (5×5 μm) of 12% OS/PS-PVP/PDP$_{1.0}$ spread from CHCl$_3$ solution (block copolymer concentration 1.8 mg/ml) at 20°C, and transferred onto mica at $\pi = 10$ mN/m. Ratio between styrene repeat units in OS and PS is 1:2.

4.3.4. Effect of Molecular Weight on the Morphology (PS-PVP$_{12\%}$/PDP)

The effect of the total block copolymer molecular weight on the LB film morphology was investigated using PS-PVP$_{12\%}$ of a much higher and a much lower molecular weight (see Table 4-1) compared to the 12%[†] copolymer used elsewhere in this thesis, and which shows broken planar aggregates without PDP present and the nanostrand network with PDP present. For reference, the Langmuir compression isotherms for these copolymers with and without equimolar PDP present are shown in Figure 4-17. The area per polymer molecule increases with increase of total molecular weight of PS-PVP, as is to be expected. On the other hand, the area per VP unit is expected to remain constant, at least at low surface pressure. The latter is observed for 12$_L$% and 12$_M$% copolymer, but the mean area per VP unit for high molecular weight PS-PVP is less, which might be explained by the fact that the very long polymer chains may have not enough time to spread on the water surface

---

[†] In this section, we call it 12$_M$% (M – medium) to distinguish it from the 12% samples of low and high molecular weights.

before solvent evaporates and some PVP chains can “freeze” at the top of features formed. In the case of complexes, three isotherms represented on pressure–area per VP unit (bottom right image in Figure 4-17) have a constant shift along the area axis, which can be indirect evidence of full complexation (otherwise, the amount of uncomplexed PDP molecules would be different, which would affect the area on the isotherms as observed but without the regularity in shift).

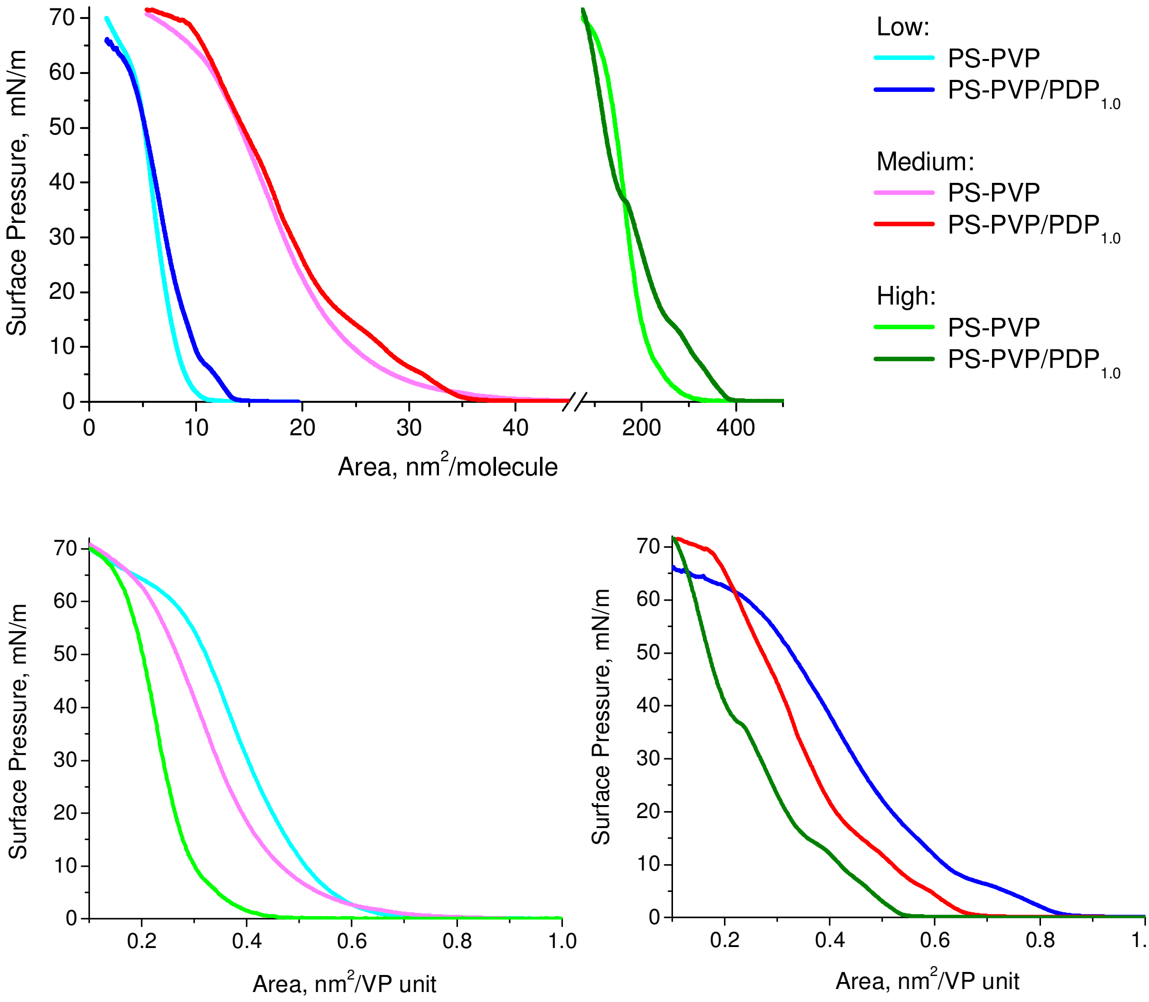

Figure 4-17. Langmuir compression isotherms of PS-PVP block copolymers of 12 % PVP with and without equimolar PDP. 1.8 mg/ml $CHCl_3$ solutions were spread at 20 ±0.5°C. Total molecular weight of polymers are: 13,700 (low); 45,600 (medium); 610,000 (high). The area is presented per polymer molecule (top) or per polymer molecule (bottom).

The LB film morphologies obtained with these copolymers of low and high molecular weights are shown in Figure 4-18 (morphologies of $12_M\%$ have been shown previously). The heights of low and high MW 12% PS-PVP, calculated using the rms end-to-end disitance of PS chains in a theta solvent and the Kumaki diameter (see Chapter 3, equation 1 and 2), are in good agreement with experimental data (Table 4-4).

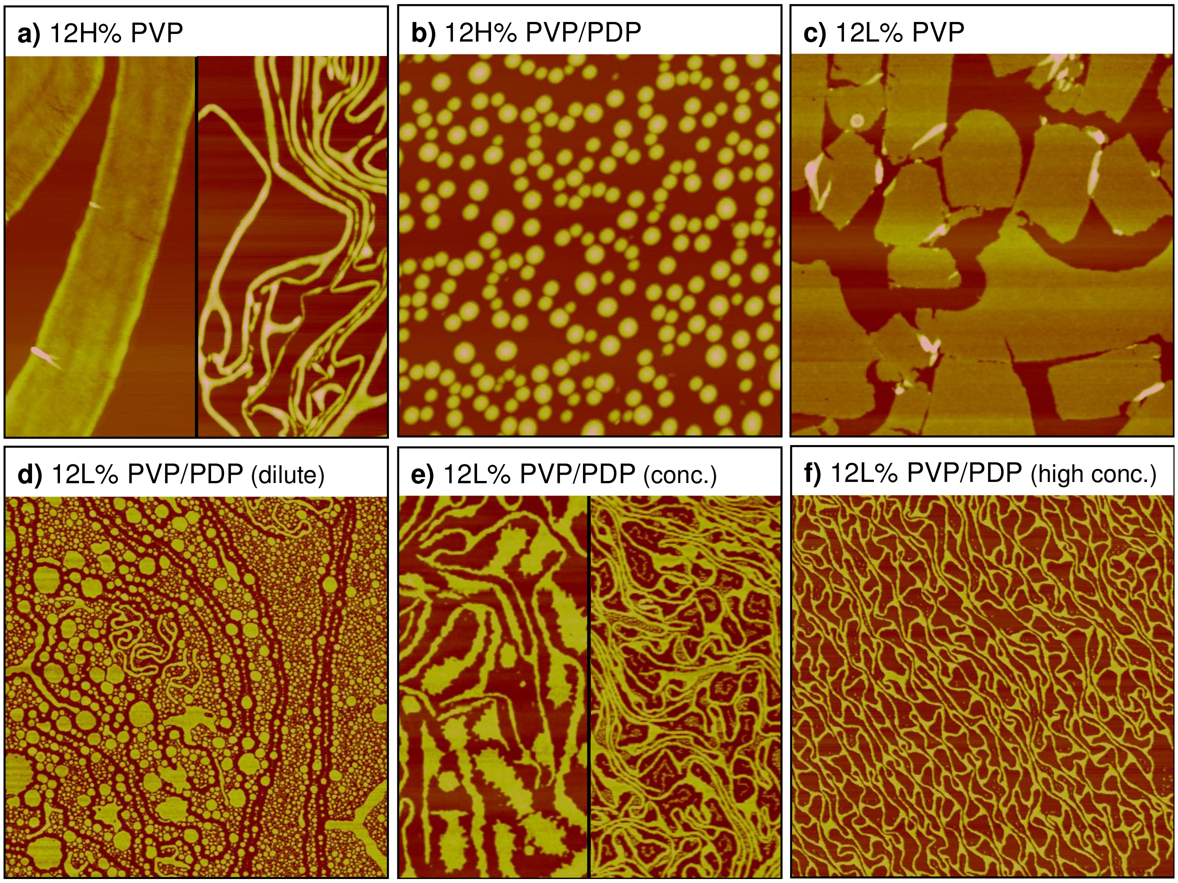

Figure 4-18. AFM height images of LB films of PS-PVP$_{12\%}$ with and without PDP spread from $CHCl_3$ solutions at 21±0.5°C, and transferred at $\pi = 3$–5 mN/m. a) $12_H\%$ PS-PVP; b) $12_H\%$ PS-PVP/PDP$_{1.0}$; c) $12_L\%$ PS-PVP; d–f) $12_L\%$ PS-PVP/PDP$_{1.0-1.3}$. Concentration of solutions: a–c,e) 1.80 mg/mL; d) 0.35 mg/mL; f) 4.06 mg/mL. Scan size, μm: 5×5 (a,e: 5×2.5 each). Z-scale, nm: a) 35, 20; b) 70; c) 18; d–f) 10.

Table 4-4. Calculated values of the rms end-to-end distance of PS (*R*) and the Kumaki diameter of a PS sphere (*d*), and comparison with the experimental height (AFM) of PS-PVP/PDP$_{1.0}$ at $\pi = 3$ mN/m.

Sample	Calculated height of features (nm)		Measured height of features (nm)
	R	*d*	
12_L%	2.5	3.1	*ca.* 3.3
12_H%	16.5	21.5	> 20

The very high molecular weight copolymer without PDP present, spread from a high concentration solution (1.80 mg/mL), shows mixed morphologies (Figure 4-18a) of ribbons and strands of variable thickness as well as some more elongated planar aggregates and other irregular structures (where there is material, since the surface coverage is poor due to a low transfer ratio). These resemble diverse "dewetted structures" shown by Moffitt and coll.,[22,23] particularly for pure PS.[24] Given that the composition of this copolymer puts it in the planar regime, the diversity of structures that can be attributed to competition between polymer association and continuous film dewetting, exacerbated by the slower kinetics of high molecular weight chains, is not surprising, as explained in Chapter 3. It is noteworthy that the rims around the planar structures are particularly high, *ca.* 4 nm (compared to less than 1 nm for the lower MW polymers with planar structures described in Chapter 3). With the presence of equimolar or a small excess of PDP (1.0:1.0 to 1.0:1.3 VP:PDP, Figure 4-18b), whether spreading is from high or low concentration solutions, the morphology is in the form of variably sized and irregularly spaced circular micelles (simply pushed closer together for transfers done at 15 compared to 3 mN/m).[25] The same morphology was observed for the 14_H% copolymer having half the molecular weight of the high MW 12_H%, attributed to the slow kinetics of high MW chains that cause diffusion limitation (creating depletion in the vicinity of growing aggregates) to set in much earlier during the spreading/evaporation process (see Chapter 3). It is noteworthy that the isotherm for this copolymer shows a distinct (although short) plateau at a surface pressure of *ca.* 35–40 mN/m, reflective of the micellar morphology.

The much lower MW 12_L% copolymer (13,700) without PDP (studied at high concentration only) has a morphology consisting mainly of large platelets, often with fairly straight edges and sides, with sharp angles, indicative of broken planar aggregates (Figure 4-18c), as in the intermediate MW 12_M% copolymer. In the presence of PDP (1.0:1.0 or 1.0:1.3), low concentration spreading solutions (0.35 mg/mL, Figure 4-18d) lead to a morphology consisting mainly of circular-type aggregates of widely varying sizes, often with edge irregularities, along with a small fraction of strand-like objects. High concentration solutions (1.80 mg/mL, Figure 4-18e) greatly increase the nanostrand population, with which the planar-type aggregates (no longer circular, but with quite irregular or serrated edges) are interconnected. Much higher concentrations (4.06 mg/mL shown in Figure 4-18f) are required for the morphology to be dominated by the nanostrands (which nevertheless still have thickened areas, especially at network junctions). The greater tendency for planar-type aggregates in this copolymer can be explained by the shortness of the VP block, which can have several consequences. One is that, with a block length that is similar to that of the 4% copolymer in Chapter 3, it lies as a monolayer almost exclusively beneath the PS phase, which is enough to rationalize the planar-type morphologies. Another consequence is the reduction in block repulsion, up to block miscibility for low enough molecular weight blocks. This would clearly have a consequence on the phase separation in the form of ultrathin films, at least in part by varying the “stickiness” (attractive interactions with the surface) of the respective blocks, as modeled in ref. 26 for ultrathin films on solid planar surfaces.

A third consequence is that the lower molecular weight of the PS block means that it has a lower T_g, possibly also with significantly greater PDP incorporation (since miscibility increases with decreasing molecular weight), which would reduce its T_g even further. Thus, this system may be expected to maintain greater mobility at the air/water interface for a longer time than the higher molecular weight analogs. This is supported by the morphologies of LB films transferred at high surface pressure (40 mN/m). Similar to the 12_M% PVP/PDP copolymer, which shows buckling at $\pi > 30$ mN/m (see Chapter 2), the 12_L% PVP/PDP copolymer also exhibits collapse at high surface pressure but simultaneously it forms significant (quasi-)fusion of aggregates (see Figure 4-19). It can thus be concluded that for low molecular weight copolymers, it is not only the block weight fractions that dictate morphologies, but also the absolute molecular weights of the blocks.

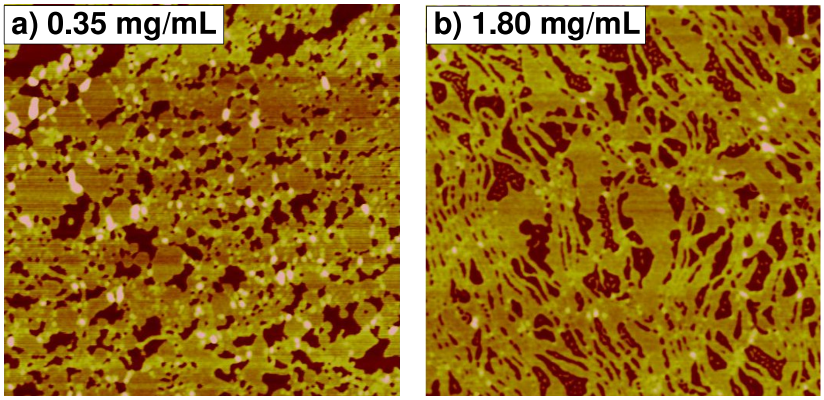

Figure 4-19. AFM height images of $12_L\%$ PS-PVP/PDP$_{1.3}$ spread from dilute (a) and concentrated (b) $CHCl_3$ solutions at 20°C, and transferred onto mica at $\pi = 40$ mN/m. Scan size: 3×3 µm.

It is of additional interest that the use of tetrachloroethane as spreading solvent (1.8 mg/mL concentration) and low subphase temperature, which produced a "perfected" nanostrand morphology for $12_M\%$ PVP/PDP, attributed to the maintenance of mobility for a longer time during the morphology formation process (Chapter 2), gives larger and more circular aggregates containing tiny holes (thus resembling "nanofoams"[27]) for $12_L\%$ PVP/PDP (Figure 4-20). Again, when the aggregates are compressed together at higher surface pressure, there are signs of interconnections forming among them (similar to Figure 4-19) that are suggestive of remaining PS mobility.

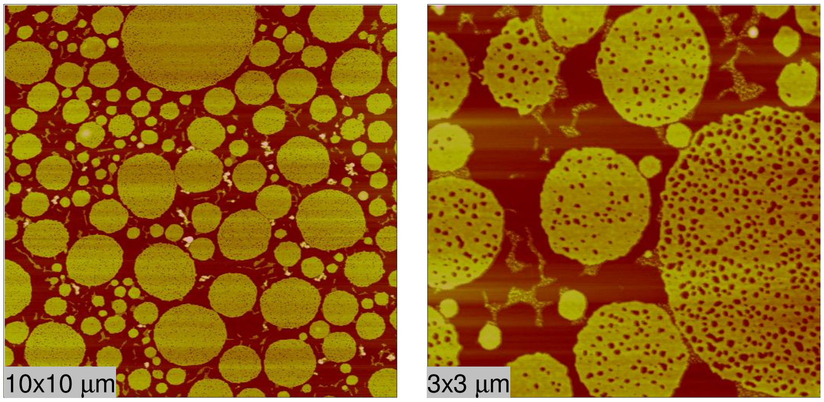

Figure 4-20. AFM height images of $12_L\%$ PS-PVP/PDP$_{1.3}$ spread from $C_2H_2Cl_4$ solution (concentration 1.80 mg/ml) at 9°C, and transferred onto mica at $\pi = 5$ mN/m.

The variety of morphological forms observed for these very high and very low molecular weight 12% VP copolymers are reminiscent of the various morphologies and “dewetted structures” observed by Moffitt and coll. for PS-PEO copolymers.[22–24] The latter, in considering the effect of molecular weight on “dewetted structures”, argued that structures corresponding to dots, strands and planar aggregates are favoured in the order of low to high molecular weight. This was explained on the basis that dewetting originates from a continuous film (formed by the polymer solution of a given deposited drop), which first form nanoholes that then grow to form interconnected rims; then these rims break up into strands and finally the strands break up into dots via the Rayleigh instability mechanism. LB film morphologies are thus viewed as resulting from freezing in at different stages along this pathway. Since the mobility of polymers decreases with increasing molecular weight, it was therefore concluded that the higher the molecular weight, the earlier the stage at which the morphology freezes in. Similarly, higher solution concentration implies higher viscosity, which also slows down kinetics, and should thus favour morphologies at earlier stages of dewetting compared to lower concentrations.

A number of the images presented here do not appear to be in agreement with that picture of dewetting. In particular, we see predominantly dot-like features for 12_H% PVP/PDP and a much higher tendency for planar features for 12_L% PVP/PDP (and nanostrands for medium molecular weight, Chapter 2), which is contrary to what is expected from the dewetting model. Furthermore, the 12_L% PVP/PDP films obtained from the lowest concentration solution show both nanodots and large planar aggregates, compared to an increased tendency for nanostrand-type structures with increasing solution concentration. These observations support our discussion in Chapter 3, notably that the block composition first of all dictates the equilibrium type of morphology to which the film tends, and that the spreading/evaporation process that freezes in non-equilibrium morphologies is complex, and in particular, must involve a competition between both association and dewetting, where association proceeds from small to large aggregates (*i.e.* opposite to dewetting). Furthermore, the mechanism of dewetting is itself influenced by any nanostructure that forms in the spreading film of evaporating solution.

Finally, it is of interest to mention that the theoretical analysis by Potemkin and Möller of ultrathin films on solid surfaces shows that nanoholes (at the bottom of which is the adsorbed monolayer) may form in films where the more hydrophobic block also has some degree of "stickiness" with the surface when in the planar morphology regime, and that the composition range where this morphology occurs increases with increase in degree of stickiness of the more hydrophobic block.[26] This might be one explanation for the nanofoam morphology observed in Figure 4-20, particularly if some PVP is blended with the PS block due to their very low molecular weight. It is, furthermore, conceivable that if such nanofoam structures occur in the course of spreading, that further spreading enlarges these holes by the dewetting process described by Moffitt and coll.,[23] which may account for the appearance of the particular form of the nanostrand network observed in Figure 4-18 for the film spread from the highest concentration solutions.

4.4. CONCLUSIONS

Using PS-PVP diblock copolymers of various molecular weights and block ratios as well as various small molecules complexed to VP, we have established the following. First, by using AFM, we have shown the existence of coronae around spheres and strands, and thus, confirmed the surface micelle structure proposed previously. Second, for the first time (to our knowledge), it has been shown that the plateau observed in pressure–area isotherms of nanodot-forming polymers is associated with a pressure-induced order–order transition (*i.e.* nanodot re-ordering), which occurs simultaneously with alkyl chain reorientation. This is the most important result of this chapter, and even of this thesis. Third, we demonstrated that acetone treatment of LB nanostrand films confers an internal structure to the nanostrands in the form of a displaced double row of nanodots. This led to a discussion speculating about the initial stages of polymer chain association following drop spreading as suggested by this internal structure. Fourth, use of various surfactants complexed to the copolymer has added to knowledge of the role of small molecules in supramolecular self-assembly at the air/water interface. Last, we have shown that control over structure formation is directed not only by the ratio between blocks, but by the total molecular weight of the block copolymer, which introduces additional factors governing morphology formation, thus complementing the discussion of Chapter 3.

References to Chapter 4:

1. Chapter 3 of this thesis.
2. Zhu, J.; Eisenberg, A.; Lennox, R. B. Interfacial behavior of block polyelectrolytes. 5. Effect of varying block lengths on the properties of surface micelles. *Macromolecules* **1992**, *25*, 6547–6555.
3. Spatz, J. P.; Sheiko, S.; Möller, M. Substrate-induced lateral micro-phase separation of a diblock copolymer. *Adv. Mater.* **1996**, *8*, 513–517.
4. Spatz, J. P.; Möller, M; Noeske,M.; Behm, R. J.; Pietralla, M. Nanomosaic surfaces by lateral phase separation of a diblock copolymer. *Macromolecules* **1997**, *30*, 3874–3880.
5. Kramarenko, E. Y.; Potemkin, I. I.; Khokhlov, A. R.; Winkler, R. G.; Reineker, P. Surface micellar nanopattern formation of adsorbed diblock copolymer systems. *Macromolecules* **1999**, *32*, 3495–3501.
6. Perepichka, I. I.; Badia, A.; Bazuin, C. G. Nanostrand formation of block copolymers at the air/water interface. *ACS Nano*, **2010**, *4*, 6825–6835. (Chapter 2 of this thesis).
7. Shin, K.; Rafailovich, M. H.; Sokolov, J.; Chang, D. M. Cox, J. K.; Lennox, R. B.; Eisenberg, A.; Gibaud, A.; Huang, J.; Hsu, S. L.; Satija, S. K. Observation of surface ordering of alkyl side chains in polystyrene/polyelectrolytes diblock copolymer Langmuir films, *Langmuir* **2001**, *17*, 4955–4961.
8. Li, Z.; Zhao, W.; Quinn, J.; Rafailovich, M. H.; Sokolov, J.; Lennox, R. B.; Eisenberg, A.; Wu, X. Z.; Kim, M. W.; Sinha, S. K.; Tolan, M. X-ray reflectivity of diblock copolymer monolayers at the air/water interface. *Langmuir* **1995**, *11*, 4785–4792.
9. Zhu, J.; Eisenberg, A.; Lennox, R. B. Interfacial behavior of block polyelectrolytes. 1. Evidence for novel surface micelle formation. *J. Am. Chem. Soc.* **1991**, *113*, 5583–5588.
10. Gaussian 03, Revision D.01. Frisch, M. J.; Trucks, G. W.; Schlegel, H. B.; Scuseria, G. E.; Robb, M. A.; Cheeseman, J. R.; Montgomery, J. A.; Vreven, Jr. T.; Kudin, K. N.; Burant, J. C.; Millam, J. M.; Iyengar, S. S.; Tomasi, J.; Barone, V.; Mennucci, B.; Cossi, M.; Scalmani, G.; Rega, N.; Petersson, G. A.; Nakatsuji, H.; Hada, M.; Ehara, M.; Toyota, K.; Fukuda, R.; Hasegawa, J.; Ishida, M.; Nakajima, T.; Honda, Y.; Kitao, O.; Nakai, H.; Klene, M.; Li, X.; Knox, J. E.; Hratchian, H. P.; Cross, J. B.; Bakken, V.; Adamo, C.; Jaramillo, J.; Gomperts, R.; Stratmann, R. E.; Yazyev, O.; Austin, A. J.; Cammi, R.; Pomelli, C.; Ochterski, J. W.; Ayala, P. Y.; Morokuma, K.; Voth, G. A.; Salvador, P.; Dannenberg, J. J.; Zakrzewski, V. G.; Dapprich, S.; Daniels, A. D.; Strain, M. C.; Farkas, O.; Malick, D. K.; Rabuck, A. D.; Raghavachari, K.; Foresman, J. B.; Ortiz, J. V.; Cui, Q.; Baboul, A. G.; Clifford, S.; Cioslowski, J.; Stefanov, B.

B.; Liu, G.; Liashenko, A.; Piskorz, P.; Komaromi, I.; Martin, R. L.; Fox, D. J.; Keith, T.; Al-Laham, M. A.; Peng, C. Y.; Nanayakkara, A.; Challacombe, M.; Gill, P. M. W.; Johnson, B.; Chen, W.; Wong, M. W.; Gonzalez C.; Pople, J. A. Gaussian Inc., Wallingford CT, 2004.

11. HyperChem For Windows Release 8.0 Scholar, Copyright 2007 Hypercube Inc.
12. Dicko, A.; Bourque, H.; Pézolet, M. Study by infrared spectroscopy of the conformation of dipalmitoylphosphatidylglycerol monolayers at the air–water interface and transferred on solid substrates. *Chem. Phys. Lipids* **1998**, *96*, 125–139.
13. van Zoelen, W.; Alberda van Ekenstein, G.; Ikkala, O.; ten Brinke, G. Incorporation of PPE in lamellar self-assembled PS-b-PVP(PDP) supramolecules and PS-b-PVP diblock copolymers. *Macromolecules* **2006**, *39*, 6574–6579.
14. de Moel, K.; Alberda van Ekenstein, G. O. R.; Nijland, H.; Polushkin, E.; ten Brinke, G.; Mäki-Ontto, R.; Ikkala, O. Polymeric nanofibers prepared from self-organized supramolecules. *Chem. Mater.* **2001**, *13*, 4580–4583.
15. Laforgue, A.; Bazuin, C. G.; Prud'homme, R. E. A study of the supramolecular approach in controlling diblock copolymer nanopatterning and nanoporosity on surfaces. *Macromolecules* **2006**, *39*, 6473–6482.
16. Brandrup. J.; Immergut, E. H. *Polymer Handbook*. 2nd Ed., Wiley Interscience: New York, 1975.
17. Tashmukhamedov, S. A.; Tsagarayev, E. T.; Tillayev, R. S.; Usmanov, K. U. Eletron-microscope study of the structure of acetyl cellulose–polyvinyl pyridine graft copolymers. *Vysokomol. Soyed.* **1973**, *A15*, 2082–2085.
18. Roe, S.; Sherrington, D. C.; Hysteresis-like behaviour in the swelling/deswelling of polystyrene based crosslinked resins using acetone/water mixtures. *Eur. Polymm. J.* **1987**, *23*, 195–199.
19. Sidorenko, A.; Minko, S.; Schenk-Meuser, K.; Duschner, H.; Stamm, M. Switching of polymer brushes. *Langmuir* **1999**, *15*, 8349–8355.
20. Lee, J. Y.; Painter, P. C.; Coleman, M. M. Hydrogen bonding in polymer blends. 4. Blends involving polymers containing methacrylic acid and vinylpyridine groups. *Macromolecules* **1988**, *21*, 954–960.
21. Ruokolainen, J.; Torkkeli, M.; Serimaa, R.; Vahvaselkä, S.; Saariaho, M.; ten Brinke, G.; Ikkala, O. Critical interaction strength for surfactant–induced mesomorphic structures in polymer–surfactant systems. *Macromolecules* **1996**, *29*, 6621–6628.
22. Cheyne, R. B.; Moffitt, M. G. Novel two-dimensional "ring and chain" morphologies in Langmuir-Blodgett monolayers of PS-b-PEO block copolymers: Effect of spreading solution concentration on self-assembly at the air/water interface. *Langmuir* **2005**, *21*, 5453–5460.

23. Cheyne, R. B.; Moffitt, M. G. Self-assembly of polystyrene-block-poly(ethylene oxide copolymers at the air–water interface: Is dewetting the genesis of surface aggregate formation? *Langmuir* **2006**, *22*, 8387–8396.

24. Price, E. W.; Harirchian-Saei, S.; Moffitt, M. G. Strands, network, and continents from homopolystyrene dewetting at the air/water interface: Implications for amphiphilic block copolymer self-assembly. *Langmuir* **2011**, *27*, 1364–1372.

25. Dr. Qing Lu, using the solvent-assisted technique on this copolymer with equimolar PDP, also observed a morphology of circular micelles, but interconnected to some extent as if partly fused.

26 Potemkin, I. I.; Möller, M. Microphase separation in ultrathin films of diblock copolymers with variable stickiness of one of the blocks to the surface. *Macromolecules* **2005**, *38*, 2999–3006.

27. Meszaros, M.; Eisenberg, A.; Lennox, R. B. Block Copolymer Self-Assembly in Two Dimensions: Nanoscale Emulsions and Foams. *Faraday Discuss.* **1994**, *98*, 283–294.

Appendix to Chapter 4

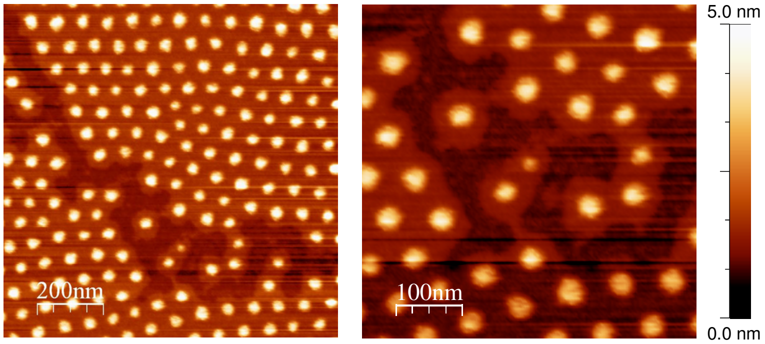

Figure SI-4-1. AFM height image (obtained with Nanoscope AFM) of the 46% PS–PVP/PDP$_{1.0}$ LB film spread from CHCl$_3$ solution of 0.6 mg/mL copolymer concentration and transferred onto mica at π = 15 mN/m. Scan size: 1×1 µm (left) and 515×515 nm (right).

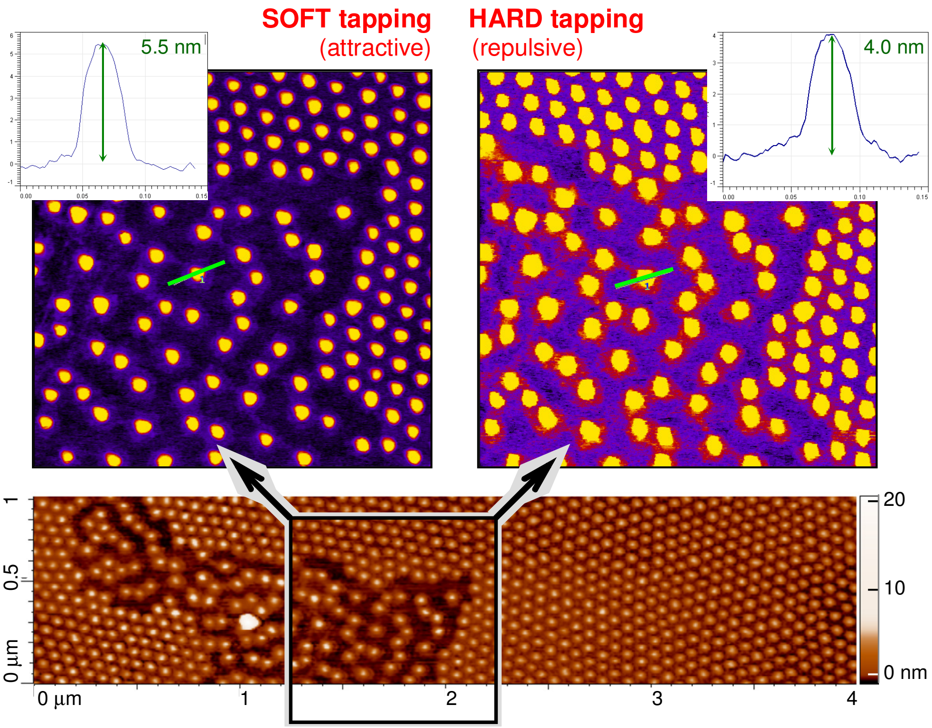

Figure SI-4-2. AFM height images (obtained with AIST-NT's SmartSPM) and section profiles (along the green lines) of the 46% PS–PVP/PDP$_{1.0}$ LB film (the same film as on Figure SI-4-1). Scan size: 1×1 µm (top) and 1×4 µm (bottom).

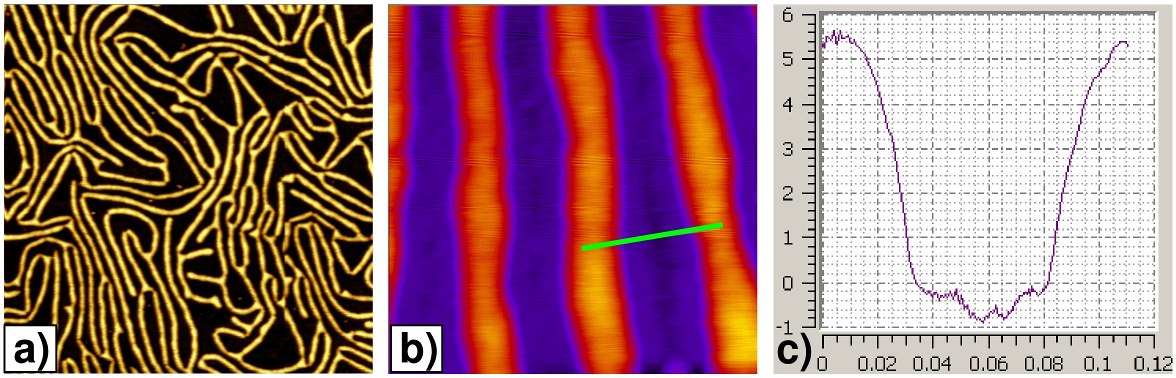

Figure SI-4-3. AFM height images of the 12 % PS–PVP/PDP$_{1.0}$ LB film (π = 5 mN/m). Image (c) is the profile section along the green line in image (b). Scan size: a) 3×3 µm; b) 300×300 nm.

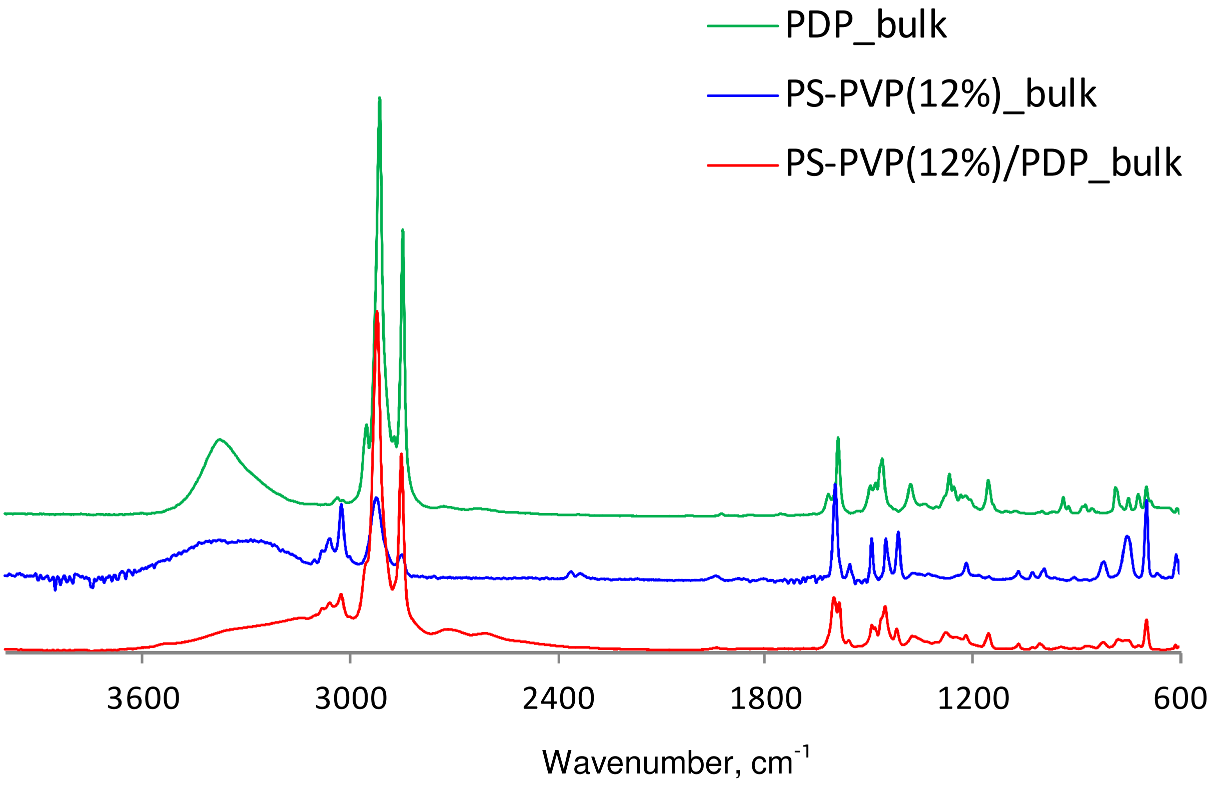

Figure SI-4-4. ATR-IR spectra of 12% PS-PVP, PDP, and 12% PS-PVP/PDP$_{1.0}$ in bulk. (Expanded spectra are presented in Figure 4-4).

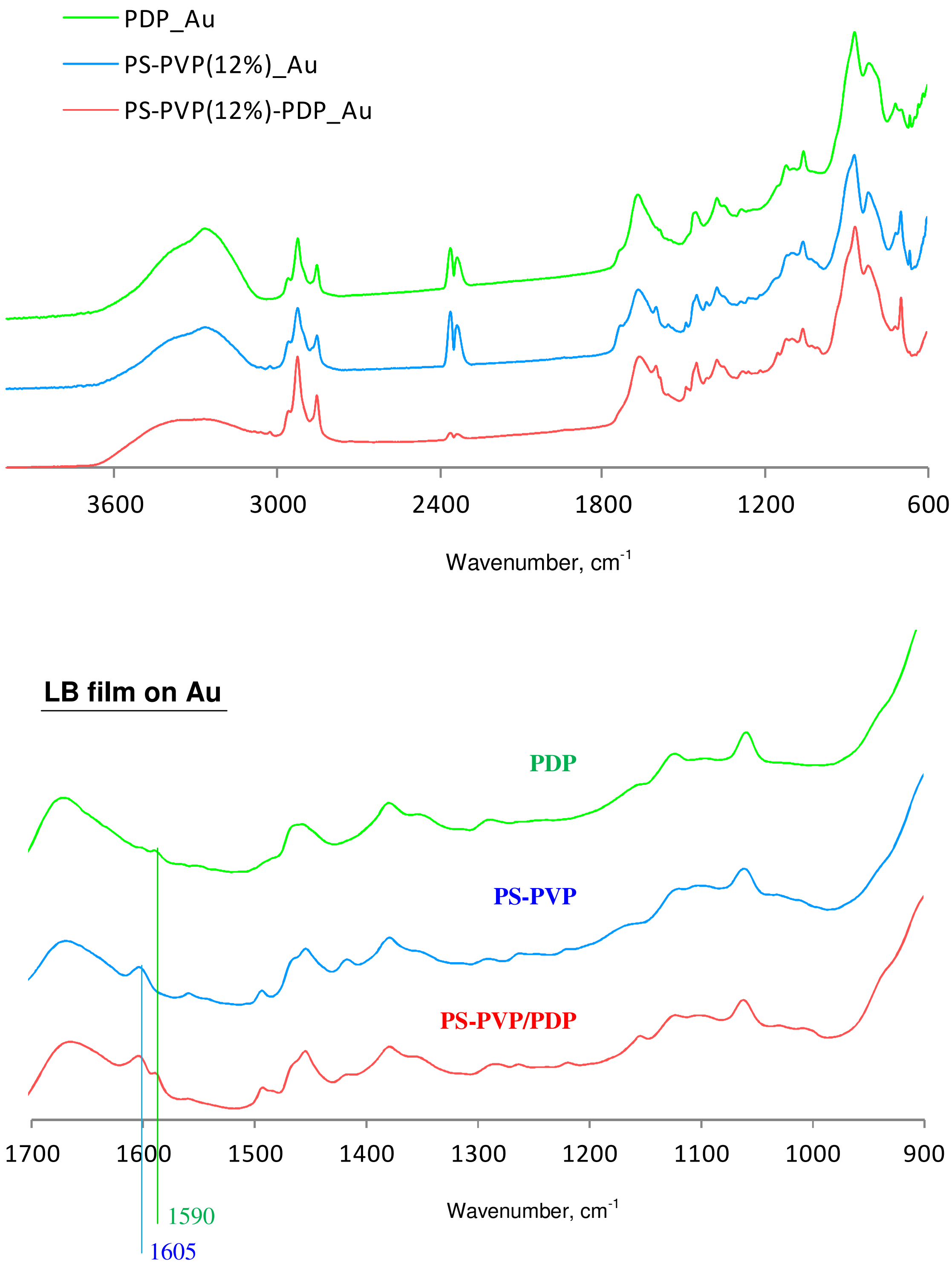

Figure SI-4-5. ATR-IR spectra of 12% PS-PVP, PDP, and 12% PS-PVP/$PDP_{1.0}$ LB films transferred at π = 20 mN/m onto gold substrate.

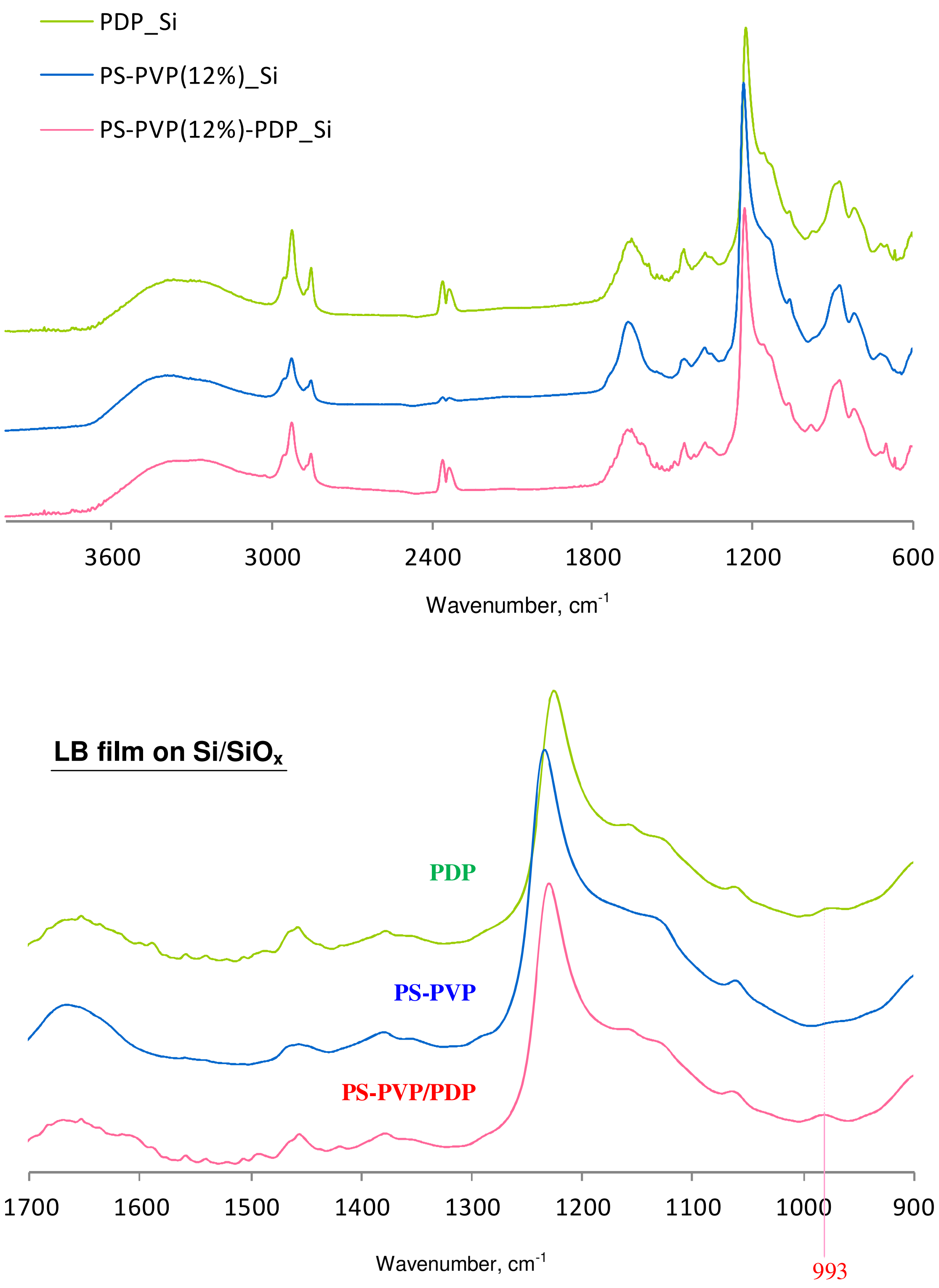

Figure SI-4-6. ATR-IR spectra of 12% PS-PVP, PDP, and 12% PS-PVP/PDP$_{1.0}$ LB films transferred at π = 20 mN/m onto silicon wafer.

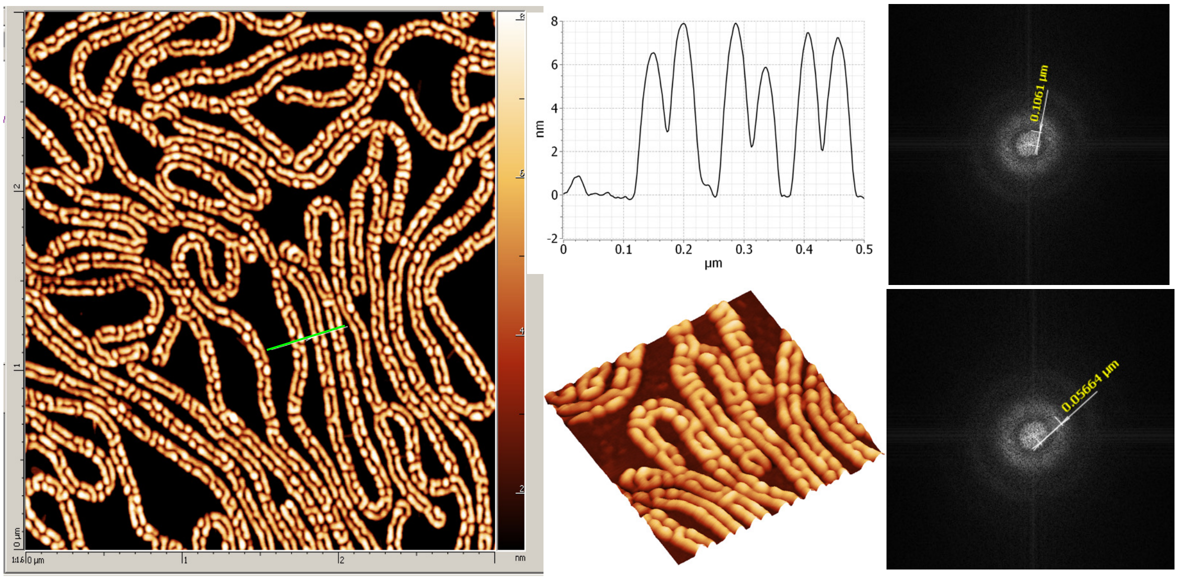

Figure SI-4-7. AFM topography images with cross-section (along the green line) and FFT analysis of 12% PS-PVP/PDP LB film after soaking in acetone for 30 min. Scan size: 3×3 μm (2D image), 1×1 μm (3D image).

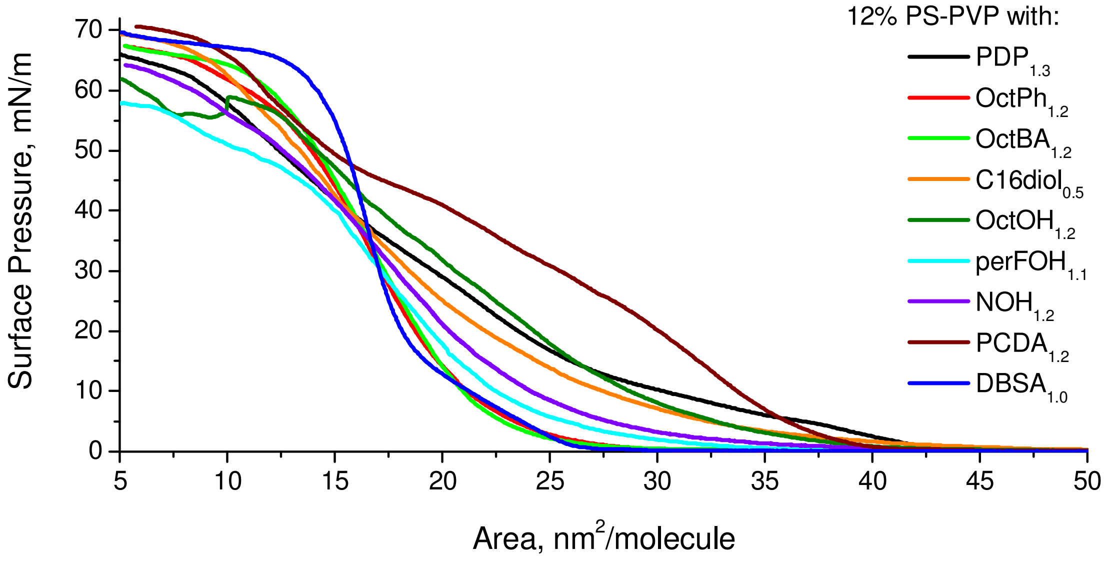

Figure SI-4-8. Langmuir compression isotherms of 12% PS-PVP with various small molecules spread from concentrated (1.8–20 mg/ml) $CHCl_3$ solutions at 21±1°C.

Chapter 5

General Conclusions and Perspectives

Solution concentration: *high density of polymer chains on the surface*

Temperature: *dynamics of drop spreading, chain mobility*

Ratio between copo and small molecules: *maximum complexation*

Area of spreading: *self-assembly occurs quickly, then structure is frozen*

Nature of small molecules: *surfactants capable to form hydrogen bonds*

Diblock copolymer: f_{PVP} = 10–20 mol %; $MW_{Ps\text{-}PVP}$ < 60,000 Da

Solvent: *less volatile to optimize time for self-assembly*

Diblock copolymer: f_{PVP} > 20 mol % for complex, > 30 mol% for copo

Orientation of PDP: *gauche-to-trans (when area is compressed)*

Transition plateau: *hexagonal-to-rectangular order–order transition*

Surface pressure: *distance between surface micelles*

5.1. General Conclusions

The initial objective of this work was to find conditions, using the standard Langmuir technique, that gives good control over nanostrand network morphology in LB films of a PS-PVP/PDP diblock copolymer shown previously to give this morphology using the so-called "solvent-assisted" (highly user-dependent) method, and to try to understand the mechanism of their self-assembly. This aim was achieved, as described in Chapter 2. We have shown the conditions that allow this morphology to be obtained with high "purity", and have proposed a novel mechanism for the formation of the nanostrand network, based on the idea of disassembly (or dewetting) of an initially continuous film that had self-assembled in the course of spreading in the form of a fingerprint (or stripe) morphology of alternating stripes of hydrophobic PS (raised above the water surface) and hydrophilic PVP (adsorbed as a monolayer on the water surface). The PS stripes can be viewed as having dewetted on top of the continuous PVP monolayer in this continuous film, making it nanostructured. The disassembly of this film is proposed to occur at the level of the exposed PVP stripes (*i.e.* not covered by PS), and can be viewed as dewetting of the nanostructured continuous film on the water surface.

Subsequently, our studies were extended to a wide series of PS-PVP copolymers, where many molecular and experimental parameters were systematically varied, often over a wide range of: block ratio (usually expressed as mol% PVP content), total copolymer molecular weight, VP/PDP ratio (particularly, comparing no PDP and equimolar PDP), spreading solvent concentration (particularly, "high" *vs*. "low"), *etc*. This, along with literature results on other block copolymer systems, has allowed us to clarify a number of relationships between film morphologies and molecular and experimental parameters, and thereby deepen our understanding of pattern formation in these LB films.

In chapter 3, we showed first of all that the primary (thermodynamic) factor controlling the type of morphology (planar, strand, or dot) is the molar ratio between blocks. We have determined the composition limits for each of these main morphologies, which are very different with and without equimolar PDP present (Table 3-2), and also have shown that a transition from one structure to another is possible for the same PVP molar ratio when PDP is added. This explains, for example, why the 12% PVP copolymer shows a planar-type morphology without PDP and the nanostrand network in the presence of equimolar PDP, as first observed in Chapter 2. As in some literature systems, we have shown the direct relation between nanofeature dimensions and the length of each block: the micellar height is controlled by the molecular weight of PS and the distance between surface micelles is limited by the length of the surface-adsorbed PVP. The transition compositions can be related, at least in part, to critical ratios of the surface areas occupied by the two blocks (another contribution may come from changes in interfacial energies, particularly of the hydrophilic block with air and PS). The PVP/PS critical surface area ratio is higher for the rod/dot transition than for the planar/rod transition. From comparison with literature systems (Table 3-2), it seems that the presence or not of an alkyl group is particularly important in determining the stability ranges of the three morphologies. The presence of an ionic group (as in the alkylated PS-PVP systems) reduces the transition compositions a little in comparison. This might be explained, at least in part, by the alkyl group causing greater expansion of the PVP monolayer on the water surface for steric reasons (and the ionic groups through electrostatic repulsion), as shown experimentally by the onset and limiting areas associated with the Langmuir isotherms. Greater PVP expansion means greater surface area per VP, or, in other words, a higher PVP/PS surface area ratio, for a given block molar ratio. This will decrease the transition compositions if they are determined primarily by the PVP/PS surface area ratios.

In addition, we have shown, complementing other literature results, that the principal morphologies can be modified, sometimes drastically, by various kinetic effects that accompany the complex drop spreading and solvent evaporation process at the air/water interface. This has the greatest consequences for the planar and nanostrand morphologies, and is especially put into evidence by the spreading solution concentration and total block copolymer molecular weight. This has been discussed (mainly in Chapter 3, complemented in Chapter 4) in relation to (1) polymer chain aggregation (which may or may not include chain entanglements), since the solutions are initially well below the critical overlap concentration, (2) decrease and then cessation of polymer chain mobility as solvent evaporation causes the T_g of at least one of the blocks (PS) to approach and then go above the working temperature, thus freezing in non-equilibrium morphologies and (3) dewetting phenomena. Dewetting in the course of drop spreading can occur both in terms of one block relative to the other (here, PS relative to the surface-adsorbed PVP monolayer) and in terms of a continuous block copolymer film relative to the water surface. The former can be considered as equilibrium morphologies in the instantaneous conditions under which they occur. The latter can lead to a wide variety of forms. Furthermore, this can occur from both unstructured films (*e.g.* those with the planar morphology) and nanostructured films (those with stripe and nanodot morphologies), this last accounting for the nanostrand morphology as said in the first paragraph of this section.

In the course of the research, other discoveries – essentially serendipitous – were made. The most important one concerns the nature of the transition associated with the high pressure plateau in the Langmuir isotherms for films with the nanodot morphology. When examining a nanodot LB PS-PVP/PDP film transferred at high surface pressure (above the plateau pressure), we were surprised to see not only direct evidence of the vertical reorientation (relative to the water surface) of the PDP molecules (detected by *in-situ* FTIR previously in the literature, and which we could also observe), but also that a transition in the packing order of the nanodots occurs, from hexagonal to rectangular. To our knowledge, this is the first time that an order–order transition, induced here by surface pressure, has been shown for a block copolymer monolayer spread at the air/water interface. It sheds completely new light on the isotherm plateau transition.

In preliminary experiments to use nanostrands as a template, which involved subsequent washing out of PDP (*i.e.* to provide better access to the PVP functional group, pyridine), we discovered the new morphology of nanostrands with an internal structure of two lengthwise parallel rows of nanodots. This resulted in not only a discussion of possible new insights into the early stages of the morphology formation, but this substructure itself is of particular interest. To our knowledge, this is the first time this type of pattern has been observed, and this particular arrangement of nanodots cannot be obtained by any other self-assembling method.

Finally, it is worth adding that preliminary results on the stability of LB nanostrand films in aqueous solutions of various pH show that the morphology is stable in water ($pH = 7$), aqueous acetic acid ($pH = 2$), and aqueous sodium bicarbonate ($pH = 9$) for a long period of time (several days). Minor changes (revealed as breaks of long strands into shorter ones) were observed after soaking the samples in H_2O and $NaHCO_3$ at 65–70°C (for 2½ hours);

and major disruptions of the film occurred after CH_3COOH treatment at this temperature. Aqueous hydrochloric acid (pH = 2), especially with heating, was observed to destroy the monolayer completely. The above changes can be associated with the solubility of PVP in the acidic solutions, and in addition, with an interaction of PVP with HCl. It is believed that UV crosslinking can be used for stabilizing the film before subjecting it to chemical reactions.

5.2. Ideas for Future Work

In this dissertation, comprehensive research work has been done that has given many significant and new results and improved understanding of block copolymer LB films. However, various additional experiments can be proposed to further extend the work (though, they will, in turn, generate new ideas to be explored). The following describes several further ideas and experiments that are of interest to follow up on.

Use of the nanostrand LB film as a template. It is intriguing to use the nanostrand monolayer as a unique template for selective deposition of various other substances. Here we mention one example. It will be difficult to directly detect the presence and location of deposited small molecules by AFM, and FTIR intensity may be not enough to resolve potential shifts of PVP signals (broad signals) even if new complex is formed (although their presence if not their location might be detectable). Thus, relatively big molecules (or nanoparticles) ought to be used. We actually did some preliminary trials with a fullerene derivative. LB films of a nanostrand LB film rinsed in acetone was immersed for three days in an acetone solution of fullerenemalonic acid [$C_{60}(COOH)_2$]. It showed a uniform coverage of the entire surface by spherical features of *ca.* 1 nm height (the van der Waals diameter of C_{60} molecule is 1.1 nm). It is assumed that the use of a mica substrate could be a reason for the non-selective deposition of $C_{60}(COOH)_2$ because organic acids have also an affinity to aluminosilicates. In this case, the use of a silicon-oxide substrate can improve the selectivity.

Influence of high surface pressure on the nanodot morphology produced from pure PS-PVP. A very important result concerns the surface pressure-induced hexagonal-to-rectangular order–order transition of nanodots, accompanied by PDP reorientation, as observed by AFM with the 29_4% PS-PVP/PDP complex. It will be of great interest to verify if the isotherm plateau observed for other block copolymers also involves an order–order (or disorder) transition. In particular, what happens in the LB film of 46% PS-PVP without PDP present? A hint of what happens is shown in Figure SI-3-1 in the Appendix of Chapter 3. The image, taken from a film transferred at π = 15 mN/m (above the plateau pressure of *ca.* 6 mN/m), shows various bundles of nanodots between which the hexagonal order is clearly perturbed, perhaps with a tendency to rectangular order. The presence of the bundles suggests that the adsorbed PVP monolayer has been displaced vertically and the fact the height of these bundles is the same as that of the isolated nanodots suggests that the displacement is upwards along the nanodots (if they submerged into the water subphase, it would be expected that the bundles would be higher than the isolated nanodots). It will be of interest to explore this system in greater detail at various transfer pressures to clarify what is really happening. For example, if much higher surface pressures are applied, will there be much greater extent of bundling?

***In-situ* FTIR spectroscopy.** Exploratory *in-situ* PM-IRRAS experiments were undertaken to investigate the alkyl chain conformation and also to detect H-bonding directly on the water surface. A change in alkyl chain conformation was detected weakly at high surface pressures for the 46% PS-PVP/PDP, possibly because only part of the surface actually shows alkyl chain reorientation according to the AFM (Figure 4-5). H-bonding could not be detected at all, in part because the IR bands involved are not very strong. With the very recent knowledge gained concerning the plateau transition, it will be of interest to redo and optimize the *in-situ* PM-IRRAS experiments on this system to better clarify the alkyl chain reorientation. In comparison, the pure block copolymer can also be investigated to determine how much of CH_2 stretching band shift, corresponding to the *gauche*-to-*trans* conformation, if any, is related to the CH_2 in the vinyl backbone. To detect *in-situ* H-bonding, it will probably be more useful to use a benzoic acid surfactant (like OctBA in Chapter 4), since its C=O IR band is both strong and sensitive to H-bonding.

PS-PVP/DBSA. We used 4-dodecylbenzenesulfonic acid (DBSA) purchased a long time ago in the experiment with this chemical described in Chapter 4. Its main interest is the fact that ionic interactions instead of H-bonding are involved. Considering the possible aging of the chemical, it is advised to redo the experiments using fresh DBSA before final conclusions regarding structure obtained from PS-PVP/DBSA are made. Furthermore, the commercially available DBSA contains a mixture of isomers. For a more rigorous study of complexes with ionic bonds, the use of *meta*-alkylsulfonic acid (that can be synthesized with an *n*-alkyl tail) may be considered.

Complexes with perfluoro molecules. Perfluorocarbon derivatives possess quite different properties from hydrocarbon derivatives. Functional perfluoro molecules that interact with PVP may thus provide new insights into supramolecular self-assembly. The data shown in Chapter 4 on 1H,1H,2H,2H-perfluoro-1-octanol (FOH) indicates that little if any complexation with PVP was achieved in this case, since the morphology is the same as that obtained for pure PS-PVP. In principle, the H-bond with this molecule should be stronger than with OctOH, which should increase the degree of complexation compared to OctOH. However, the much greater immiscibility of perfluoro chains compared to alkyl chains with PVP and/or steric effects due to the size of F compared to H, can account for the low complexation. It might be possible to compensate the repulsion between the perfluoro chains and PVP by using a functional group with a stronger H-bond, particularly a phenol function, like in PDP, or a benzoic acid group. For this reason, and because it is not commercially available, we attempted to synthesize (perfluorooctyl)phenol in our lab (octyl being chosen to be in parallel with several of the other small molecules shown in Figure 4-14 of Chapter 4). The direct synthesis[*] of 4-(perfluorooctyl)phenol from 1-bromo-4-(heptadecafluorooctyl)benzene using Pd_2dba_3 catalyst, and the Suzuki reaction of 1-bromo-4-(heptadecafluoro-octyl)benzene with 4-carboxyphenylboronic acid [the product of which should be 4′-(heptadecafluorooctyl)-biphenyl-1-carboxylic acid] did not lead to the desired compounds, since it was found that perfluoroalkanes are not stable in KOH (used in the above reactions). Thus, another synthetic approach has to be used to be able to pursue this line of additional research.

Acetone treatment of LB films obtained from pure diblock copolymer. In the acetone treatment of the nanostrands obtained using 12% PS-PVP/PDP, it was thought that some PDP may be located in the PS and therefore play some role in revealing the zig-zag double

---

[*] Anderson, K. W.; Ikawa, T.; Tundel, R. E.; Buchwald, S. L. The selective reaction of aryl halides with KOH: Synthesis of phenols, aromatic ethers, and benzofurans. *JACS* **2006**, *128*, 10694–10695.

line of nanodots along the strand backbone. To test this further, the same experiment should be done on a 19% PS-PVP (without PDP), since this copolymer also gives a nanostrand morphology (though less perfectly than the PDP-containing material). If the same substructure is observed, then this would indicate that the change is mainly related to the swelling of PS by acetone.

Fabrication of gold nanodot arrays. Last but not least, it would be of interest to use the hexagonal dot morphology as a template to fabricate, for example, arrays of gold nanodots of variable spacings (and later, gold nanowires using the nanostrands) onto glass surfaces. The surface arrays of gold nanostructures are expected to exhibit enhanced optical properties that can be characterized by surface plasmon resonance spectroscopy (SPR) and UV-vis spectroscopy. This could initiate a new long-term project.

Epilogue

“All truths are easy to understand once they are discovered; the point is to discover them”

Galileo Galilei